US 20230158507A1

(19) **United States**

(12) **Patent Application Publication**

Himbert et al.

(10) **Pub. No.: US 2023/0158507 A1**

(43) **Pub. Date: May 25, 2023**

(54) **BIOLOGICAL MEMBRANE-BASED SENSOR**

(71) Applicant: **McMaster University**, Hamilton (CA)

(72) Inventors: **Sebastian Himbert**, Hamilton (CA); **Maikel Rheinstadter**, Hamilton (CA)

(21) Appl. No.: **18/097,781**

(22) Filed: **Jan. 17, 2023**

Related U.S. Application Data

(63) Continuation of application No. 16/229,487, filed on Dec. 21, 2018, now Pat. No. 11,577,248.

(60) Provisional application No. 62/608,680, filed on Dec. 21, 2017.

Publication Classification

(51) **Int. Cl.**

B01L 3/00	(2006.01)
G01N 27/327	(2006.01)
G01N 33/53	(2006.01)
G01N 33/49	(2006.01)

(52) **U.S. Cl.**

CPC ***B01L 3/5085*** (2013.01); ***B01L 3/502715*** (2013.01); ***G01N 27/3272*** (2013.01); ***G01N 33/5306*** (2013.01); ***G01N 27/3277*** (2013.01); ***G01N 33/49*** (2013.01); ***G01N 27/3275*** (2013.01)

(57) **ABSTRACT**

Provided herein is a biosensor suitable for use in measuring membrane fluidity or membrane permeability. The biosensor is formed of a solid substrate having a lipid bilayer compatible surface and a multi-lamellar lipid membrane structure localized on the lipid bilayer compatible surface. The multi-lamellar lipid membrane structure can be derived from a biological cell further comprising one or more synthetic lipids. An electrode forming all or part of the lipid bilayer compatible surface may be used to detect disruptions in the lipid membrane structure and hemolytic activity in a test sample.

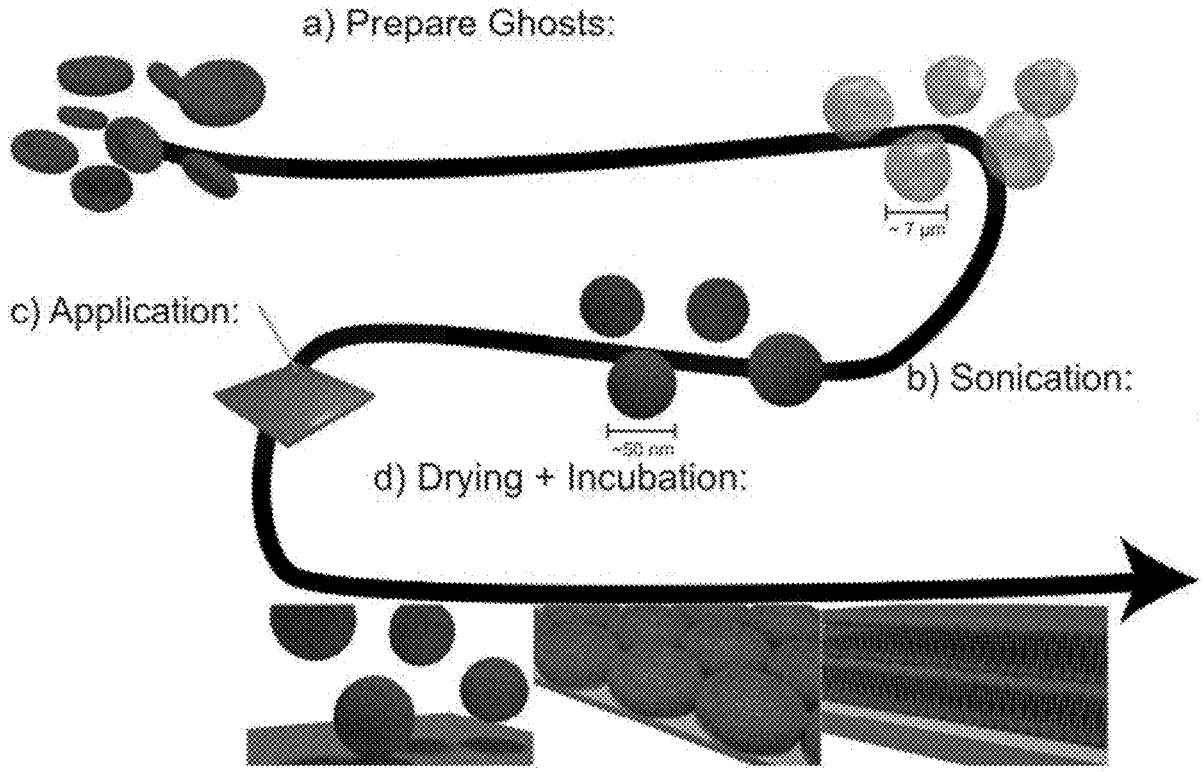

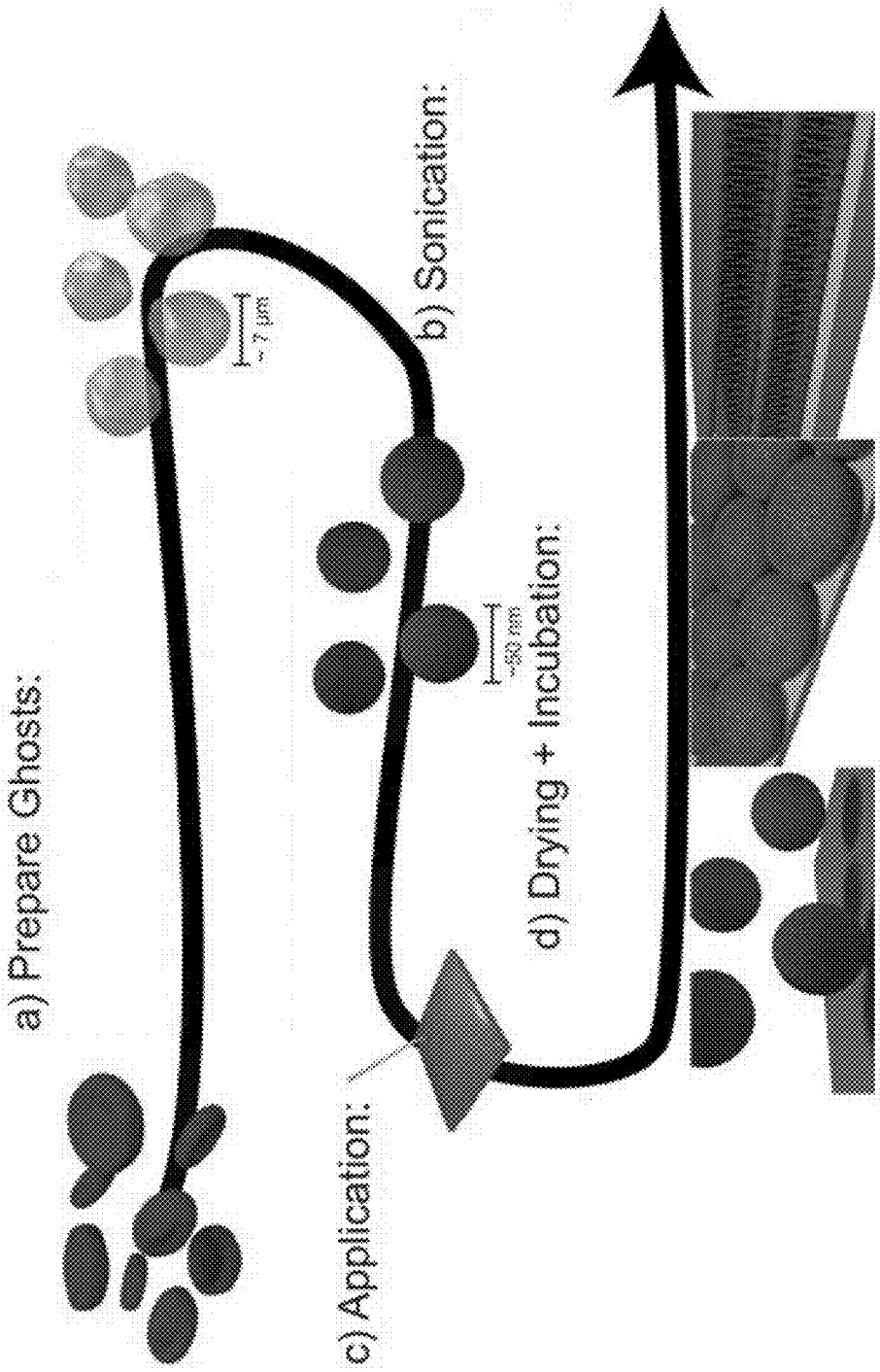
a) Prepare Ghosts:
~7 µm
b) Sonication:
~50 nm
c) Application:
d) Drying + Incubation:

FIG. 1

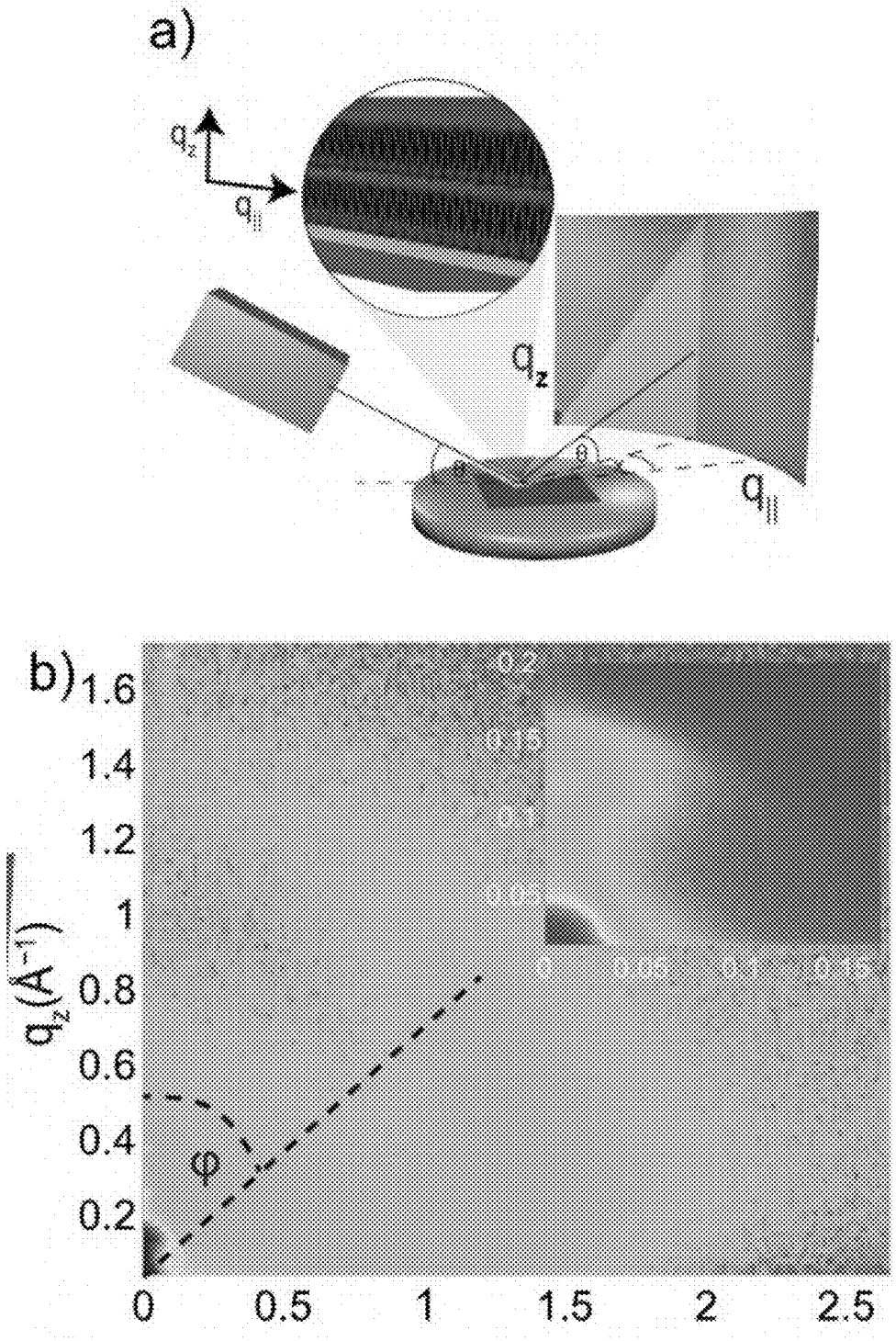

FIG. 2

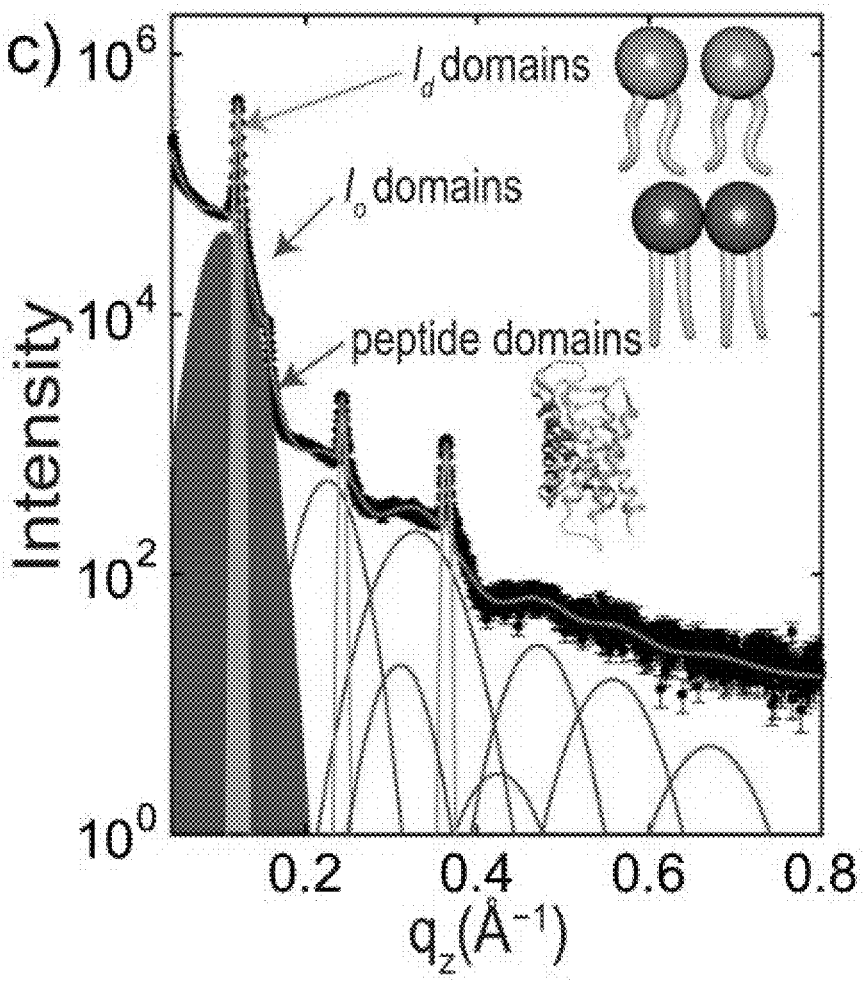
c)
10^6
10^4
10^2
10^0
Intensity
l_d domains
l_o domains
peptide domains
0.2
0.4
0.6
0.8
q_z(Å^{-1})

FIG. 2 (CONT.)

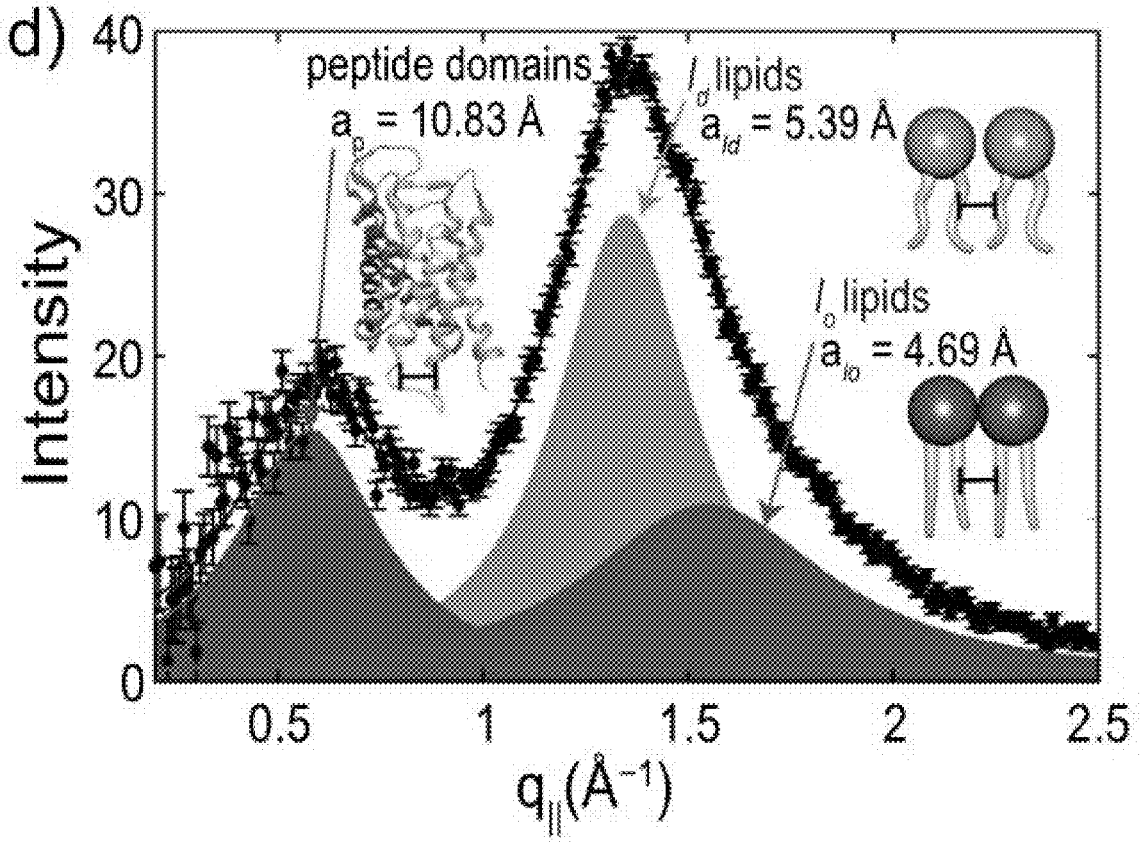
d)
peptide domains
a_p = 10.83 Å
l_d lipids
a_{ld} = 5.39 Å
l_o lipids
a_{lo} = 4.69 Å
Intensity
0
10
20
30
40
0.5
1
1.5
2
2.5
$q_{||}$(Å^{-1})

FIG. 2 (CONT.)

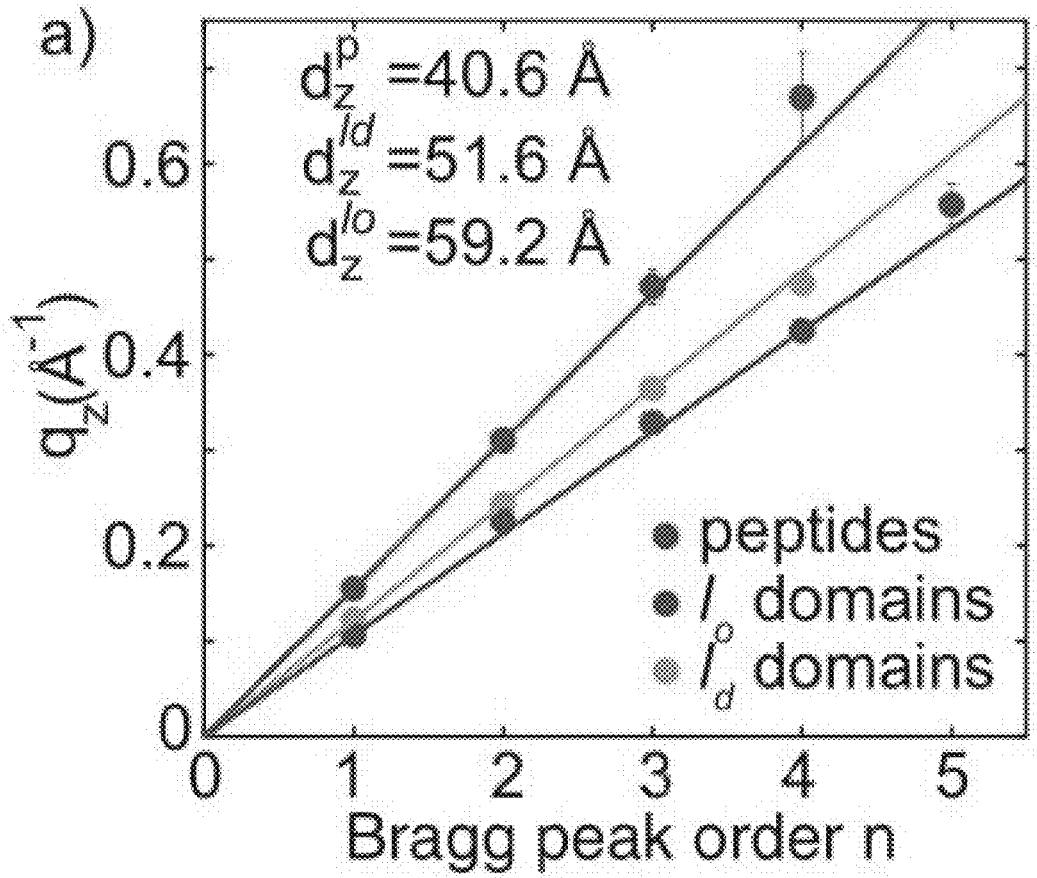
a)
d_z^p =40.6 Å
d_z^{ld} =51.6 Å
d_z^{lo} =59.2 Å
q_z(Å^{-1})
0
0.2
0.4
0.6
0
1
2
3
4
5
Bragg peak order n
peptides
l_d domains
l_d^o domains

FIG. 3

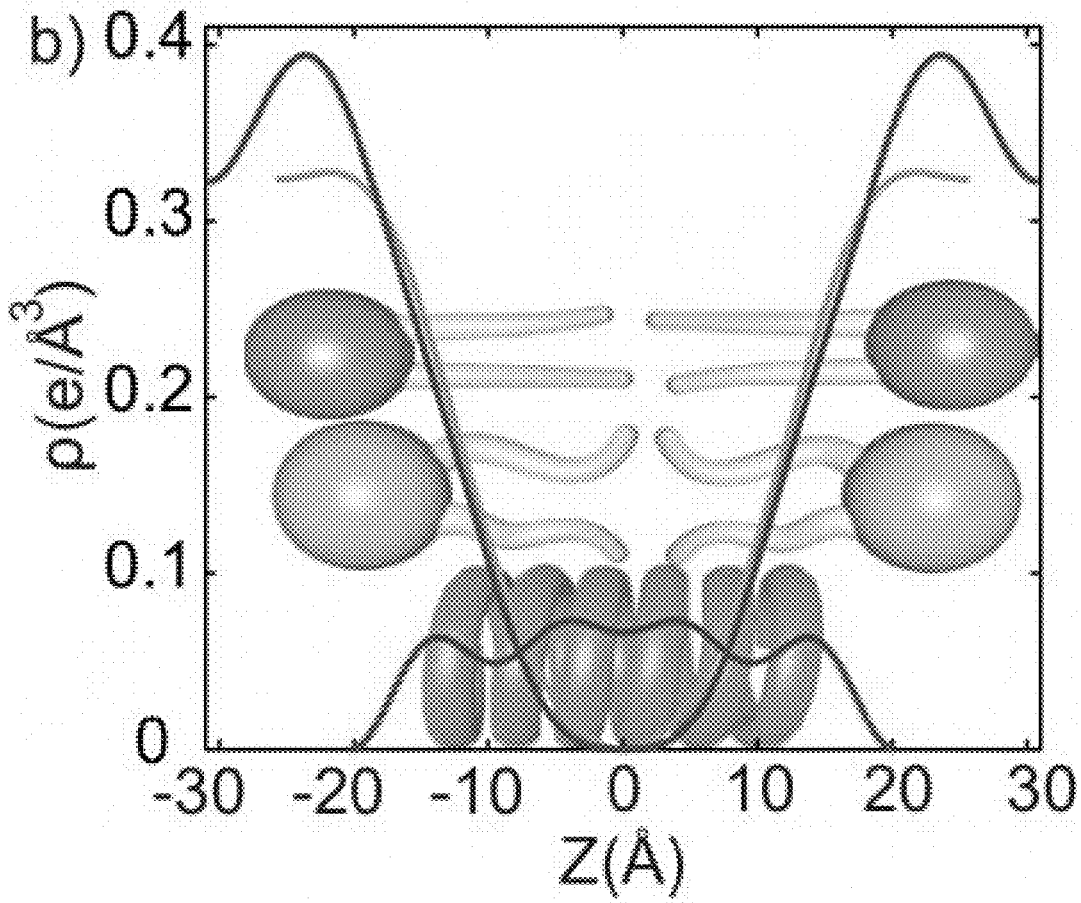

FIG. 3 (CONT.)

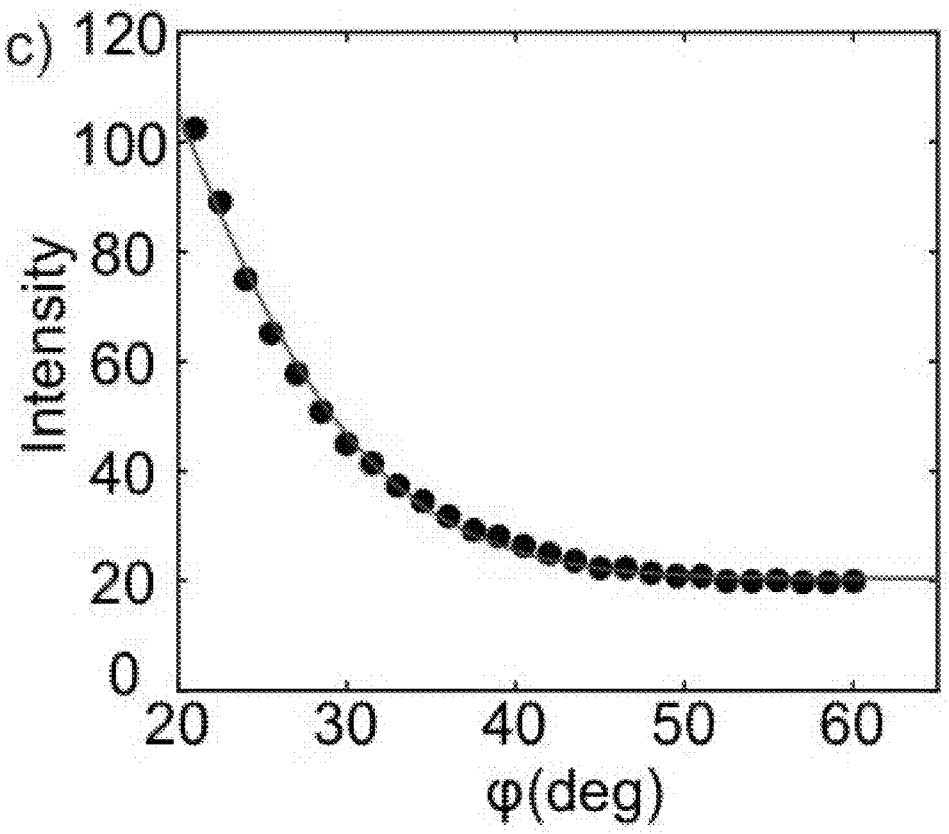

FIG. 3 (CONT.)

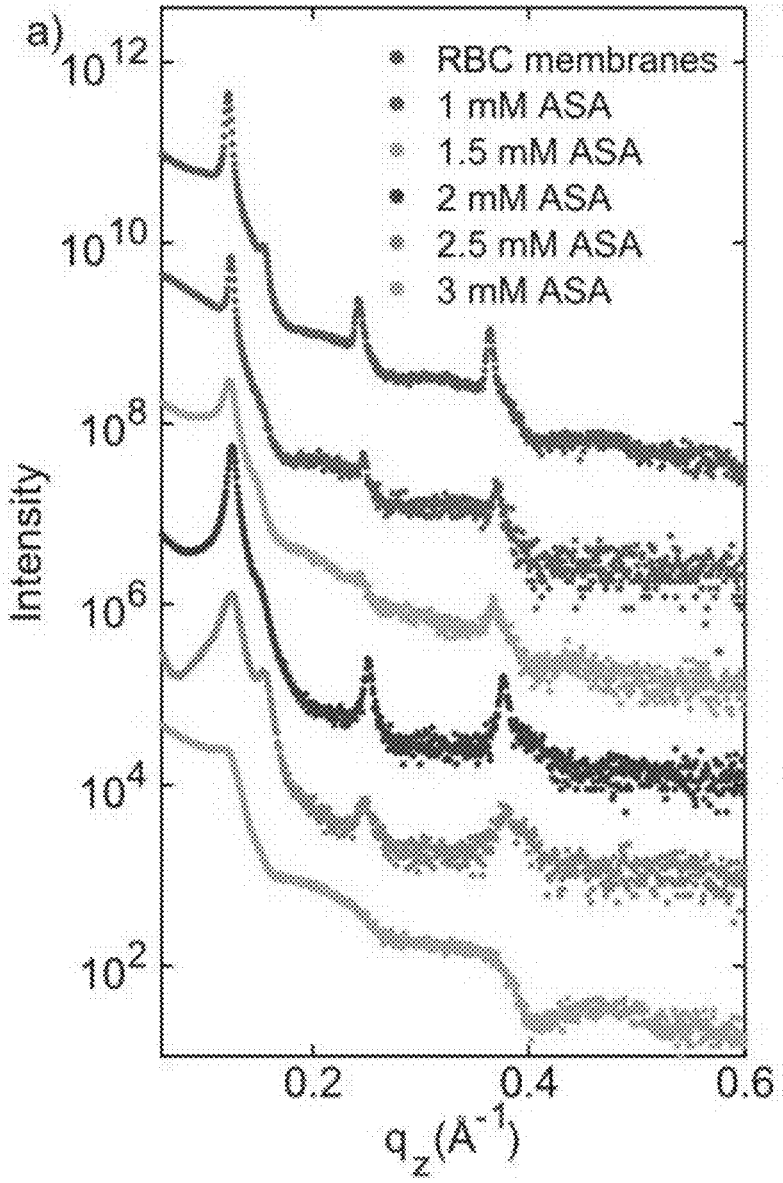
a)
RBC membranes
1 mM ASA
1.5 mM ASA
2 mM ASA
2.5 mM ASA
3 mM ASA
Intensity
10^{12}
10^{10}
10^{8}
10^{6}
10^{4}
10^{2}
0.2
0.4
0.6
$q_z(Å^{-1})$

FIG. 4

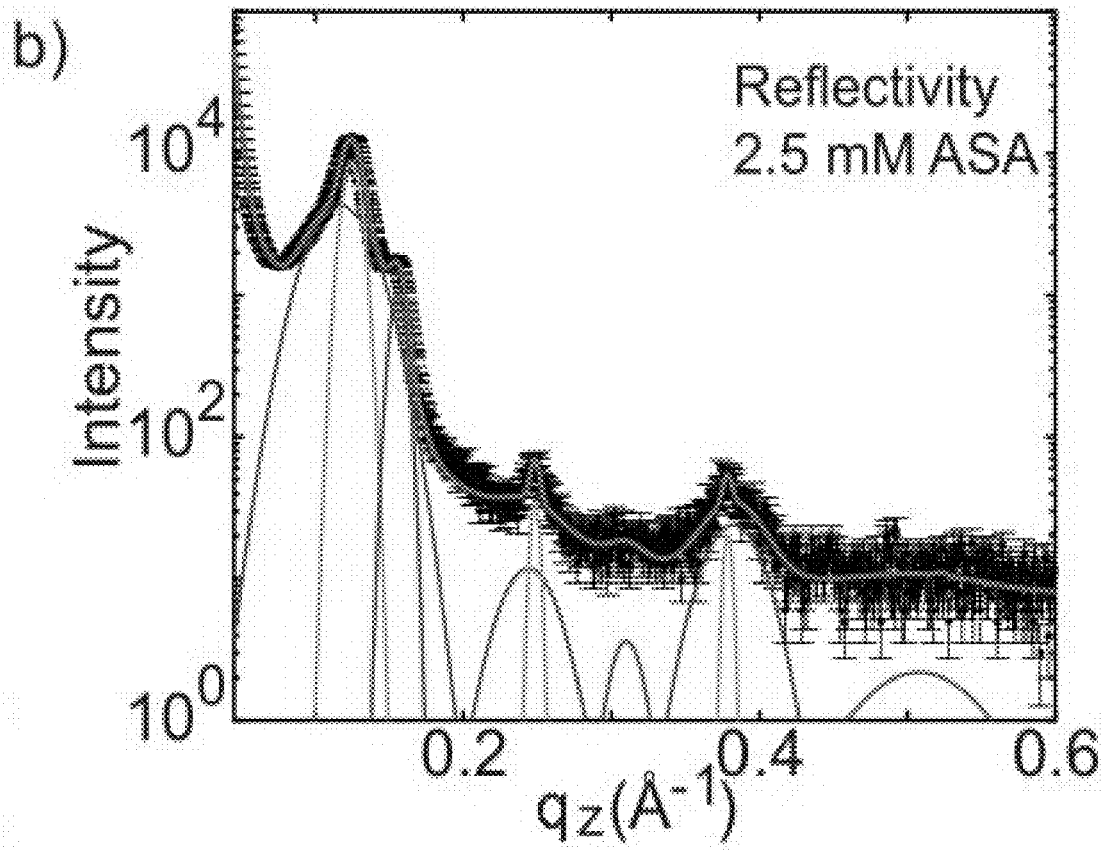

FIG. 4 (CONT.)

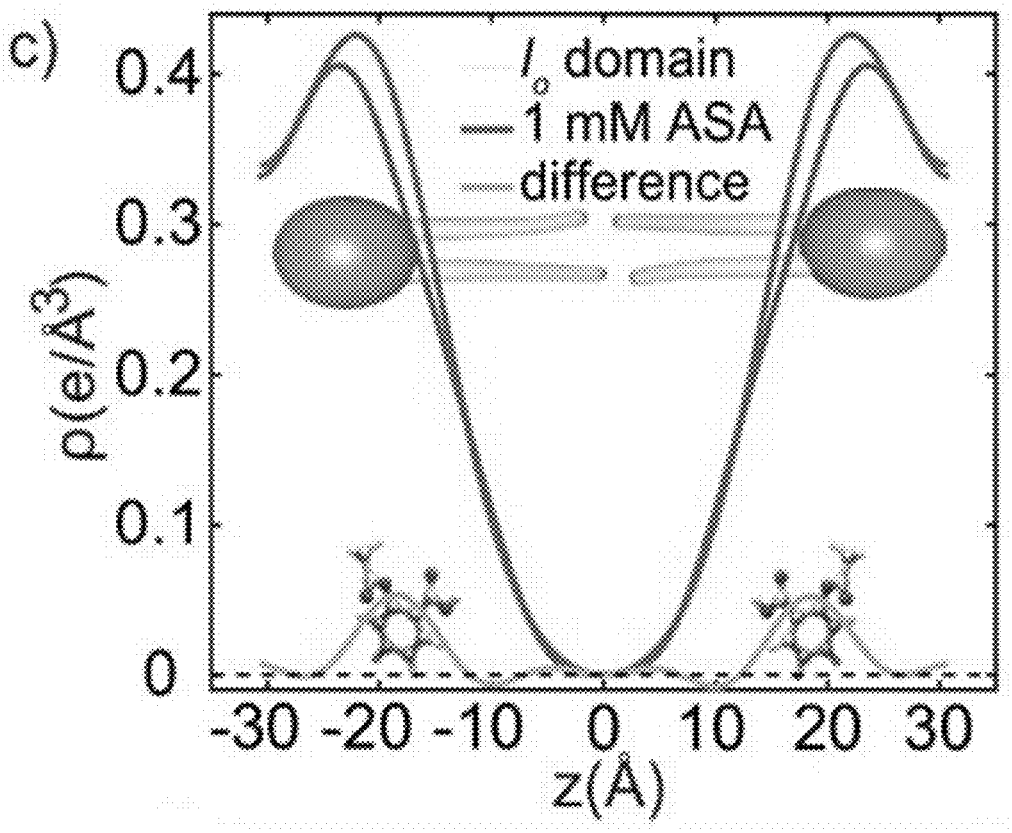
c)
0.4
0.3
0.2
0.1
0
ρ(e/Å³)
I₀ domain
1 mM ASA
difference
-30 -20 -10 0 10 20 30
z(Å)

FIG. 4 (CONT.)

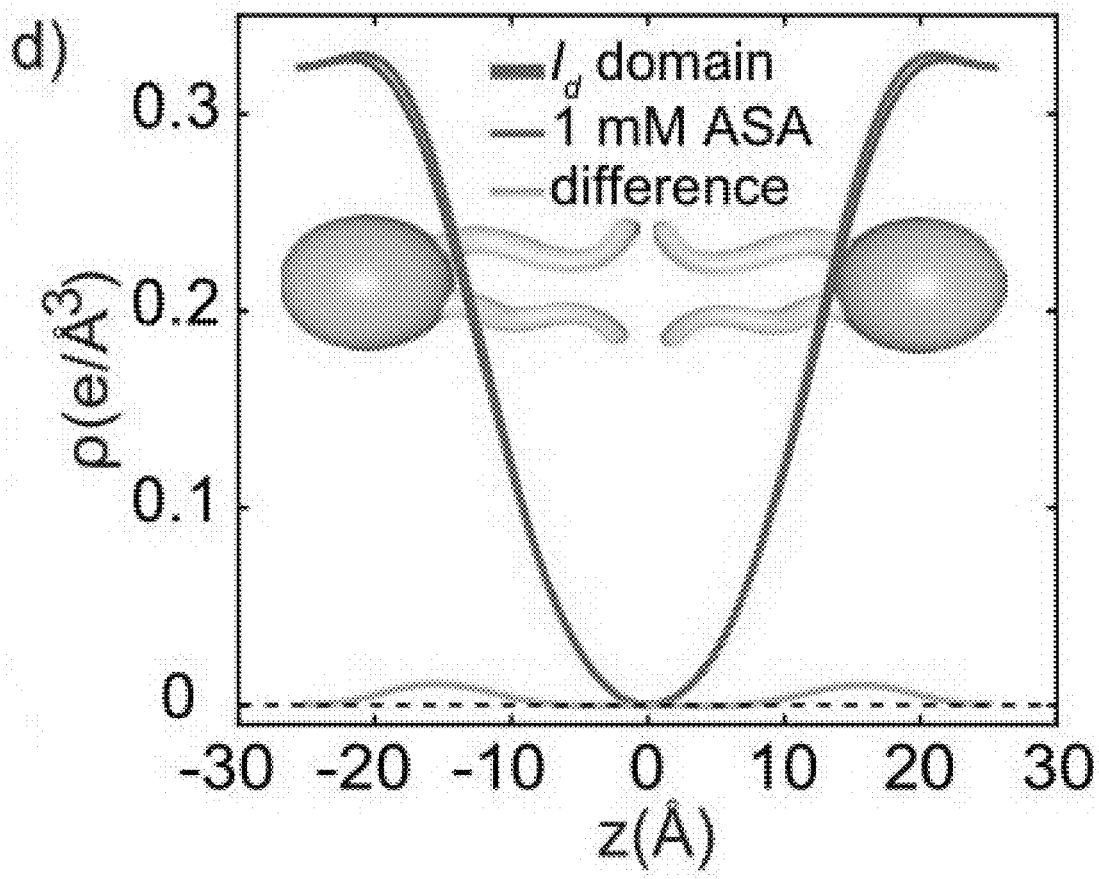
d)
I_d domain
1 mM ASA
difference
0.3
0.2
0.1
0
ρ(e/Å^3)
-30
-20
-10
0
10
20
30
z(Å)

FIG. 4 (CONT.)

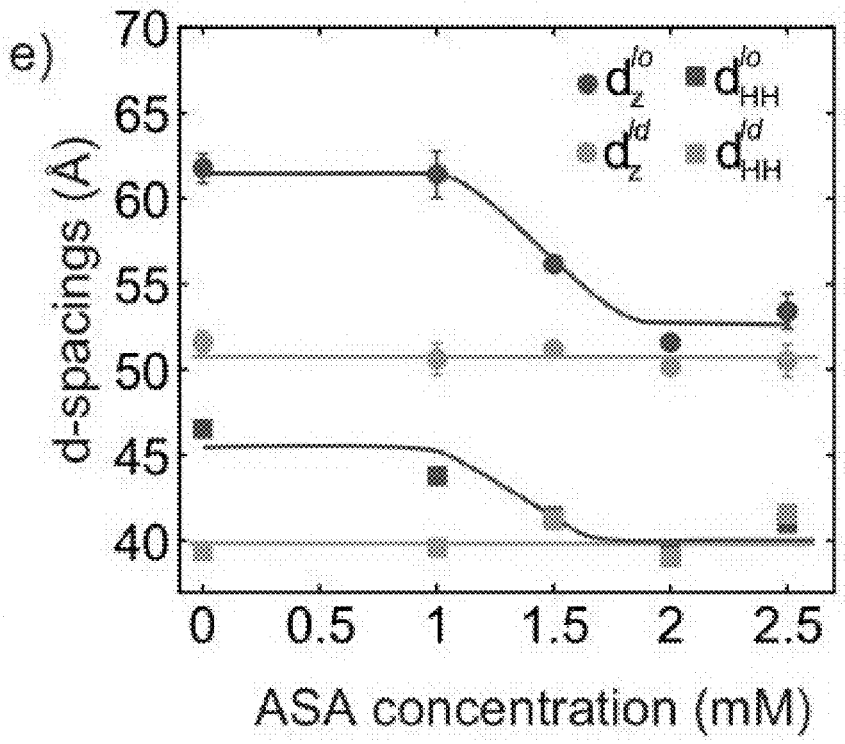
e)
70
65
60
55
50
45
40
d-spacings (Å)
0
0.5
1
1.5
2
2.5
ASA concentration (mM)
d_z^{lo}
d_{HH}^{lo}
d_z^{ld}
d_{HH}^{ld}

FIG. 4 (CONT.)

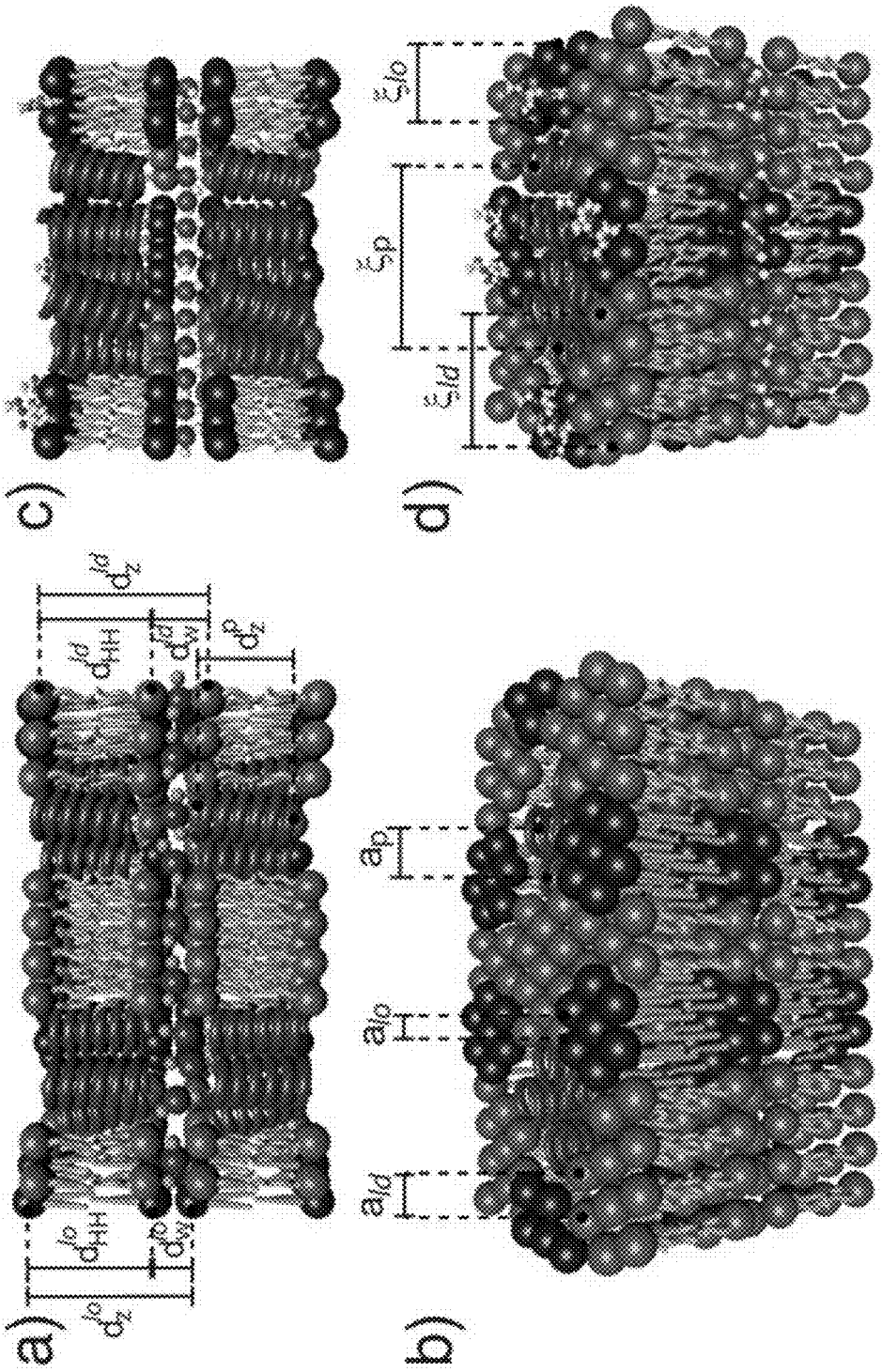

FIG. 5

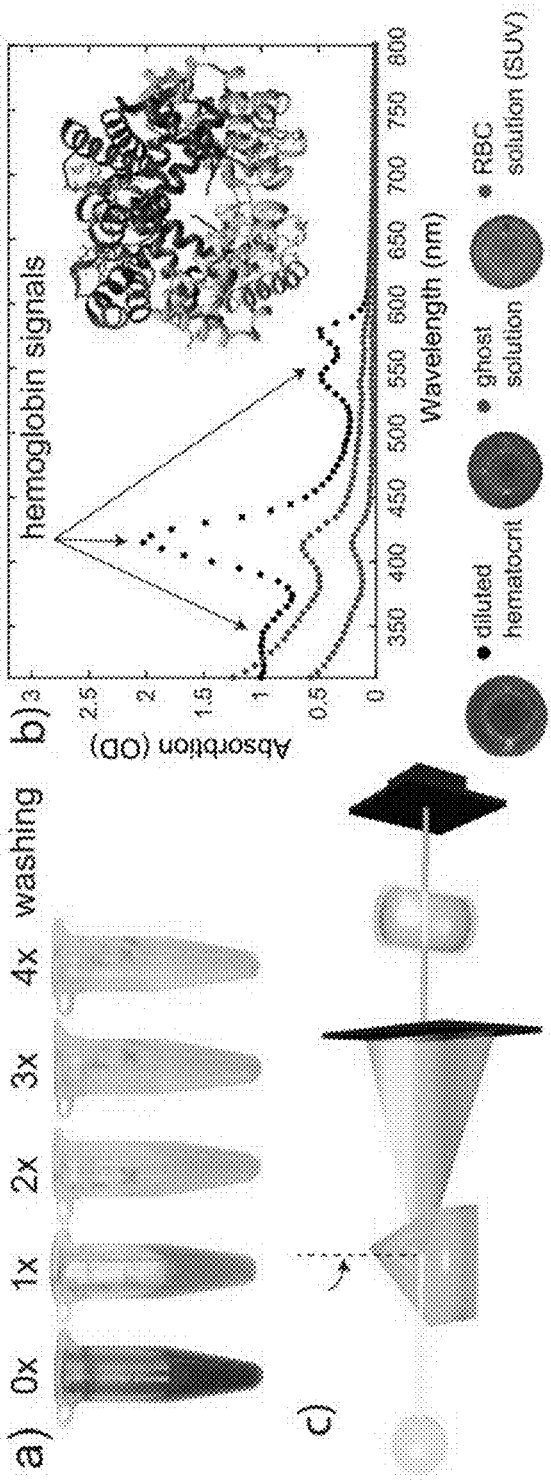
a)
0x
1x
2x
3x
4x
washing
b)
hemoglobin signals
Absorption (OD)
Wavelength (nm)
c)
diluted hematocrit
ghost solution
RBC solution (SUV)

FIG. 6

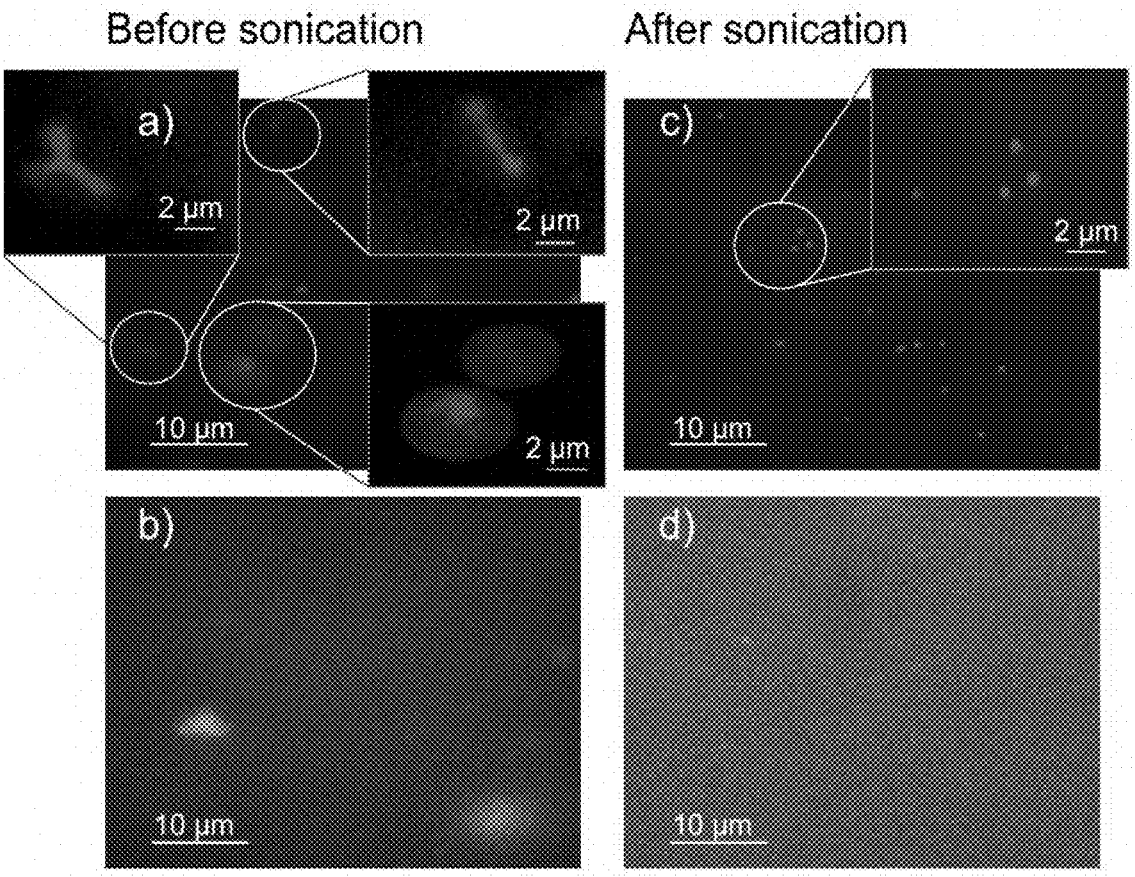
Before sonication
After sonication
a)
2 µm
2 µm
10 µm
2 µm
c)
2 µm
10 µm
b)
10 µm
d)
10 µm

FIG. 7

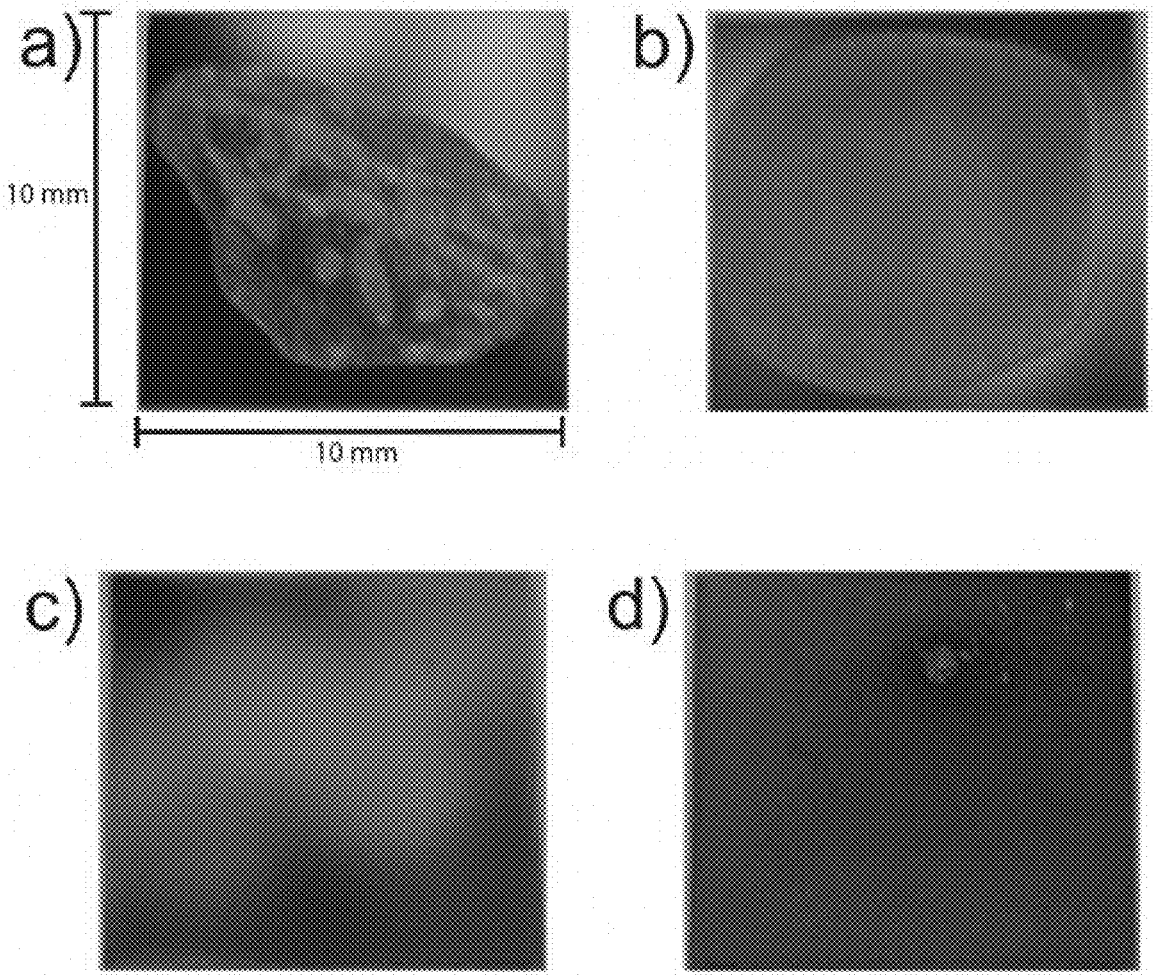

FIG. 8

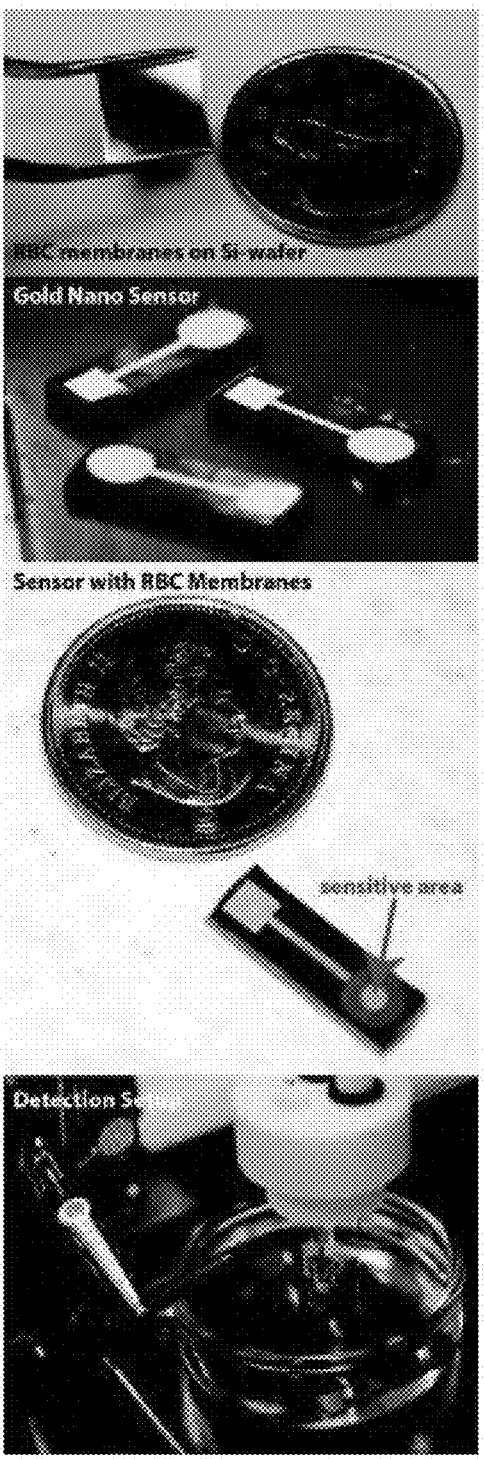
RBC membranes on Si wafer
Gold Nano Sensor
Sensor with RBC Membranes
sensitive area
Detection S

FIG. 9

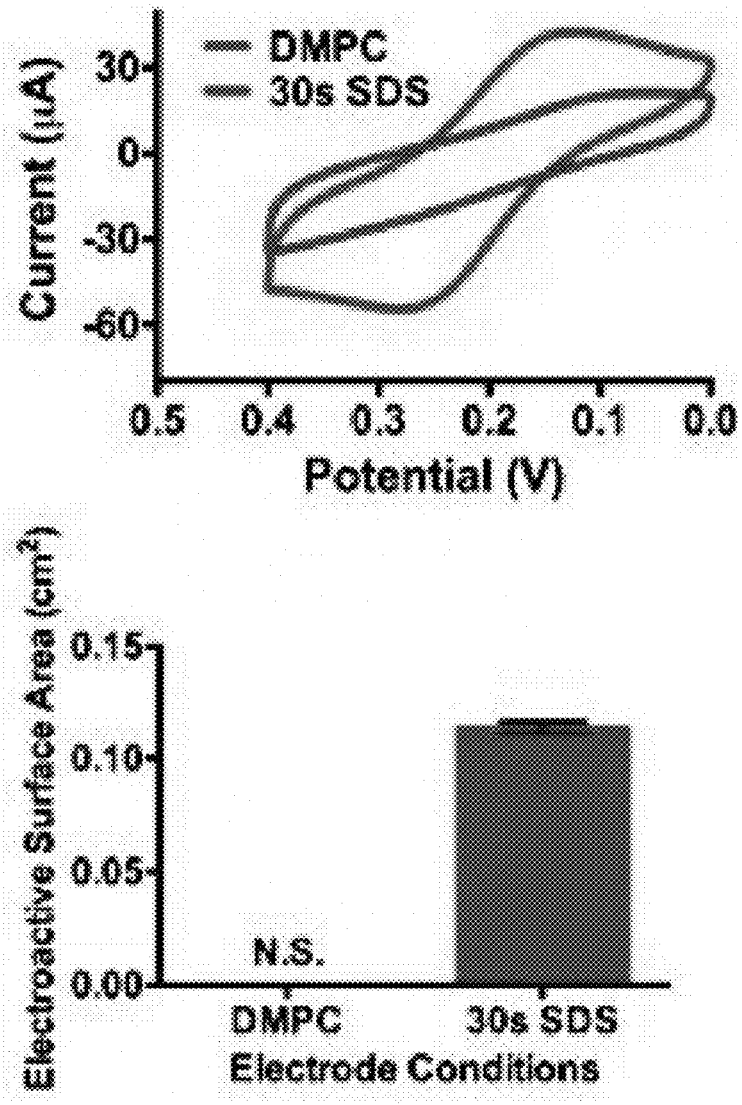
DMPC
30s SDS
Current (μA)
30
0
-30
-60
0.5
0.4
0.3
0.2
0.1
0.0
Potential (V)
Electroactive Surface Area (cm²)
0.15
0.10
0.05
0.00
N.S.
DMPC
30s SDS
Electrode Conditions

FIG. 10

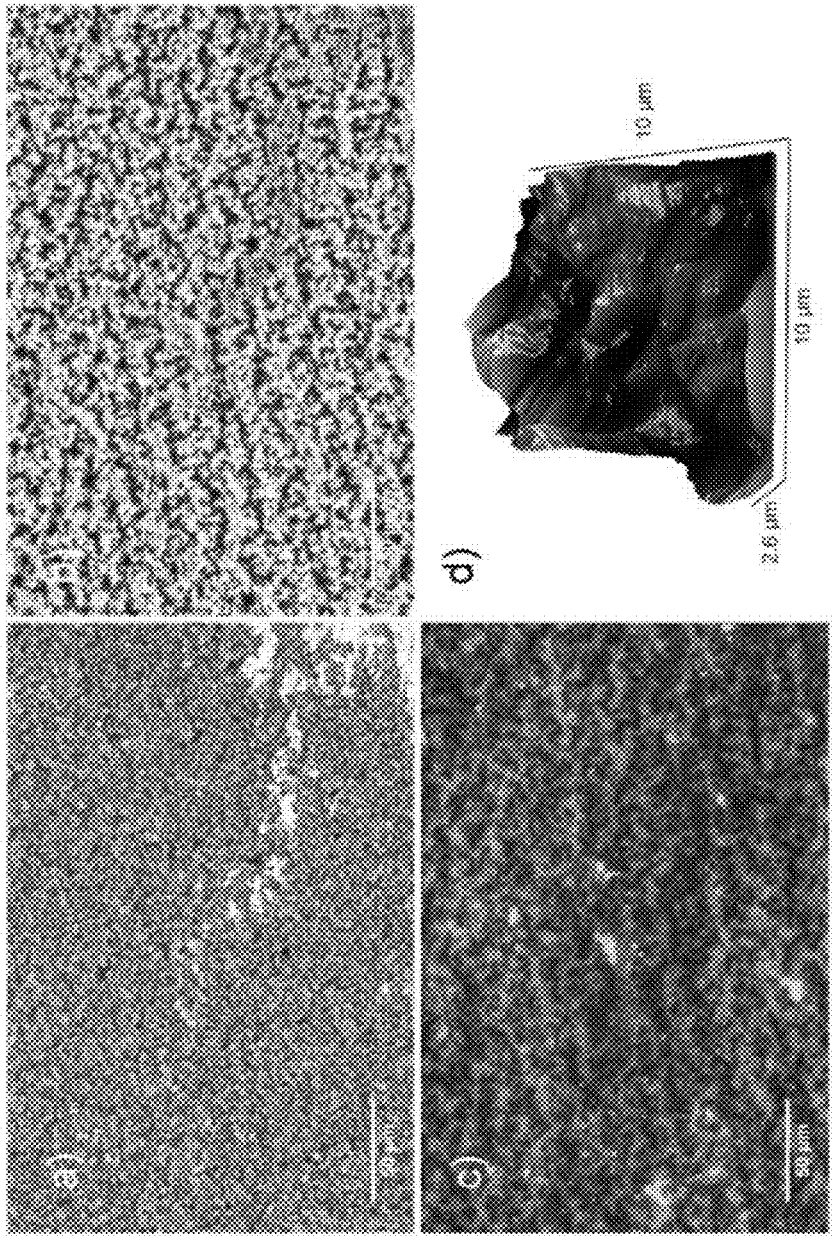

FIG. 11

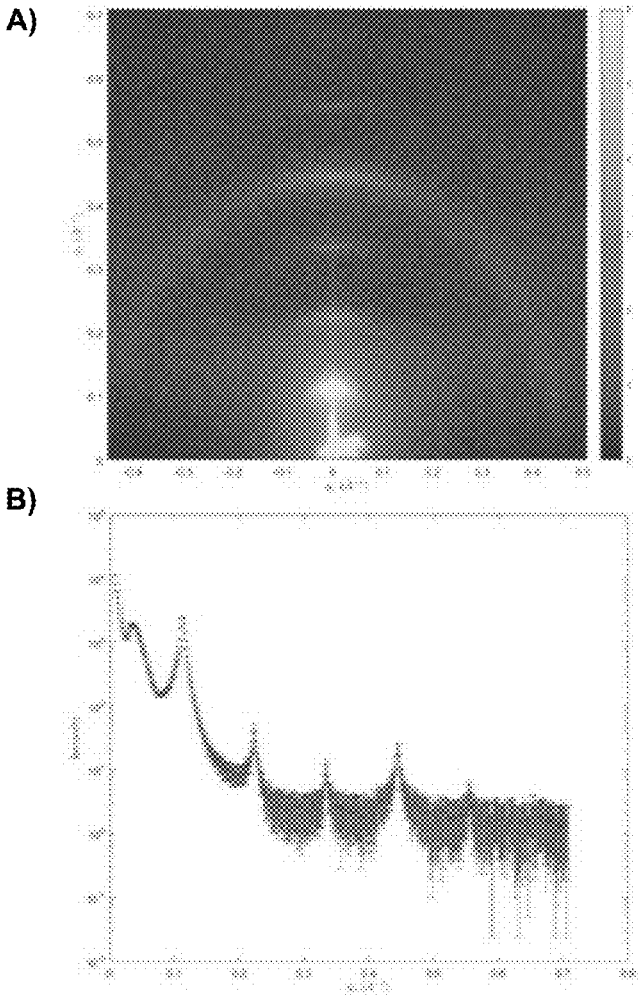

FIG. 12

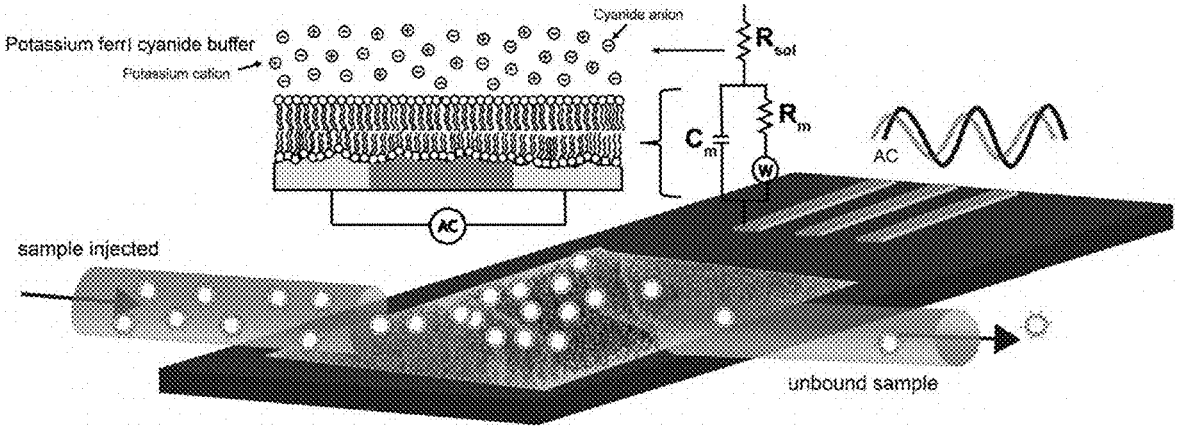

FIG. 13A

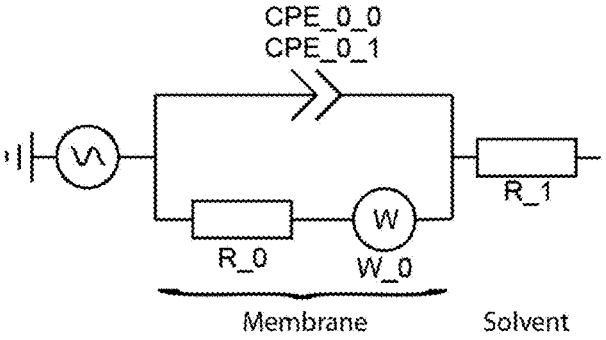

FIG. 13B

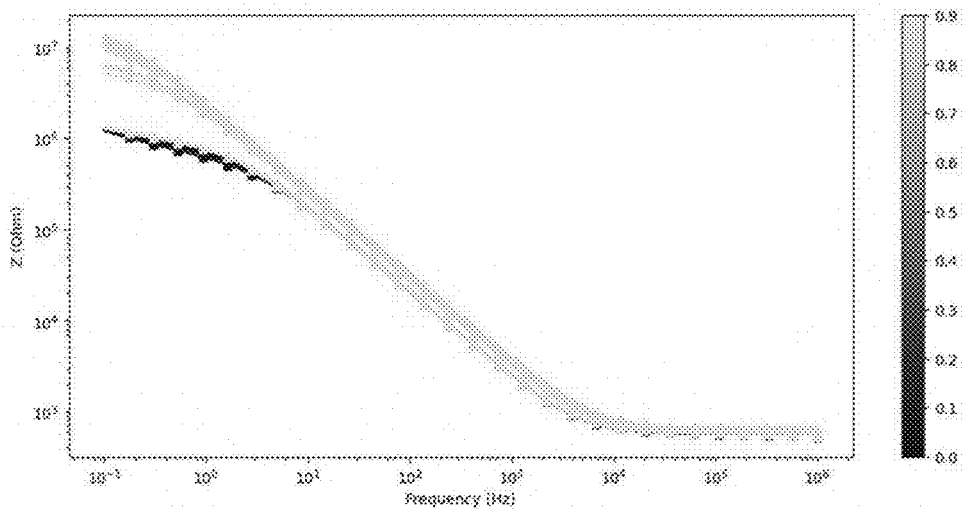

FIG. 14A

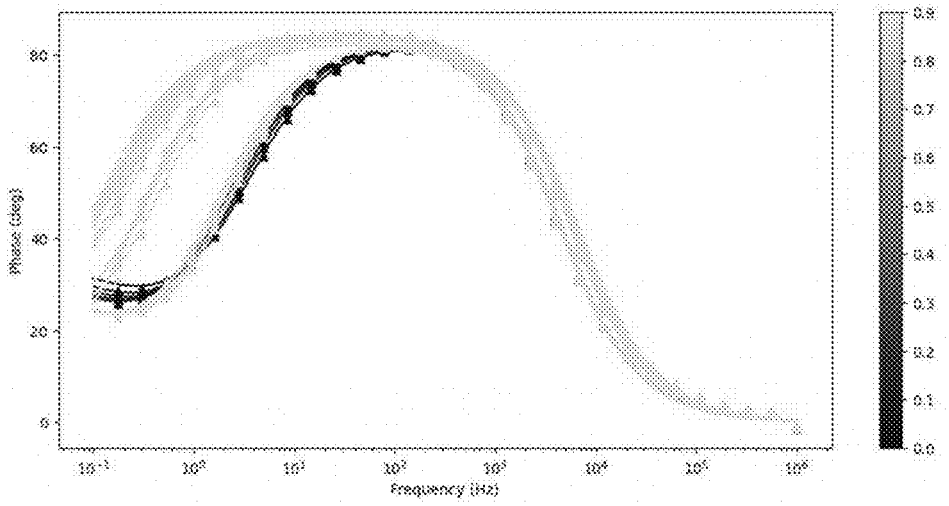

FIG. 14B

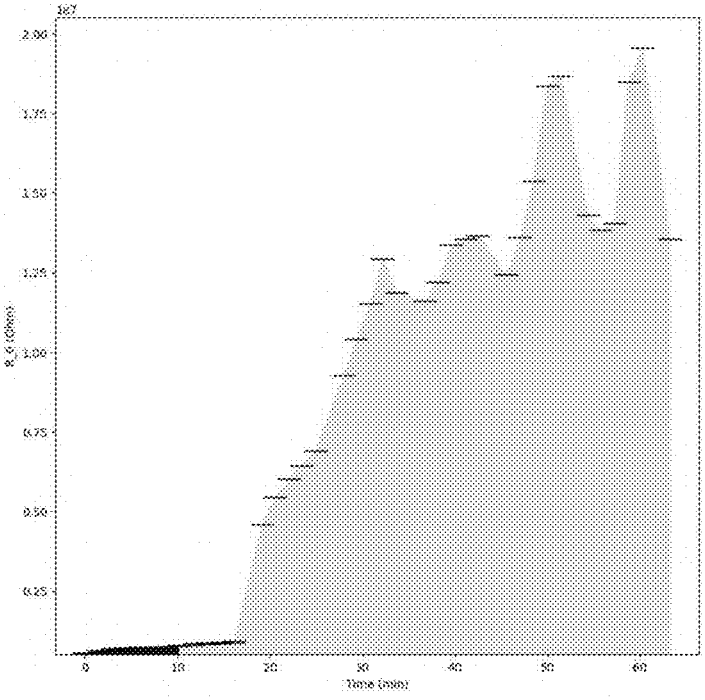

FIG. 14C

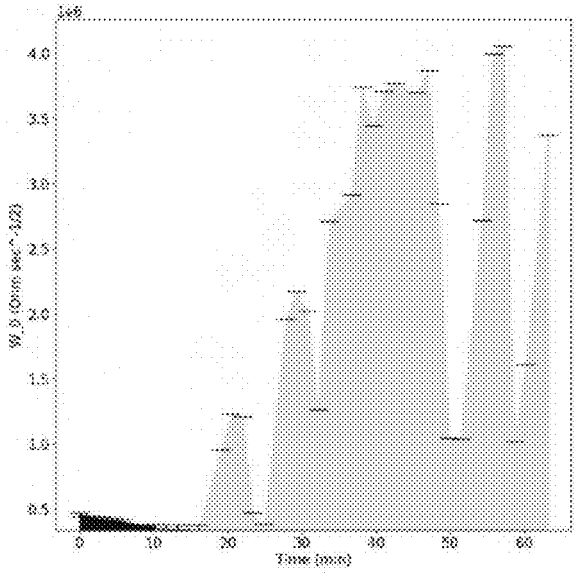

FIG. 14D

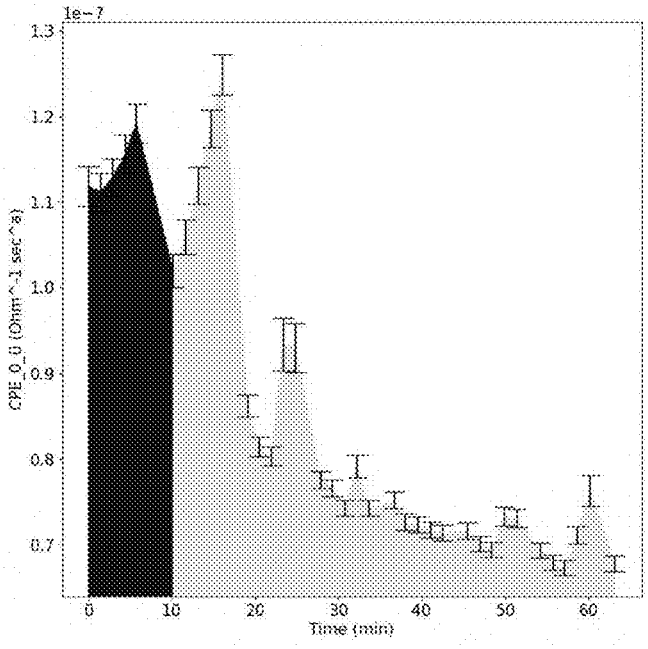

FIG. 14E

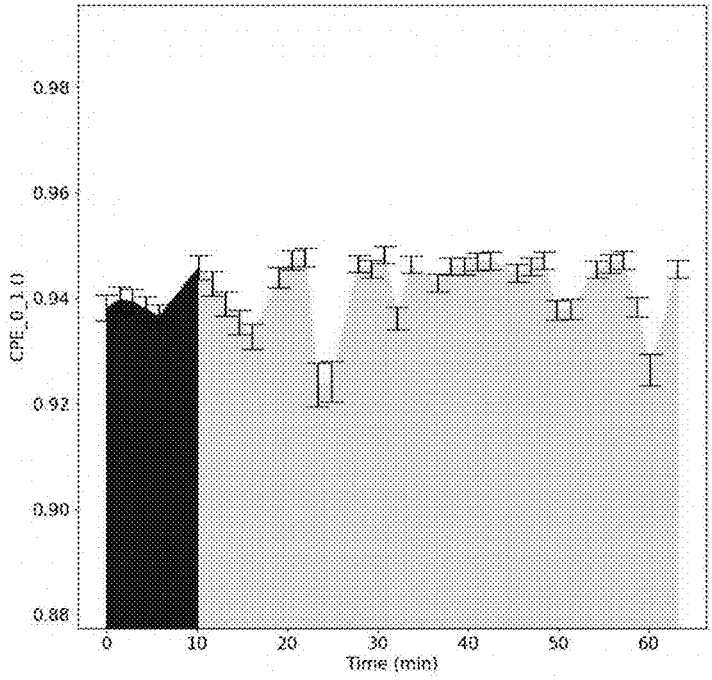

FIG. 14F

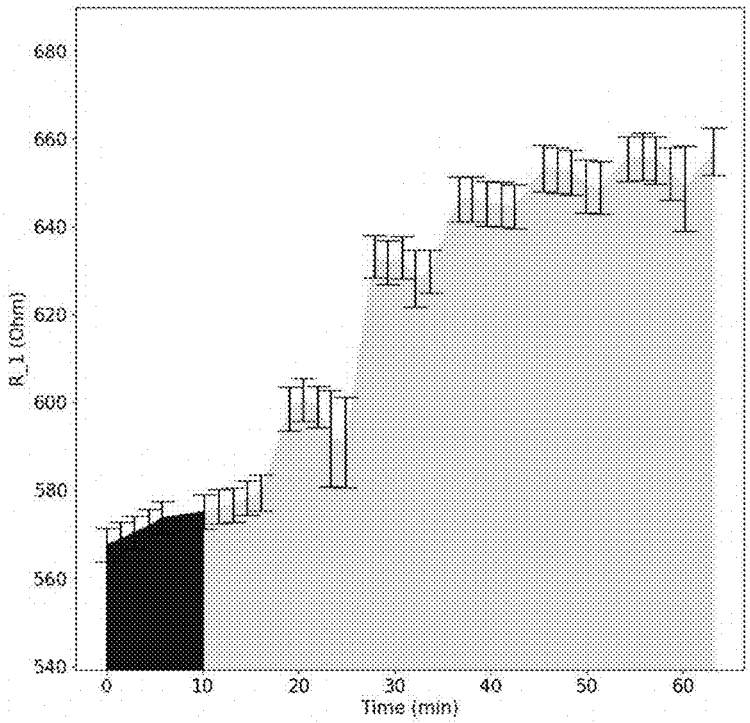

FIG. 14G

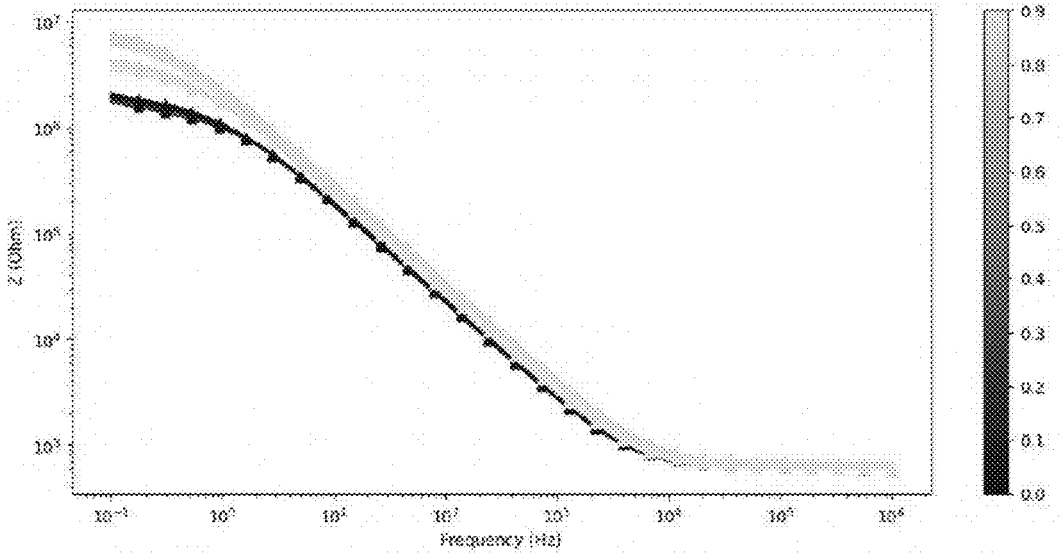

FIG. 15A

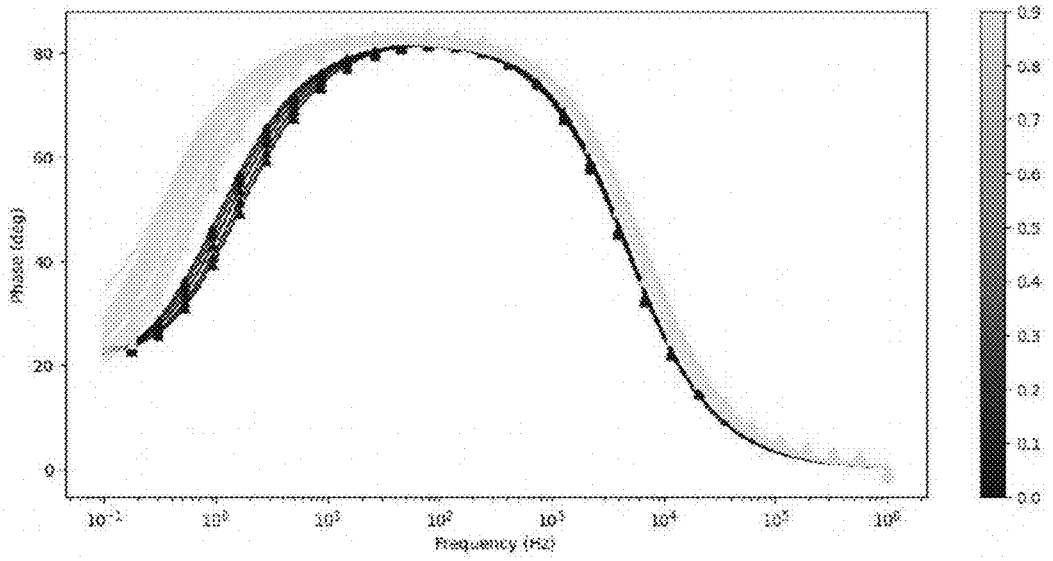

FIG. 15B

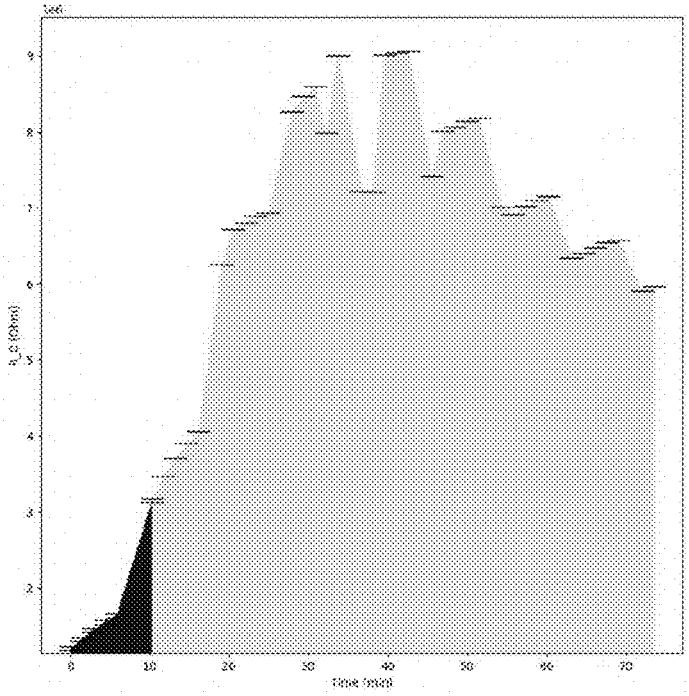

FIG. 15C

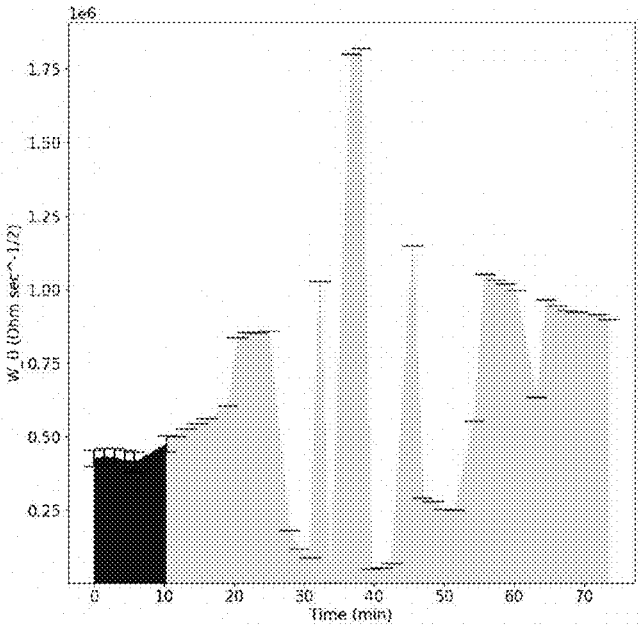

FIG. 15D

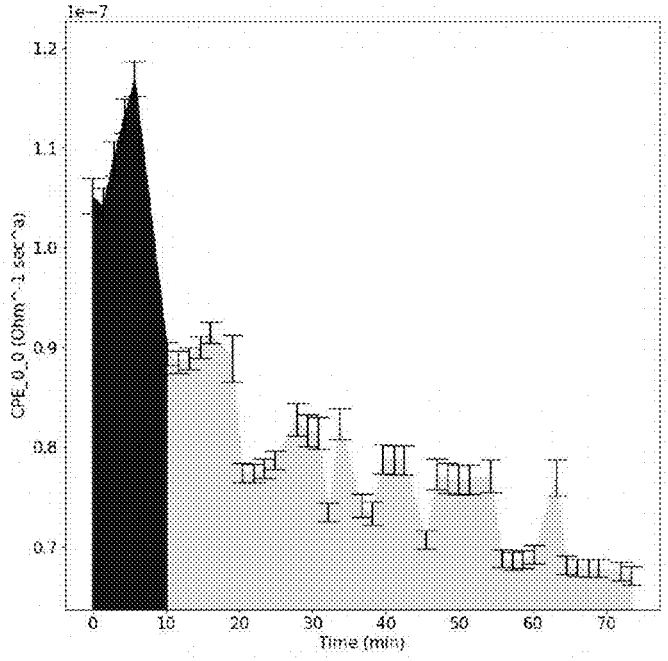

FIG. 15E

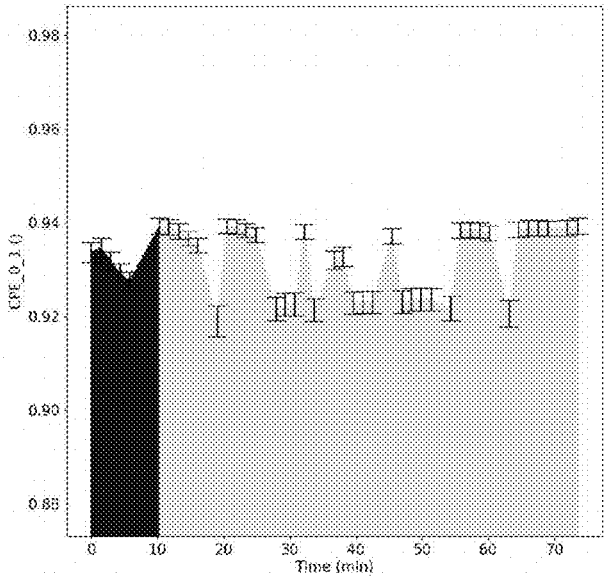

FIG. 15F

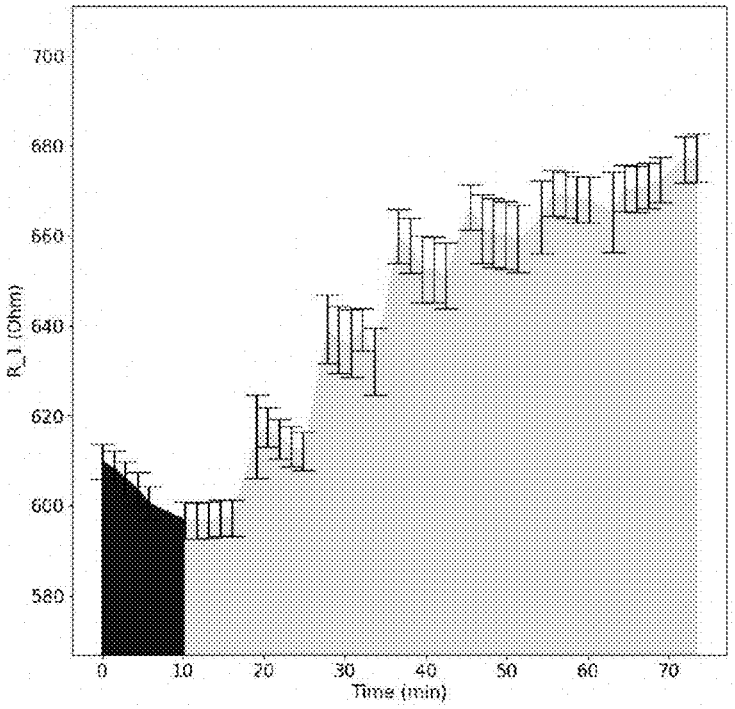

FIG. 15G

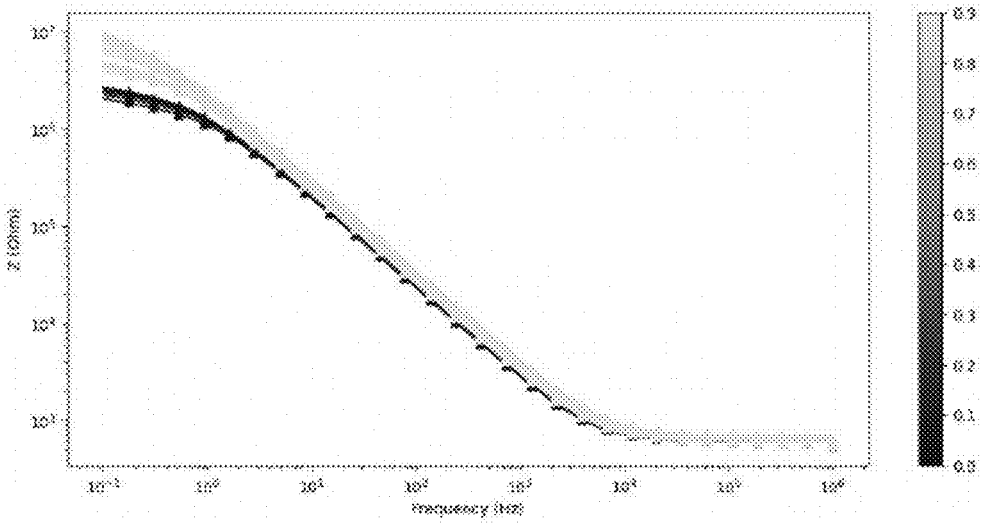

FIG. 16A

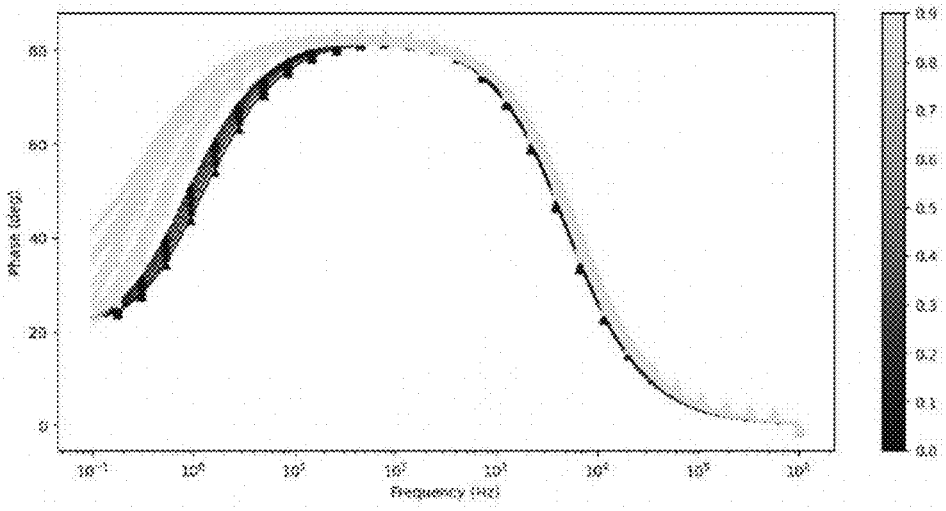

FIG. 16B

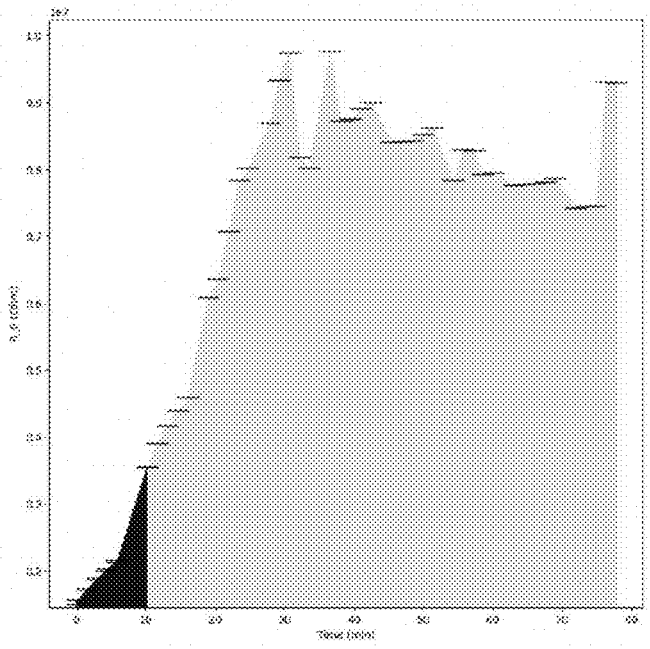

FIG. 16C

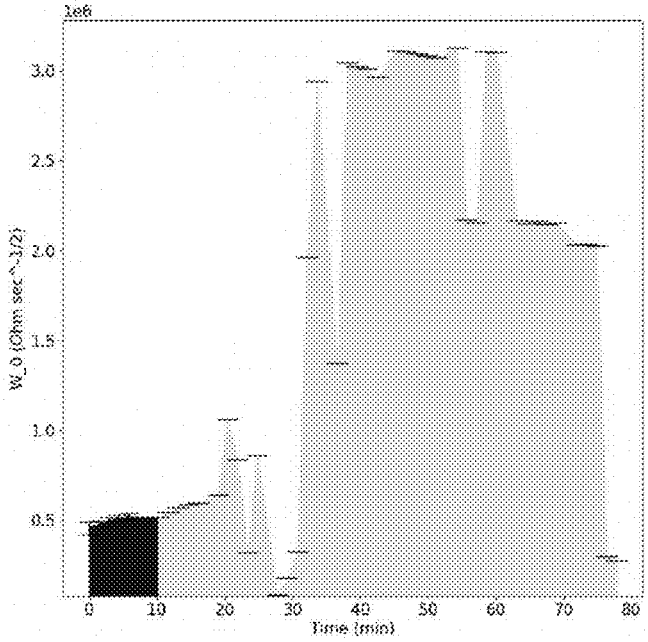

FIG. 16D

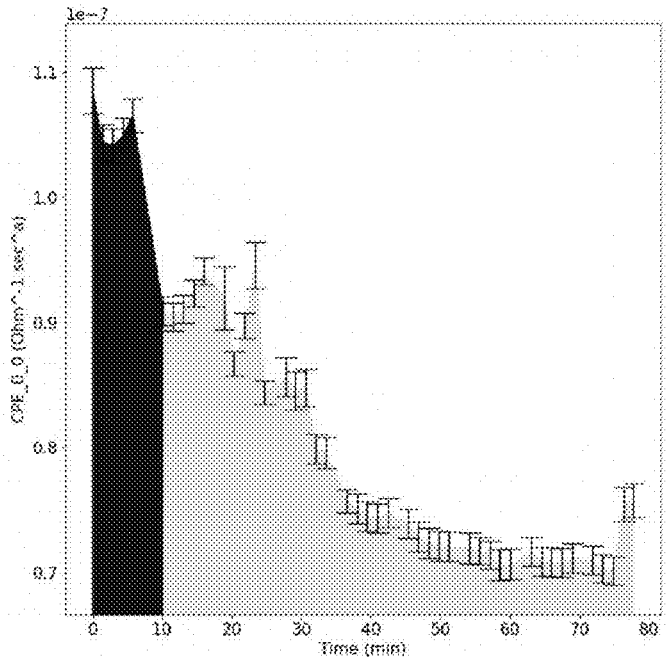

FIG. 16E

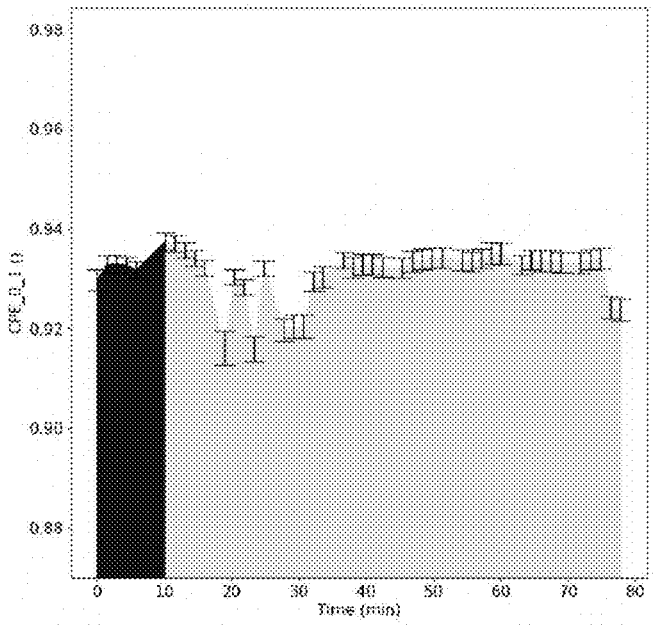

FIG. 16F

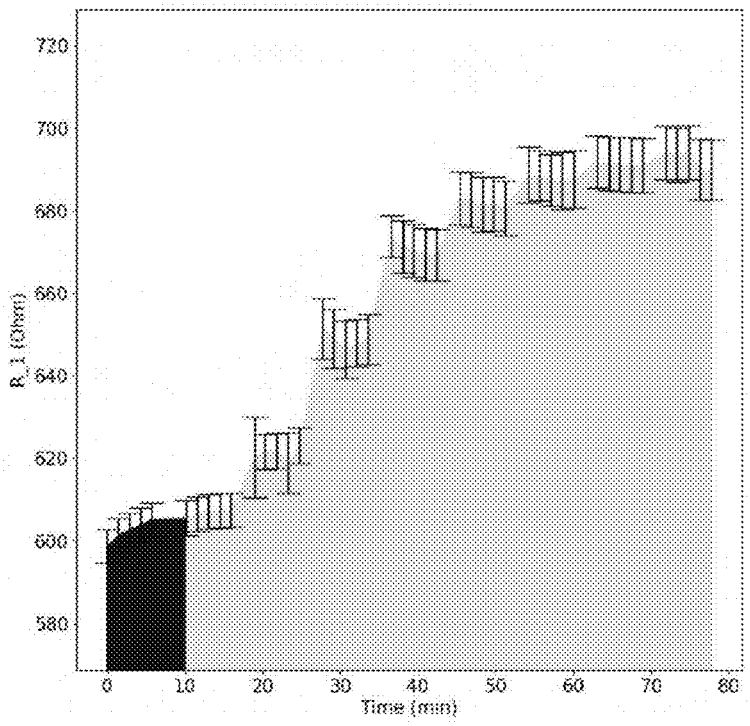
720
700
680
660
640
620
600
580
R_1 (Ohm)
0
10
20
30
40
50
60
70
80
Time (min)

FIG. 16G

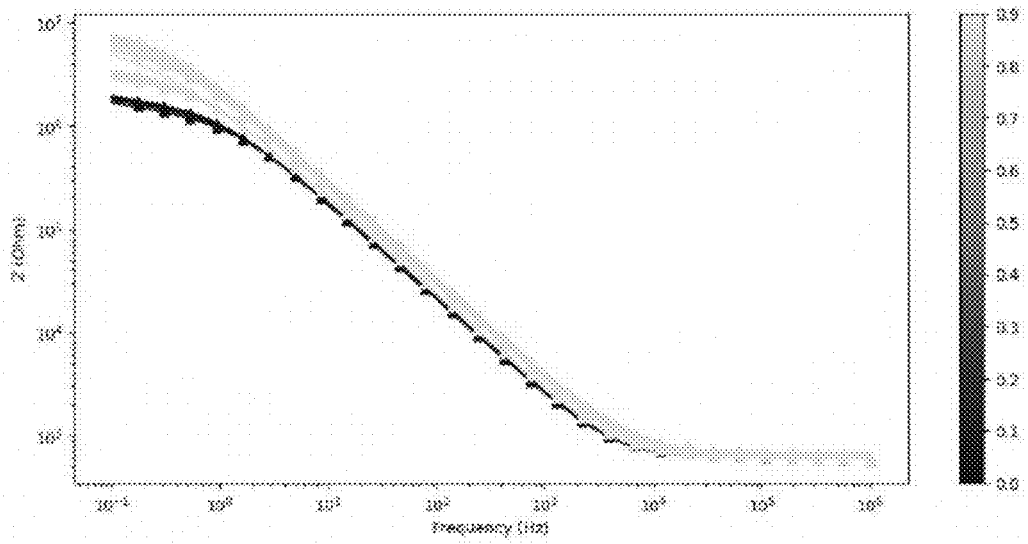

FIG. 17A

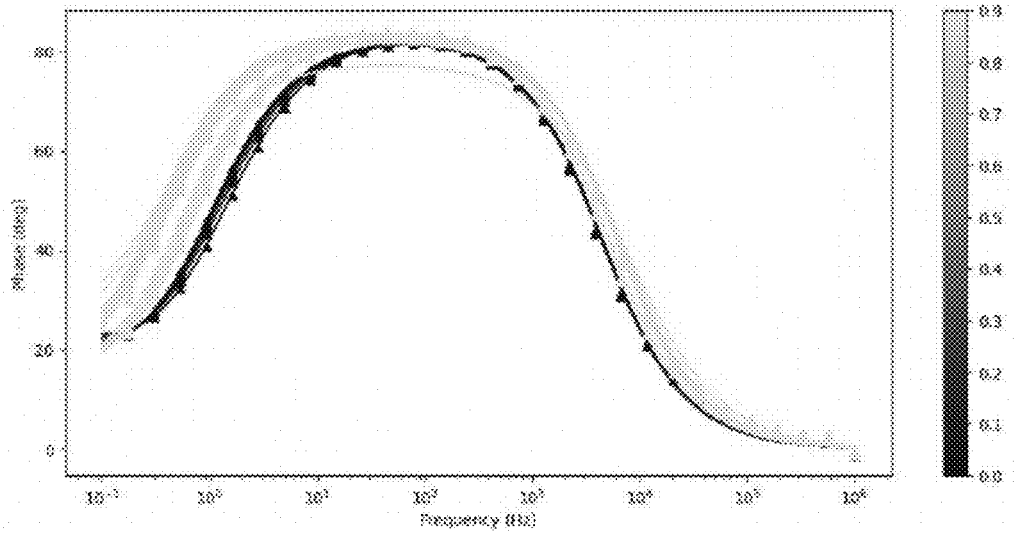

FIG. 17B

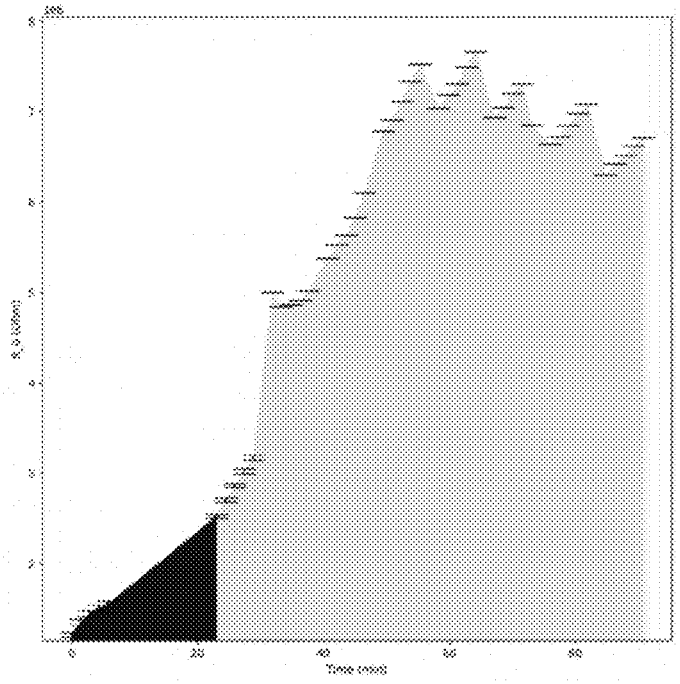

FIG. 17C

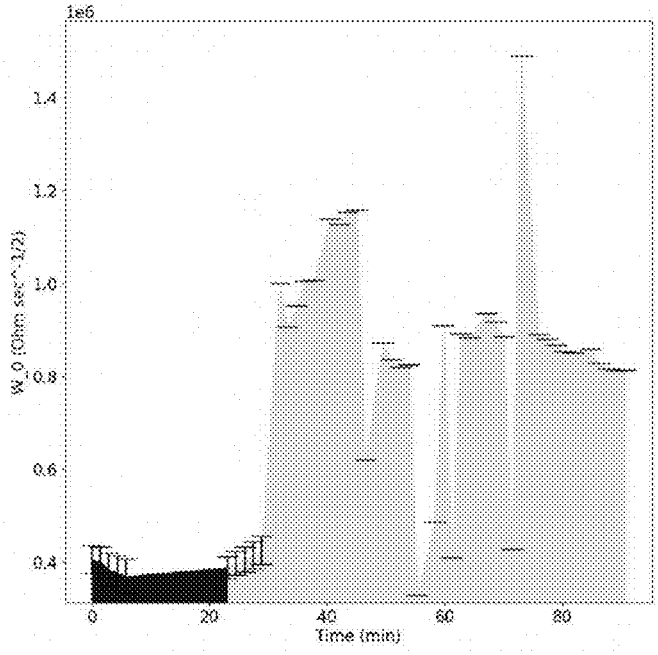

FIG. 17D

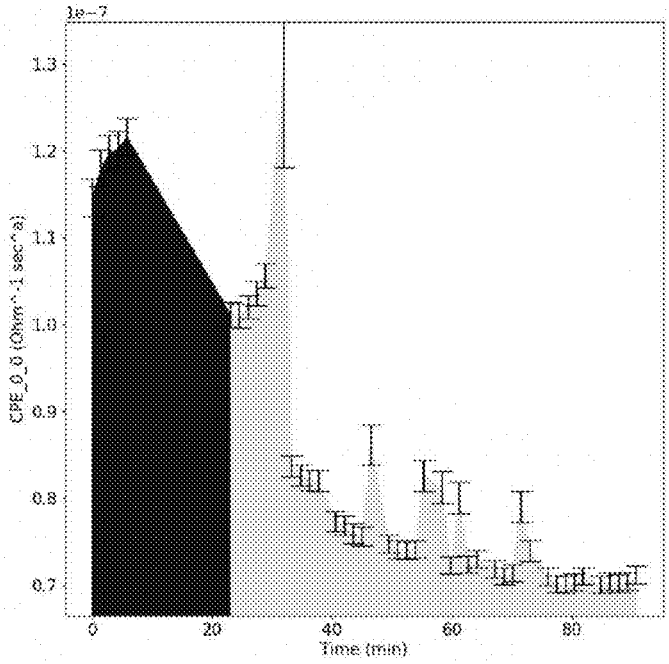

FIG. 17E

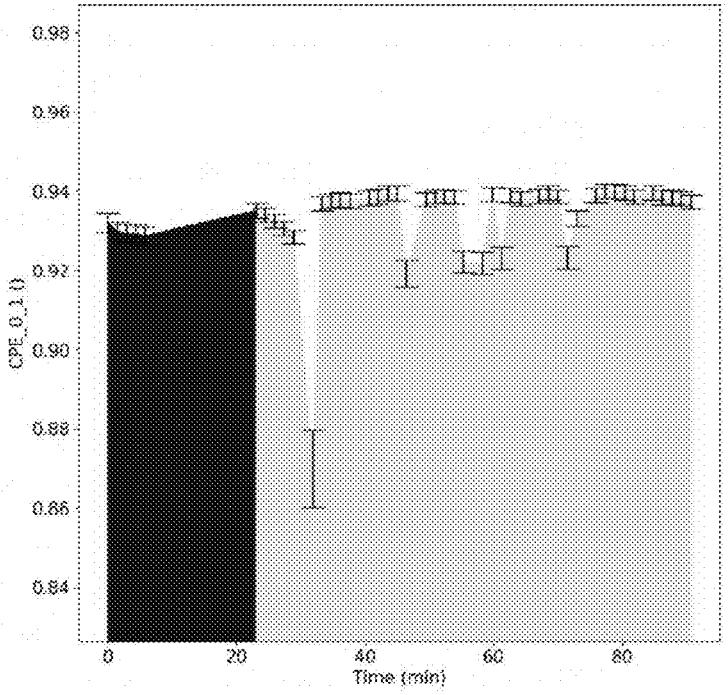

FIG. 17F

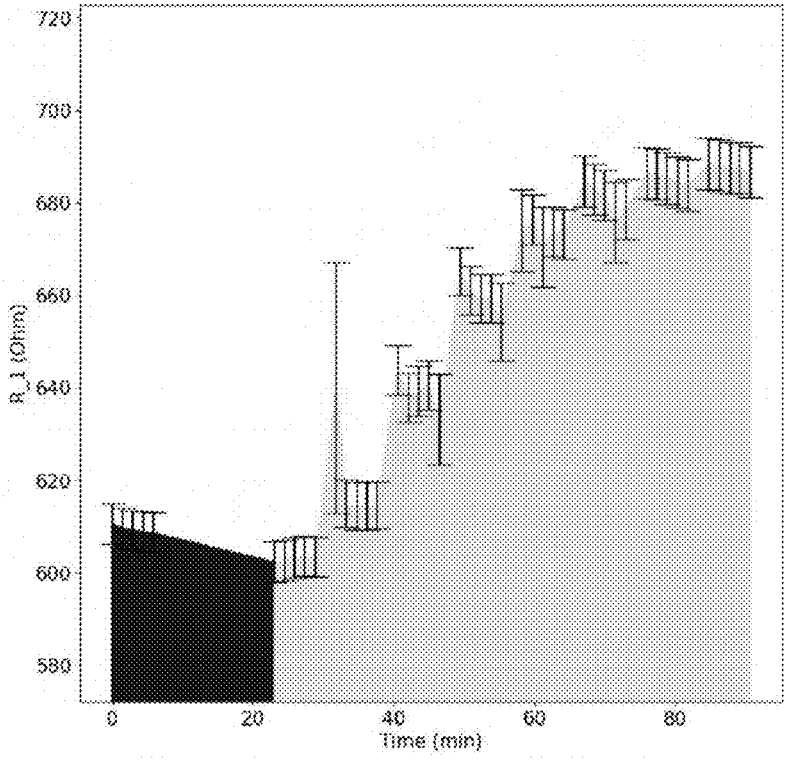

FIG. 17G

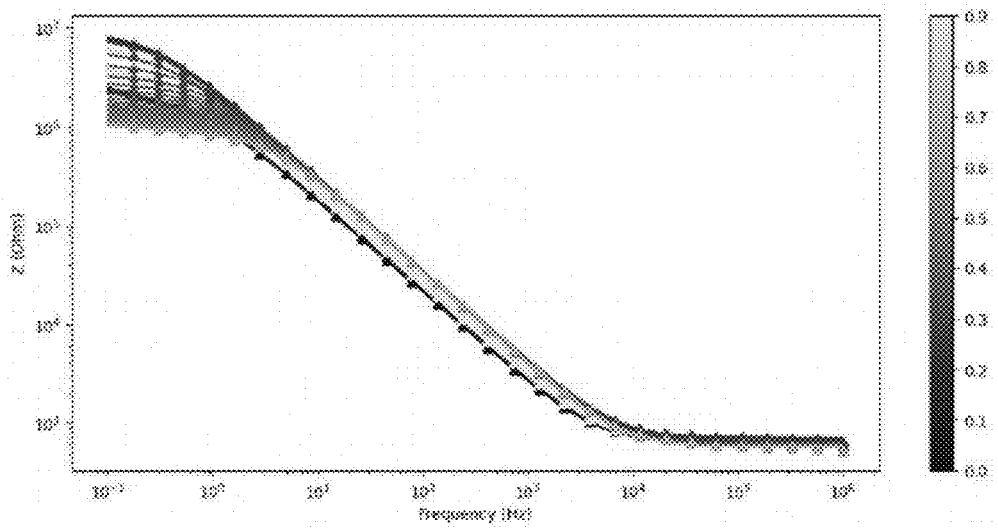

FIG. 18A

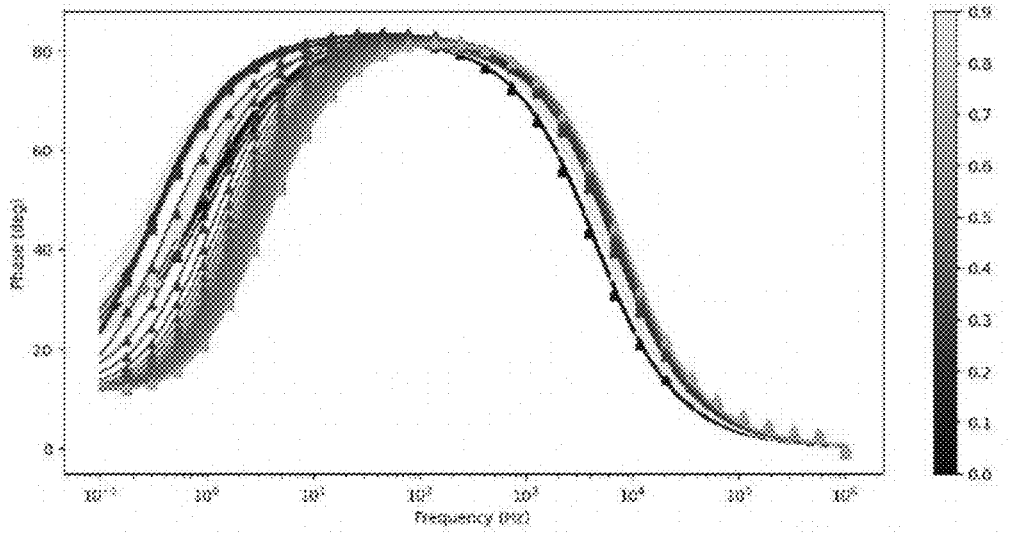

FIG. 18B

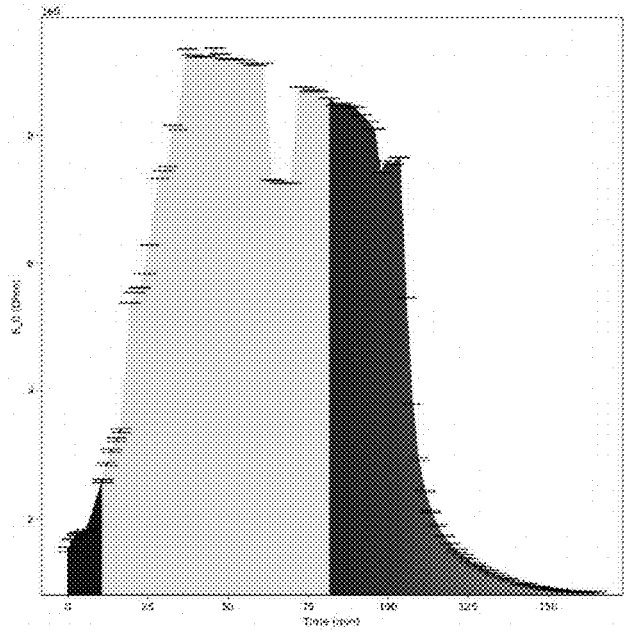

FIG. 18C

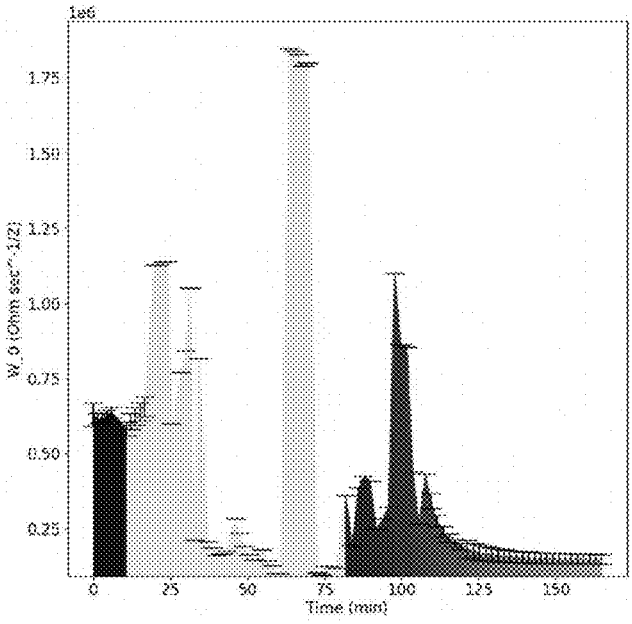

FIG. 18D

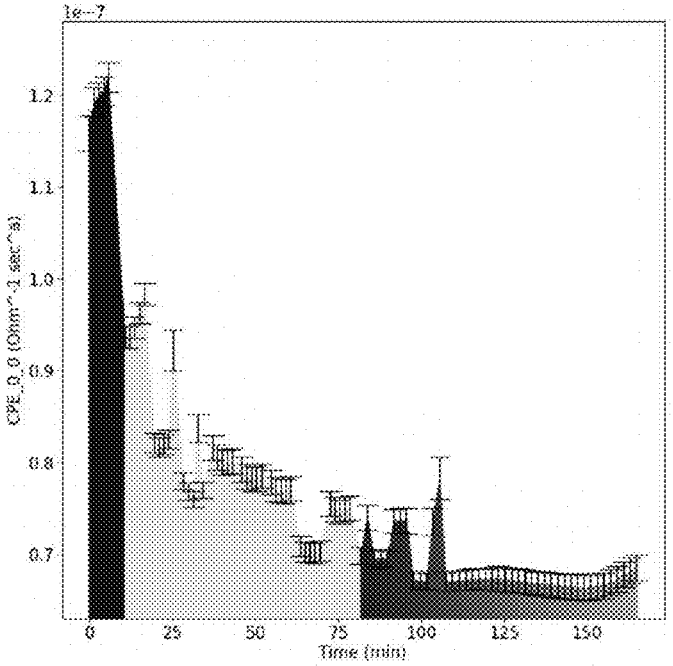

FIG. 18E

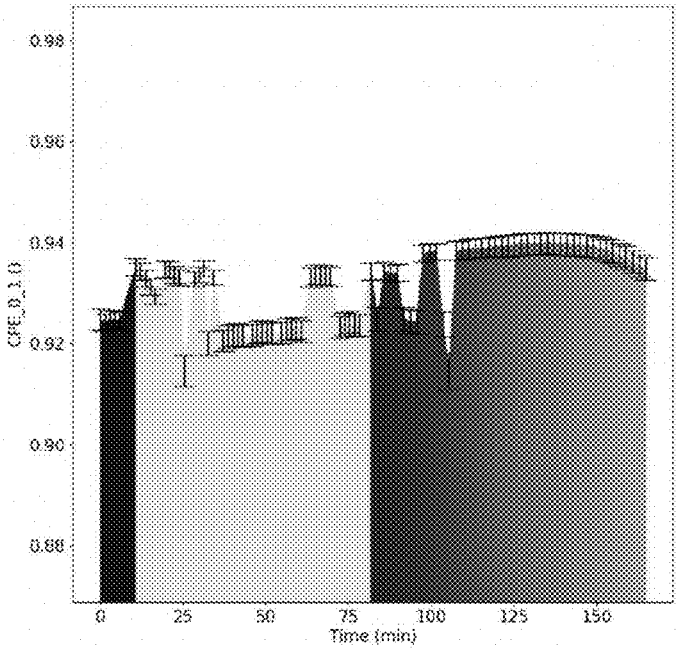

FIG. 18F

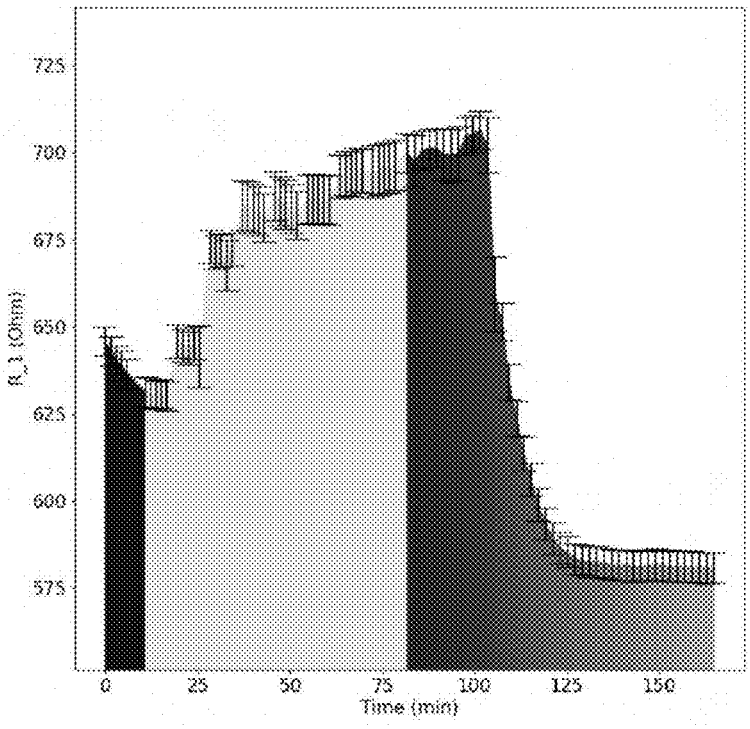

FIG. 18G

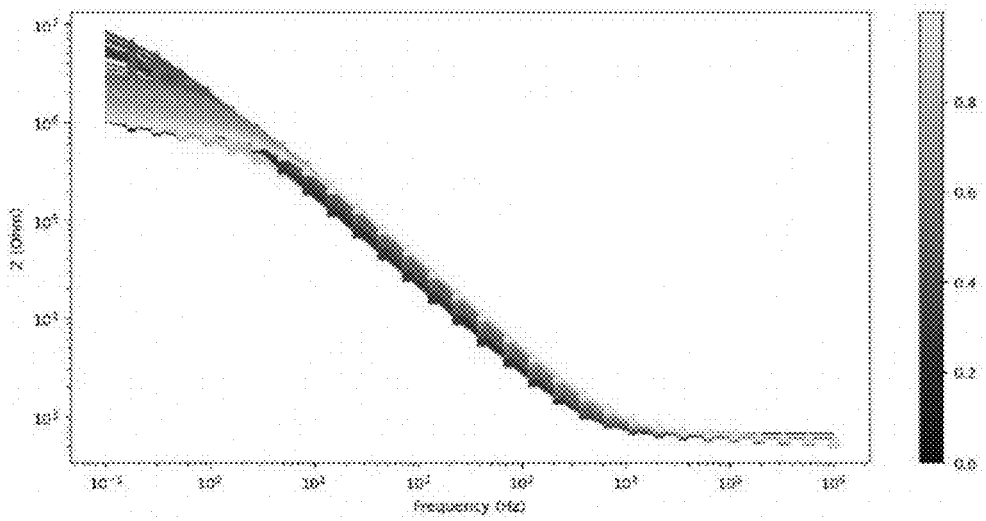

FIG. 19A

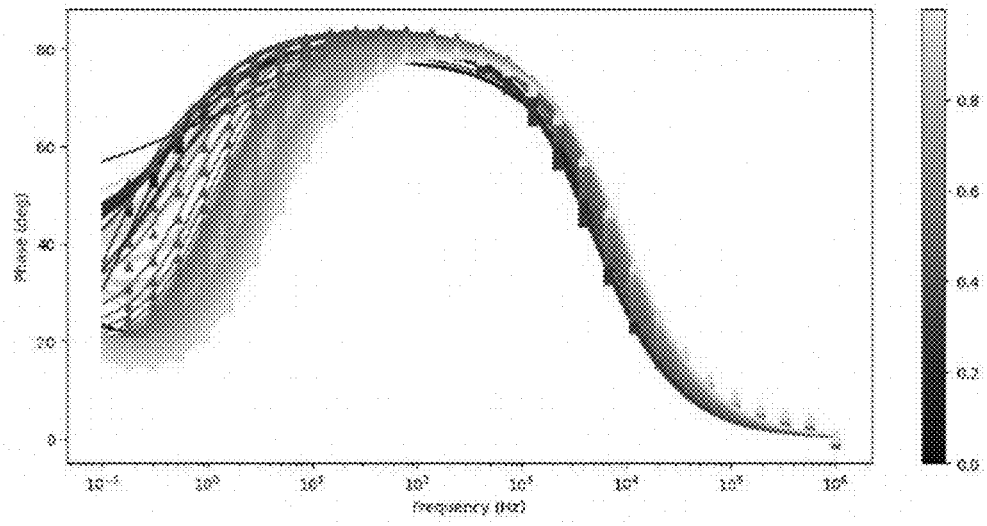

FIG. 19B

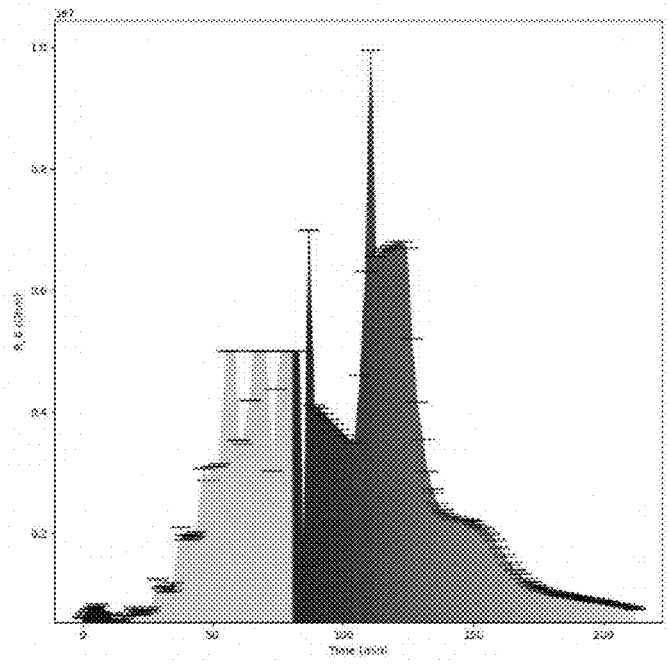

FIG. 19C

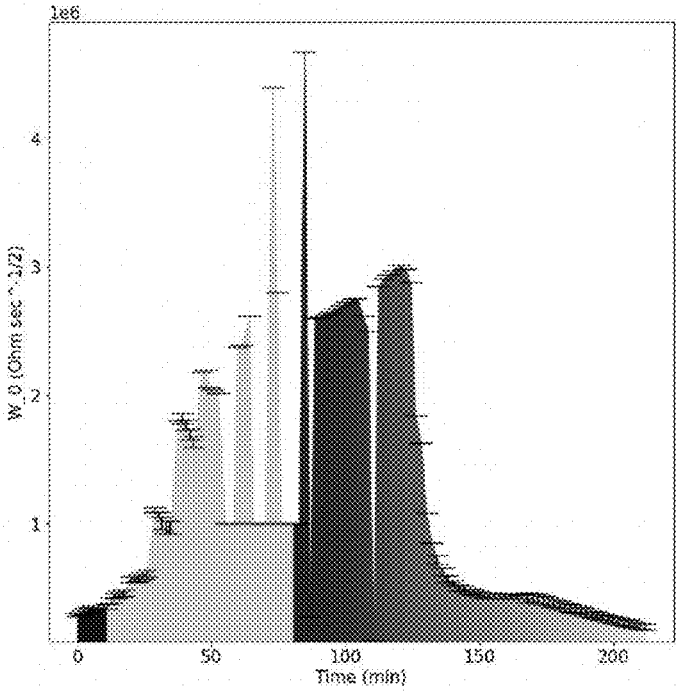

FIG. 19D

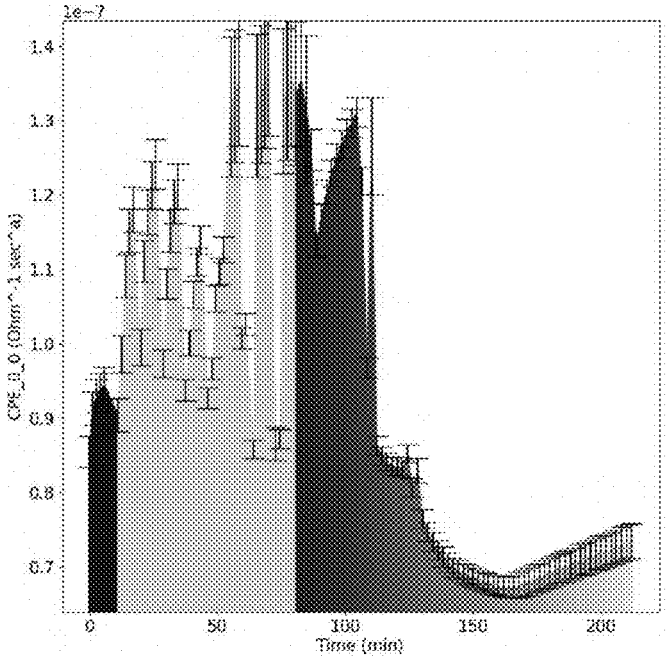

FIG. 19E

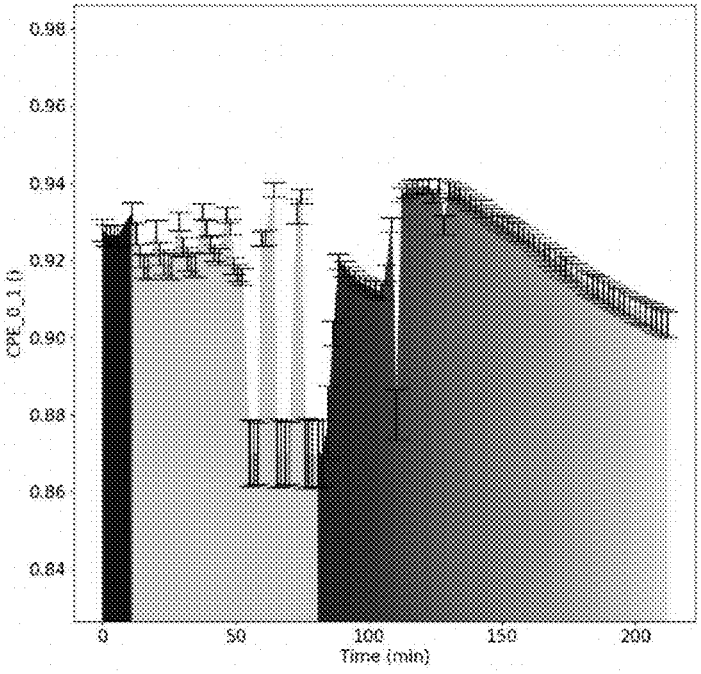

FIG. 19F

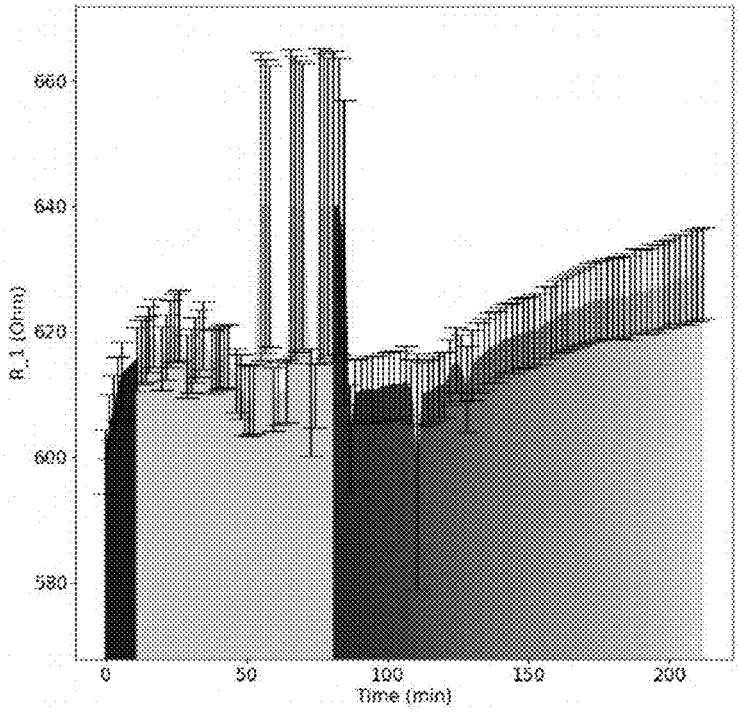

FIG. 19G

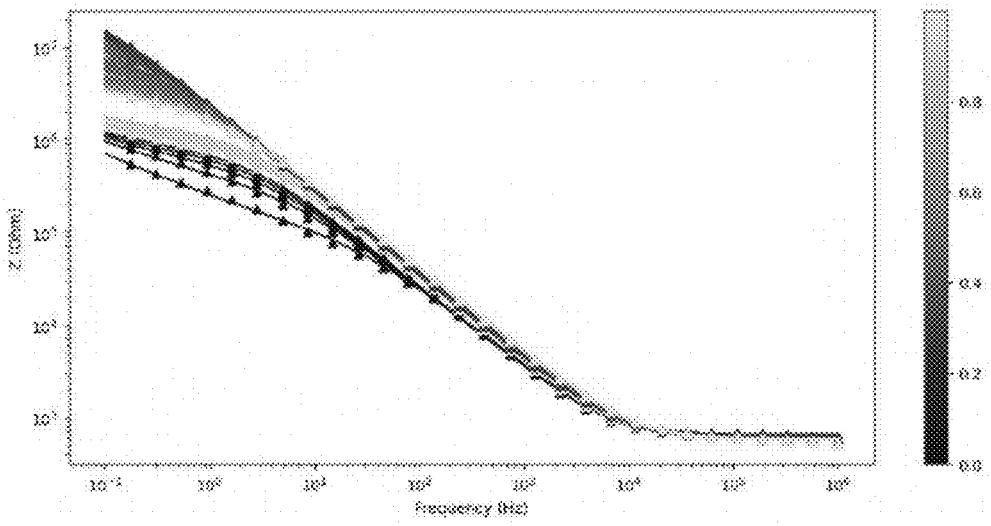

FIG. 20A

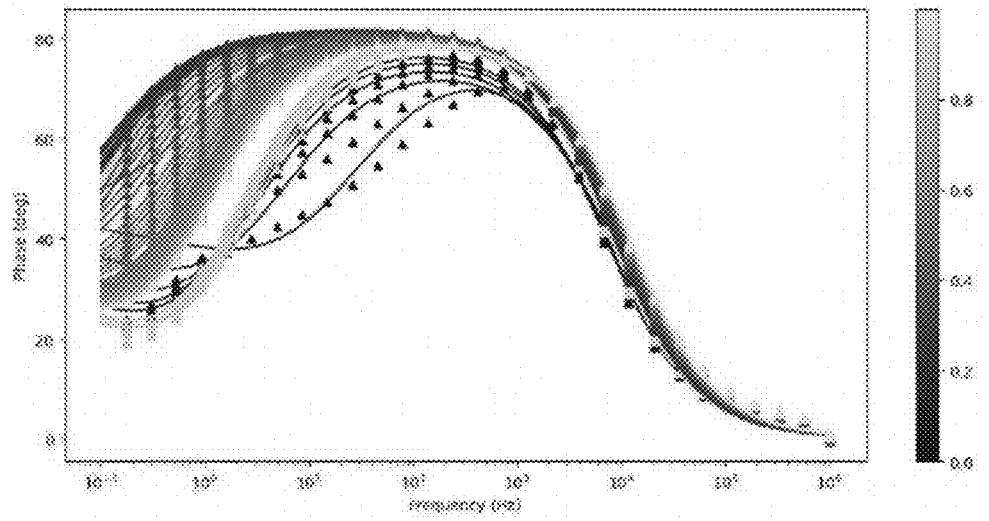

FIG. 20B

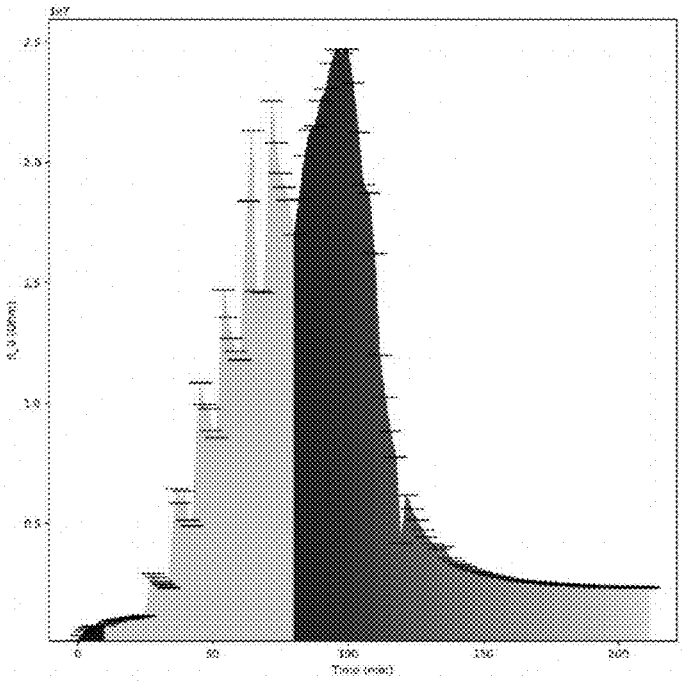

FIG. 20C

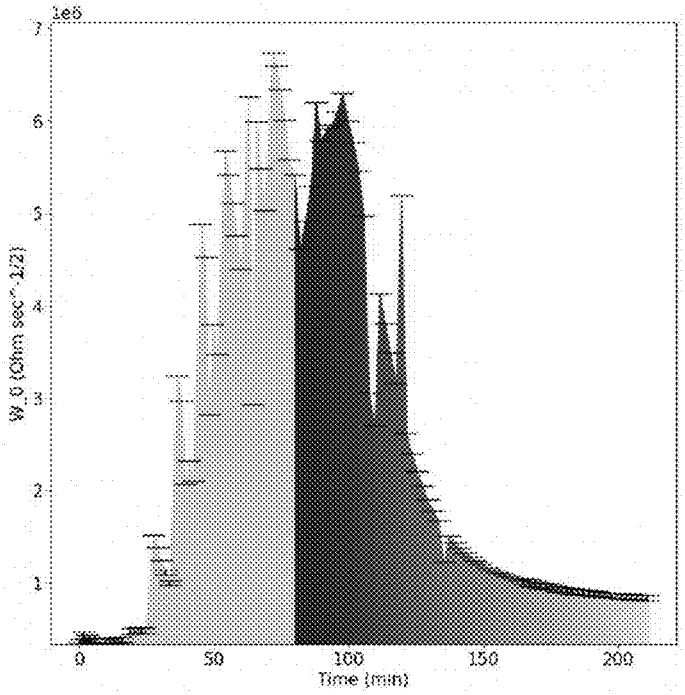

FIG. 20D

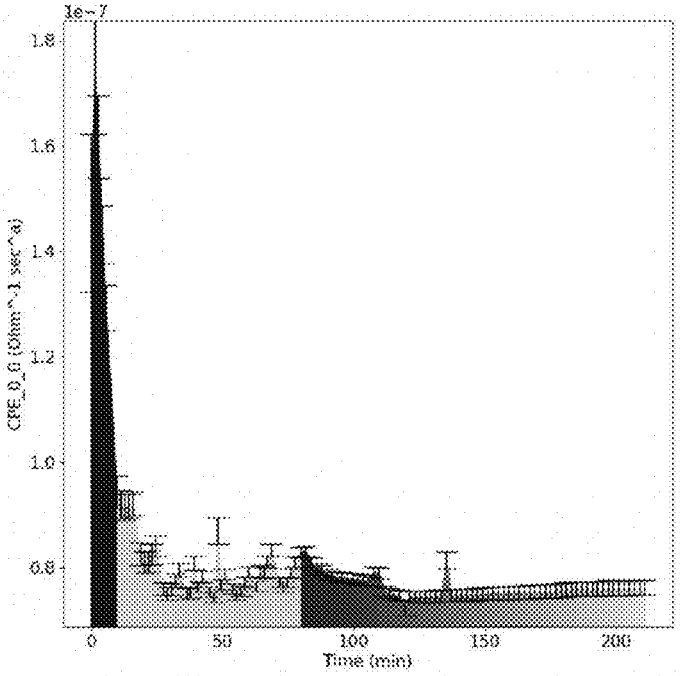

FIG. 20E

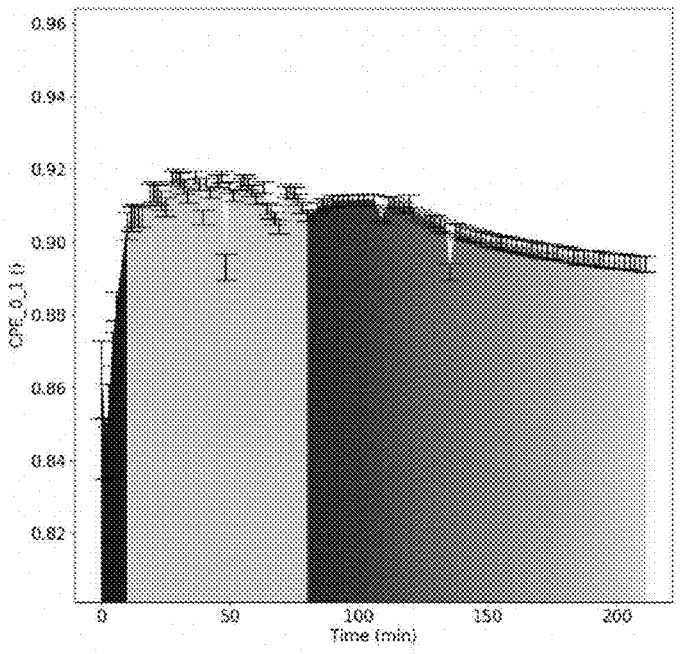

FIG. 20F

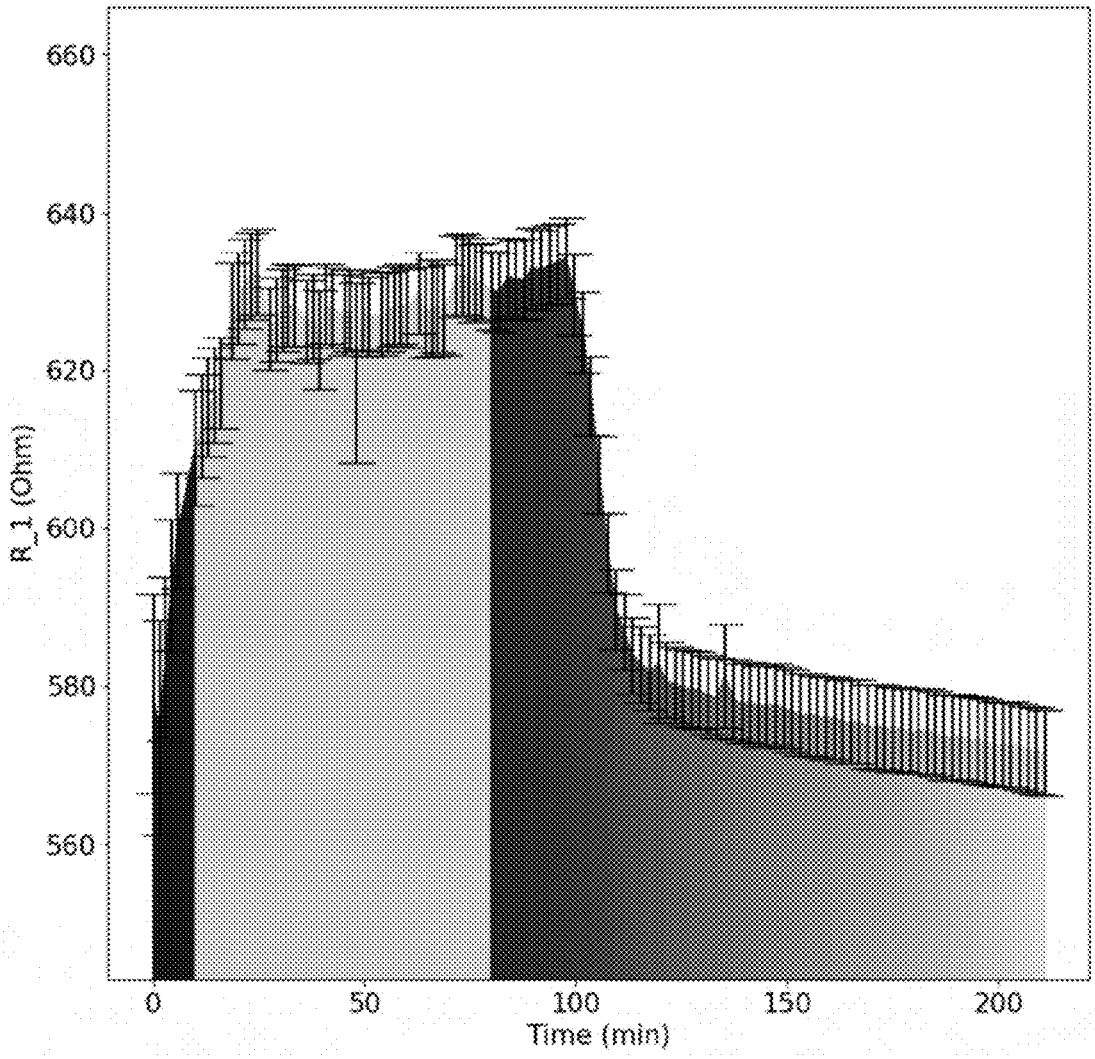

FIG. 20G

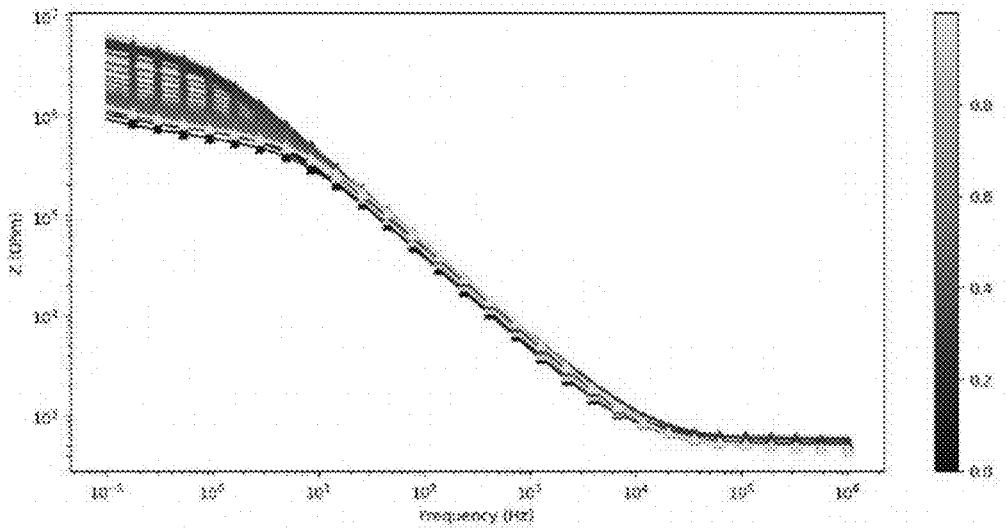

FIG. 21A

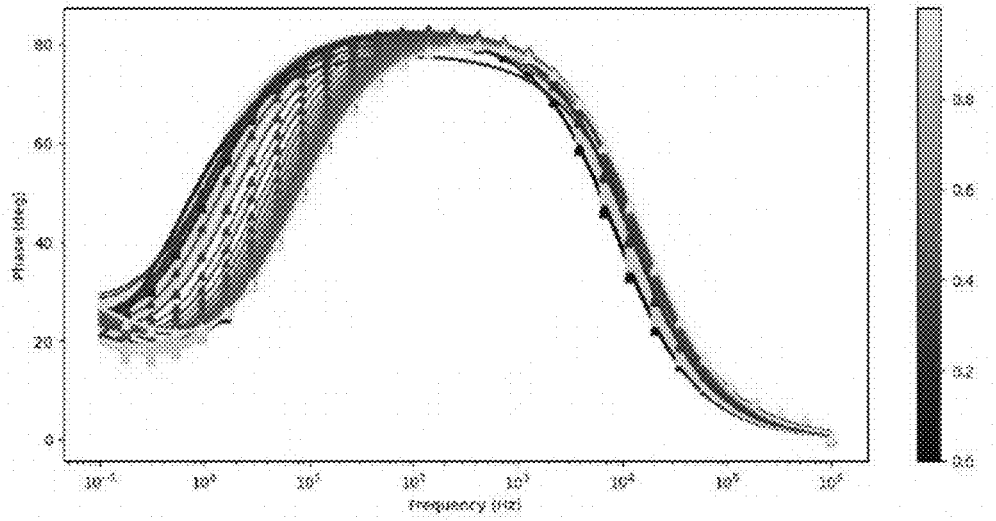

FIG. 21B

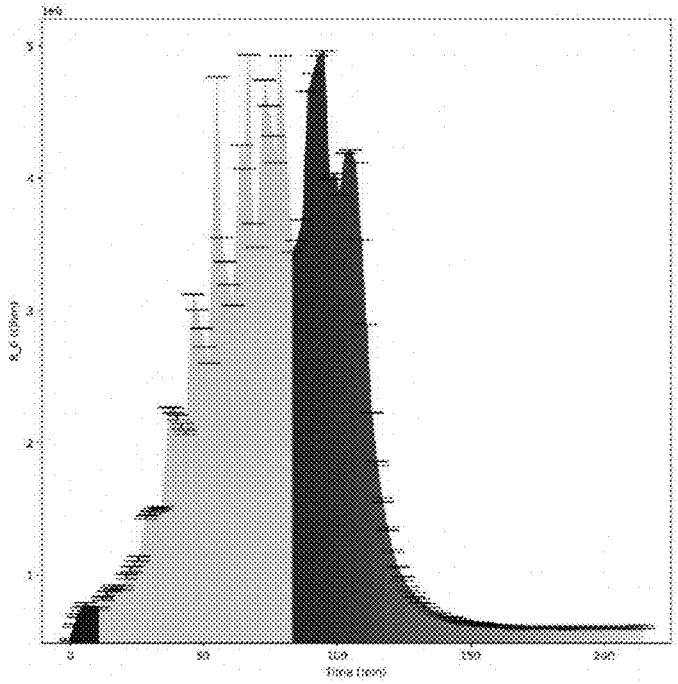

FIG. 21C

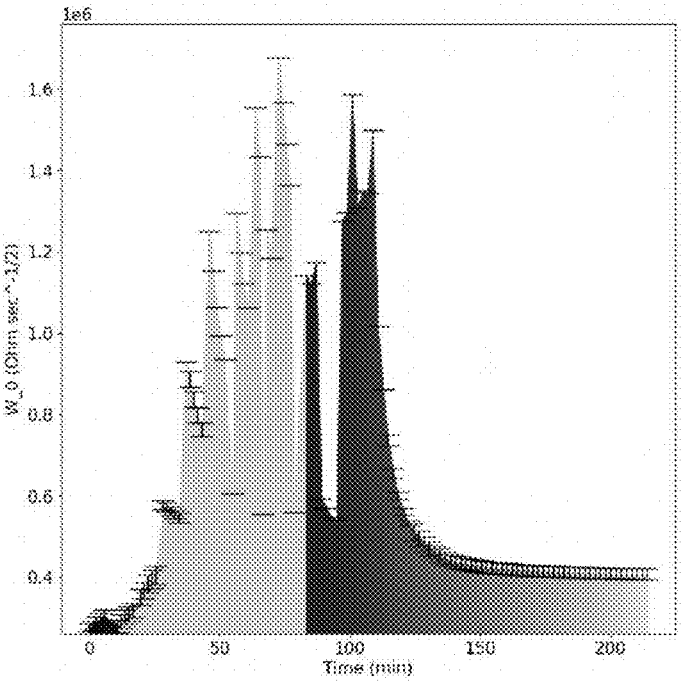

FIG. 21D

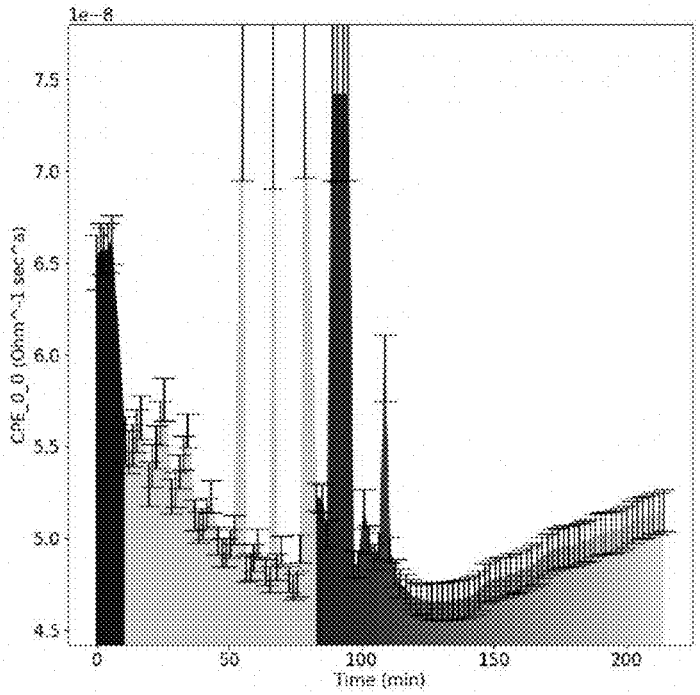

FIG. 21E

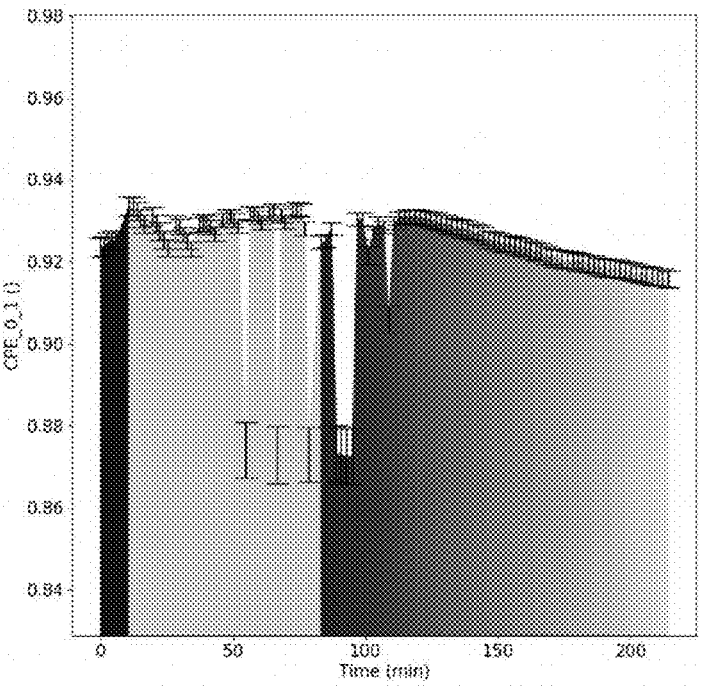

FIG. 21F

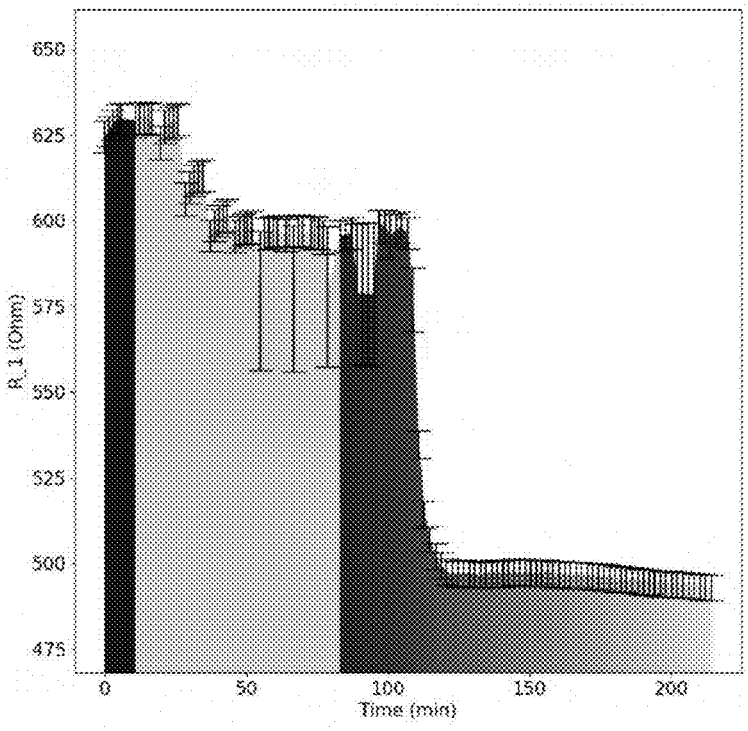

FIG. 21G

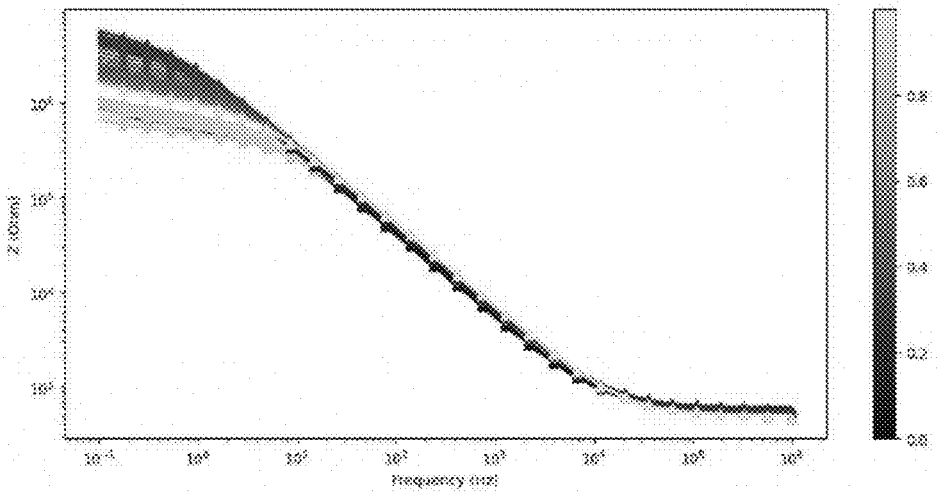

FIG. 22A

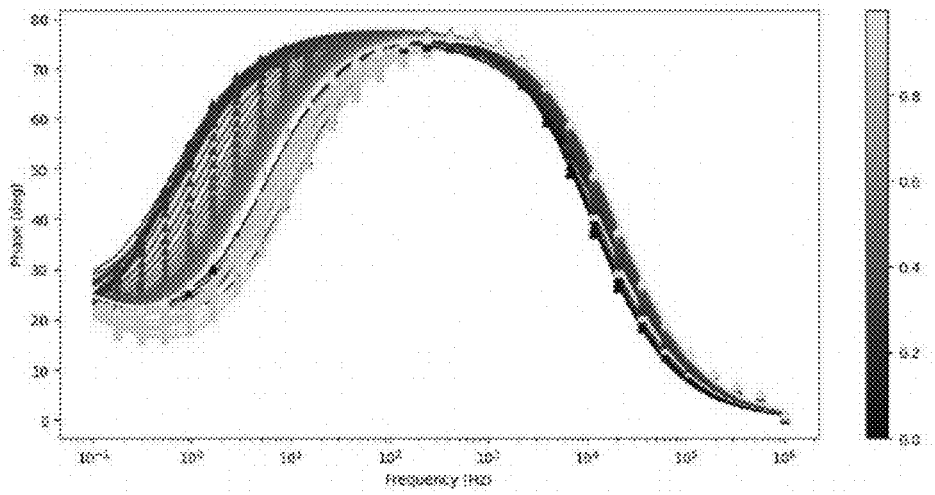

FIG. 22B

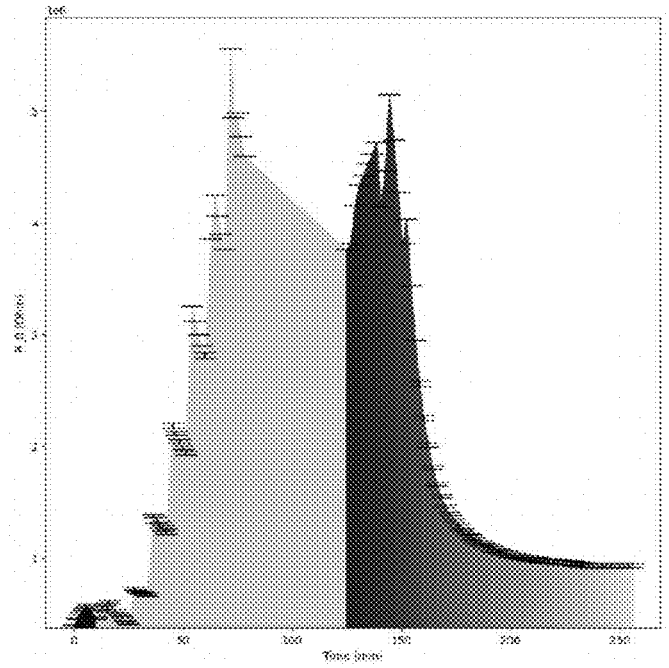

FIG. 22C

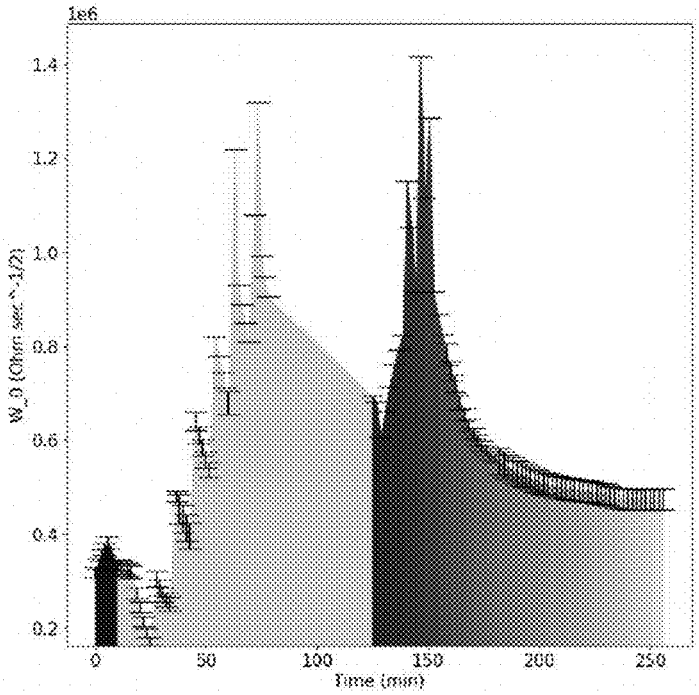

FIG. 22D

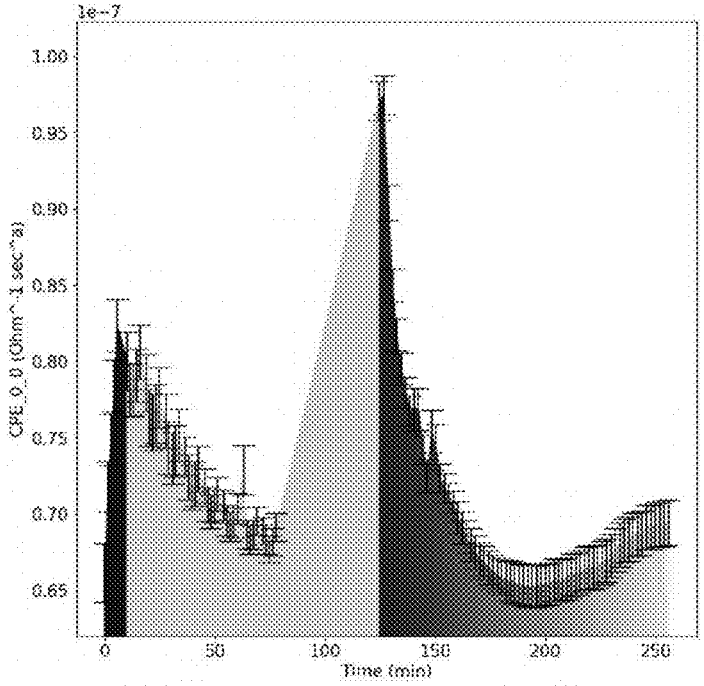

FIG. 22E

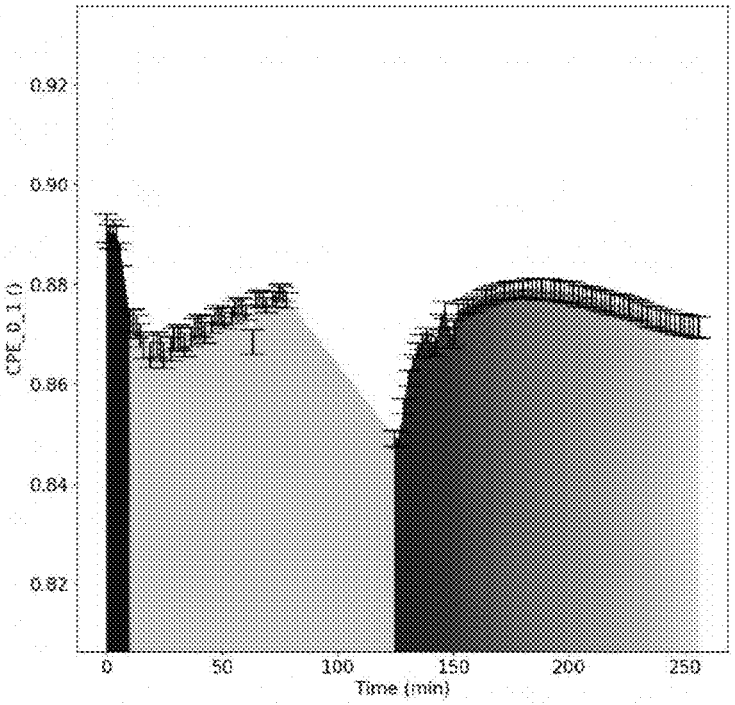

FIG. 22F

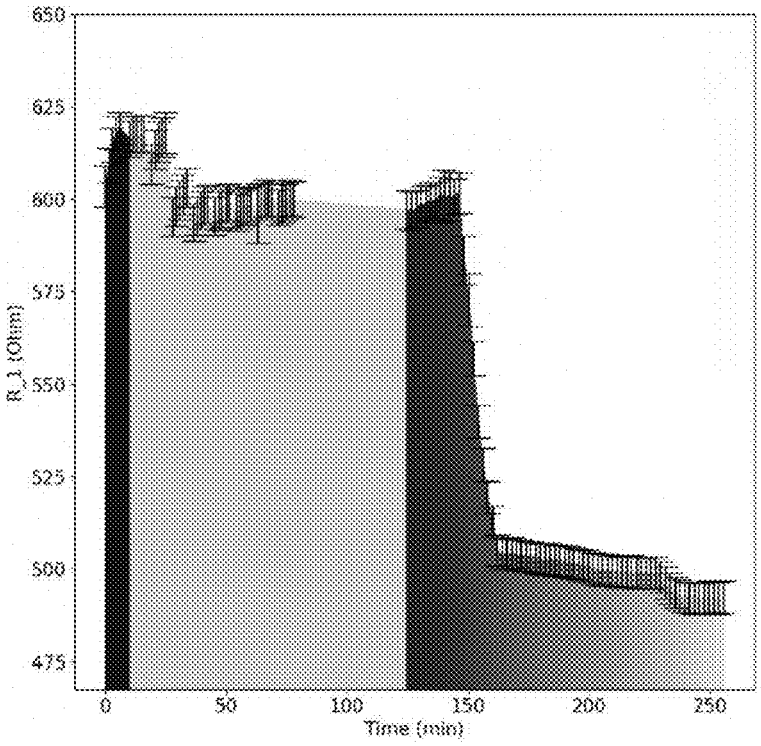
650
625
600
575
550
525
500
475
R_1 (Ohm)
0
50
100
150
200
250
Time (min)

FIG. 22G

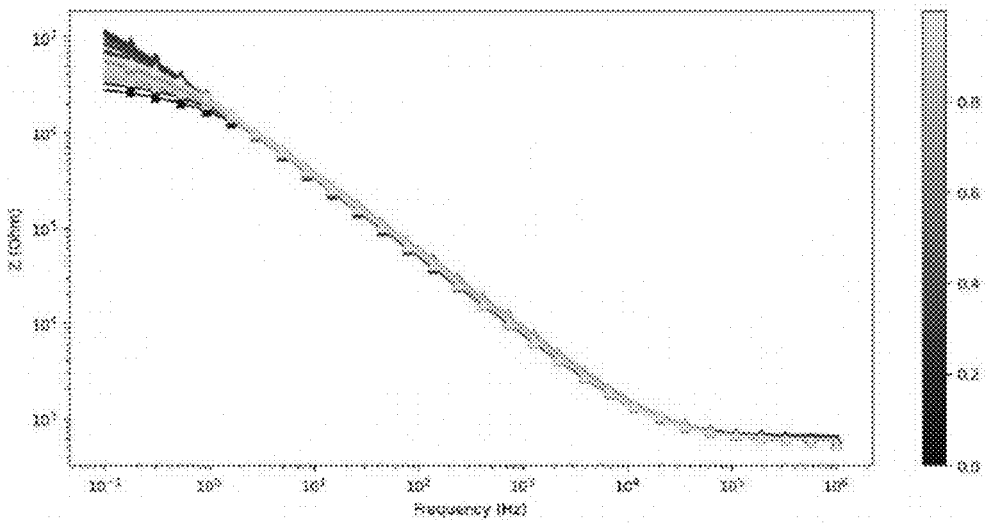

FIG. 23A

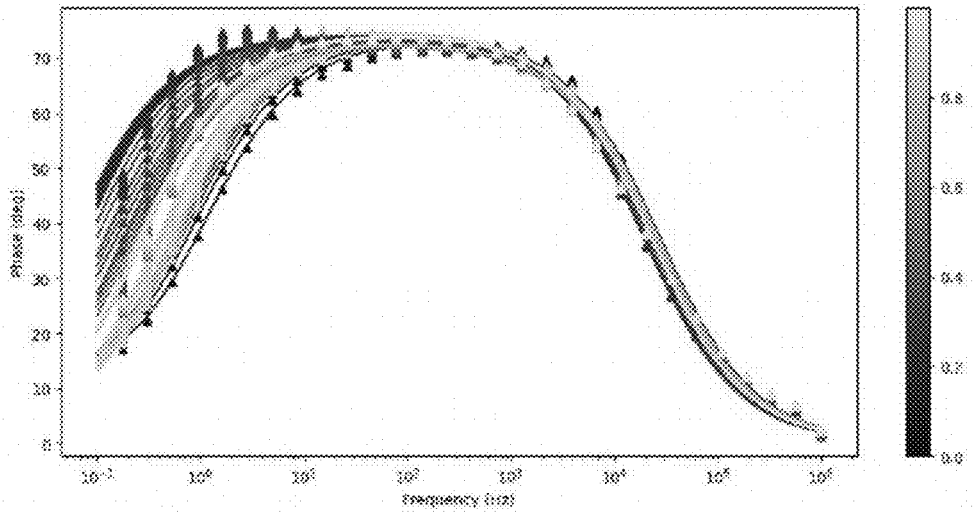

FIG. 23B

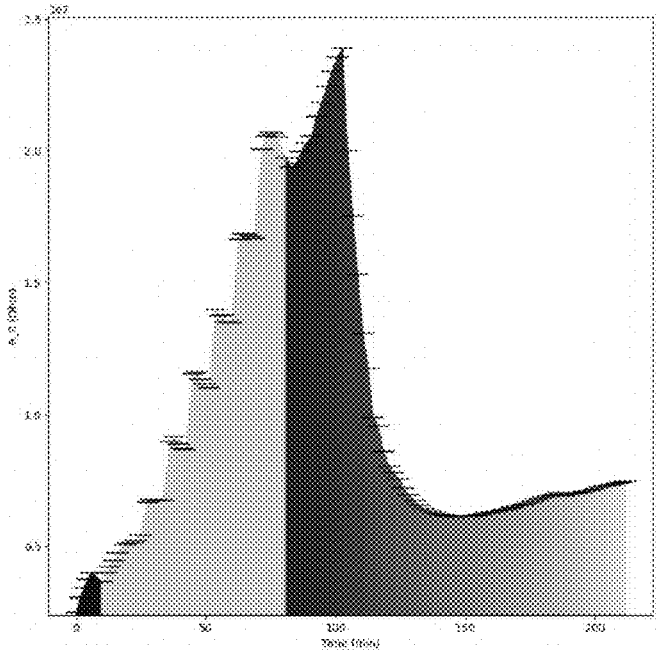

FIG. 23C

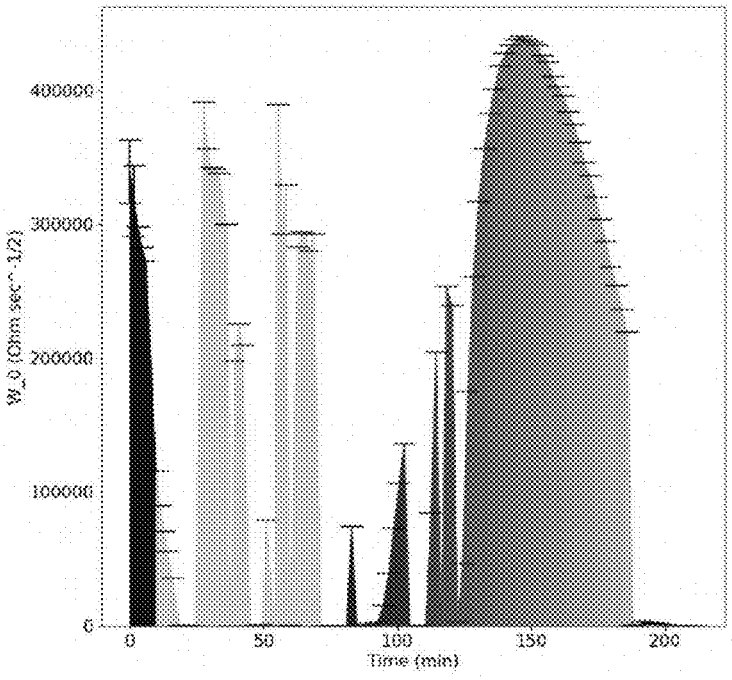

FIG. 23D

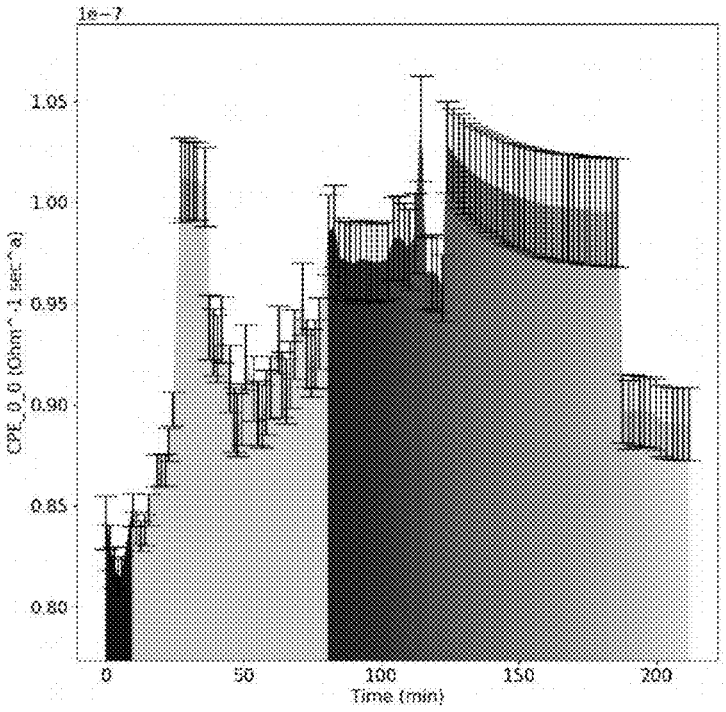

FIG. 23E

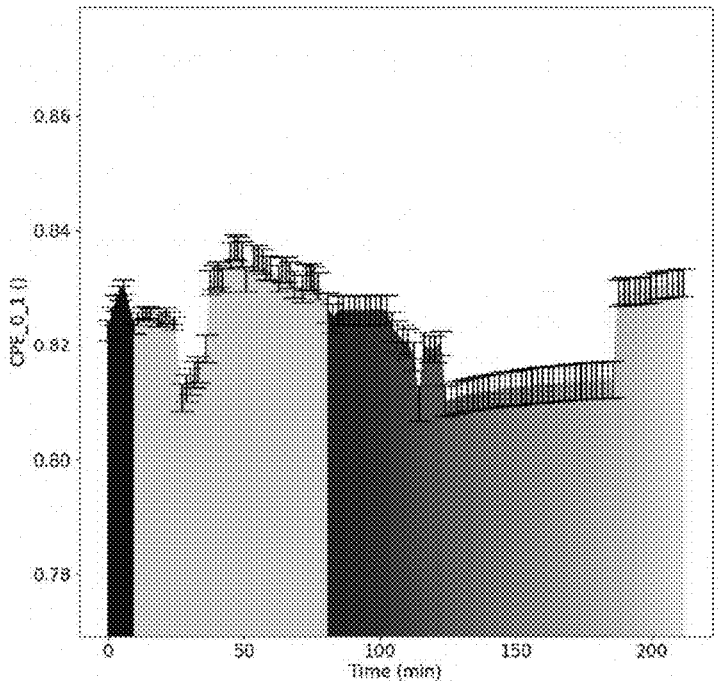

FIG. 23F

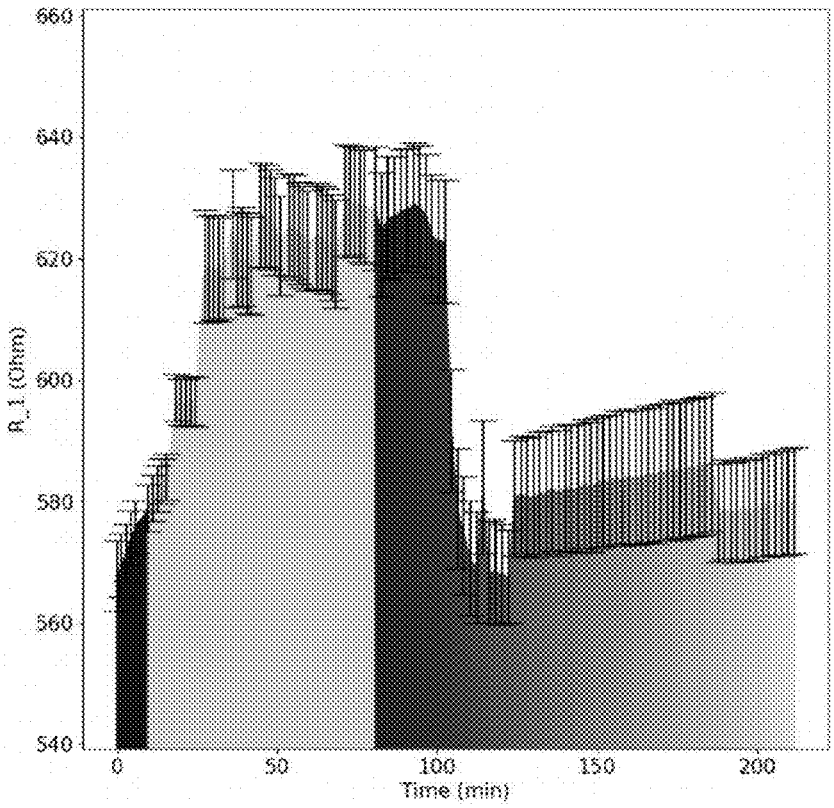

FIG. 23G

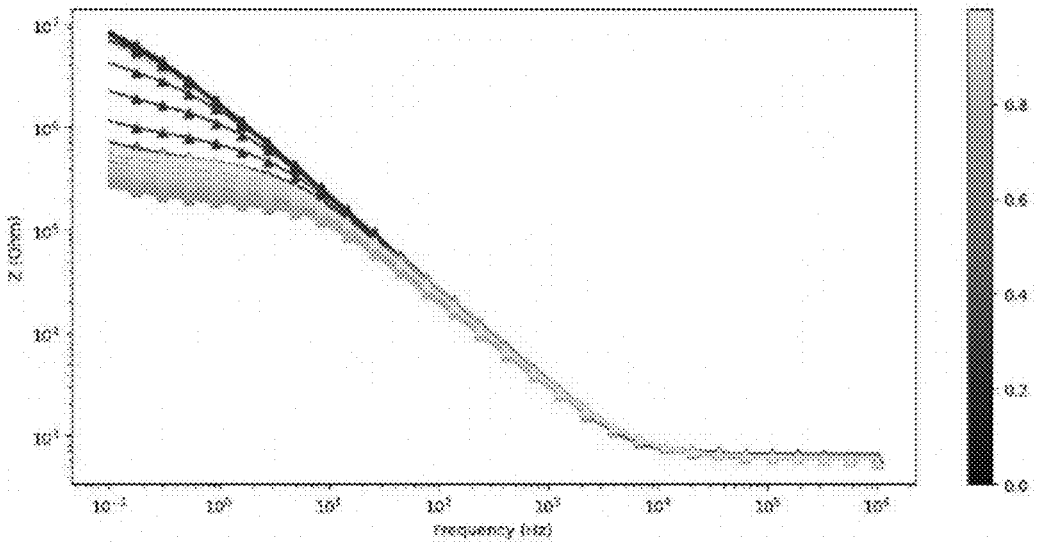

FIG. 24A

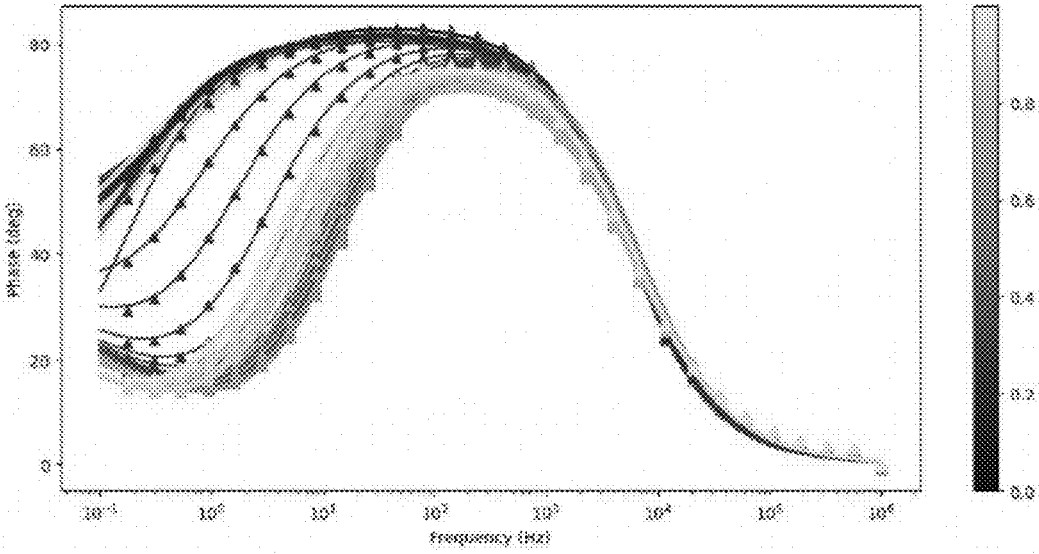

FIG. 24B

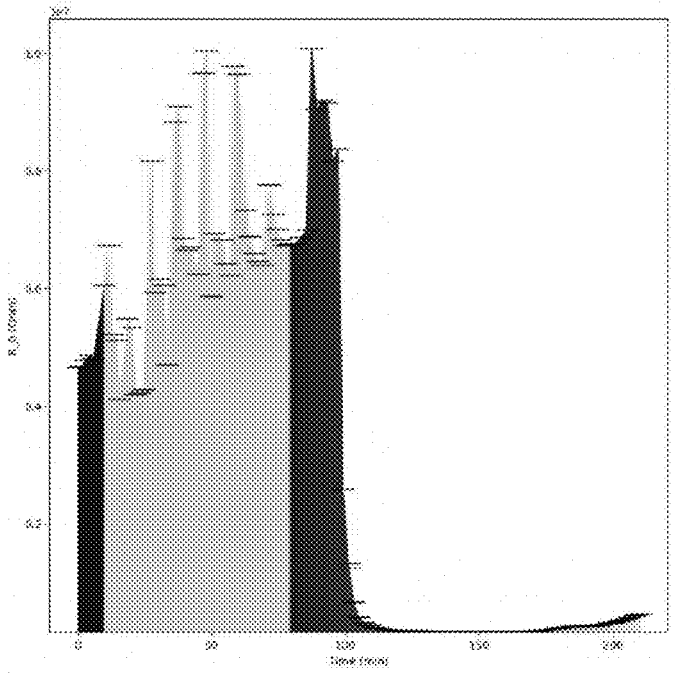

FIG. 24C

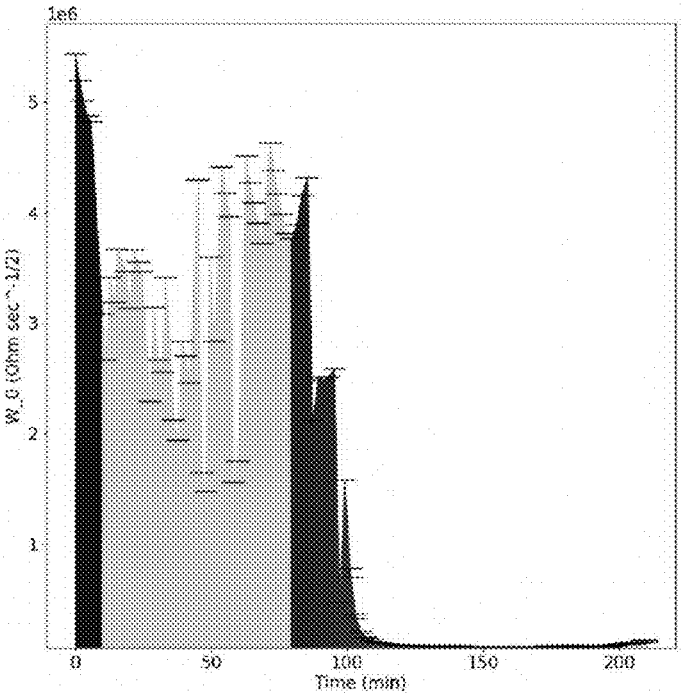

FIG. 24D

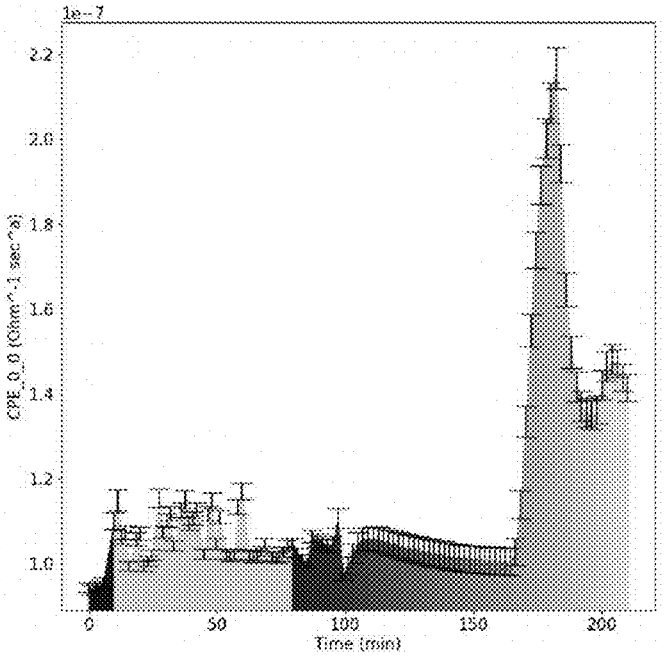

FIG. 24E

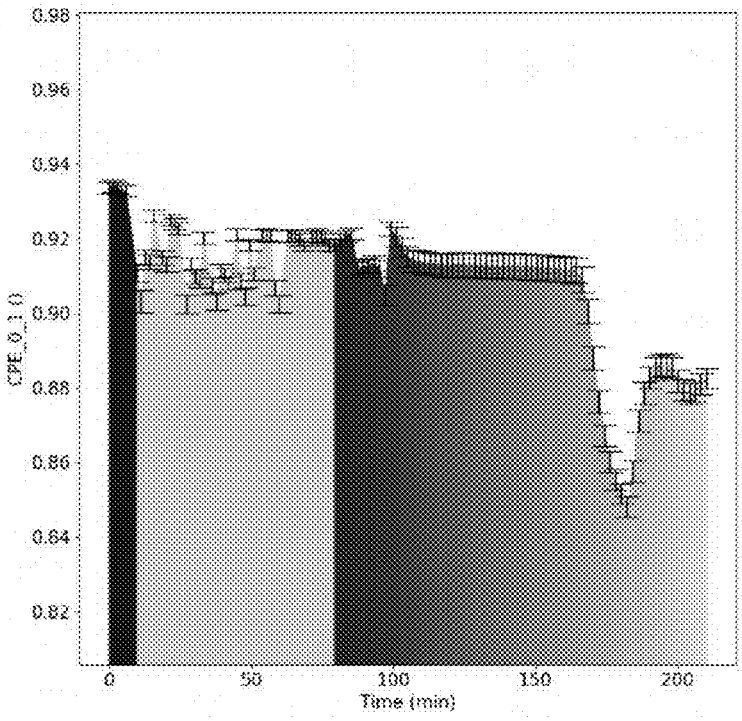

FIG. 24F

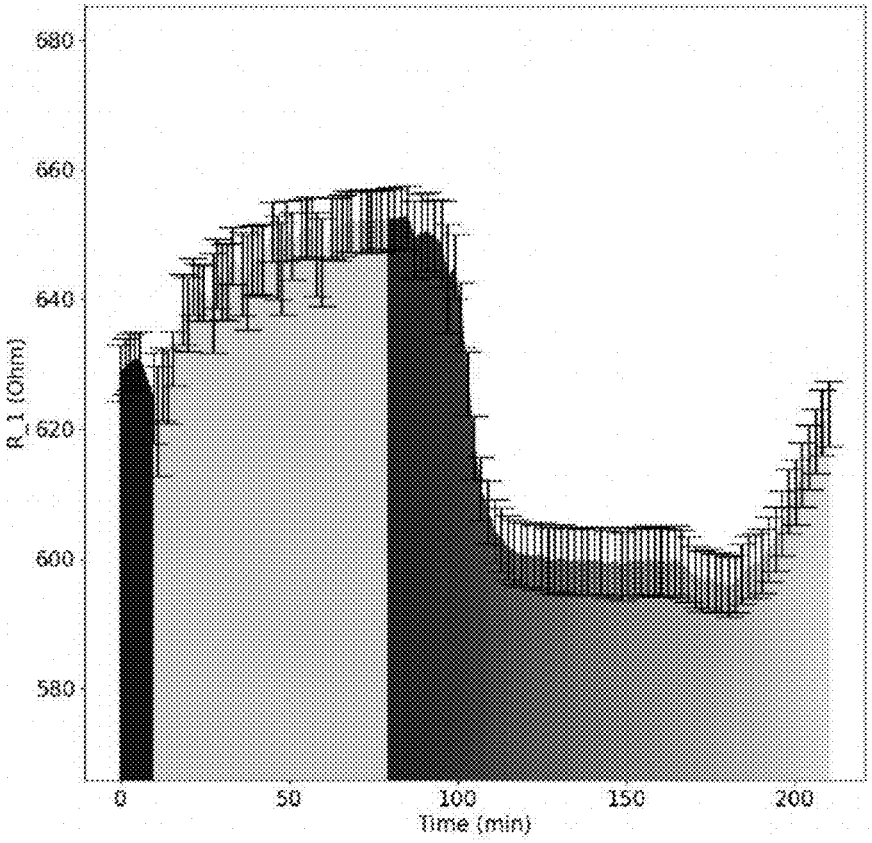

FIG. 24G

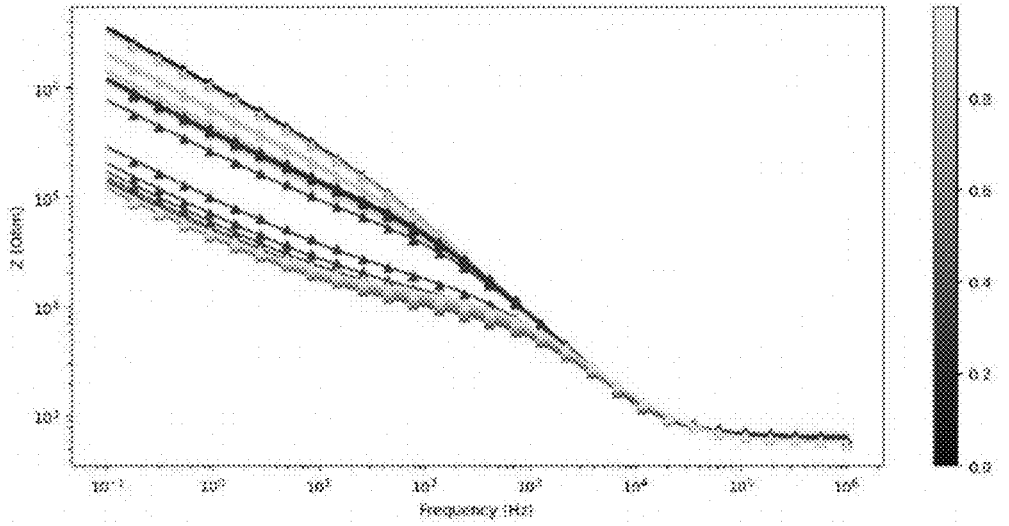

FIG. 25A

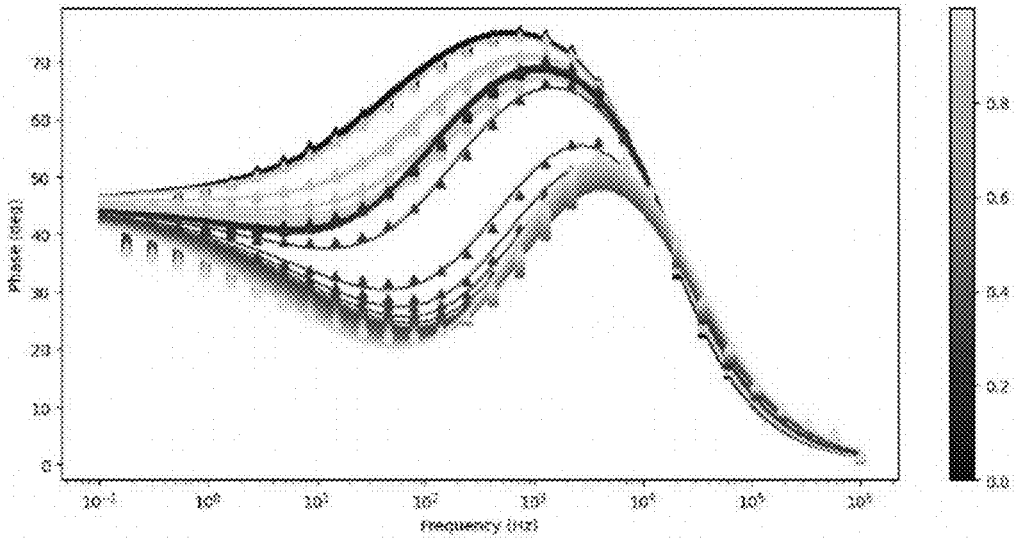

FIG. 25B

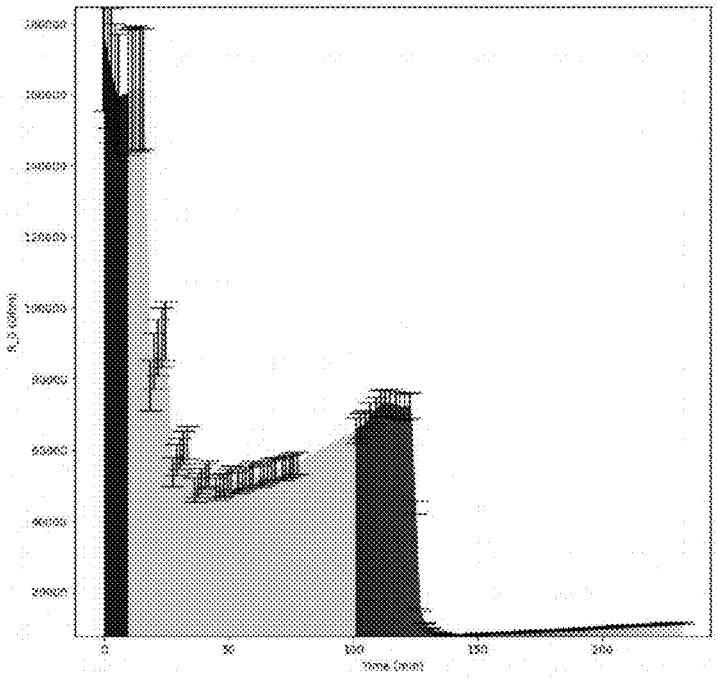

FIG. 25C

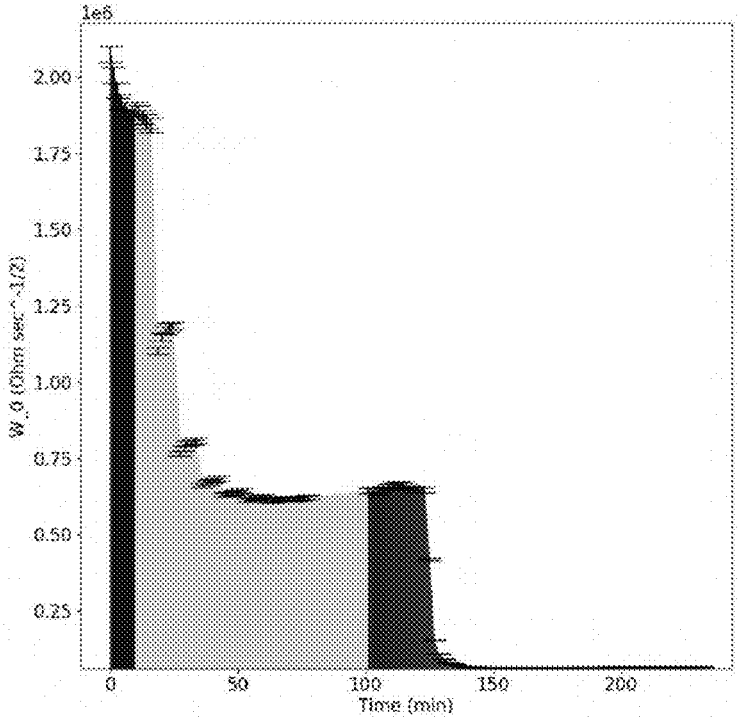

FIG. 25D

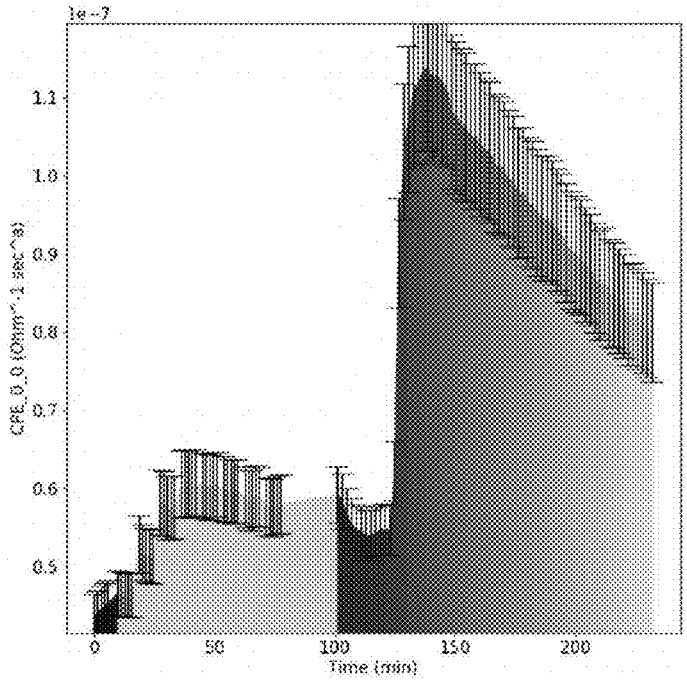

FIG. 25E

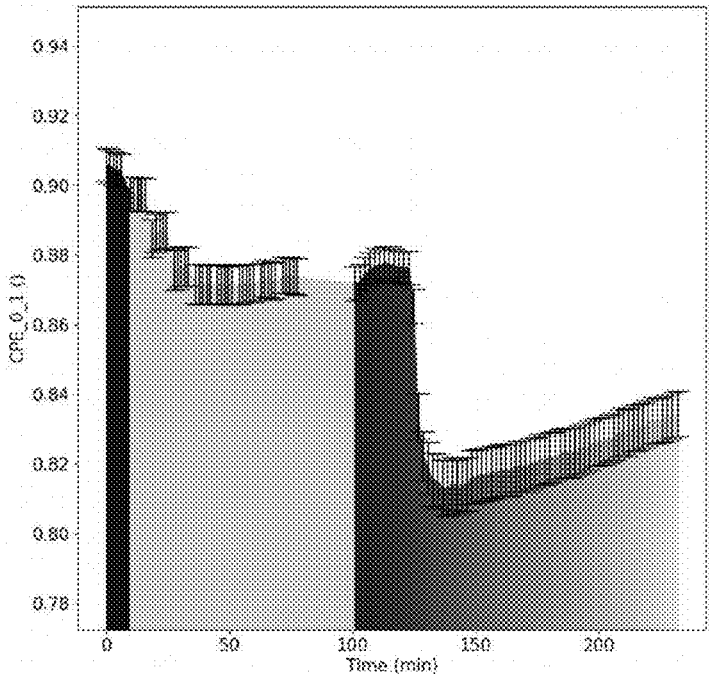

FIG. 25F

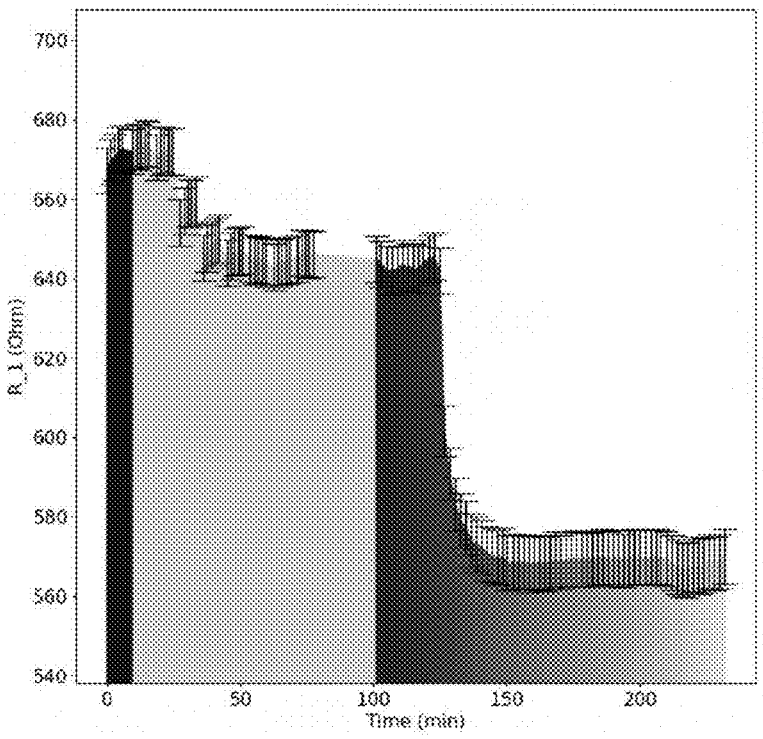
700
680
660
640
620
600
580
560
540
R_1 (Ohm)
0
50
100
150
200
Time (min)

FIG. 25G

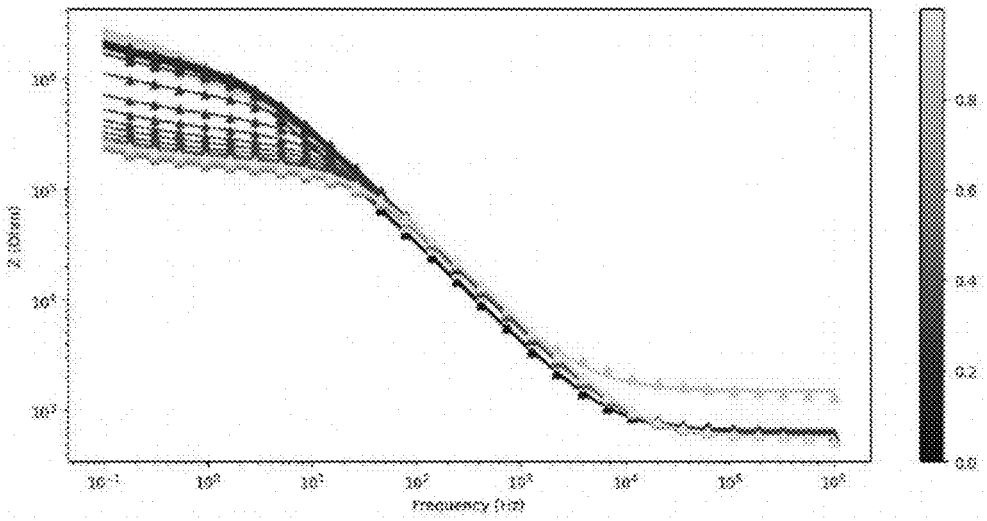

FIG. 26A

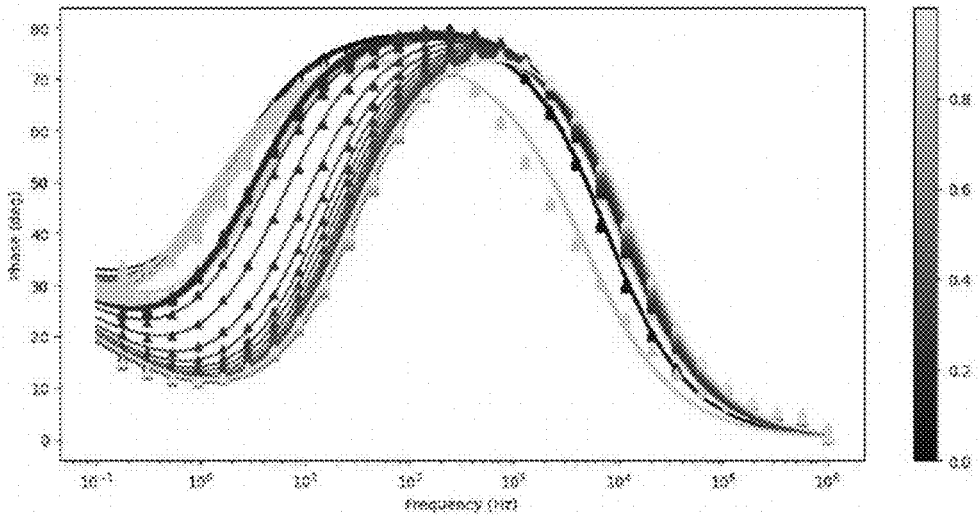

FIG. 26B

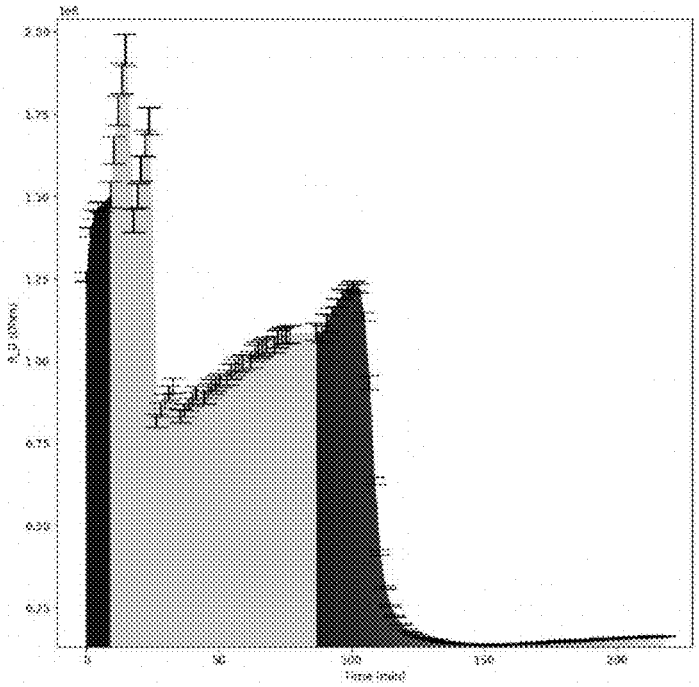

FIG. 26C

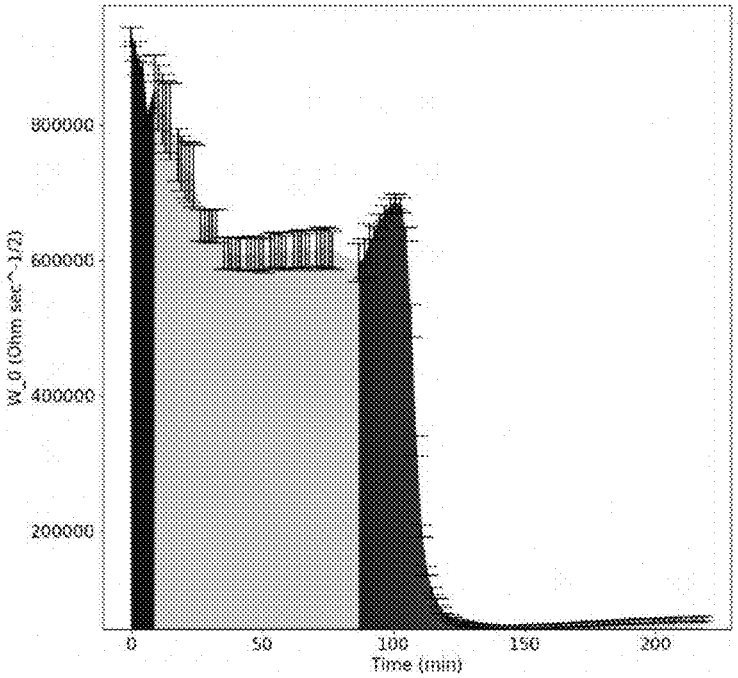

FIG. 26D

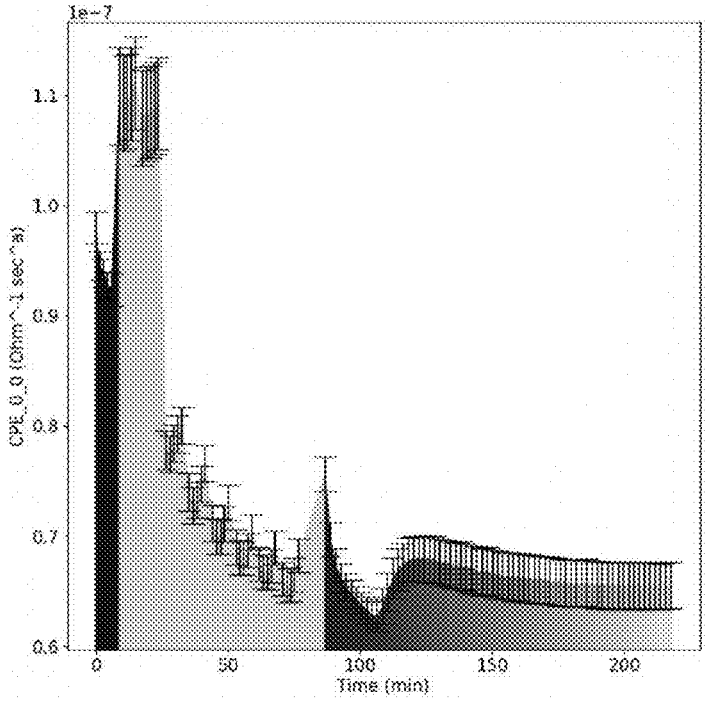

FIG. 26E

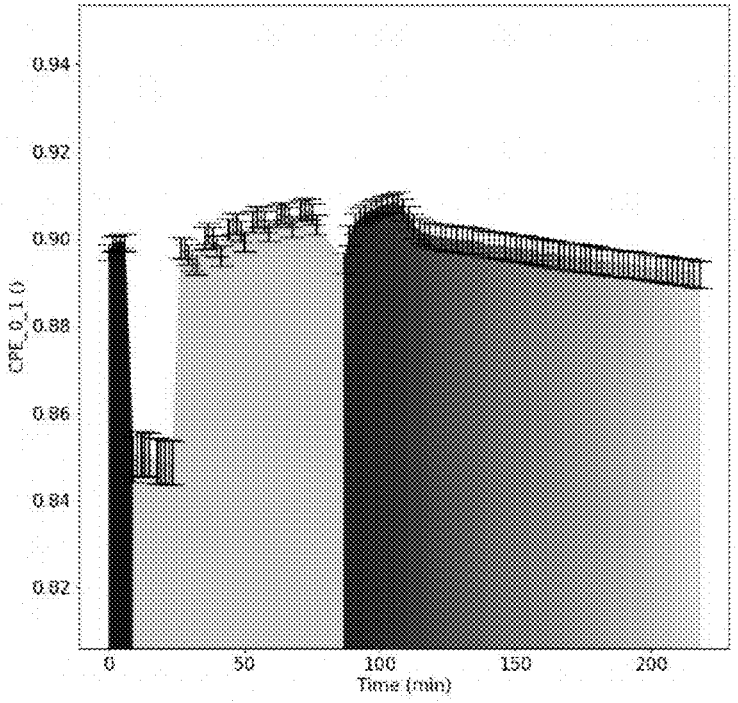

FIG. 26F

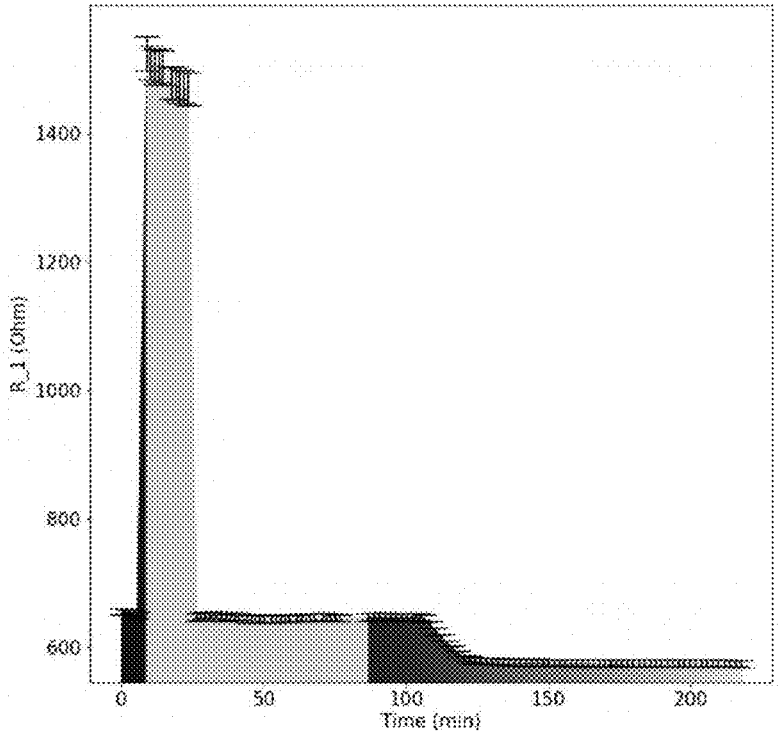

FIG. 26G

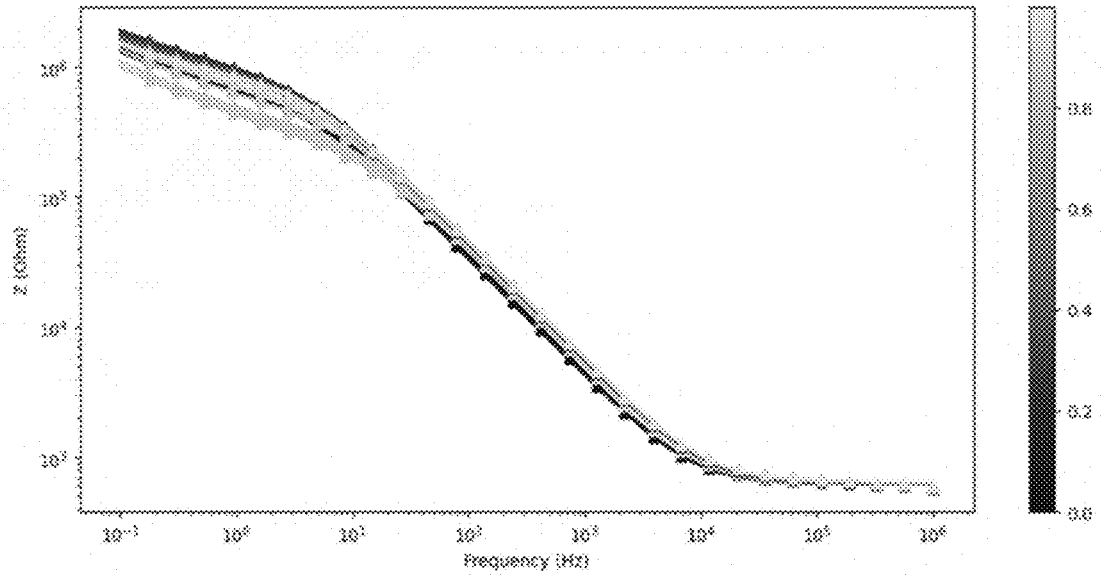

FIG. 27A

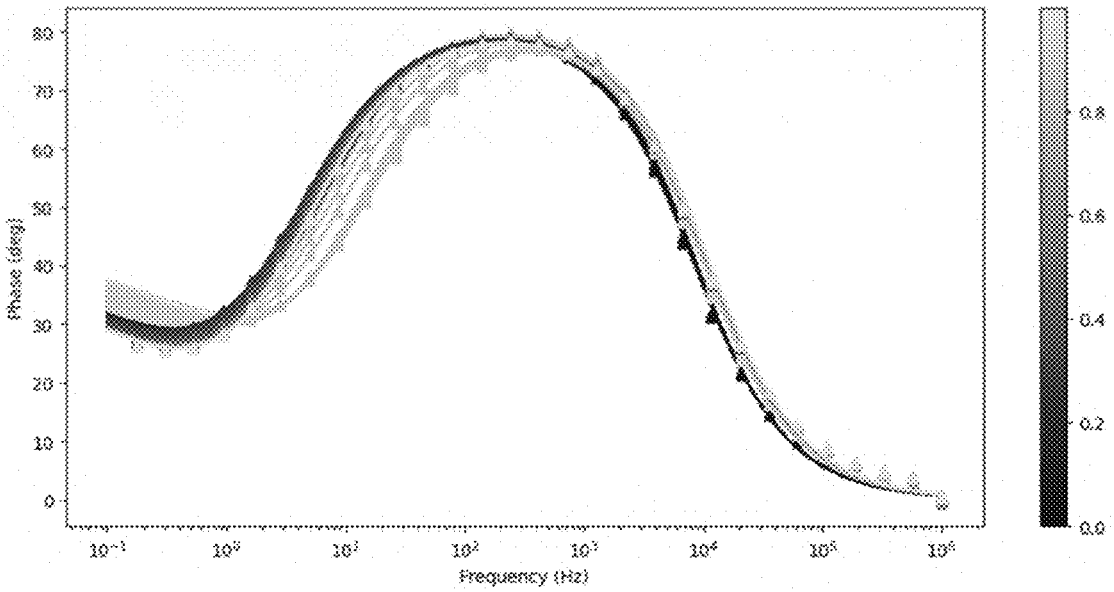

FIG. 27B

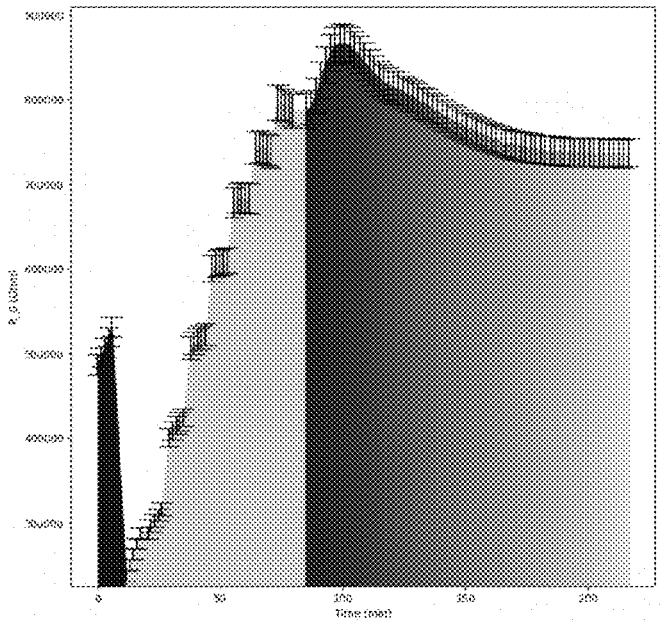

FIG. 27C

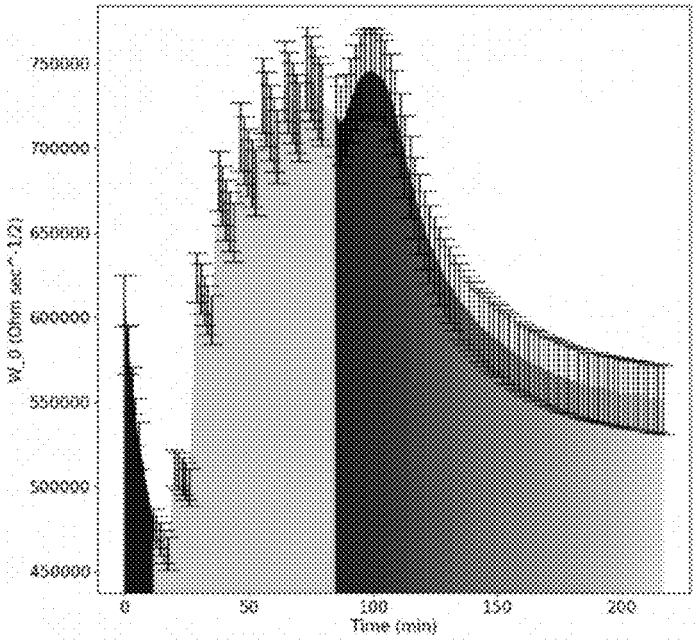

FIG. 27D

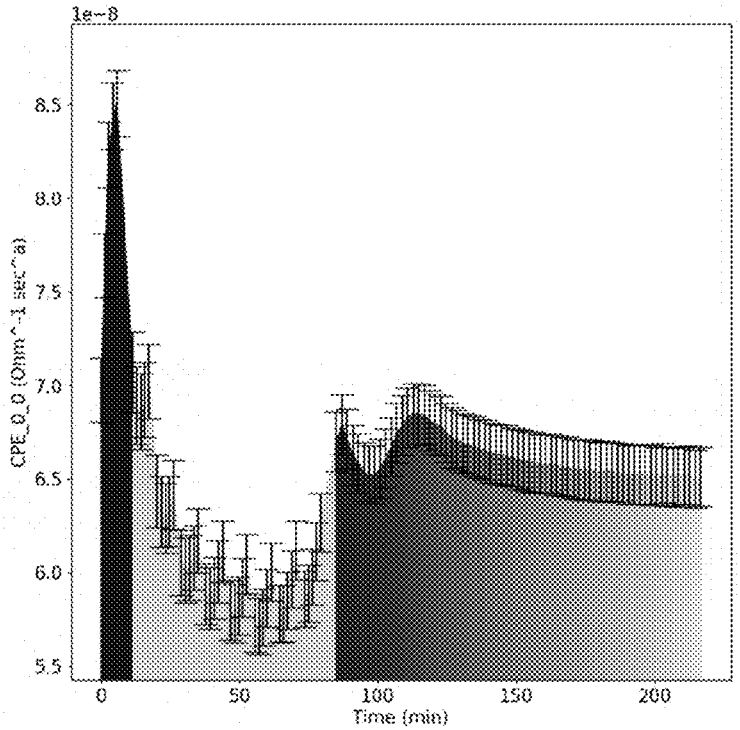

FIG. 27E

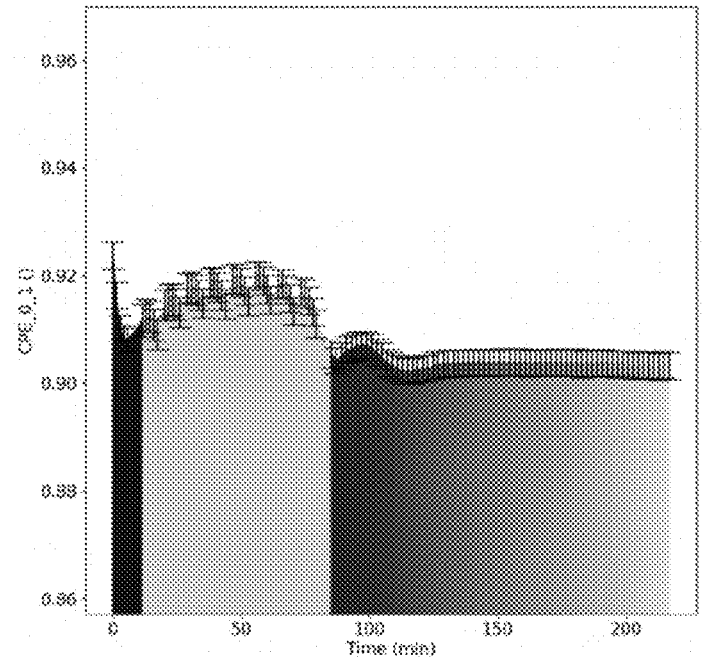

FIG. 27F

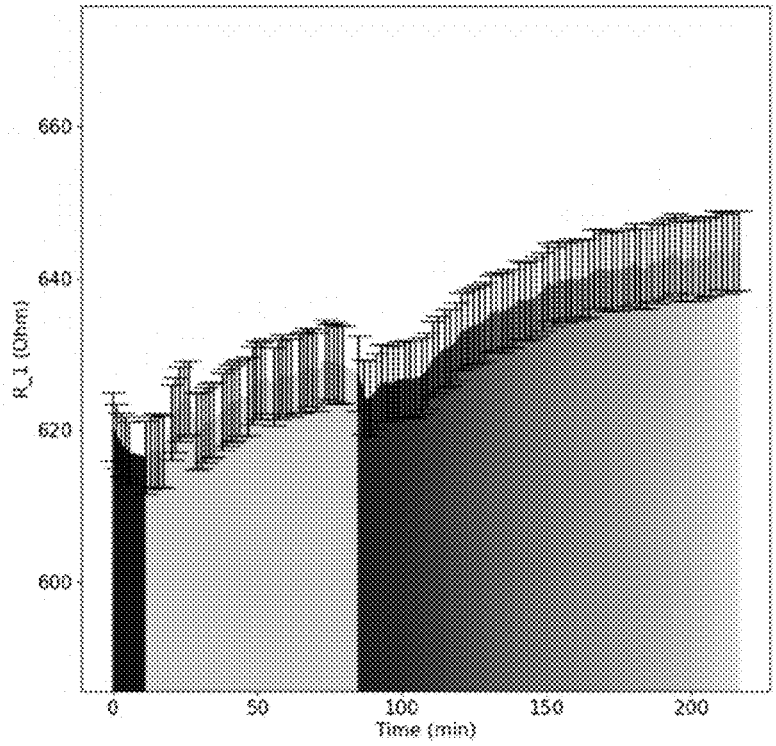

FIG. 27G

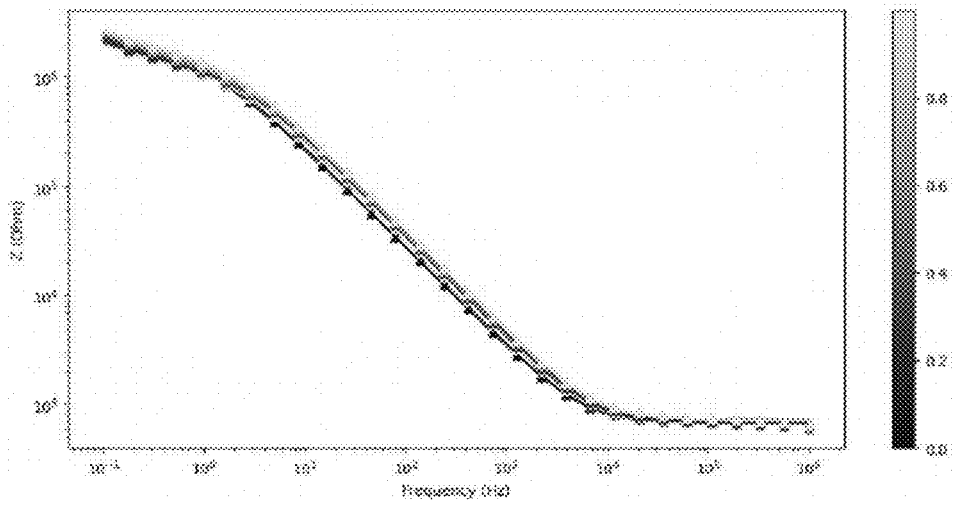

FIG. 28A

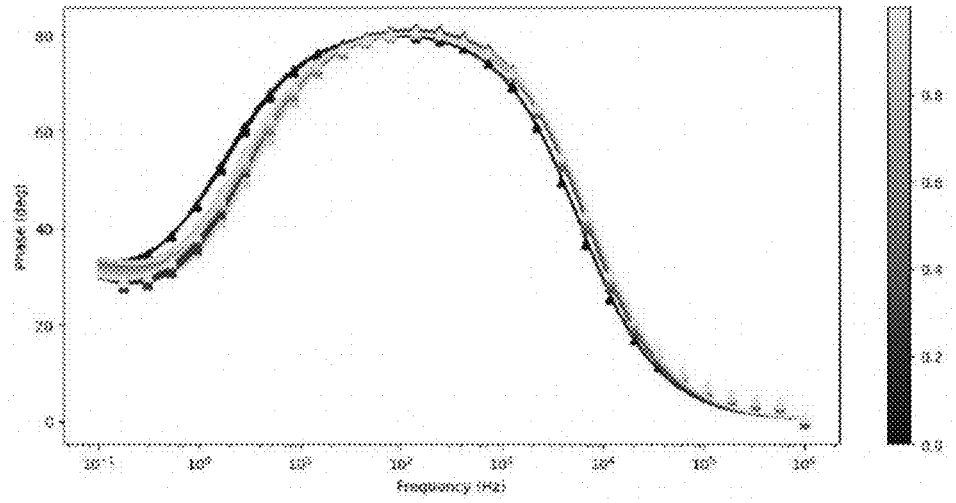

FIG. 28B

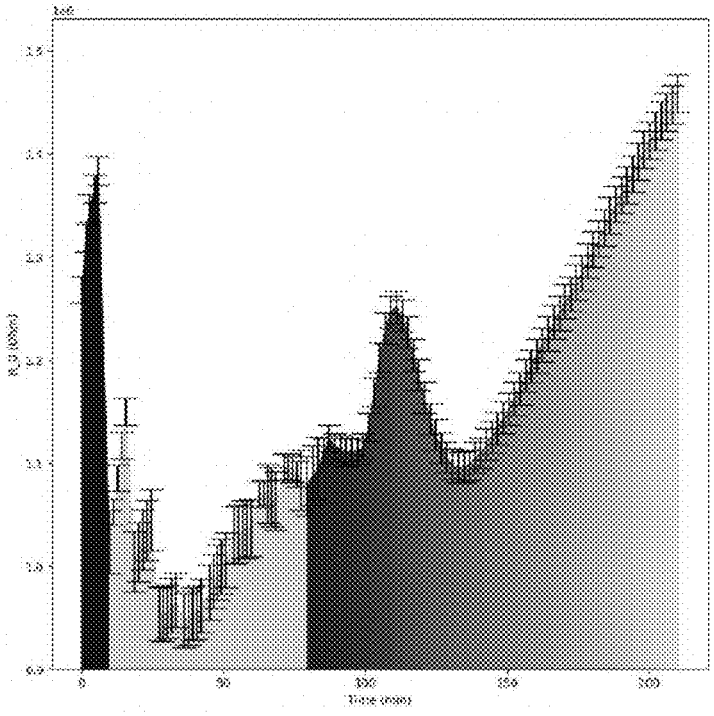

FIG. 28C

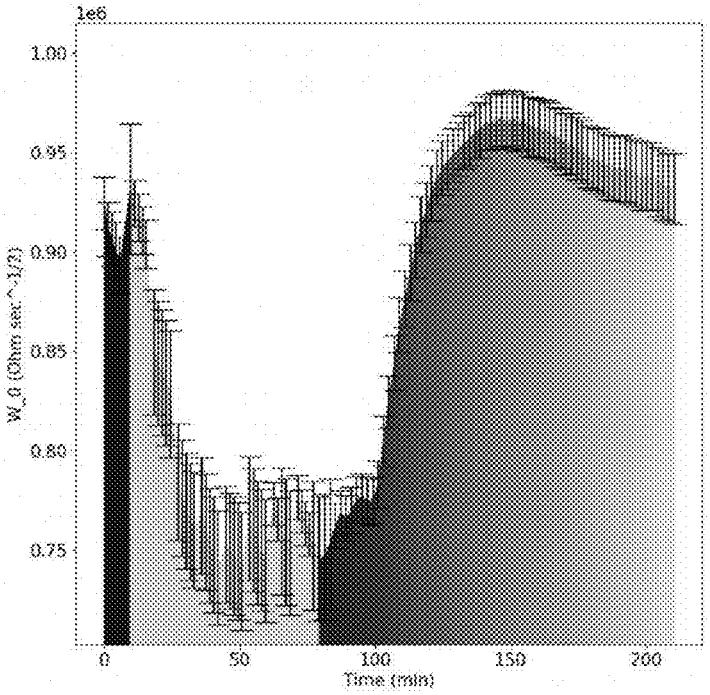

FIG. 28D

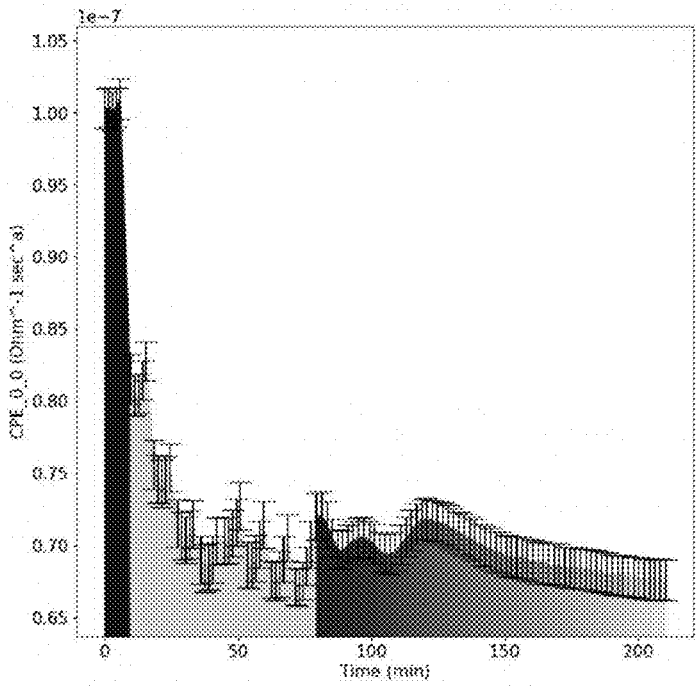

FIG. 28E

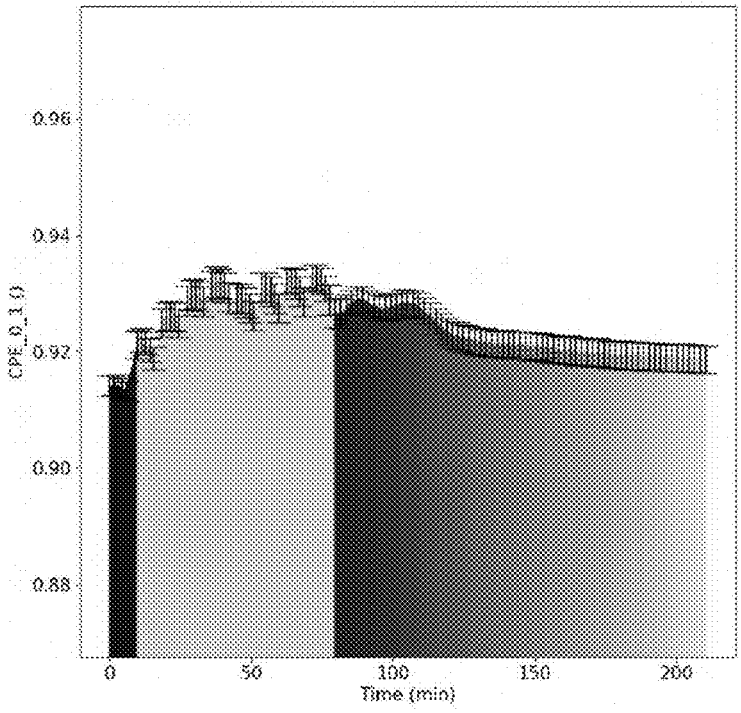

FIG. 28F

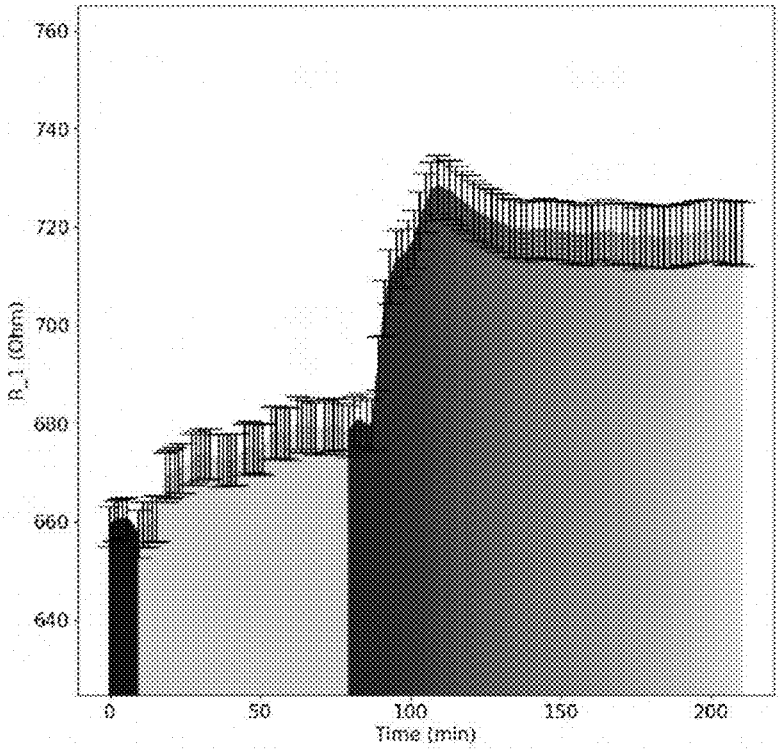

FIG. 28G

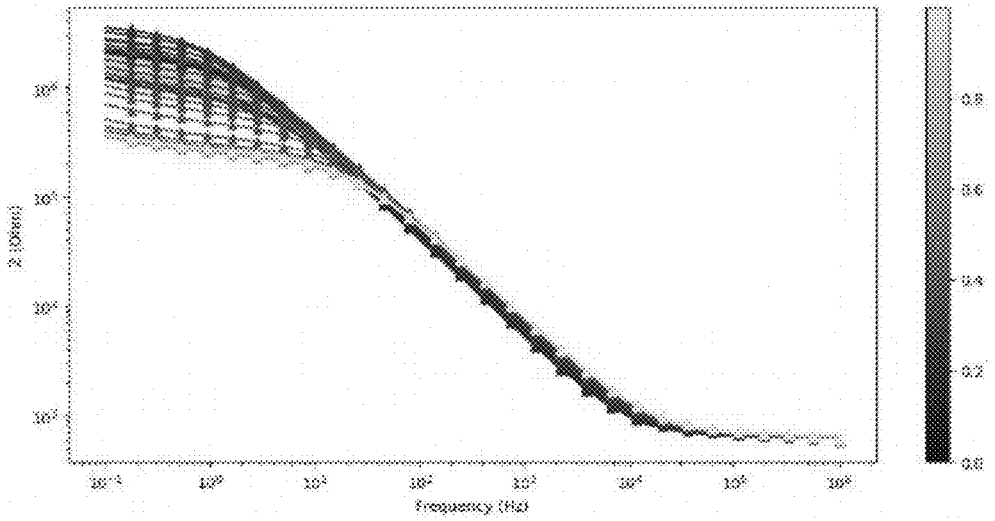

FIG. 29A

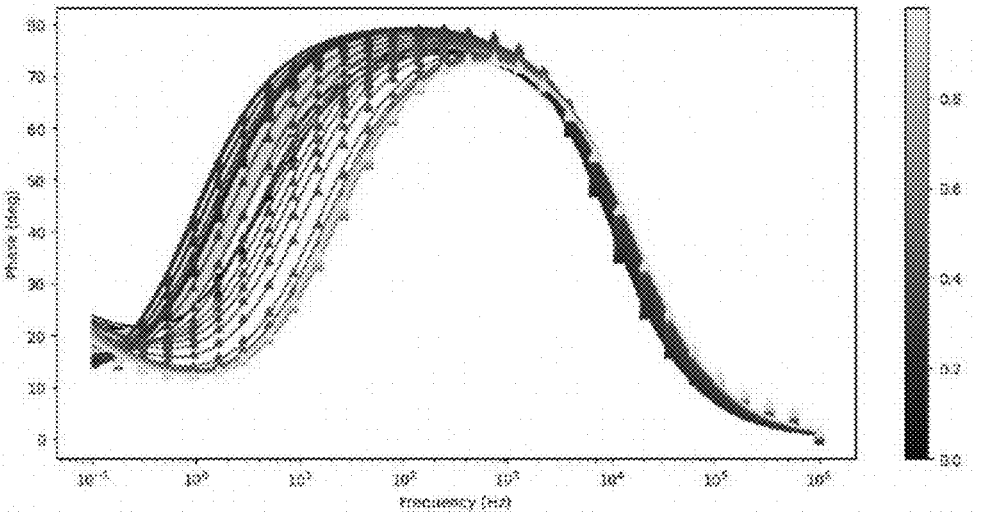

FIG. 29B

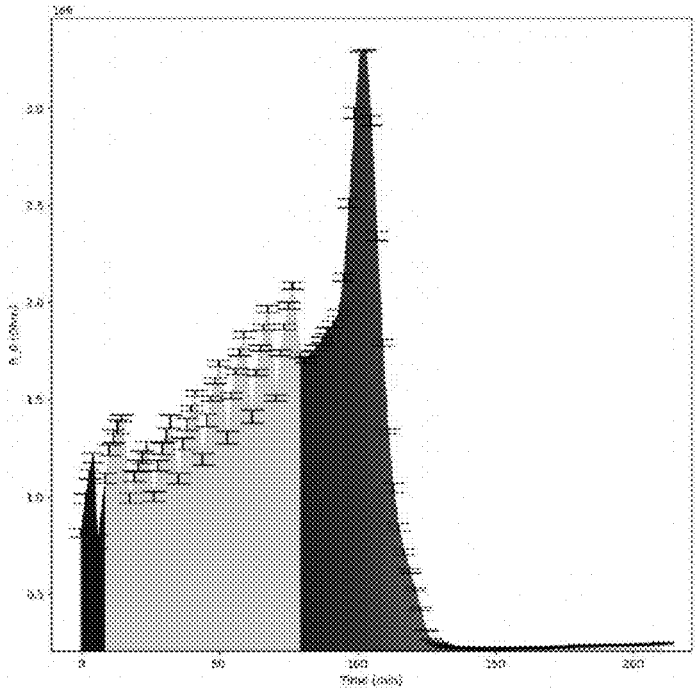

FIG. 29C

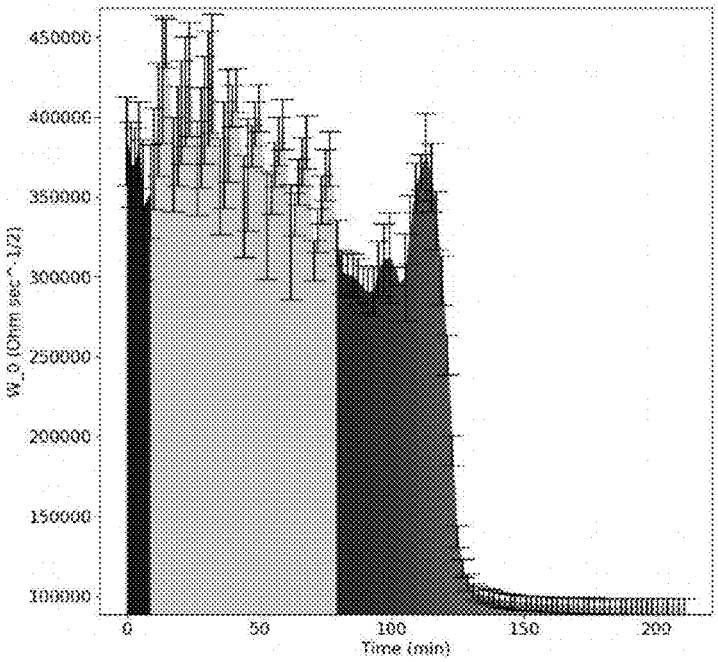

FIG. 29D

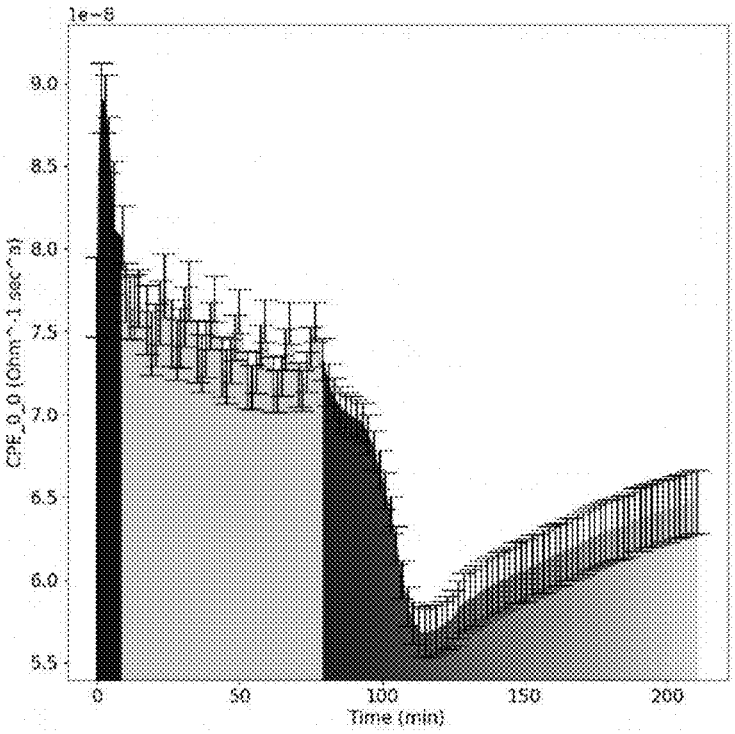

FIG. 29E

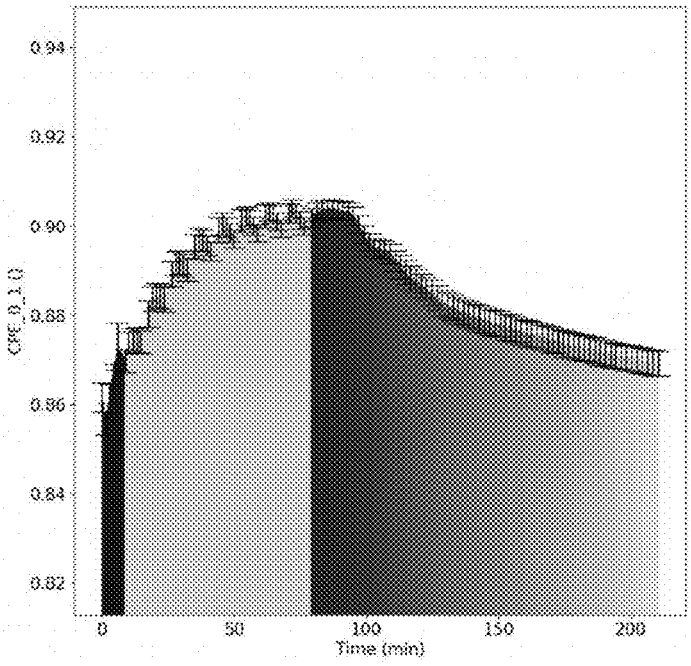

FIG. 29F

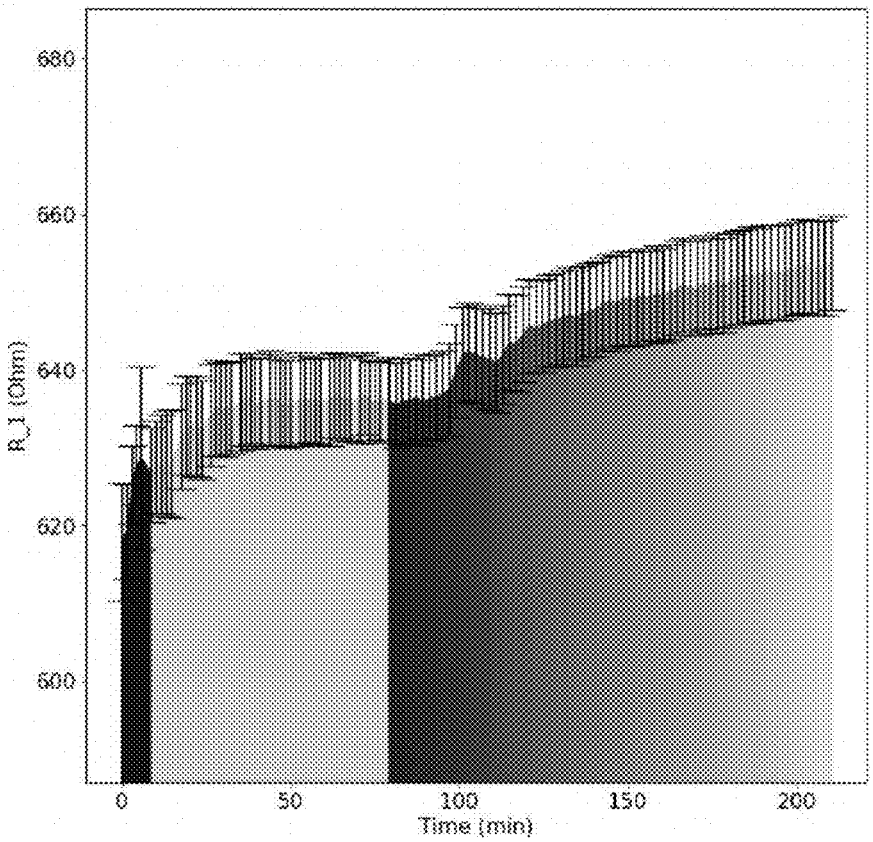

FIG. 29G

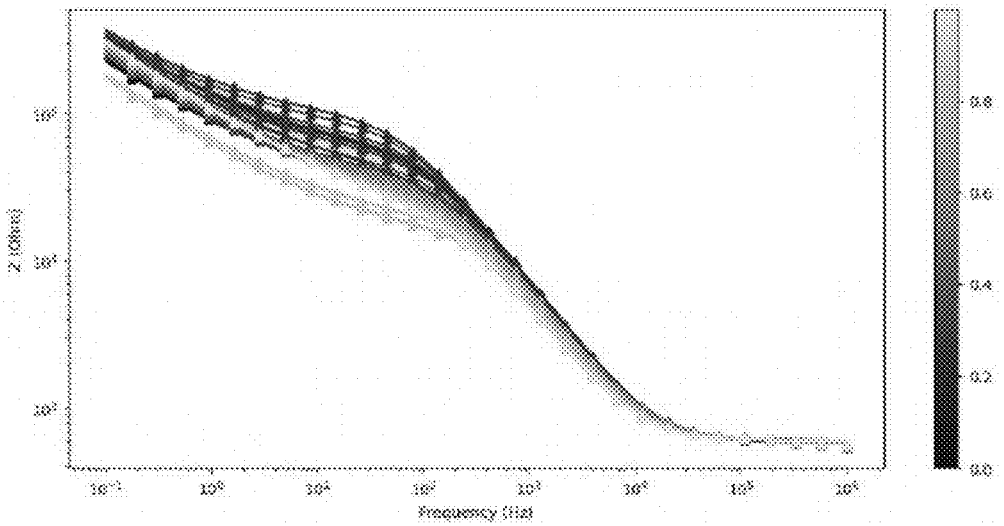

FIG. 30A

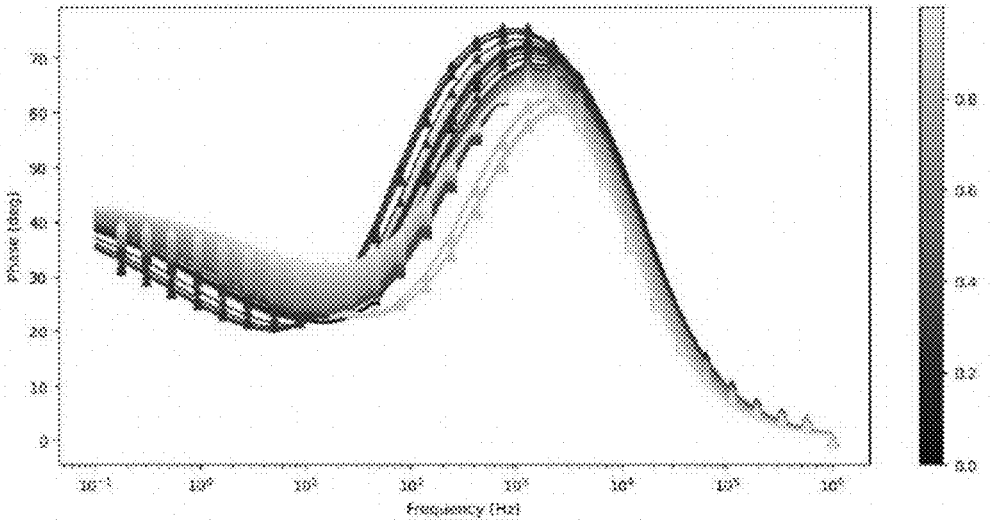

FIG. 30B

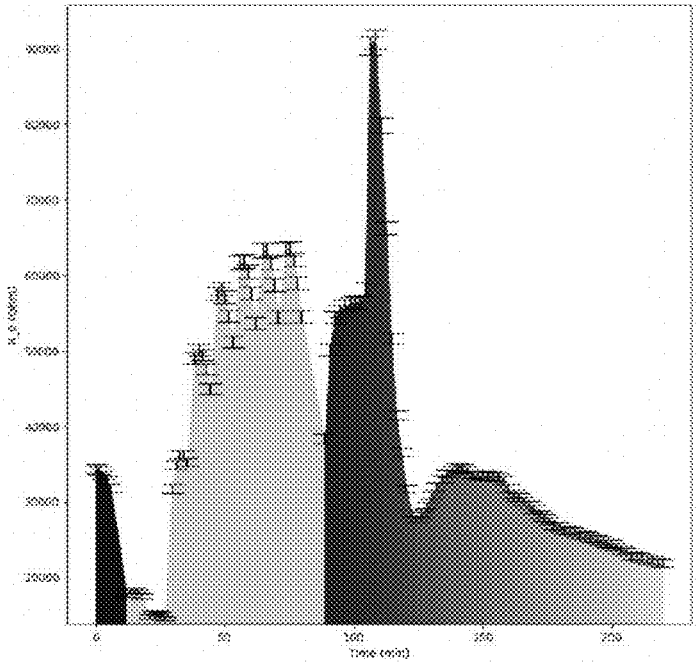

FIG. 30C

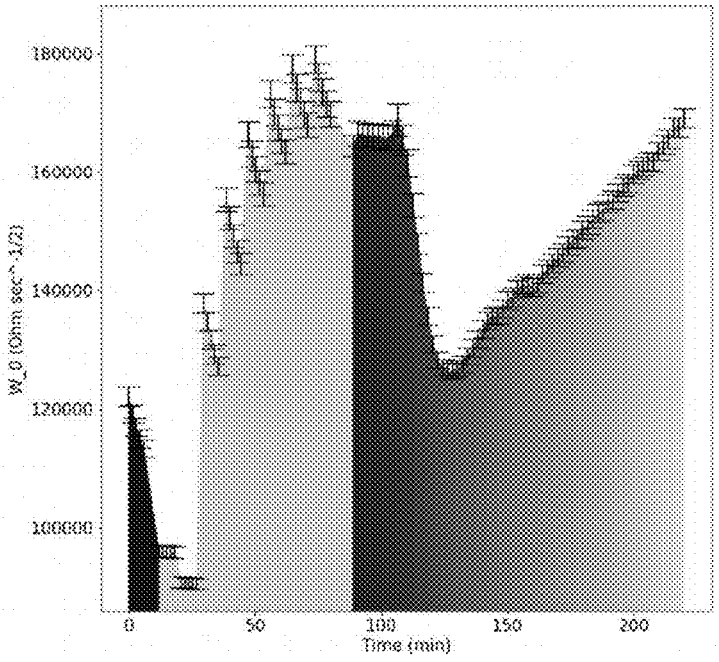

FIG. 30D

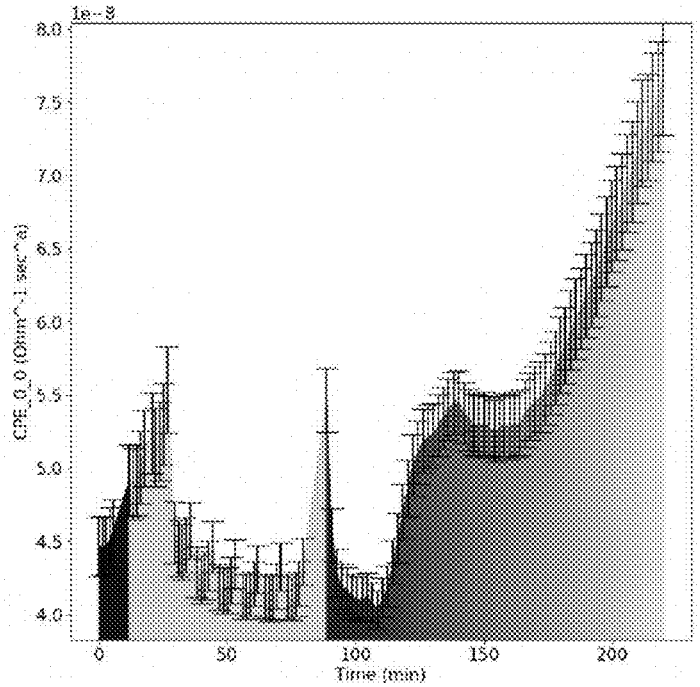

FIG. 30E

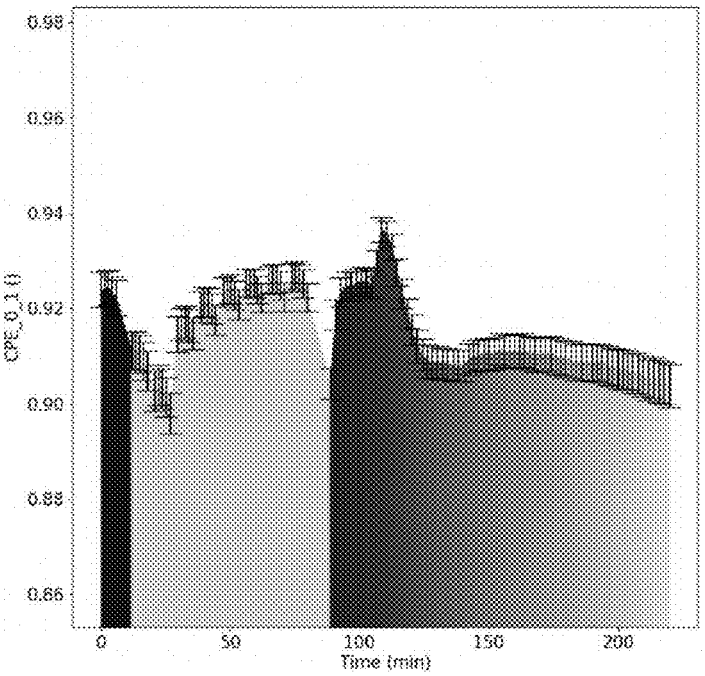

FIG. 30F

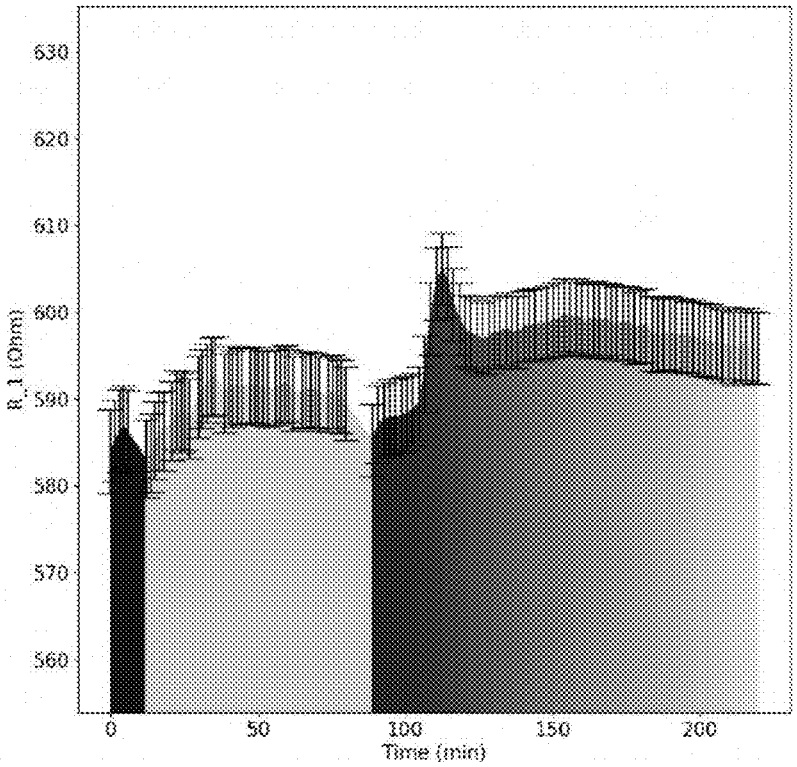

FIG. 30G

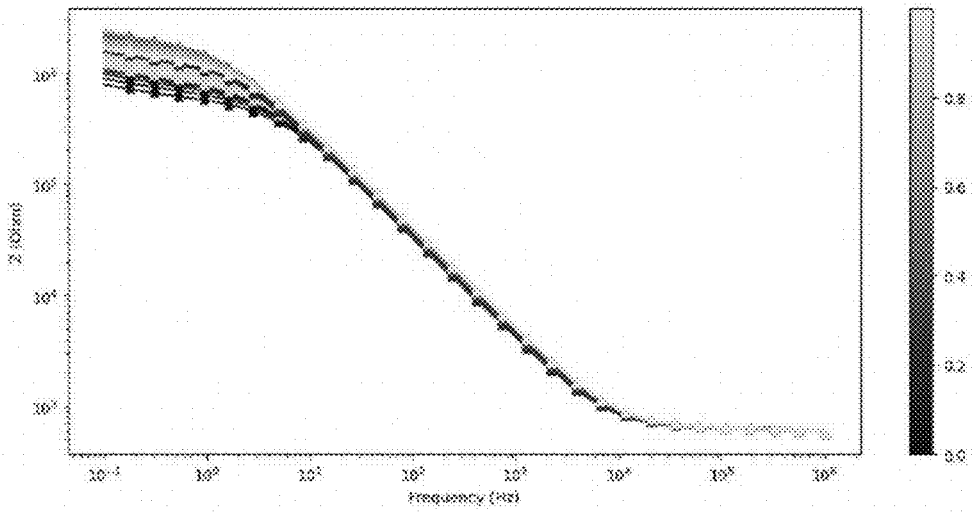

FIG. 31A

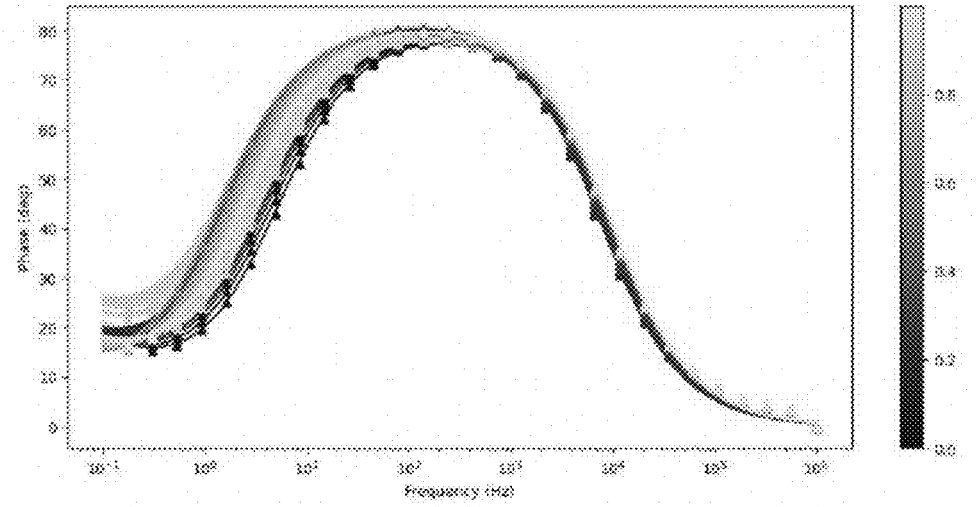

FIG. 31B

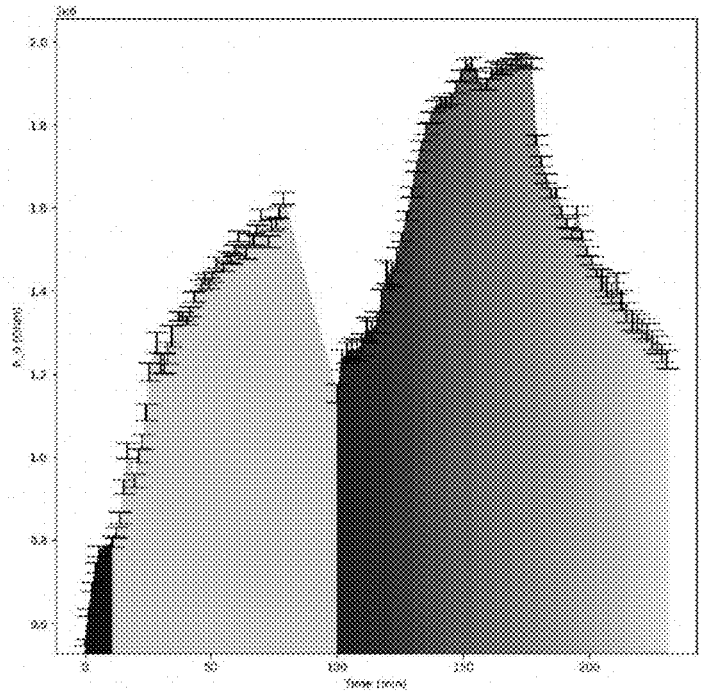

FIG. 31C

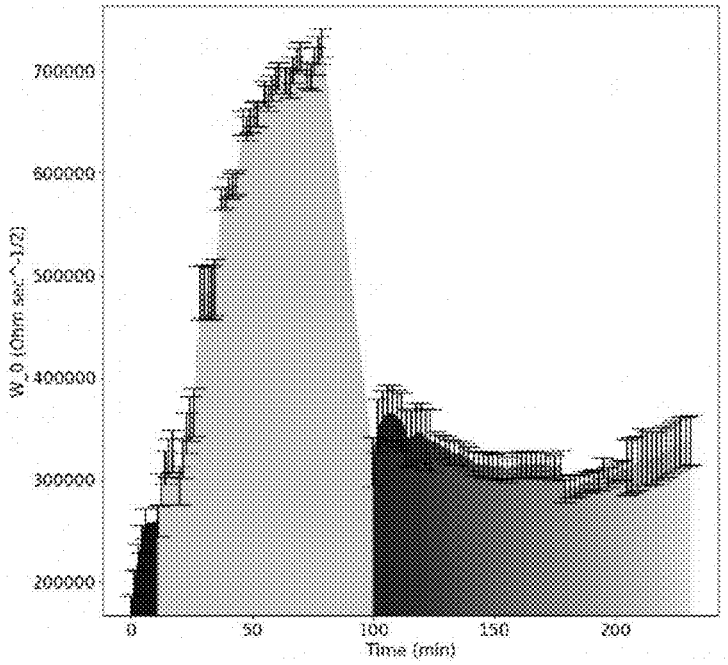

FIG. 31D

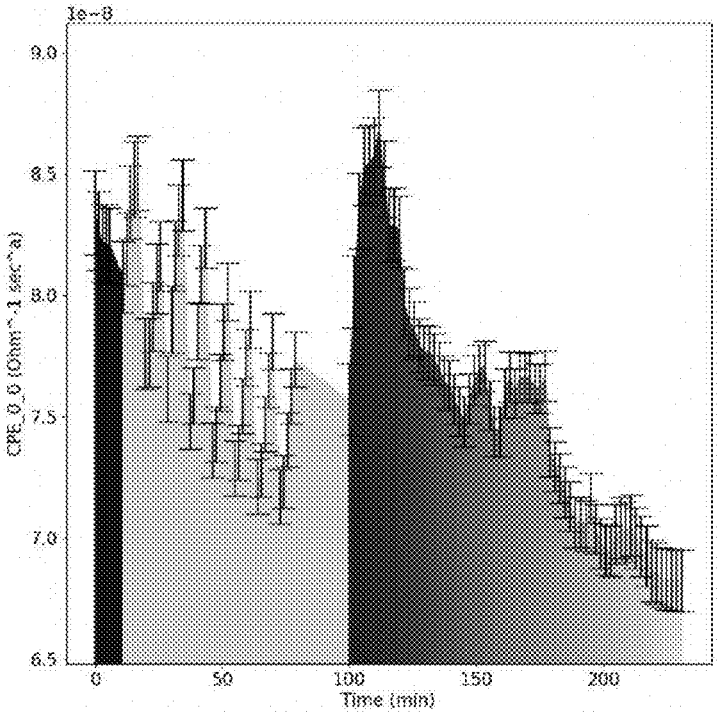

FIG. 31E

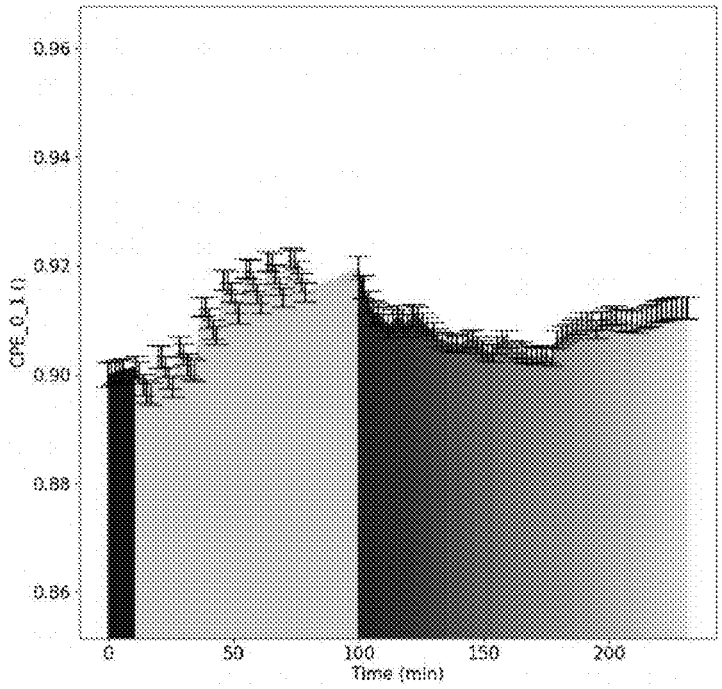

FIG. 31F

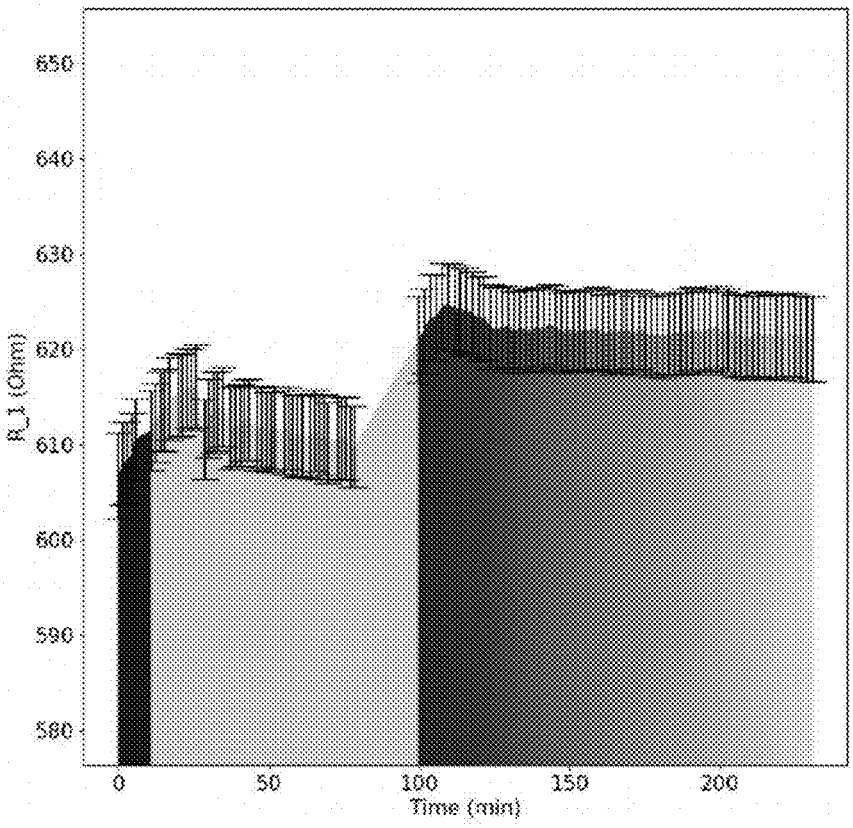

FIG. 31G

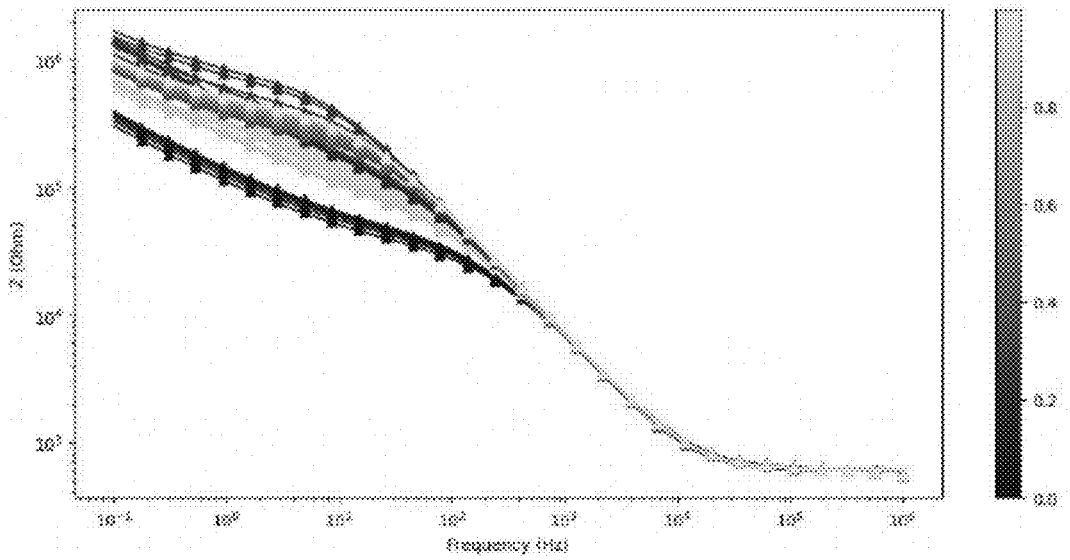

FIG. 32A

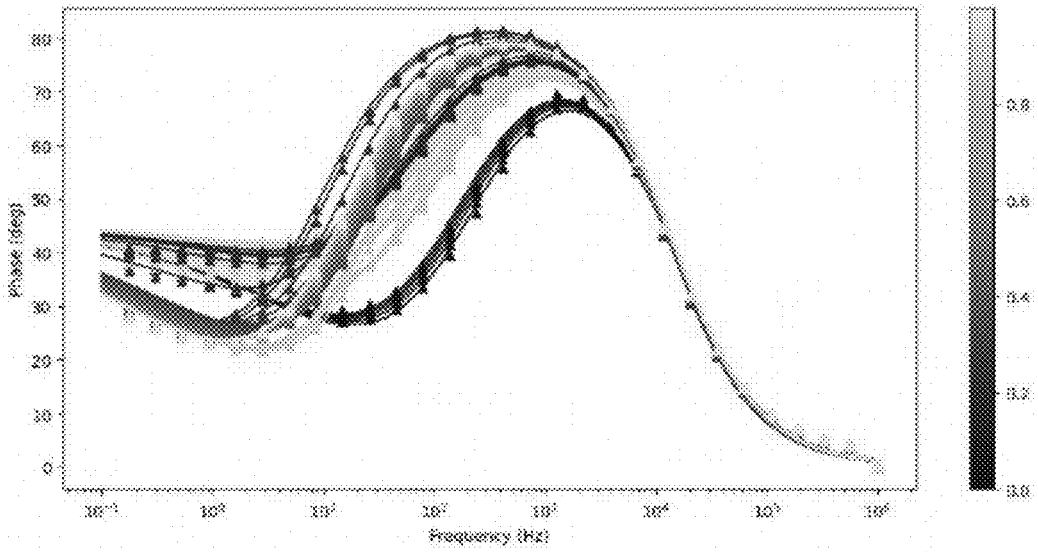

FIG. 32B

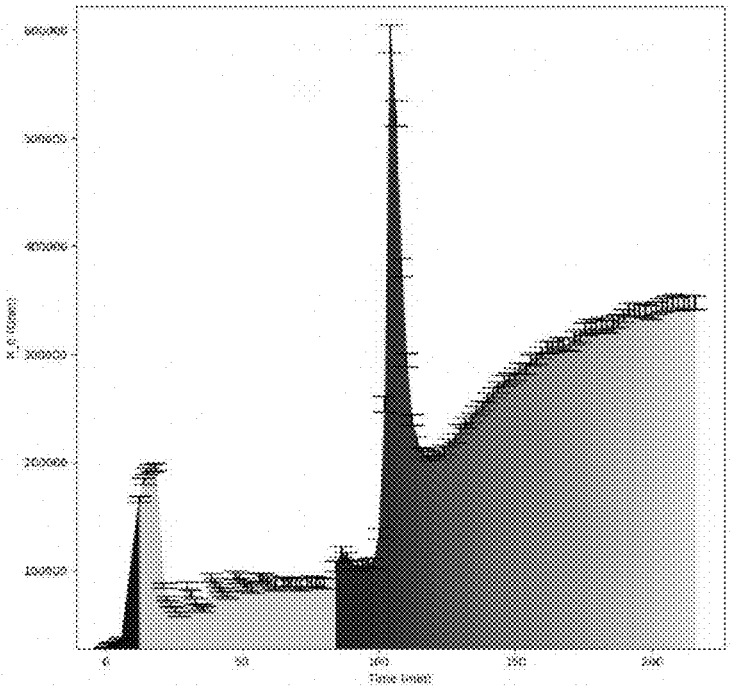

FIG. 32C

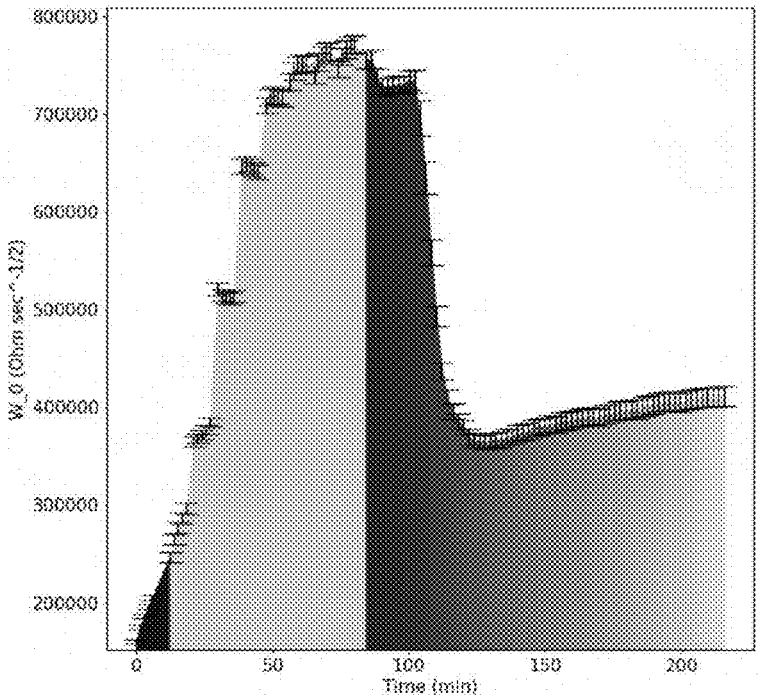

FIG. 32D

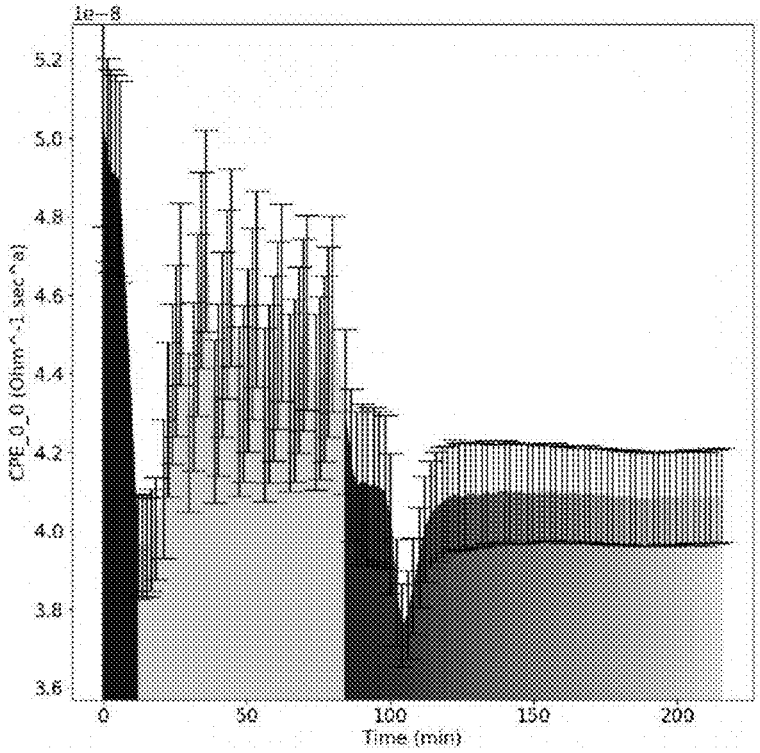

FIG. 32E

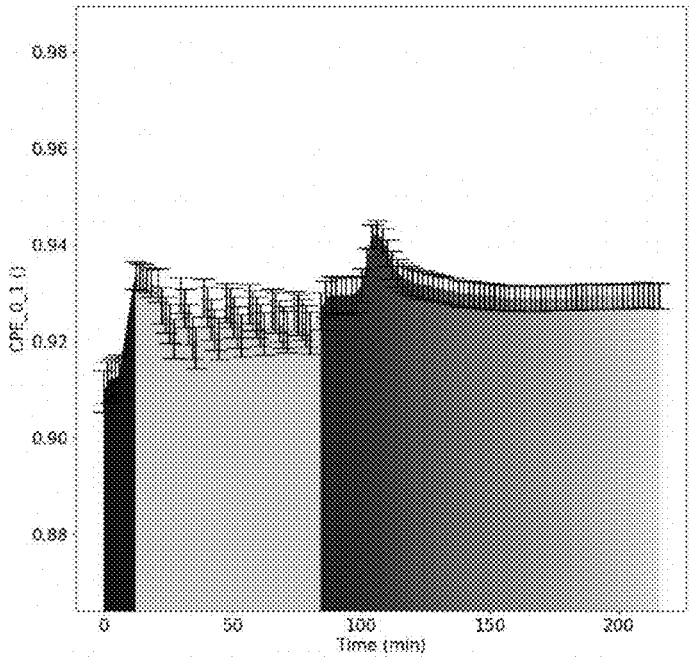

FIG. 32F

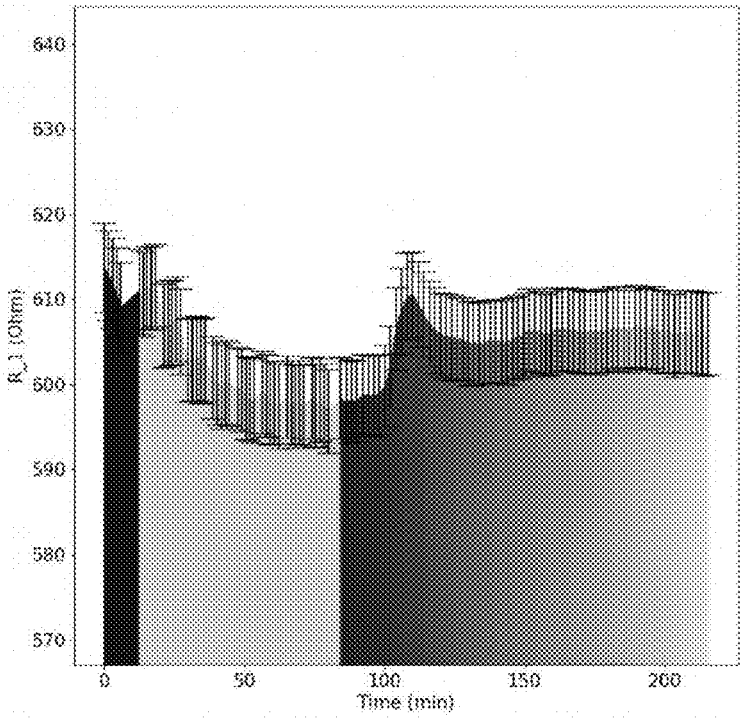

FIG. 32G

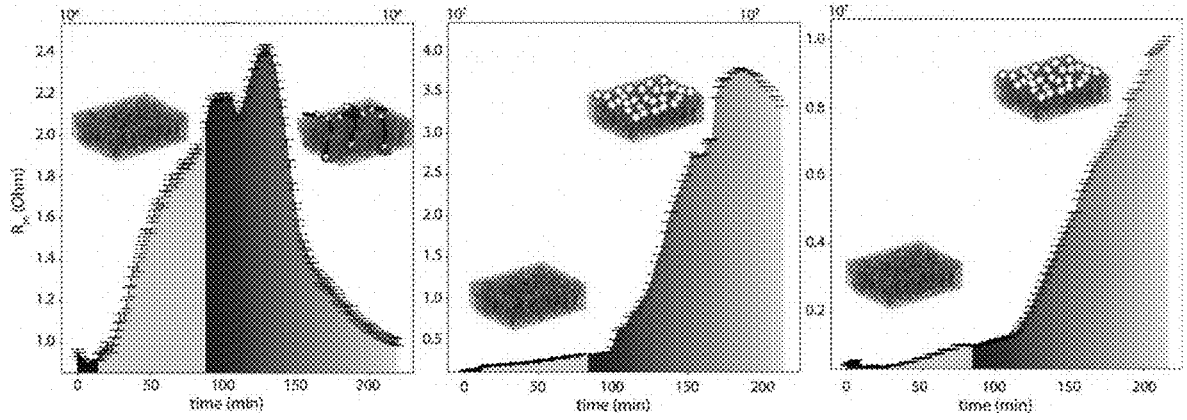

FIG. 33

BIOLOGICAL MEMBRANE-BASED SENSOR

RELATED APPLICATION

[0001] This application is a continuation in part of U.S. patent application Ser. No. 16/229,487, entitled Biological Membrane-Based Sensor, filed Dec. 21, 2018, which claims the benefit of U.S. Provisional Application Ser. No. 62/608,680 filed Dec. 21, 2017, the entire contents of which are hereby incorporated by reference.

FIELD

[0002] The present application relates to multi-lamellar lipid membranes and more specifically to multi-lamellar lipid membranes derived from biological cells and multi-lamellar lipid membranes that comprise synthetic lipids and their use as a biosensor.

BACKGROUND

[0003] The presence of pale cells with no internal content in a blood smear is typically indicative of a disease. These cells are produced by hemolysis and have been named red blood cell (RBC) ghosts based on their appearance under the microscope. RBC ghosts can be prepared artificially, and their preparation is a well-known protocol in biological and medical research [1-3]. The first published protocol in 1963 by Dodge, Mitchell and Hanahan describes the extraction of the cell membrane from RBCs through hemolysis and was an essential step in the development of membrane proteomics and lipidomics [4, 5]. The RBC lipid bilayer consists of equal amounts of cholesterol and phospholipids, such as phosphatidylcholine, sphingomyelin, phosphatidylethanolamine and phosphati dylserine [6].

[0004] Another well-known protocol is the preparation of highly oriented stacks of artificial supported lipid bilayers on silicon wafers [7, 8]. This technique allows the analysis of molecular structure and dynamical properties of these bilayers using biophysical techniques, such as fluorescence microscopy, atomic force microscopy, as well as X-ray and neutron scattering [8-17]. This approach has advanced significantly during the past decades and is now used to study complex, multi-component membranes and their interaction with drugs, small molecules [8, 18-27], bacteria [28, 29], and in particular lipid rafts, i.e., functional lipid domains [30-36].

[0005] Blood tests are routinely used to detect and identify infectious agents and inform therapeutic treatment. Blood agar plates are the current gold-standard tests for detecting and identifying bacteria with a hemolytic activity, i.e., bacteria which break the red blood cell (RBC) membrane. In this test, clinical swabs or specimens are spread on an agar plate (a growth medium), which typically contains 5% blood, and the plate is incubated overnight. Hemolytic activity is evaluated visually as changes to the colour of the plate and pattern formation. Typically, blood from sheep or horses is used for these tests as human blood has the potential to expose hospitals and technicians to dangerous pathogens.

[0006] Although this approach is used to detect hemolytic activity, there are significant limitations of the current procedures. The blood used in the manufacturing of the commonly used agar plates is of animal origin, typically sheep or bovine, as it is not feasible to produce the required large quantities of blood with human blood. However, this design inherently prevents the test from detecting pathogens specific to humans. Any test optimized for human specific pathogens thus requires minimizing the use of human blood in its design in combination with a high selectivity and sensitivity.

[0007] Electronic sensors coated with synthetic lipids are known in the art. However, these known synthetic lipids result in membranes that are not representative of real biological membranes because of their reduced complexity and, the significance of results obtained with those sensors is, therefore, limited in a clinical environment and it is not readily apparent whether and which synthetic lipids may be used in a membrane of a biosensor such that the biosensors mimics have membranes that mimic real biological membranes and may provide sufficient performance (e.g., detection and sensitivity) under certain biological test conditions.

SUMMARY

[0008] As demonstrated herein, coating sensors with real biological membranes overcome certain limitations of existing sensors and increase the clinical significance of those sensors. It is further demonstrated herein that by doping the biological membranes on the sensor surface with certain synthetic lipids described herein, the selectivity and sensitivity of the membrane-based sensor to specific toxins and pathogens can be drastically enhanced. For instance, by increasing the electric charge of the membrane through incorporation of charged synthetic lipids, the attachment of toxins of opposite charge can be increased. Incorporation of PEGylated lipids allows the attachment of protein linkers to attach antibodies that specifically bind to certain antigens. Through this mechanism, the sensor can be made sensitive and specific to detect certain types of bacteria for instance.

[0009] Accordingly, in one aspect there is provided a biosensor comprising:

[0010] a solid substrate having a lipid bilayer compatible surface; and

[0011] a multi-lamellar lipid membrane structure localized on the lipid bilayer compatible surface, the multi-lamellar lipid membrane structure being prepared from red blood cells or red blood cell ghosts and comprises one or more synthetic lipids.

[0012] In at least one embodiment, the one or more synthetic lipids comprises a phosphatidylcholine (PC), a phosphatidylethanolamine (PE), a phosphatidylglycerol (PG) and/or a phosphatidylserine (PS).

[0013] In at least one embodiment, the one or more synthetic lipids are selected from the group consisting of 1,2-dimyristoyl-sn-glycero-3-phosphocholine (DMPC), 1-palmitoyl oleoyl-glycero-3-phosphocholine (POPC), 1-palmitoyl-2-oleoyl-sn-glycero-3-phospho-L-serine (POPS), 1,2-dimyristoyl-sn-glycero-3-phospho-L-serine (DMPS), and 1-palmitoyl-2-oleoyl-sn-glycero-3-phospho-(1'-rac-glycerol) (POPG).

[0014] In at least one embodiment, the multi-lamellar lipid membrane structure further comprises one or more lipids conjugated with polyethylene glycol (PEGylated lipids).

[0015] In at least one embodiment, the one or more PEGylated lipids comprises PEGylated phosphatidylethanolamine (PE). In at least one embodiment, the one or more PEGylated lipids comprises PEGylated cholesterol.

[0016] In at least one embodiment, the one or more PEGylated lipids comprises a functionalized PEGylated lipid.

[0017] In at least one embodiment, the polyethylene glycol is methoxy polyethylene glycol.

[0018] In another aspect, there is provided a biosensor comprising:

[0019] a solid substrate having a lipid bilayer compatible surface; and

[0020] a multi-lamellar lipid membrane structure localized on the lipid bilayer compatible surface, the multi-lamellar lipid membrane structure comprises two or more synthetic lipids comprising a phosphatidylethanolamine (PE), a phosphatidylglycerol (PG), a phosphatidylcholine (PC), a phosphatidylserine (PS), a cholesterol, and/or a cardiolipin (CL).

[0021] In at least one embodiment, the PE comprises 1-palmitoyl-2-oleoyl-sn-glycero-3-phosphoethanolamine (POPE) and/or 1,2-dimyristoyl-sn-glycero-3-phosphoethanolamine (DMPE).

[0022] In at least one embodiment, the PG comprises 1-palmitoyl-2-oleoyl-sn-glycero-3-phospho-(1'-rac-glycerol) (POPG) and/or 1,2-dimyristoyl-sn-glycero-3-phospho-(1'-rac-glycerol) (DMPG).

[0023] In at least one embodiment, the PC comprises 1,2-dimyristoyl-sn-glycero-3-phosphocholine (DMPC).

[0024] In at least one embodiment, the PS comprises 1,2-dimyristoyl-sn-glycero phospho-L-serine (DMPS).

[0025] In yet another aspect, there is provided a method of detecting membrane disruption activity in a sample, the method comprising: (a) contacting the sample with the biosensor of claim **1**; and (b) detecting a change in the multi-lamellar lipid membrane structure in response to the sample.

[0026] In yet another aspect, there is provided at least one method of making the biosensor disclosed herein, the method comprising: (a) preparing an aqueous solution of hybrid membranes comprising membranes prepared from red blood cells or red blood cell ghosts and the one or more synthetic lipids; and (b) generating the multi-lamellar lipid membrane structure localized on the lipid bilayer compatible surface by successively providing the aqueous solution of hybrid membranes on the lipid bilayer compatible surface.

[0027] Other features and advantages of the present application will become apparent from the following detailed description. It should be understood, however, that the detailed description and the specific examples, while indicating embodiments of the application, are given by way of illustration only and the scope of the claims should not be limited by these embodiments but should be given the broadest interpretation consistent with the description as a whole.

DRAWINGS

[0028] The embodiments of the application will now be described in greater detail with reference to the attached drawings in which:

[0029] FIG. **1**. Schematic of the Blood-on-a-Chip preparation protocol. The protocol is based on the original protocol for the preparation of red blood cell ghosts (a). The RBCs are then sonicated to form small uni-lamellar vesicles and centrifuged (b) before the solution is applied to silicon wafers (c). The membranes are dried and annealed (d) to form well developed multi-lamellar stacks of red blood cell membranes supported on silicon wafers.

[0030] FIG. **2**. Removal of hemoglobin from the erythrocyte blood fraction after induced lysis in hypotonic buffer. a) Ghost samples lose their characteristic red color through sequential centrifugation and washes. b) Comparison of UV-vis absorbance curves at different stages within ghost preparation. Characteristic hemoglobin absorbance signatures are significantly reduced in the final solution after the procedure. c) Schematic of the UV-vis setup.

[0031] FIG. **3**. Fluorescence microscopy images of the ghost solution before and after sonication. The membrane was labelled using DiI in parts a) and c), while Alexa Fluor 488 labelled phalloidin was used to label the F-actin network in b) and d). Before sonication, ghosts of highly irregular shape and a large size distribution are observed including 'ghosts inside of ghosts'. The solution also contains large clusters of actin. Small uni-lamellar vesicles are observed after sonication and no actin particles (within the resolution of the microscope used).

[0032] FIG. **4**. Photos of the silicon chips after a) application of the RBC solution on a hydrophilic wafer and fast drying, b) application on a hydrophobic wafer after slow drying. c) and d) show hydrophilic wafers after slow drying and slow drying and annealing, respectively. See text for details.

[0033] FIG. **5**. Overview of the X-ray diffraction results. The setup is schematically shown in a). The highly aligned membranes are oriented on the X-ray diffractometer, such that q_z measures out-of-plane, and $q_{||}$in-plane membrane structure. b) Two-dimensional data. The main features are a series of intensities along the q_z-axis and two broad signals along the in-plane axis $q_{||}$. c) shows a cut along q_z. The data are well fit by three series of Bragg peaks corresponding to three different lamellar spacings assigned to l_o and ld lipid domains (green and blue) and coiled-coil α-helical peptide domains (red). d) The in-plane signals show three correlation peaks corresponding to the packing of α-helices in the peptide domains (ap=10.83 Å) and packing distances of ld (ald=5.39 Å) and l_o lipid tails (alo=4.69 Å) in the hydrophobic membrane core.

[0034] FIG. **6**. Analysis of the X-ray diffraction data in FIG. **5**. The lamellar spacings of the peptide, and the l_o and ld lipid domains are determined from the slopes of q_z vs. n plots. b) Shows the corresponding electron densities as determined through Fourier analysis of the out-of-plane diffraction data. The densities for the l_o and l_d lipid domains agree well with literature values. The peptide domain shows an almost constant density in the hydrophobic membrane core, indicative of trans-membrane peptide domains. c) Membrane orientation is determined from radial integration of the scattered intensity along the meridional degree, ϕ. The solid line is a fit using a Gaussian profile. RBC membranes are 90.9% oriented with respect to the silicon substrate.

[0035] FIG. **7**. Analysis of the RBC/aspirin complexes. a) Shows all reflectivity curves for complexes containing between 0 and 3 mM ASA. b) The pattern for the 2.5 mM sample is well fit by three series of peaks corresponding to l_o, l_d and peptide domains. c) The location of the ASA molecule is determined by comparing the electron density of a pure RBC membrane with a low concentration of 1 mM ASA. Aspirin is found to partition the l_o lipid domains of RBC membranes and locate in the head group region, at |z|-values of 22.8 Å, d) Small partitioning of aspirin is observed in l_d lipid domains, indicative that aspirin preferably interacts with l_o domains. e) Lamellar spacing, d_z, and membrane thickness, d_{HH} of the l_o lipid domains decrease significantly with increasing ASA concentration until thickness of l_o and l_d domains coincide.

[0036] FIG. **8**. The structural findings are summarized in cartoons of pure RBC membranes (a) and RBC membranes containing aspirin (b). While domains of saturated, unsaturated lipids and coiled-coil peptides are observed in pure RBC membranes, with significantly different membrane thicknesses, the addition of aspirin leads to an overall thinning of the membranes and an increase of the lipid spacings, indicative of a fluidification. Aspirin mainly interacts with the $l_o$lipid domains. Structural parameters determined in this study are given in the figures.

[0037] FIG. **9**. Nanostructured gold electrodes with RBC membranes applied to the sensors.

[0038] FIG. **10**. Modelling hemolytic activity based on membranes disrupted using the surfactant, sodium dodecyl sulfate (SDS).

[0039] FIG. **11**. Microscopy images of an exemplary biosensor. (a) and (b) are standard images at different resolutions. (c) shows a fluorescent image where the red blood cell membranes are illuminated, indicating that the red blood cell membranes are annealed to the sensor. (d) shows an electron microscopy image of an enlarged section of the surface of multi-lamellar structure on a biosensor.

[0040] FIG. **12** shows the improved quality of the membrane coating obtained using the protocol of Example 3. (a) shows a 2D x-ray image, (b) shows the reflectivity Bragg peaks.

[0041] FIGS. **13**A-**13**B show a setup of Electrochemical Impedance Spectroscopy (EIS) according to one embodiment. **13**B depicts the "Randles circuit" which is used to model EIS data recorded on immobilized hybrid red blood cell membranes.

[0042] FIGS. **14**A-**14**G are graphs showing results of electrochemical impedance spectroscopy (EIS) of hybrid RBC membrane with 10% POPS (Hybrid POPS Sensor 1).

[0043] FIGS. **14**A and **14**B show the real and imaginary component of the impedance signal recorded on immobilized lipid bilayer. Measurements were made while a sequence of two buffers was successively pumped into the chamber: (1) Buffer A: Potassium hexacyanoferrate(III) ($K_3[Fe(CN)_6]$) at a concentration of 5 mM. (2) Buffer B: Vesicles formed from the hybrid membrane solution in 5 mM Potassium hexacyanoferrate(III) ($K_3[Fe(CN)_6]$). Buffer A is pumped into the chamber. Ten EIS spectra are recorded in time intervals of ~1 min (darker colors in the graphs). Afterwards, Buffer B is pumped into the chamber. EIS spectra are monitored for 90 min in time intervals of ~1 min (lighter colors in the graphs). The buffer B inside the chamber is exchanged after every 5 measurements. FIG. **14**C shows the time-behavior of the membrane resistance R_0 (see Randles circuit in FIG. **13**B). The darker and the lighter sections indicate the signals from the blank sensor and the membrane coating process respectively. FIG. **14**D shows the time-behavior of the Warburg element W_0 (see Randles circuit in FIG. **13**B). The darker and the lighter sections indicate the signals from the blank sensor and the membrane coating process respectively. FIG. **14**E and **14**F show the time-behavior of the constant phase element parameters CPE_0 and CPE_1 (see Randles circuit in FIG. **13**B). The darker and the lighter sections indicate the signals from the blank sensor and the membrane coating process respectively. FIG. **14**G shows the time-behavior of the solvent resistance R_1 (see Randles circuit in FIG. **13**B). The darker and the lighter sections indicate the signals from the blank sensor and the membrane coating process respectively. Importantly, the increase in R_0, the increase in the Warburg coefficient as well as decrease in the constant phase element coefficient CPF_0_0 during the elution of Buffer B indicates the coating of the sensor with the hybrid membrane.

[0044] FIGS. **15**A-**15**G are graphs showing results of electrochemical impedance spectroscopy (EIS) of hybrid RBC membrane with 10% POPS (Hybrid POPS Sensor 2). For the description of individual figures, see the description for FIGS. **14**A-**14**G above.

[0045] FIGS. **16**A-**16**G are graphs showing results of electrochemical impedance spectroscopy (EIS) of hybrid RBC membrane with 10% POPC (Hybrid_10percent POPC_Sensor1). For the description of individual figures, see the description for FIGS. **14**A-**14**G above.

[0046] FIGS. **17**A-**17**G are graphs showing results of electrochemical impedance spectroscopy (EIS) of hybrid RBC membrane with 10% POPC (Hybrid_10percent POPC_Sensor2). For the description of individual figures, see the description for FIGS. **14**A-**14**G above.

[0047] FIGS. **18**A-**18**G are graphs showing results of electrochemical impedance spectroscopy (EIS) of hybrid RBC membrane with 50% POPC (Hybrid_50percent POPC_Sensor1). FIGS. **18**A and **18**B show the real and imaginary component of the impedance signal recorded on immobilized lipid bilayer. FIG. **18**C-**18**G show the time-behavior of the corresponding dielectric properties. Measurements were performed while a sequence of three buffers was successively pumped into the measurement chamber: (1) Buffer A: Potassium hexacyanoferrate(III) ($K_3[Fe(CN)_6]$) at a concentration of 5 mM. (2) Buffer B: Vesicles formed from the synthetic lipids in 5 mM Potassium hexacyanoferrate (III) ($K_3[Fe(CN)_6]$). (3) Buffer C: A sample buffer consisting of 25 μg/mL PmB in 5 mM Potassium hexacyanoferrate(III) ($K_3[Fe(CN)_6]$). In a first step, the flow chamber is flushed with Buffer A. Ten EIS spectra are recorded in time intervals of ~1 min (left most section in the resulting graphs). Afterwards, Buffer B is pumped into the chamber. EIS spectra are monitored for 90 min in time intervals of ~1 min (middle section in the resulting graphs). The buffer B inside the chamber is exchanged after every 5 measurements. Finally, Buffer C is pumped into the chamber. EIS spectra are recorded immediately after every movement of the syringe pump (see the right most section in the resulting graphs). FIG. **18**C shows the time-behavior of the membrane resistance R_0 (see Randles circuit in FIG. **13**B). The three distinct sections in the graph indicate the signals from the blank sensor, the membrane coating process and the PmB buffer respectively. FIG. **18**D shows the time-behavior of the Warburg element W_0 (see Randles circuit in FIG. **13**B). The three distinct sections in the graph indicate the signals from the blank sensor, the membrane coating process and the PmB buffer respectively. FIG. **18**E and 18F show the time-behavior of the constant phase element parameters CPE_0 and CPE_1 (see Randles circuit in FIG. **13**B). The three distinct sections in the graph indicate the signals from the blank sensor, the membrane coating process and the PmB buffer respectively. FIG. **18**G shows the time-behavior of the solvent resistance R_1 (see Randles circuit in FIG. **13**B). The three distinct sections in the graph indicate the signals from the blank sensor, the membrane coating process and the PmB buffer respectively. Importantly, the increase in R_0, the increase in the Warburg coefficient as well as decrease in the constant phase element coefficient CPF_0_0 during the

elution of Buffer B indicates the coating of the sensor with the hybrid membrane. Consequently, the decrease in the membrane's resistance R_0 after the introduction of Buffer 3 indicates a PmB induced damage.

[0048] FIGS. **19**A-**19**G are graphs showing results of electrochemical impedance spectroscopy (EIS) of synthetic *E. coli* membrane with POPE:POPG:CL at a molar ratio of 67:23.2:9.8 (Synthetic_E_coli_PEPGCL_Sensor_1). For the description of individual figures, see the description for FIGS. **18**A-**18**G above. Importantly, the increase in R_0, the increase in the Warburg coefficient as well as decrease in the constant phase element coefficient CPF_0_0 during the elution of Buffer B indicates the coating of the sensor with the hybrid membrane. Consequently, the decrease in the membrane's resistance R_0 after the introduction of Buffer 3 indicates a PmB induced damage.

[0049] FIGS. **20**A-**20**G are graphs showing results of electrochemical impedance spectroscopy (EIS) of synthetic *E. coli* membrane with POPE:POPG:CL at a molar ratio of 67:23.2:9.8 (Synthetic_E_coli_PEPGCL Sensor2). For the description of individual figures, see the description for FIGS. **18**A-**18**G above. Importantly, the increase in R_0, the increase in the Warburg coefficient as well as decrease in the constant phase element coefficient CPF_0_0 during the elution of Buffer B indicates the coating of the sensor with the lipid bilayer. Consequently, the decrease in the membrane's resistance R_0 after the introduction of Buffer 3 indicates a PmB induced damage.

[0050] FIGS. **21**A-**21**G are graphs showing results of electrochemical impedance spectroscopy (EIS) of synthetic *E. coli* membrane with POPE:POPG:CL at a molar ratio of 67:23.2:9.8 (Synthetic_E_coli PEPGCL_Sensor3). For the description of individual figures, see the description for FIGS. **18**A-**18**G above. Importantly, the increase in R_0, the increase in the Warburg coefficient as well as decrease in the constant phase element coefficient CPF_0_0 during the elution of Buffer B indicates the coating of the sensor with the lipid bilayer. Consequently, the decrease in the membrane's resistance R_0 after the introduction of Buffer 3 indicates a PmB induced damage.

[0051] FIGS. **22**A-**22**G are graphs showing results of electrochemical impedance spectroscopy (EIS) of synthetic *E. coli* membrane with POPE:POPG:CL at a molar ratio of 67:23.2:9.8 (Synthetic_E_coli_PEPGCL_Sensor4). For the description of individual figures, see the description for FIGS. **18**A-**18**G above. Importantly, the increase in R_0, the increase in the Warburg coefficient as well as decrease in the constant phase element coefficient CPF_0_0 during the elution of Buffer B indicates the coating of the sensor with the lipid bilayer. Consequently, the decrease in the membrane's resistance R_0 after the introduction of Buffer 3 indicates a PmB induced damage.

[0052] FIGS. **23**A-**23**G are graphs showing results of electrochemical impedance spectroscopy (EIS) of synthetic *E. coli* membrane with POPE:POPG:CL at a molar ratio of 78:21:0 (Synthetic_*E_coli*_PEPG_Sensor1). For the description of individual figures, see the description for FIGS. **18**A-**18**G above. Importantly, the increase in R_0, the increase in the Warburg coefficient as well as decrease in the constant phase element coefficient CPF_0_0 during the elution of Buffer B indicates the coating of the sensor with the lipid bilayer. Consequently, the decrease in the membrane's resistance R_0 after the introduction of Buffer 3 indicates a PmB induced damage.

[0053] FIGS. **24**A-**24**G are graphs showing results of electrochemical impedance spectroscopy (EIS) of synthetic *E. coli* membrane with POPE:POPG:CL at a molar ratio of 78:21:0 (Synthetic_*E_coli*_PEPG_Sensor2). For the description of individual figures, see the description for FIGS. **18**A-**18**G above. Importantly, the increase in R_0, the increase in the Warburg coefficient as well as decrease in the constant phase element coefficient CPF_0_0 during the elution of Buffer B indicates the coating of the sensor with the lipid bilayer. Consequently, the decrease in the membrane's resistance R_0 after the introduction of Buffer 3 indicates a PmB induced damage.

[0054] FIGS. **25**A-**25**G are graphs showing results of electrochemical impedance spectroscopy (EIS) of synthetic *E. coli* membrane with POPE:POPG:CL at a molar ratio of 78:21:0 (Synthetic_*E_coli*_PEPG_Sensor3). For the description of individual figures, see the description for FIGS. **18**A-**18**G above. Importantly, the increase in R_0, the increase in the Warburg coefficient as well as decrease in the constant phase element coefficient CPF_0_0 during the elution of Buffer B indicates the coating of the sensor with the lipid bilayer. Consequently, the decrease in the membrane's resistance R_0 after the introduction of Buffer 3 indicates a PmB induced damage.

[0055] FIGS. **26**A-**26**G are graphs showing results of electrochemical impedance spectroscopy (EIS) of synthetic *E. coli* membrane with POPE:POPG:CL at a molar ratio of 78:21:0 (Synthetic_*E_coli*_PEPG_Sensor4). For the description of individual figures, see the description for FIGS. **18**A-**18**G above. Importantly, the increase in R_0, the increase in the Warburg coefficient as well as decrease in the constant phase element coefficient CPF_0_0 during the elution of Buffer B indicates the coating of the sensor with the lipid bilayer. Consequently, the decrease in the membrane's resistance R_0 indicates 0 after the introduction of Buffer 3 indicates a PmB induced damage.

[0056] FIGS. **27**A-**27**G are graphs showing results of electrochemical impedance spectroscopy (EIS) of synthetic *E. coli* membrane with POPE:POPG:CL at a molar ratio of 90:0:10 (Synthetic_*E_coli*_PECL_Senso1). For the description of individual figures, see the description for FIGS. **18**A-**18**G above. Importantly, the increase in R_0, the increase in the Warburg coefficient as well as decrease in the constant phase element coefficient CPF_0_0 during the elution of Buffer B indicates the coating of the sensor with the lipid bilayer. Consequently, the increase in the membrane's resistance R_0 after the introduction of Buffer 3 indicates an accumulation of PmB on the membrane's surface.

[0057] FIGS. **28**A-**28**G are graphs showing results of electrochemical impedance spectroscopy (EIS) of synthetic *E. coli* membrane with POPE:POPG:CL at a molar ratio of 90:0:10 (Synthetic_*E_coli*_PECL_Sensor2). For the description of individual figures, see the description for FIGS. **18**A-**18**G above. Importantly, the increase in R_0, the increase in the Warburg coefficient as well as decrease in the constant phase element coefficient CPF_0_0 during the elution of Buffer B indicates the coating of the sensor with the lipid bilayer. Consequently, the increase in the membrane's resistance R_0 after the introduction of Buffer 3 indicates an accumulation of PmB on the membrane's surface.

[0058] FIGS. **29**A-**29**G are graphs showing results of electrochemical impedance spectroscopy (EIS) of synthetic

E. coli membrane with POPE:POPG:CL at a molar ratio of 0:80:20 (Synthetic_*E_coli*_PGCL_Sensor1). For the description of individual figures, see the description for FIGS. **18**A-**18**G above. Importantly, the increase in R_0, the increase in the Warburg coefficient as well as decrease in the constant phase element coefficient CPF_0_0 during the elution of Buffer B indicates the coating of the sensor with the lipid bilayer. Consequently, the decrease in the membrane's resistance R 0 after the introduction of Buffer 3 indicates a PmB induced damage.

[0059] FIGS. **30**A-**30**G are graphs showing results of electrochemical impedance spectroscopy (EIS) of *E. coli* membrane (*E_coli*_Sensor1). For the description of individual figures, see the description for FIGS. **18**A-**18**G above. Importantly, the increase in R_0, the increase in the Warburg coefficient as well as decrease in the constant phase element coefficient CPF_0_0 during the elution of Buffer B indicates the coating of the sensor with the lipid bilayer. Consequently, the decrease in the membrane's resistance R_0 after the introduction of Buffer 3 indicates a PmB induced damage.

[0060] FIGS. **31**A-**31**G are graphs showing results of electrochemical impedance spectroscopy (EIS) of *E. coli* membrane (*E_coli*_Sensor2). For the description of individual figures, see the description for FIGS. **18**A-**18**G above. Importantly, the increase in R_0, the increase in the Warburg coefficient as well as decrease in the constant phase element coefficient CPF_0_0 during the elution of Buffer B indicates the coating of the sensor with the lipid bilayer. Consequently, the decrease in the membrane's resistance R_0 after the introduction of Buffer 3 indicates a PmB induced damage.

[0061] FIGS. **32**A-**32**G are graphs showing results of electrochemical impedance spectroscopy (EIS) of *E. coli* membrane (*E_coli*_Sensor3).

[0062] FIG. **33** is a series of graphs showing membrane resistance. Renal membrane analogues were formed on a gold sensor, and dielectric membrane properties were measured by EIS. Membrane resistance (R_m) is a very sensitive measure to detect membrane damage as this resistance drops when pores form and the redox-active molecule ferricyanide can reach the electrode. A sample buffe consisting of either 25 μg/mL polymyxin B (PmB), 25 μg/mL of PmB in the erythro-PmBs, or 4.5 mg/mL of erythrocyte liposomes in 5 mM potassium hexacyanoferrate(III) ($K_3[Fe(CN)_6]$) was pumped into the chamber. (Left panel) For free PmB, R. initially increases when the membrane is formed on the sensor. When treated with PmB, the PmB molecules start to accumulate on the membrane surface and resistance increases before sharply dropping as a result of membrane damage. (Middle panel) When exposed to erythrocyte liposomes, the increase of R. is indicative of liposomes attaching to the membrane on the sensor. (Right panel) For erythro-PmBs, R. keeps increasing as a result of liposome attachment. There is no drop in resistance, which would be indicative of membrane damage.

[0063] Further aspects and features of the example embodiments described herein will appear from the following description taken together with the accompanying drawings.

DETAILED DESCRIPTION

[0064] Unless otherwise indicated, the definitions and embodiments described in this and other sections are intended to be applicable to all embodiments and aspects of the present application herein described for which they are suitable as would be understood by a person skilled in the art.

[0065] In understanding the scope of the present application, the term "comprising" and its derivatives, as used herein, are intended to be open ended terms that specify the presence of the stated features, elements, components, groups, integers, and/or steps, but do not exclude the presence of other unstated features, elements, components, groups, integers and/or steps. The foregoing also applies to words having similar meanings such as the terms, "including", "having" and their derivatives. The term "consisting" and its derivatives, as used herein, are intended to be closed terms that specify the presence of the stated features, elements, components, groups, integers, and/or steps, but exclude the presence of other unstated features, elements, components, groups, integers and/or steps. The term "consisting essentially of", as used herein, is intended to specify the presence of the stated features, elements, components, groups, integers, and/or steps as well as those that do not materially affect the basic and novel characteristic(s) of features, elements, components, groups, integers, and/or steps.

[0066] Terms of degree such as "substantially", "about" and "approximately" as used herein mean a reasonable amount of deviation of the modified term such that the end result is not significantly changed. These terms of degree should be construed as including a deviation of at least ±5% of the modified term if this deviation would not negate the meaning of the word it modifies.

[0067] More specifically, the term "about" means plus or minus 0.1 to 20%, 5-20%, or 10-20%, 10%-15%, preferably 5-10%, most preferably about 5% of the number to which reference is being made.

[0068] The recitation of numerical ranges by endpoints herein includes all numbers and fractions subsumed within that range (e.g., 1 to 5 includes 1, 1.5, 2, 2.75, 3, 3.90, 4, and 5). It is also to be understood that all numbers and fractions thereof are presumed to be modified by the term "about."

[0069] The term "and/or" as used herein means that the listed items are present, or used, individually or in combination. In effect, this term means that "at least one of" or "one or more" of the listed items is used or present.

[0070] In one aspect, there is provided a biosensor comprising a multi-lamellar lipid membrane structure. An example multi-lamellar lipid membrane structure comprising two lipid bilayers is shown in FIG. **5**. In at least one embodiment, the biosensor comprises a solid substrate having a lipid bilayer compatible surface and a multi-lamellar lipid membrane structure derived from a plurality of biological cells and localized on the lipid bilayer compatible surface. In at least one embodiment, there is an aqueous layer interposed between each lipid layer of the multi-lamellar lipid membrane structure.

[0071] In at least one embodiment, the substrate comprises a lipid bilayer compatible surface that is selected or configured to allow for the localization of the multi-lamellar lipid membrane structure adjacent to the surface. In an example embodiment, the surface is a planar surface. In one embodiment, the lipid bilayer compatible surface is hydrophilic.

[0072] In at least one embodiment, the multi-lamellar lipid membrane structure may be derived or prepared from red blood cells. In at least one embodiment, the multi-lamellar

lipid membrane structure is derived from red blood cell ghosts. As shown in FIG. **1** and detailed in the Examples, incubating a preparation of red blood cell ghosts on a lipid bilayer compatible surface results in the annealing of the individual cell ghosts into a multi-lamellar lipid membrane structure adjacent to the lipid bilayer compatible surface. In at least one embodiment, the multi-lamellar lipid membrane structure is a single bilayer. In at least one embodiment, the multi-lamellar lipid membrane structure is made of between 2 and about 1,000 stacked lipid bilayers. In at least one embodiment, the multi-lamellar lipid membrane structure is made of two stacked lipid bilayers.

[0073] In at least one embodiment, the multi-lamellar lipid membrane structure is formed by incubating the lipid bilayer compatible surface with the preparation of red blood cell ghosts, wherein the red blood cell ghosts anneal to form the multi-lamellar lipid membrane structure. In at least one embodiment, the cell ghosts are incubated at a temperature greater than about 30° C., 35° C., or 40° C. In at least one embodiment, the cell ghosts are incubated at a temperature between about 30° C. and 60° C. In one embodiment, the temperature is about 30° C., 35° C., 37° C., 40° C., 45° C. or 50° C. In at least one embodiment the temperature is between about 35° C. and 55° C., or between about 35° C. and 40° C.

[0074] As demonstrated in the Examples, the formation of a multi-lamellar lipid membrane structure is improved under humid conditions. Accordingly, in at least one embodiment the cell ghosts are incubated at a relative humidity greater than 50%. In one at least embodiment, the relative humidity is greater than 50%, 60%, 70%, 80%, 85% or 90%. In at least one embodiment, the relative humidity is between about 70% and 100%, optionally between about 80% and 95%.

[0075] In at least one embodiment, the biological cells, optionally cell ghosts, are incubated in the presence of a salt or salt solution. For example, in at least one embodiment the substrate is incubated on a platform above a salt solution. In at least one embodiment, the salt solution is a potassium sulfate solution, optionally a saturated potassium sulfate solution. In at least one embodiment, the salt is potassium sulfate, lithium chloride, potassium acetate, magnesium chloride, potassium carbonate, magnesium nitrate, sodium chloride, potassium chloride, potassium nitrate, potassium sulfate, or combinations thereof

[0076] In another aspect, provided herein in at least one embodiment is a biosensor comprising a solid substrate having a lipid bilayer compatible surface; and a multi-lamellar lipid membrane structure localized on the lipid bilayer compatible surface, the multi-lamellar lipid membrane structure being prepared from red blood cells or red blood cell ghosts and comprises one or more synthetic lipids.

[0077] The term "synthetic lipid" as used herein refers to a lipid that is not wholly derived from a natural source. A synthetic lipid can be, for example, obtained by a chemical or biotechnological process. A synthetic lipid can also be prepared from a compound that is derived from a natural source, so that a portion of the synthetic lipid molecule is derived from that natural source. For example, a synthetic lipid can be prepared from glycerol or glycerol-3-phosphocholine (GPC) derived from a plant or animal source.

[0078] In at least one embodiment, the one or more synthetic lipids comprises a phosphatidylcholine (PC).

[0079] In at least one embodiment, the concentration of the PC in the multi-lamellar lipid membrane structure is between about 10 mass % to about 90 mass %. In at least one embodiment, the concentration of the PC in the multi-lamellar lipid membrane structure is between about 20 mass % to about 80 mass %. In at least one embodiment, the concentration of the PC in the multi-lamellar lipid membrane structure is between about 30 mass % to about 70 mass %. In at least one embodiment, the concentration of the PC in the multi-lamellar lipid membrane structure is between about 40 mass % to about 60 mass %. In at least one embodiment, the concentration of the PC in the multi-lamellar lipid membrane structure is between about 45 mass % to about 55 mass %.

[0080] In at least one embodiment, the concentration of the PC in the multi-lamellar lipid membrane structure is about 10 mass %. In at least one embodiment, the concentration of the PC in the multi-lamellar lipid membrane structure is about 20 mass %. In at least one embodiment, the concentration of the PC in the multi-lamellar lipid membrane structure is about 50 mass %. In at least one embodiment, the concentration of the PC in the multi-lamellar lipid membrane structure is about 80 mass %. In at least one embodiment, the concentration of the PC in the multi-lamellar lipid membrane structure is about 90 mass %.

[0081] In at least one embodiment, the PC comprises 1,2-dimyristoyl-sn-glycero-3-phosphocholine (DMPC).

[0082] In at least one embodiment, the concentration of the DMPC in the multi-lamellar lipid membrane structure is between about 10 mass % to about 90 mass %. In at least one embodiment, the concentration of the DMPC in the multi-lamellar lipid membrane structure is between about 20 mass % to about 80 mass %. In at least one embodiment, the concentration of the DMPC in the multi-lamellar lipid membrane structure is between about 30 mass % to about 70 mass %. In at least one embodiment, the concentration of the DMPC in the multi-lamellar lipid membrane structure is between about 40 mass % to about 60 mass %. In at least one embodiment, the concentration of the DMPC in the multi-lamellar lipid membrane structure is between about 45 mass % to about 55 mass %.

[0083] In at least one embodiment, the concentration of the DMPC in the multi-lamellar lipid membrane structure is about 10 mass %. In at least one embodiment, the concentration of the DMPC in the multi-lamellar lipid membrane structure is about 20 mass %. In at least one embodiment, the concentration of the DMPC in the multi-lamellar lipid membrane structure is about 50 mass %. In at least one embodiment, the concentration of the DMPC in the multi-lamellar lipid membrane structure is about 80 mass %. In at least one embodiment, the concentration of the DMPC in the multi-lamellar lipid membrane structure is about 90 mass %.

[0084] In at least one embodiment, the PC comprises and 1-palmitoyl-2-oleoyl-glycero-3-phosphocholine (POPC).

[0085] In at least one embodiment, the concentration of the POPC in the multi-lamellar lipid membrane structure is between about 10 mass % to about 90 mass %. In at least one embodiment, the concentration of the POPC in the multi-lamellar lipid membrane structure is between about 20 mass % to about 80 mass %. In at least one embodiment, the concentration of the POPC in the multi-lamellar lipid membrane structure is between about 30 mass % to about 70 mass %. In at least one embodiment, the concentration of the POPC in the multi- lamellar lipid membrane structure is

between about 40 mass % to about 60 mass %. In at least one embodiment, the concentration of the POPC in the multi-lamellar lipid membrane structure is between about 45 mass % to about 55 mass %.

[0086] In at least one embodiment, the concentration of the POPC in the multi-lamellar lipid membrane structure is about 10 mass %. In at least one embodiment, the concentration of the POPC in the multi-lamellar lipid membrane structure is about 20 mass %. In at least one embodiment, the concentration of the POPC in the multi-lamellar lipid membrane structure is about 50 mass %. In at least one embodiment, the concentration of the POPC in the multi-lamellar lipid membrane structure is about 80 mass %. In at least one embodiment, the concentration of the POPC in the multi-lamellar lipid membrane structure is about 90 mass %.

[0087] In at least one embodiment, the one or more synthetic lipids comprises a phosphatidylethanolamine (PE).

[0088] In at least one embodiment, the concentration of the PE in the multi-lamellar lipid membrane structure is between about 10 mass % to about 90 mass %. In at least one embodiment, the concentration of the PE in the multi-lamellar lipid membrane structure is between about 20 mass % to about 80 mass %. In at least one embodiment, the concentration of the PE in the multi-lamellar lipid membrane structure is between about 30 mass % to about 70 mass %. In at least one embodiment, the concentration of the PE in the multi-lamellar lipid membrane structure is between about 40 mass % to about 60 mass %. In at least one embodiment, the concentration of the PE in the multi-lamellar lipid membrane structure is between about 45 mass % to about 55 mass %.

[0089] In at least one embodiment, the concentration of the PE in the multi-lamellar lipid membrane structure is about 10 mass %. In at least one embodiment, the concentration of the PE in the multi-lamellar lipid membrane structure is about 20 mass %. In at least one embodiment, the concentration of the PE in the multi-lamellar lipid membrane structure is about 50 mass %. In at least one embodiment, the concentration of the PE in the multi-lamellar lipid membrane structure is about 80 mass %. In at least one embodiment, the concentration of the PE in the multi-lamellar lipid membrane structure is about 90 mass %.

[0090] In at least one embodiment, the one or more synthetic lipids comprises a phosphatidylserine (PS).

[0091] In at least one embodiment, the concentration of the PS in the multi-lamellar lipid membrane structure is between about 10 mass % to about 50 mass %. In at least one embodiment, the concentration of the PS in the multi-lamellar lipid membrane structure is between about 20 mass % to about 40 mass %. In at least one embodiment, the concentration of the PS in the multi-lamellar lipid membrane structure is between about 23 mass % to about 35 mass %.

[0092] In at least one embodiment, the concentration of the PS in the multi-lamellar lipid membrane structure is about 10 mass %. In at least one embodiment, the concentration of the PS in the multi-lamellar lipid membrane structure is about 20 mass %. In at least one embodiment, the concentration of the PS in the multi-lamellar lipid membrane structure is about 50 mass %.

[0093] In at least one embodiment, the PS comprises 1-palmitoyl-2-oleoyl-sn-glycero-3-phospho-L-serine (POPS).

[0094] In at least one embodiment, the concentration of the POPS in the multi-lamellar lipid membrane structure is between about 10 mass % to about 50 mass %. In at least one embodiment, the concentration of the POPS in the multi-lamellar lipid membrane structure is between about 20 mass % to about 40 mass %. In at least one embodiment, the concentration of the POPS in the multi-lamellar lipid membrane structure is between about 23 mass % to about 35 mass %.

[0095] In at least one embodiment, the concentration of the POPS in the multi-lamellar lipid membrane structure is about 10 mass %. In at least one embodiment, the concentration of the POPS in the multi-lamellar lipid membrane structure is about 20 mass %. In at least one embodiment, the concentration of the POPS in the multi-lamellar lipid membrane structure is about 50 mass %.

[0096] In at least one embodiment, the PS comprises 1,2-dimyristoyl-sn-glycero-3-phospho-L-serine (DMFS).

[0097] In at least one embodiment, the concentration of the DMPS in the multi-lamellar lipid membrane structure is between about 10 mass % to about 50 mass %. In at least one embodiment, the concentration of the DMPS in the multi-lamellar lipid membrane structure is between about 20 mass % to about 40 mass %. In at least one embodiment, the concentration of the DMPS in the multi-lamellar lipid membrane structure is between about 23 mass % to about 35 mass %.

[0098] In at least one embodiment, the concentration of the DMPS in the multi-lamellar lipid membrane structure is about 10 mass %. In at least one embodiment, the concentration of the DMPS in the multi-lamellar lipid membrane structure is about 20 mass %. In at least one embodiment, the concentration of the DMPS in the multi-lamellar lipid membrane structure is about 50 mass %.

[0099] In at least one embodiment, the one or more synthetic lipids comprises a phosphatidylglycerol (PG).

[0100] In at least one embodiment, the concentration of the PG in the multi-lamellar lipid membrane structure is between about 10 mass % to about 50 mass %. In at least one embodiment, the concentration of the PG in the multi-lamellar lipid membrane structure is between about 20 mass % to about 40 mass %. In at least one embodiment, the concentration of the PG in the multi-lamellar lipid membrane structure is between about 23 mass % to about 35 mass %.

[0101] In at least one embodiment, the concentration of the PG in the multi-lamellar lipid membrane structure is about 10 mass %. In at least one embodiment, the concentration of the PG in the multi-lamellar lipid membrane structure is about 20 mass %. In at least one embodiment, the concentration of the PG in the multi-lamellar lipid membrane structure is about 50 mass %.

[0102] In at least one embodiment, the PG comprises 1-palmitoyl-2-oleoyl-sn-glycero-3-phospho-(1'-rac-glycerol) (POPG).

[0103] In at least one embodiment, the concentration of the POPG in the multi-lamellar lipid membrane structure is between about 10 mass % to about 50 mass %. In at least one embodiment, the concentration of the POPG in the multi-lamellar lipid membrane structure is between about 20 mass % to about 40 mass %. In at least one embodiment, the concentration of the POPG in the multi-lamellar lipid membrane structure is between about 23 mass % to about 35 mass %.

[0104] In at least one embodiment, the concentration of the POPG in the multi-lamellar lipid membrane structure is

about 10 mass %. In at least one embodiment, the concentration of the POPG in the multi-lamellar lipid membrane structure is about 20 mass %. In at least one embodiment, the concentration of the POPG in the multi-lamellar lipid membrane structure is about 50 mass %.

[0105] In at least one embodiment, the one or more synthetic lipids are selected from the group consisting of 1,2-dimyristoyl-sn-glycero-3-phosphocholine (DMPC), 1-palmitoyl oleoyl-glycero-3-phosphocholine (POPC), 1-palmitoyl-2-ol eoyl- sn-glycero-3-phospho-L-serine (POPS), 1,2-dimyristoyl-sn-glycero-3-phospho-L-serine (DMPS), and 1-palmitoyl-2-oleoyl-sn-glycero-3-phospho-(1'-rac-glycerol) (POPG).

[0106] As known by a person skilled in the art, a fatty acid chain on a lipid can be described by the number of carbons in the fatty acid chain and the number of double bonds in the fatty acid chain. The numbers are generally presented in the format X:Y, where X means the number of carbons in fatty acid chain and Y means the number of double bonds in fatty acid chain. For example, 18:1 means 18 carbons in the fatty acid chain with one double bonds. For lipids containing two fatty acid chains such as a phospholipid, when only one X:Y is given it means that both fatty acids are the same.

[0107] In at least one embodiment, the one or more synthetic lipids comprises at least one fatty acid chain, wherein each fatty acid chain can have between 12 carbons and 40 carbons with up to 6 double bonds.

[0108] In at least one embodiment, the fatty acid chain has 12 carbons. In at least one embodiment, the fatty acid chain has 13 carbons. In at least one embodiment, the fatty acid chain has 14 carbons. In at least one embodiment, the fatty acid chain has 15 carbons. In at least one embodiment, the fatty acid chain has 16 carbons. In at least one embodiment, the fatty acid chain has 17 carbons. In at least one embodiment, the fatty acid chain has 18 carbons. In at least one embodiment, the fatty acid chain has 19 carbons. In at least one embodiment, the fatty acid chain has 20 carbons. In at least one embodiment, the fatty acid chain has 21 carbons. In at least one embodiment, the fatty acid chain has 22 carbons. In at least one embodiment, the fatty acid chain has 23 carbons. In at least one embodiment, the fatty acid chain has 24 carbons. In at least one embodiment, the fatty acid chain has 25 carbons. In at least one embodiment, the fatty acid chain has 26 carbons. In at least one embodiment, the fatty acid chain has 27 carbons. In at least one embodiment, the fatty acid chain has 28 carbons. In at least one embodiment, the fatty acid chain has 29 carbons. In at least one embodiment, the fatty acid chain has 30 carbons. In at least one embodiment, the fatty acid chain has 31 carbons. In at least one embodiment, the fatty acid chain has 32 carbons. In at least one embodiment, the fatty acid chain has 33 carbons. In at least one embodiment, the fatty acid chain has 34 carbons. In at least one embodiment, the fatty acid chain has 35 carbons. In at least one embodiment, the fatty acid chain has 36 carbons. In at least one embodiment, the fatty acid chain has 37 carbons. In at least one embodiment, the fatty acid chain has 38 carbons. In at least one embodiment, the fatty acid chain has 39 carbons. In at least one embodiment, the fatty acid chain has 40 carbons.

[0109] In at least one embodiment, the fatty acid chain has no double bond. In at least one embodiment, the fatty acid chain has 1 double bond. In at least one embodiment, the fatty acid chain has 2 double bonds. In at least one embodiment, the fatty acid chain has 3 double bonds. In at least one embodiment, the fatty acid chain has 4 double bonds. In at least one embodiment, the fatty acid chain has 5 double bonds. In at least one embodiment, the fatty acid chain has 6 double bonds.

[0110] In at least one embodiment, the multi-lamellar lipid membrane structure further comprises one or more lipids conjugated with polyethylene glycol (PEGylated lipids).

[0111] In at least one embodiment, the concentration of the one or more synthetic lipids is in the multi-lamellar lipid membrane structure up to about 10 mass % and the concentration of the PEGylated lipids in the multi-lamellar lipid membrane structure is up to about 10 mass %.

[0112] In at least one embodiment, the PEG has an average molecular weight of about 44 g/mol to about 5000 g/mol.

[0113] In at least one embodiment, the PEG is PEG 350. In at least one embodiment, the PEG is PEG550. In at least one embodiment, the PEG is PEG 750. In at least one embodiment, the PEG is PEG1000. In at least one embodiment, the PEG is PEG2000. In at least one embodiment, the PEG is PEG3000. In at least one embodiment, the PEG is PEG5000.

[0114] In at least one embodiment, the one or more PEGylated lipids comprises PEGylated phosphatidylethanolamine (PE).

[0115] In at least one embodiment, the PEGylated PE comprises 1,2-dioleoyl-sn-glycero-3-phosphoethanolamine (DOPE).

[0116] In at least one embodiment, the fatty acid chains of the DOPE have a length of 18 carbons. In one embodiment, the fatty acid chains of the DOPE have a length of 16 carbons. In at least one embodiment, the fatty acid chains of the DOPE have a length of 14 carbons.

[0117] In at least one embodiment, the fatty acid chains of the DOPE have one double bond. In one embodiment, the fatty acid chains of the DOPE have zero double bond.

[0118] In at least one embodiment, the PEGylated lipid is 18:1 PEG350 DOPE. In one embodiment, the PEGylated lipid is 18:0 PEG350 DOPE. In at least one embodiment, the PEGylated lipid is 14:0 PEG350 DOPE. In at least one embodiment, the PEGylated lipid is 16:0 PEG350 DOPE.

[0119] In at least one embodiment, the PEGylated lipid is 18:1 PEG550 DOPE. In at least one embodiment, the PEGylated lipid is 18:0 PEG550 DOPE. In at least one embodiment, the PEGylated lipid is 14:0 PEG550 DOPE. In at least one embodiment, the PEGylated lipid is 16:0 PEG550 DOPE.

[0120] In at least one embodiment, the PEGylated lipid is 18:1 PEG750 DOPE. In at least one embodiment, the PEGylated lipid is 18:0 PEG750 DOPE. In at least one embodiment, the PEGylated lipid is 14:0 PEG750 DOPE. In at least one embodiment, the PEGylated lipid is 16:0 PEG750 DOPE.

[0121] In at least one embodiment, the PEGylated lipid is 18:1 PEG1000 DOPE. In at least one embodiment, the PEGylated lipid is 18:0 PEG1000 DOPE. In at least one embodiment, the PEGylated lipid is 14:0 PEG1000 DOPE. In at least one embodiment, the PEGylated lipid is 16:0 PEG1000 DOPE.

[0122] In at least one embodiment, the PEGylated lipid is 18:1 PEG2000 DOPE. In one embodiment, the PEGylated lipid is 18:0 PEG2000 DOPE. In at least one embodiment, the PEGylated lipid is 14:0 PEG2000 DOPE. In at least one embodiment, the PEGylated lipid is 16:0 PEG2000 DOPE.

[0123] In at least one embodiment, the PEGylated lipid is 18:1 PEG3000 DOPE. In at least one embodiment, the PEGylated lipid is 18:0 PEG3000 DOPE. In at least one embodiment, the PEGylated lipid is 14:0 PEG3000 DOPE. In at least one embodiment, the PEGylated lipid is 16:0 PEG3000 DOPE.

[0124] In at least one embodiment, the PEGylated lipid is 18:1 PEG5000 DOPE. In one embodiment, the PEGylated lipid is 18:0 PEG5000 DOPE. In at least one embodiment, the PEGylated lipid is 14:0 PEG5000 DOPE. In at least one embodiment, the PEGylated lipid is 16:0 PEG5000 DOPE.

[0125] In at least one embodiment, the PEGylated PE comprises PEGylated 1,2-Distearoyl-sn-glycero-3-phosphoethanolamine (DSPE).

[0126] In at least one embodiment, the fatty acid chains of the DSPE have a length of 18 carbons. In at least one embodiment, the fatty acid chains of the DSPE have a length of 16 carbons. In at least one embodiment, the fatty acid chains of the DSPE have a length of 14 carbons.

[0127] In at least one embodiment, the fatty acid chains of the DSPE have one double bond. In at least one embodiment, the fatty acid chains of the DSPE have zero double bond.

[0128] In at least one embodiment, the PEGylated lipid is 18:1 PEG350 DSPE. In one embodiment, the PEGylated lipid is 18:0 PEG350 DSPE. In at least one embodiment, the PEGylated lipid is 14:0 PEG350 DSPE. In at least one embodiment, the PEGylated lipid is 16:0 PEG350 D DSPE.

[0129] In at least one embodiment, the PEGylated lipid is 18:1 PEG550 DSPE. In at least one embodiment, the PEGylated lipid is 18:0 PEG550 DSPE. In at least one embodiment, the PEGylated lipid is 14:0 PEG550 DSPE. In at least one embodiment, the PEGylated lipid is 16:0 PEG550 DSPE.

[0130] In at least one embodiment, the PEGylated lipid is 18:1 PEG750 DSPE. In at least one embodiment, the PEGylated lipid is 18:0 PEG750 DSPE. In at least one embodiment, the PEGylated lipid is 14:0 PEG750 DSPE. In at least one embodiment, the PEGylated lipid is 16:0 PEG750 DSPE.

[0131] In at least one embodiment, the PEGylated lipid is 18:1 PEG1000 DSPE. In at least one embodiment, the PEGylated lipid is 18:0 PEG1000 DSPE. In at least one embodiment, the PEGylated lipid is 14:0 PEG1000 DSPE. In at least one embodiment, the PEGylated lipid is 16:0 PEG1000 DSPE.

[0132] In at least one embodiment, the PEGylated lipid is 18:1 PEG2000 DSPE. In one embodiment, the PEGylated lipid is 18:0 PEG2000 DSPE. In at least one embodiment, the PEGylated lipid is 14:0 PEG2000 DSPE. In at least one embodiment, the PEGylated lipid is 16:0 PEG2000 DSPE.

[0133] In at least one embodiment, the PEGylated lipid is 18:1 PEG3000 DSPE. In at least one embodiment, the PEGylated lipid is 18:0 PEG3000 DSPE. In at least one embodiment, the PEGylated lipid is 14:0 PEG3000 DSPE. In at least one embodiment, the PEGylated lipid is 16:0 PEG3000 DSPE.

[0134] In at least one embodiment, the PEGylated lipid is 18:1 PEG5000 DSPE. In one embodiment, the PEGylated lipid is 18:0 PEG5000 DSPE. In at least one embodiment, the

[0135] PEGylated lipid is 14:0 PEG5000 DSPE. In at least one embodiment, the PEGylated lipid is 16:0 PEG5000 DSPE.

[0136] In at least one embodiment, the one or more PEGylated lipids comprises cholesterol. In at least one embodiment, the PEG is PEG600.

[0137] In at least one embodiment, the one or more PEGylated lipids comprises cholesterol-PEG600.

[0138] In at least one embodiment, the one or more PEGylated lipids comprises a functionalized PEGylated lipid, the functionalized PEG lipid comprises a functionalized group. A functionalized group can be, for example, maleimide, biotin, succinyl, cyanur, folate, pyridyldithio propionyl (pdp), carboxylic acid, a squarate, benzylguanine, carboxy N-Hydroxysuccinimide ester (NHS), dibenzocyclooctyl (DBCO), azide, 6-chlorohexylcarbonyltriethylene glycol or an amine.

[0139] In at least one embodiment, the functionalized PEGylated lipid comprises 1,2-Distearoyl-sn-glycero-3-phosphoethanolamine (DSPE). In at least one embodiment, the PEGylated is PEG2000 or PEG5000. In at least one embodiment, the functionalized group is maleimide, biotin, or amine.

[0140] In at least one embodiment, the PEGylated lipid comprises DSPE-PEG(2000) maleimide. In at least one embodiment, the PEG lipid comprises DSPE-PEG(2000) biotin. In at least one embodiment, the PEG lipid comprises DSPE-PEG(5000) amine. In at least one embodiment, the PEG lipid comprises DSPE-PEG(5000) maleimide. In at least one embodiment, the PEG lipid comprises DSPE-PEG (2000) amine.

[0141] In at least one embodiment, the PEG is methoxy PEG (mPEG).

[0142] In at least one embodiment, the multi-lamellar lipid membrane structure derived from red blood cells or red blood cell ghosts and comprises 1-palmitoyl-2-oleoyl-sn-glycero-3-phospho-L-serine (POPS) and one or more PEGylated lipids. In at least one embodiment, the lipid membrane structure derived from red blood cells or red blood cell ghosts and comprises 1,2-dimyristoyl-sn-glycero-3-phospho-L-serine (DMPS) and one or more PEGylated lipids.

[0143] In at least one embodiment, the concentration of 1-palmitoyl-2-oleoyl-sn-glycero-3-phospho-L-serine (POPS) or 1,2-dimyristoyl-sn-glycero-3-phospho-L-serine (DMPS) in the multi-lamellar lipid structure is up to about 10 mass %. In at least one embodiment, the concentration of PEGylated lipids in the multi-lamellar lipid membrane structure is up to about 10mass %.

[0144] In at least one embodiment, the concentration of 1-palmitoyl-2-oleoyl-sn-glycero-3-phospho-L-serine (POPS) in the multi-lamellar lipid structure is up to about 10 mass % and the concentration of PEGylated lipids in the multi-lamellar lipid membrane structure is up to about 10 mass %.

[0145] In at least one embodiment, the concentration of 1,2-dimyristoyl-sn-glycero phospho-L-serine (DMFS) in the multi-lamellar lipid structure is up to about 10 mass % and the concentration of PEGylated lipids in the multi-lamellar lipid membrane structure is up to about 10 mass %.

[0146] In another aspect, provided herein in at least one embodiment is a biosensor comprising a solid substrate having a lipid bilayer compatible surface; and a multi-lamellar lipid membrane structure localized on the lipid bilayer compatible surface, the multi-lamellar lipid membrane structure comprises two or more synthetic lipids comprising a phosphatidylethanolamine (PE), a phosphati-

dylglycerol (PG), a phosphatidylcholine (PC), a phosphatidylserine (PS), a cholesterol, and/or a cardiolipin (CL).

[0147] In at least one embodiment, the two or more synthetic lipids are PE, PG and CL. In at least one embodiment, the concentration of the PE in the multi-lamellar lipid membrane structure is between about 67 mass % to about 71 mass %. In at least one embodiment, the concentration of the PG is in the multi-lamellar lipid membrane structure is between about 23 mass % to about 27 mass %. In at least one embodiment, the concentration of the CL in the multi-lamellar lipid membrane structure is between about 3 mass % to about 10 mass %.

[0148] In at least one embodiment, the two or more synthetic lipids are PE and CL. In at least one embodiment, the concentration of the PE in the multi-lamellar lipid membrane structure is about 90 mass % and the concentration of the CL in the multi-lamellar lipid membrane structure is about 10 mass %.

[0149] In at least one embodiment, the two or more synthetic lipids are PE and PG. In at least one embodiment, the concentration of the PE in the multi-lamellar lipid membrane structure is about 78 mass % and the concentration of the PG in the multi-lamellar lipid membrane structure is about 22 mass %.

[0150] In at least one embodiment, the two or more synthetic lipids are PG and CL. In at least one embodiment, the concentration of the PG in the multi-lamellar lipid membrane structure is about 80 mass % and the concentration of the CL in the multi-lamellar lipid membrane structure is about 20 mass %.

[0151] In at least one embodiment, the PE comprises 1-palmitoyl-2-oleoyl-sn-glycero-3-phosphoethanolamine (POPE). In at least one embodiment, the PE comprises 1,2-dimyristoyl-sn-glycero-3-phosphoethanol amine (DMPE).

[0152] In at least one embodiment, the PG comprises 1-palmitoyl-2-oleoyl-sn-glycero-3-phospho-(1'-rac-glycerol) (POPG). In at least one embodiment, the PG comprises 1,2-dimyristoyl-sn-glycero-3-phospho-(1'-rac-glycerol) (DMPG).

[0153] In at least one embodiment, the PC comprises 1,2-dimyristoyl-sn-glycero-3-phosphocholine (DMPC).

[0154] In at least one embodiment, the PS comprises 1,2-dimyristoyl-sn-glycero-3-phospho-L-serine (DMPS).

[0155] In at least one embodiment, the multi-lamellar lipid membrane structure consists of 1-palmitoyl-2-oleoyl-sn-glycero-3-phosphoethanolamine (POPE), 1-palmitoyl-2-oleoyl-sn-glycero-3-phospho-(1'-rac-glycerol) (POPG) and Cardiolipin (CL).

[0156] In at least one embodiment, the concentration of 1-palmitoyl-2-oleoyl-sn-glycero-3-phosphoethanolamine (POPE) in the multi-lamellar lipid membrane structure is between about 67 mass % to about 71 mass %.

[0157] In at least one embodiment, the concentration of 1-palmitoyl-2-oleoyl-sn-glycero-3-phospho-(1'-rac-glycerol) (POPG) in the multi-lamellar lipid membrane structure is between about 23 mass % to about 27 mass %.

[0158] In at least one embodiment, the concentration of cardiolipin (CL) in the multi-lamellar lipid membrane structure is between about 3 mass % to about 10 mass %.

[0159] In at least one embodiment, the concentration of 1-palmitoyl-2-oleoyl-sn-glycero-3-phosphoethanolamine (POPE) in the multi-lamellar lipid membrane structure is about 70.5 mass %, the concentration of 1-palmitoyl-2-oleoyl-sn-glycero-3-phospho-(1'-rac-glycerol) (POPG) in the multi-lamellar lipid membrane structure is about 26.5 mass %, and the concentration of cardiolipin (CL) in the multi-lamellar lipid membrane structure is about 3 mass %.

[0160] In at least one embodiment, the concentration of 1-palmitoyl-2-oleoyl-sn-glycero-3-phosphoethanolamine (POPE) in the multi-lamellar lipid membrane structure is about 69.5 mass %, the concentration of 1-palmitoyl-2-oleoyl-sn-glycero-3-phospho-(1'-rac-glycerol) (POPG) in the multi-lamellar lipid membrane structure is about 25.5 mass %, and the concentration of cardiolipin (CL) in the multi-lamellar lipid membrane structure is about 5 mass %.

[0161] In at least one embodiment, the concentration of 1-palmitoyl-2-oleoyl-sn-glycero-3-phosphoethanolamine (POPE) in the multi-lamellar lipid membrane structure is about 67 mass %, the concentration of 1-palmitoyl-2-oleoyl-sn-glycero-3-phospho-(1'-rac-glycerol) (POPG) in the multi-lamellar lipid membrane structure is about 23 mass %, and the concentration of cardiolipin (CL) in the multi-lamellar lipid membrane structure is about 10 mass %.

[0162] In at least embodiment, the lipid membrane structure consists of 1-palmitoyl oleoyl-sn-glycero-3-phosphoethanolamine (POPE) and cardiolipin (CL).

[0163] In at least one embodiment, the concentration of 1-palmitoyl-2-oleoyl-sn-glycero-3-phosphoethanolamine (POPE) in the multi-lamellar lipid membrane structure is about 90 mass % and the concentration of cardiolipin (CL) in the multi-lamellar lipid membrane structure is about 10 mass %.

[0164] In at least embodiment, the multi-lamellar lipid membrane structure consists of 1-palmitoyl-2-oleoyl-sn-glycero-3-phosphoethanolamine (POPE) and 1-palmitoyl-2-oleoyl-sn-glycero-3-phospho-(1'-rac-glycerol) (POPG).

[0165] In at least one embodiment, the concentration of 1-palmitoyl-2-oleoyl-sn-glycero-3-phosphoethanolamine (POPE) in the multi-lamellar lipid membrane structure is about 78 mass % and the concentration of 1-palmitoyl-2-oleoyl-sn-glycero-3-phospho-(1'-rac-glycerol) (POPG) in the multi-lamellar lipid membrane structure is about 22 mass 1%.

[0166] In at least embodiment, the multi-lamellar lipid membrane structure consists of 1-palmitoyl-2-oleoyl-sn-glycero-3-phospho-(1'-rac-glycerol) (POPG) and cardiolipin (CL).

[0167] In at least one embodiment, the concentration of 1-palmitoyl-2-oleoyl-sn-glycero-3-phospho-(1'-rac-glycerol) (POPG) in the multi-lamellar lipid membrane structure is about 80 mass % and the concentration of Cardiolipin (CL) in the multi-lamellar lipid membrane structure is about 20 mass %.

[0168] In at least one embodiment, the multi-lamellar lipid membrane structure consists of 1,2-dimyristoyl-sn-glycero-3-phosphoethanolamine (DMPE), 1,2-dimyristoyl-sn-glycero-3-phospho-(1'-rac-glycerol) (DMPG), and cardiolipin (CL).

[0169] In at least one embodiment, the concentration of 1,2-dimyristoyl-sn-glycero-3-phosphoethanolamine (DMPE) in the 1 multi-lamellar lipid membrane structure is between about 67 mass % to about 71 mass %.

[0170] In at least one embodiment, the concentration of 1,2-dimyristoyl-sn-glycero-3--phospho-(1'-rac-glycerol) (DMPG) in the multi-lamellar lipid membrane structure is between about 23 mass % to about 27 mass %.

[0171] In at least one embodiment, the concentration of cardiolipin (CL) in the multi-lamellar lipid membrane structure is between about 3 mass % to about 10 mass %.

[0172] In at least one embodiment, the concentration of 1,2-dimyristoyl-sn-glycero phosphoethanolamine (DMPE) in the multi-lamellar lipid membrane structure is about 70.5 mass %, the concentration of 1,2-dimyristoyl-sn-glycero-3-phospho-(1'-rac-glycerol) (DMPG) in the multi-lamellar lipid membrane structure is about 26.5 mass %, and the concentration of cardiolipin (CL) in the multi-lamellar lipid membrane structure is about 3 mass %.

[0173] In at least one embodiment, the concentration of 1,2-dimyristoyl-sn-glycero-3-phosphoethanolamine (DMPE) in the multi-lamellar lipid membrane structure is about 69.5 mass %, the concentration of 1,2-dimyristoyl-sn-glycero-3-phospho-(1'-rac-glycerol) (DMPG) in the multi-lamellar lipid membrane structure is about 25.5 mass 1%, and the concentration of cardiolipin (CL) in the multi-lamellar lipid membrane structure is about 5 mass %.

[0174] In at least one embodiment, the concentration of 1,2-dimyristoyl-sn-glycero-3-phosphoethanolamine (DMPE) in the multi-lamellar lipid membrane structure is about 67 mass %, the concentration of 1,2-dimyristoyl-sn-glycero-3-phospho-(1'-rac-glycerol) (DMPG) in the multi-lamellar lipid membrane structure is about 23 mass %, and the concentration of cardiolipin (CL) in the multi-lamellar lipid membrane structure is about 10 mass %.

[0175] In at least one embodiment, the multi-lamellar lipid membrane structure consists of 1,2-dimyristoyl-sn-glycero-3-phosphoethanolamine (DMPE) and cardiolipin (CL).

[0176] In at least one embodiment, the concentration of 1,2-dimyristoyl-sn-glycero-3-phosphoethanolamine (DMPE) in the multi-lamellar lipid membrane structure is about 90 mass % and the concentration of Cardiolipin (CL) in the multi-lamellar lipid membrane structure is about 10 mass %.

[0177] In at least one embodiment, the multi-lamellar lipid membrane structure consists of 1,2-dimyristoyl-sn-glycero-3-phosphoethanolamine (DMPE) and 1,2-dimyristoyl-sn-glycero-3-phospho-(1'-rac-glycerol) (DMPG).

[0178] In at least one embodiment, the concentration of 1,2-dimyristoyl-sn-glycero-3-phosphoethanolamine (DMPE) in the multi-lamellar lipid membrane structure is about 78 mass % and the concentration of 1,2-dimyristoyl-sn-glycero-3-phospho-(1'-rac-glycerol) (DMPG) in the multi-lamellar lipid membrane structure is about 22 mass %.

[0179] In at least one embodiment, the multi-lamellar lipid membrane structure consists of 1,2-dimyristoyl-sn-glycero-3--phospho-(1'-rac-glycerol) (DMPG) and cardiolipin (CL).

[0180] In at least one embodiment, the concentration of 1,2-dimyristoyl-sn-glycero-3-phospho-(1'-rac-glycerol) (DMPG) in the multi-lamellar lipid membrane structure is about 80 mass % and the concentration of cardiolipin (CL) in the multi-lamellar lipid membrane structure is about 20 mass %.

[0181] In at least one embodiment, the two or more synthetic lipids are PC, PS, PE and cholesterol.

[0182] In at least one embodiment, the mass ratio of PC:PS:PE:cholesterol is 2:1:1:0.2. In at least one embodiment, the mass ratio of PC:PS:PE:cholesterol is 2:1:1:0.

[0183] In at least one embodiment, the PC is 1,2-dimyristoyl-sn-glycero-3-phosphocholine (DMPC). In at least one embodiment, the PS is 1,2-dimyristoyl-sn-glycero-3-phospho-L-serine (DMPS). In at least one embodiment, the PE is 1,2-dimyristoyl-sn-glycero-3-phosphoethanolamine (DMPE).

[0184] In at least one embodiment, the multi-lamellar lipid membrane structure consists of 1,2-dimyristoyl-sn-glycero-3-phosphocholine (DMPC), 1,2-dimyristoyl-sn-glycero-3-phospho-L-serine (DMPS), 1,2-dimyristoyl-sn-glycero-3-phosphoethanolamine (DMPE), and cholesterol.

[0185] In at least one embodiment, the mass ratio of DMPC:DMPS:DMPE:cholesterol is 2:1:1:0.2. In one embodiment, the mass ratio of DMPC:DMPS:DMPE:cholesterol is 2:1:1:0.

[0186] In at least one embodiment, the multi-lamellar lipid membrane structure is a bilayer. In one embodiment, the multi-lamellar lipid membrane structure comprises two stacked lipid bilayers.

[0187] Various materials known in the art may be used as the solid substrate for the biosensor. For example, the solid substrate may be made of a material such as silicon dioxide (SiO_2), glass, polydimethylsiloxane (PDMS), polymethyl methacrylate (PMMA), and/or polycarbonate (PC). In one embodiment, the solid substrate comprises SiO_2.

[0188] In at least one embodiment, the solid substrate comprises a lipid bilayer compatible surface. Optionally, the lipid bilayer compatible surface may be made of the same material as the solid substrate or a different material. In at least one embodiment, the lipid bilayer compatible surface is hydrophilic. In at least one embodiment, a hydrophilic surface promotes the formation of the multi-lamellar lipid membrane structure adjacent to the surface on the biosensor.

[0189] Various methods known in the art may be used to render a surface of the solid substrate hydrophilic. For example, the lipid bilayer compatible surface may comprise acid treated SiO_2 or poly-lysine. In at least one embodiment, the surface may be plasma-treated to render the surface hydrophilic by oxidation and formation of hydroxyl (OH) groups.

[0190] Acid-treatment may be performed by various methods known in the art. For example, in at least one embodiment SiO2 is cleaned by immersion in a sulfuric acid (H_2O_2) mixture (volume fraction of 70% concentrated H_2SO_4, 30% H_2O_2 at 40° C.) for 30 min).

[0191] In at least one embodiment, the biosensor comprises at least one electrode. In at least one embodiment, the electrode comprises all or part of the lipid bilayer compatible surface. In at least one embodiment, the lipid bilayer compatible surface of the at least one electrode has been rendered hydrophilic. The electrode may comprise gold, carbon, gold, silver, copper, aluminum, graphite, brass, platinum, palladium, titanium or a combination thereof. In at least one embodiment, the electrode comprises gold. For example, as demonstrated in Example 2 a biosensor may be formed by using a solid substrate comprising an electrode of functionalized gold that serves as the lipid bilayer compatible service. In at least one embodiment, the biosensor may comprise an electrode comprising a functionalized metal such as gold, copper, silver, or platinum.

[0192] Optionally, in at least one embodiment the biosensors described herein include at least one reference electrode.

[0193] It will be appreciated by a person skilled in the art that various means for applying potential and measuring current can be used in combination with the biosensors described herein that comprise one or more electrodes. In at

least one embodiment, the biosensor is operatively connected to a power supply or voltage source, and/or a detector for detecting a change in current and/or potential, optionally in response to a sample.

[0194] In at least one embodiment, the biosensor comprises a microfluidic device, well, or channel for receiving a sample. In one embodiment, the microfluidic device, well, or channel is in fluid communication with the lipid bilayer compatible surface. For example, in at least one embodiment, the microfluidic device, well or channel is in fluid communication with at least a portion of the surface of an electrode as described herein.

[0195] In another aspect, there is provided at least one embodiment of an array comprising a plurality of the biosensors described herein.

[0196] In another aspect, there is provided at least one embodiment of a method of detecting membrane disruption activity in a sample. In at least one embodiment, the method comprises:

[0197] contacting a biosensor as described herein with the sample; and

[0198] detecting a change in the multi-lamellar lipid membrane structure in response to the sample.

[0199] Various methods known in the art may be used to detect a change in the multi-lamellar lipid membrane structure. For example, in at least one embodiment the change in the multi-lamellar lipid membrane structure is detected optically. In at least one embodiment, the change in the multi-lamellar lipid membrane structure is detected using x-ray scattering techniques such as x-ray diffraction.

[0200] In at least one embodiment, the change is detected using voltammetry, optionally cyclic voltammetry, chronoamperometry, differential multi pulse voltammetry, double potential pulse techniques or additive differential pulse voltammetry.

[0201] In at least one embodiment, the sample further comprise a redox-indicator. The redox-indicator may be, for example, ferricyanide, o-dianisidine, viologen, 2,2'-biyridine, viologen, thionine, safranin, indigo carmine, or N-Phenylanthranilic acid. In an embodiment, the redox indicator is ferricyanide.

[0202] The sample may be any sample for which information regarding the presence or absence of membrane disruption activity in the sample is desired. For example, in at least one embodiment the sample is an environmental sample such as a water sample or food sample. In at least one embodiment, the sample comprises a test compound or agent and the method is for screening the test compound or agent for membrane disruption activity, optionally for hemolytic activity. In at least one embodiment, the sample is a biological sample, such as biological sample from a subject. In at least one embodiment, the biological sample may include is blood, tissue samples, tissue biopsies, samples taken from tissue culture, biological fluids, tissue extracts, freshly harvested cells, lysates of cells which have been incubated in cell cultures. In one embodiment, the biological fluid is urine, blood, a component of blood such as plasma or serum, sputum, or cerebral spinal fluid.

[0203] In at least one embodiment, the membrane disrupting activity is hemolysis, membrane fluidity, membrane elasticity, or membrane permeability.

[0204] In at least one embodiment, the change detected in the multi-lamellar lipid membrane structure is compared to a control. In at least one embodiment, a difference or similarity between the change detected in the multi-lamellar lipid membrane structure in response to the sample and the control may be indicative of the presence or absence of membrane disrupting activity in the sample such as a hemolytic agent. In at least one embodiment, the control is representative of a change in the multi-lamellar lipid membrane structure in response to a hemolytic agent, and a similarity between the change detected in response to the sample and the control is indicative of the presence of a hemolytic agent in the sample. In at least one embodiment, the hemolytic agent is a hemolytic bacteria.

[0205] In another aspect, the multi-lamellar lipid membrane structures described herein are useful for the investigation of molecules or compounds in association with a lipid membrane. For example, in at least one embodiment, there is provided a method comprising contacting a multi-lamellar lipid membrane structure as described herein with a molecule or compound, bombarding the multi-lamellar lipid membrane structure and measuring the resultant diffraction pattern.

[0206] In yet another aspect, there is provided at least one embodiment of a method of making the biosensor disclosed herein, the method comprising (1) preparing an aqueous solution of hybrid membranes comprising membranes prepared from red blood cells or red blood cell ghosts and the one or more synthetic lipids; and (2) generating the multi-lamellar lipid membrane structure localized on the lipid bilayer compatible surface by successively providing the aqueous solution of hybrid membranes on the lipid bilayer compatible surface.

[0207] In at least one embodiment, the aqueous solution of hybrid membranes is successively provided on the lipid bilayer compatible surface from 2 to 8 times.

[0208] In at least one embodiment, the aqueous solution of hybrid membranes is successively provided on the lipid bilayer compatible surface 2 times. In at least one embodiment, the aqueous solution of hybrid membranes is successively provided on the lipid bilayer compatible surface 3 times. In at least one embodiment, the aqueous solution of hybrid membranes is successively provided on the lipid bilayer compatible surface 4 times. In at least one embodiment, the aqueous solution of hybrid membranes is successively provided on the lipid bilayer compatible surface 5 times. In at least one embodiment, the aqueous solution of hybrid membranes is successively provided on the lipid bilayer compatible surface 6 times. In at least one embodiment, the aqueous solution of hybrid membranes is successively provided on the lipid bilayer compatible surface 7 times. In at least one embodiment, the aqueous solution of hybrid membranes is successively provided on the lipid bilayer compatible surface 8 times.

[0209] In at least one embodiment, after each providing of the aqueous solution of hybrid membranes to the lipid bilayer compatible surface, the method further comprises allowing the hybrid membranes to attach to the biosensor, and performing annealing to improve stability and reduce defects in the multi-lamellar lipid membrane structure.

EXAMPLES

[0210] The following non-limiting examples are illustrative of the present application:

Example 1: Preparation and fabrication of multi-lamellar RBC membranes on solid support.

Materials and Methods

Optical Microscopy and Total Internal Reflection Fluorescence Microscopy (TIRF)

[0211] The images were acquired through a LEICA DMI6000 B inverted microscope equipped with a Spectral Laser Merge Module for multi-wavelength illumination (Spectral, Richmond Hill, ON), adaptive focus control, a motorized X-Y stage (MCL Micro-Drive, Mad City Labs Inc., Madison, Wis.), a piezo X-Y-Z stage (MCL Nano-Drive, Mad City Labs Inc., Madison, Wis.), a LEICA 100×/1.47NA oil-immersed TIRF objective and an Andor iXon Ultra EMCCD camera. Excitation was provided by 488 and 647 nm diode-pumped solid-state lasers with 40 mW and 60 mW output power respectively (Spectral, Richmond Hill, ON). Alexa Fluor 488 labelled phalloidin (Invitrogen) was used to label the F-actin network and 1,1'-Dioctadecyl-3,3,3',3'-Tetramethylindocarbocyanine Perchlorate (Sigma-Aldrich) was used to label the membranes.

UV-Vis Spectroscopy

[0212] Ultraviolet-visible spectroscopy (UV-vis) was obtained using a M1000Pro Plate reader from Tecan. The technique is depicted in FIG. **2** c): the absorption of light in the visible and adjacent (near-UV and near-infrared) ranges is detected. Hemoglobin shows characteristic absorption lines at 335±0.4 nm, 416.4±0.2 nm 543±0.8 nm and 577±0.4 nm [77]. In order to prepare a sufficiently diluted RBC solution, 50 μL of the erythrocytes fraction was mixed with 1 mL PBS. 400 μL of this solution was afterwards diluted with 400 μL PBS. This dilution procedure has been repeated three times. For the measurement, a 96-plate from Costar was used. 200 μL of the diluted blood solution, the ghosts solution and the RBC solution were filled in the chambers of the plate. The absorption spectrum for each sample was scanned for wavelengths between 310 nm and 800 nm.

X-Ray Diffraction

[0213] X-ray scattering data was obtained using the Biological Large Angle Diffraction Experiment (BLADE) in the Laboratory for Membrane and Protein Dynamics at McMaster University. BLADE uses a 9 kW (45 kV, 200 mA) CuKα rotating anode at a wavelength of 1.5418 Å. Both source and detector are mounted on movable arms such that the membranes stay horizontal during the measurements. Focusing multi-layer optics provides a high intensity parallel beam with monochromatic X-ray intensities up to 10^{10} counts/(mm^2·s). This beam geometry provides optimal illumination of the solid supported membrane samples to maximize the scattering signal. A sketch of the scattering geometry is shown in FIG. **5** *a*). Note that there is no risk of sample damage using this in-house technique because of the large beam size and relatively low intensity of the X-ray beam as compared to synchrotron sources.

[0214] The result of an X-ray experiment is a 2-dimensional intensity map of a large area of the reciprocal space, as sketched in FIG. **5**. The corresponding real-space length scales are determined by $d=2\pi/|Q|$ and cover length scales from about 2.5 to 100 Å. All scans were measured at 28.0 and 50% relative humidity (RH) hydration. As depicted in FIG. **5** *a*), the wafers were oriented in the X-ray diffractometer, such that the q||-axis probed lateral structure, parallel to the wafer surface, and the perpendicular axis, q_z, probed out-of-plane structure, perpendicular to the substrate.

[0215] The experimental errors were determined as follows: Errors for peak positions, peak width and peak height are determined as the fit standard errors, corresponding to 95% confidence bounds, equivalent to 2 standard deviations, a. Errors for calculated parameters, such as peak area, were then calculated by applying the proper error propagation.

Calculation of Electron Densities

[0216] The out-of-plane structure of the membrane was determined using specular reflectivity. The relative electron density, ρ(z), is approximated by a 1-dimensional Fourier analysis [51, 78].

$$\rho(z) = \frac{2}{d_z}\sum_{n=1}^{N}\sqrt{I_n q_n}\, v_n \cos\left(\frac{2\pi n z}{d_z}\right).$$

N is the highest order of the Bragg peaks observed in the experiment. The integrated peak intensities, 1, are multiplied by q, to receive the form factors, F(q,) [51, 78]. The bilayer form factor $F(q_z)$, which is in general a complex quantity, is real-valued in the case of centro-symmetry. The phase problem of crystallography, therefore, simplifies to the sign problem $F(q_z)=\pm|F(q_z)|$ and the phases, v, can only take the values ±1. The phases, v, are needed to reconstruct the electron density profile from the scattering data following Eq. (1). When the membrane form factor $F(q_z)$ is measured at several q_z values, a continuous function, $T(q_z)$, which is proportional to $F(q_z)$, can be fitted to the data [51, 78].

$$T(q_z) = \sum_n \sqrt{I_n q_n}\,\mathrm{sinc}\left(\frac{1}{2}d_z q_z - \pi n\right).$$

[0217] Once an analytical expression for $T(q_z)$ has been determined from fitting the experimental peak intensities, the phases v, can be assessed from $T(q_z)$. The phase array v, =[−1−1 1−1 1] was used for all samples.

[0218] The electron densities determined by Eq. (1) are on a relative scale. In order to compare the electron densities in FIGS. **6** *c*) and **7** *c*), ρ in the membrane centre at z=0 was set to 0 and the electron density at the boundaries (z values between 25 and 30 Å depending on the lamellar spacing), which probe the water layer between the stacked membranes, were scaled to the electron density of water of $\rho=0.33\ e^-/Å^3$.

Membrane Orientation

[0219] To determine the degree of orientation of the membranes in the stack the correlation peak intensities were integrated as function of the meridonal angle ϕ (the angle relative to the q_z axis). The corresponding intensity was fit

with a Gaussian distribution centered at 0, which was then used to calculate the degree of orientation using Hermans orientation function:

$$H = \frac{3 < \cos^2\delta > -1}{2}.$$

[0220] The degree of orientation, H, of the RBC membranes was measured to be 90.9%.

Determination of Domain Sizes

[0221] The average size of the different lipid and peptide domains was estimated from the widths of the corresponding in-plane correlation peaks in FIG. **5** *d*) by applying Scherrer's equation [79]:

$$L = \frac{0.94\lambda}{B(2\theta)\cos(\theta)},$$

where λ is the wavelength of the X-ray beam, θ is the diffraction angle and B(2θ) is the width of the correlation peak in radians. Scherrer's equation is an established way to estimate crystallite sizes of up to ý100 nm in X-ray diffraction experiments. Note that the equation has limitations to quantitatively determine sizes of small domains of a few nanometers, only. The determined values present upper limits of the domain sizes.

[0222] The preparation protocol is schematically depicted in FIG. **1** and consists of two main parts: In the first step, RBC ghosts are produced from blood samples. In the second step, these RBC ghosts are applied onto silicon wafers and annealed to form multi-lamellar RBC membrane stacks.

Preparation of Ghosts

[0223] The preparation of RBC ghosts was first published in 1963 by Dodge, Mitchell and Hanahan [1]: 10 mL of venous blood were drawn from a participating individual. The blood was collected in venous blood collection tubes from BD (Product Number: BD 367874), coated with sodium heparin as anticoagulant. The tube was centrifuged at 3,000 g for 10 min at room temperature. After this process, a clear separation between an erythrocyte fraction and a plasma fraction was observed. The white blood cells and platelets form a layer between those two fractions.

[0224] In the original protocol, the RBC solution was then filtered by a procedure by Beutler, West and Blume [43], where the RBC solution is pushed through a cellulose filter. This process was suggested to produce pure erythrocyte preparations without the remaining leucocytes and platelets. While this protocol is well established and widely used in blood cell investigations (see, for instance, [44] for a recent review), the ghost solution produced by this protocol did not result in well-developed multi-lamellar lipid membrane stacks when applied on silicon wafers. Cellulose particles were observed under the microscope in the solution after passing through the filter, which likely inhibit the formation of well-ordered membrane stacks.

[0225] In order to avoid contamination with cellulose, the RBC solution was purified through centrifugation using the following protocol: The supernatant in the separated blood sample was removed using a pipette. PBS was added to the precipitate to achieve a volume of 10 mL and centrifuged at 3,000 g for 10 min. This process was repeated twice.

[0226] 50 μL of the RBC solution was then mixed with 1 mL of buffer solution in a 1.5 mL reaction tube. For the buffer, 16 mL of PBS and 484 mL of 18.2 MΩ·cm ultra-pure water were mixed and stored at 0° C. The solution was buffered with potassium hydroxide and hydrochloric acid to a pH of 8. This creates a hypotonic solution for the RBCs, resulting in an influx of water into the cells and their lysis. The diluted solution is vortexed for 10 s to prevent clumping. After vortexing, the reaction tube is immediately placed in ice for 30 min to slow down the re-closing of the burst cells.

[0227] Samples were then centrifuged at 18,000 g for 30 min at 0° C. After the centrifugation, a pellet is formed at the bottom of the reaction tube. The supernatant was removed by pouring the reaction tube in a beaker. 1 mL buffer solution was added to the pellet and the solution was vortexed for 10 s and centrifuged for 15 min at 18,000 g and 0° C. This process of centrifugation and removal of the supernatant was repeated 4 times. During this washing, most of the hemoglobin is removed, resulting in a transparent, colorless solution. FIG. **2** *a*) shows images of the reaction tube after different numbers of washing steps.

[0228] The removal of hemoglobin was quantitatively checked using ultraviolet-visible spectroscopy (UV-vis). The corresponding data is shown in FIG. **2** *b*). The characteristic hemoglobin absorption bands at 335 nm, 416.4 nm 543 nm and 577 nm decrease in every step; the hemoglobin content of the final solution was found to contain less than 2% of the original content.

[0229] This procedure results in solutions with typical mass concentration of RBC's of ~0.3 mg/mL. To increase the concentration, pellets from 24 such reaction tubes were collected and centrifuged at 18,000 g for 15 min. The supernatant was removed, and the tube was refilled with buffer solution to the 1 mL mark of the tube. This results in a solution with a final mass concentration of ~7 mg/mL. The ghost solution was analyzed by fluorescence microscopy, as shown in FIG. **3** *a*) and *b*). The red blood cell membrane was fluorescently labeled in part a) using 1,1'-Dioctadecyl-3,3,3',3 '-Tetramethylindocarbocyanine Perchlorate (DiI). The image shows a mix of multi-lamellar and uni-lamellar ghosts with a highly irregular shape and a large distribution of shapes and sizes, from round to long, more chain-like objects including vesicles that contain several smaller vesicles. These shapes are likely related to the presence of a cytoskeleton, whose main components are spectrin and actin in RBC [45]. To analyze this network, Alexa Fluor 488 labelled phalloidin was used to label the F-actin network in FIG. **3** *b*). Structures of ~5 μm were observed, indicative of the presence of actin.

[0230] As indicated below, the variation in size and shape of the ghosts, and the presence of an actin network likely prevents the formation of well defined, solid supported multi-lamellar RBC. To achieve a more uniform distribution of vesicle sizes and shapes, the RBC solution was tip sonicated 10 times for 5 s, each, in order to form small uni-lamellar vesicles (SUVs). The result of the sonication process is shown in FIG. **3** *c*) and *d*). In part c), the membrane was fluorescently labeled using DiI. Small dots were observed, indicative of small uni-lamellar vesicles of ~50 nm, beyond the resolution limit of the microscope.

[0231] The actin concentration was analyzed by labelling with Alexa Fluor 488 labelled phalloidin. After sonication, no more particles were observed within the resolution of the microscope used. In order to separate the SUVs and remaining actin, the solution was centrifuged for 30 min at 20,000 g. Since SUVs can only sediment in ultra-centrifuges at 120,000 g when centrifuged for more than 30 min [46], the pellet contains actin polymers and potential larger and multi-lamellar vesicles, while the SUVs stay in the supernatant. This supernatant was found to be ideal for the formation of solid supported, multi-lamellar RBC membranes, as will be discussed below.

Silicon Wafer Preparation

[0232] All membranes were prepared on single-side polished silicon wafers. 100 mm diameter, 300 μm thick silicon wafers were pre-cut into 10×10 mm^2 chips. The wafers were functionalized for deposition of the ghost solution by either preparing a hydrophobic or hydrophilic surface. To create a hydrophobic silicon surface, the wafers were pre-treated by sonication in dichloromethane (DCM) at 40° C. for 25 min. This treatment removes all organic contamination and leaves the surface in a hydrophobic state. Each wafer was then thoroughly rinsed three times by alternating with ~50 mL of ultra-pure water with a resistivity of 18.2 MΩ·cm and HPLC grade methanol.

[0233] To create a hydrophilic state, the wafers were cleaned by immersion in an H_2O_2 sulfuric acid mixture (volume fraction of 70% concentrated H_2SO_4, 30% H_2O_2 at 40° C., Piranha™ solution) for 30 min on a 3D orbital shaker (VWR) set to tilt angle 1 and speed 15). This strongly oxidizing combination removes all organic contaminants on the surface but does not disturb the native silicon oxide layer. Each wafer was then thoroughly rinsed with ~50 mL of ultra-pure water with a resistivity of 18.2 MΩ·cm. Fabrication of highly oriented, multi-lamellar solid supported RBC membranes.

[0234] The ghost solution did not spread well on hydrophobic silicon wafers, as shown in FIG. **4** *a*). For this wafer, 100 μL of concentrated ghosts solution was applied onto a 10×10 mm^2 hydrophobic silicon wafer mounted on a leveled hot plate at a temperature of 40° C. The solution was applied slowly using a 100 μL syringe to avoid spill, and the wafer typically dried within ~10 min. The membrane film was found not to cover the entire wafer and showed several wrinkles.

[0235] Slowly drying the solution to allow more time for the solution to spread and membranes to form was achieved by placing the wafers in a leveled desiccator for 5 days at 97.6±0.5% relative humidity using a saturated K2 SO4 salt solution. The slow drying resulted in a smoother film, however, still incomplete coverage of the substrate, as shown in FIG. **4** *b*). FIG. **4** *c*) shows a hydrophilic wafer prepared by applying 100 μL of concentrated SUV solution and dried for 5 days at 97.6±0.5% relative humidity. The solution covered the entire wafer indicating a homogeneous mass distribution. Only weak signals of membrane stacking in this sample were detected and thus the inventors picture the morphology of the membranes as depicted in FIG. **1** *d*), as uni-lamellar vesicles that have been dried out on the silicon substrate. This situation is similar to the preparation of single solid supported bilayers through vesicle fusion [47, 48], where small bilayer patches initially develop on the substrate, and eventually undergo a transition into a large uniform single bilayer [47]. Substrates are typically annealed for 72 h at 55° C. in an oven in air. The energy barrier for forming a lamellar structure can be overcome through gentle heating and the lamellar membrane organization becomes energetically more favorable, as it minimizes the bending energy.

[0236] However, using the same procedure and heating the RBC membranes in an oven led to destruction of the membrane film. The silicon chips were, therefore, incubated at different temperatures and under relative humidities between 50% and 100% RH by placing them in a closed container and exposure to different saturated salt solutions. The best results were obtained when the RBC chip was annealed at 50° C. and 95.8±0.5% relative humidity in a saturated $_{K2SO4}$ salt solution for 5 days, which resulted in the photo in FIG. **4** *d*). In this protocol, annealing of the RBC membranes at high temperature and humidity leads to the formation of lamellar membrane structures through membrane fusion.

Preparation of RBC/Aspirin Complexes.

[0237] In order to prepare complexes of RBC membranes containing increasing amounts of aspirin, a solution of 9 mg/mL acetylsalicylic acid (molecular weight 180 g/mol) in 18.2 MΩ·cm water was prepared. 2 μL, 3 μL, 4 μL, 5 μL, and 6 μL of this solution were added to 100 μL of the final ghosts solution resulting in acetylsalicylic acid concentrations of 1 mM, 1.5 mM, 2 mM, 2.5 mM and 3 mM. The resulting solutions were applied onto silicon wafers and dried slowly and incubated for 5 days following the above protocol.

[0238] The molar concentration of ASA in the RBC membranes can be estimated as follows: between 2 and 5 μL of the 9 mg/mL ASA solution were added to the membrane solution, resulting in between 1 10^{-7} and 2.5 10^{-7} mol. 100 μL of the 7 mg/mL RBC contain ~2 10^{-6} mol (when assuming an average molecular weight of the membranes. of 400 g/mol). This results in molar ASA concentrations between 5-10 mol %, i.e., 1 ASA molecule per 10 to 20 lipid molecules. This ASA concentration is elevated as compared to plasma concentrations of typically less than 1 mol %, however, comparable to ASA concentrations typically used in the literature [49].

Results and Discussion

Molecular Structure and Properties of RBC Membranes.

[0239] In this section, X-ray diffraction was used to determine the morphology and molecular structure of the RBC membranes. The main findings can be summarized as follows.

[0240] The protocol presented in this paper produces highly oriented, multi-lamellar RBC membranes on silicon wafers, which are highly suited for study using biophysical techniques in order to provide detailed molecular level information.

[0241] RBC membranes consist of nanometer-sized liquid ordered (l_o) and liquid disordered (ld) lipid domains and α-helical coiled-coil peptide domains, at ratios of 30.4% l_o, 45.0% ld and 24.8% coiled peptides.

[0242] As the membranes are oriented with their membrane plane parallel to the silicon substrate, the in-plane and out-of-plane structure could be determined separately but simultaneously. A schematic of the X-ray diffraction setup is

shown in FIG. **5** *a*). FIG. **5** *b*) shows the 2-dimensional X-ray diffraction pattern of a sample pre-pared with the final preparation protocol. The organization of the membranes normal to the silicon wafer is observed along the q_z-axis, while molecular organization in the plane of the membranes parallel to the substrate is observed along the q||-direction. Cuts of the diffracted intensity along the out-of-plane and in-plane direction are shown in FIGS. **5** *c*) and *d*).

Structure Perpendicular to the Membrane Plane

[0243] A lamellar membrane structure, i.e., a stack of membranes, where the bilayers are organized parallel to each other, results in a series of equally spaced and well defined Bragg reflections in diffraction experiments [8], corresponding to the 'fundamental' and the 'overtones'. The well-developed Bragg peaks along the out-of-plane axis in FIG. **5** *c*) are indicative of a lamellar organization of the RBC membranes on the substrate. The fundamental reflection for each series is colored in the Figure. Following Bragg's law ($q_z=2\pi/d_z \cdot n$), the lamellar spacing, d_z, can be determined from the slope of the curve when plotting q_z vs. the order of the Bragg peak, n. This is shown in FIGS. **6** *a*) and 3 d_z-spacings were determined: $_{dlo}$=59.2 Å, $_{dld}$=51.6 Å and d_p=40.6 Å.

[0244] Electron density profiles, ρ(z), of the bilayers were determined through Fourier analysis of the out-of-plane Bragg peaks, as described in the Materials and Methods section, and are shown in FIG. **6** *b*). The electron rich head group can be identified by the absolute maximum in the electron density profile at z~22 Å. ρ monotonically decreases to the bilayer center at z=0, where CH3 groups typically reside in the center, with a low electron density. The electron density of the $_{dlo}$=59.2 A domain (blue curve) corresponds well to a lipid bilayer with lipids in the gel state with lipid chains in an all-trans configuration [50, 51], and was, therefore, assigned to lipids in lo domains. These domains are enriched in cholesterol making them more ordered and thicker [32, 35].

[0245] The electron density corresponding to the d_{ld}=51.6 A spacing (green curve) agrees well with the electron density reported for fluid lipid bilayers, where the structure of the lipid tails in the hydrophobic membrane core is dominated by gauche-defects, as reported for instance by [52, 53]. These signals were assigned to domains of l_d lipids.

TABLE 1

	saturated lipid domains	unsaturated lipid domains	peptide domains
d_z	59.2 ± 0.5 Å	51.6 ± 0.02 Å	40.6 ± 0.06 Å
d_{HH}	46.0 ± 0.5 Å	41.0 ± 0.02 Å	—
d_w	13.2 ± 0.5 Å	10.6 ± 0.02 Å	—
a	4.68 ± 0.27 Å	5.39 ± 0.03 Å	10.88 ± 0.22 Å
A	19.04 ± 1.10 Å	25.18 ± 0.13 Å	—
Ξ	16 ± 3 Å	29 ± 2 Å	28 ± 3 Å

[0246] The 3rd spacing of d_p=40.6 Å is significantly smaller and the electron density shows an almost constant density in the hydrophobic membrane core. This density profile is well described by α-helical peptide coiled-coils, which are embedded in the membranes [26].

[0247] Lamellar spacings, d_z, membrane thicknesses, d_{HH}, and the thicknesses of the water layer, d_w were determined from the electron densities and are listed in Table 1.

In-Plane Membrane Structure

[0248] Three peaks at q||=0.58 $Å^{-1}$, q||=1.35 $Å^{-1}$, and q||=1.55 $∈^{-1}$ were observed in the in-plane diffraction in FIG. **5** *d*). These peaks fit well to distances between peptides and lipids, observed in previous investigations in single and multicomponent artificial and biological membranes [26, 35, 52, 54-56]. The peaks at q||=1.35 $Å^{-1}$ and q||=1.55 $Å^{-1}$ are in good agreement with structural features reported in model lipid membranes in their well-ordered gel and fluid phases, where the lipids tails take an all-trans conformation (gel) or are dominated by gauche defects (fluid). A correlation peak at −1.5 $Å^{-1}$ was reported in the gel phase of saturated phospholipid membranes, such as DMPC (Dimyristoyl-sn-glycero-3-phosphocholine) and DPPC (Dipalmitoyl-sn-glycero-3-phosphocholine) [32, 50, 54, 57]. Unsaturated lipids were reported to order in a structure with slightly larger nearest neighbor tail distances, leading to an acyl-chain correlation peak at −1.3 $Å^{-1}$, as reported for DOPC and POPC [27, 58]. These correlation peaks were assigned to the l_o and l_d lipid components of the plasma membranes.

[0249] The in-plane peaks are the result of a hexagonal packing of the lipid tails in the hydrophobic membrane core (planar group p6) [32]. The distance between two acyl tails is determined to be $a=4\pi/(\sqrt{3}q)$, where is the position of the corresponding correlation peak. The area per lipid chain is obtained to $AT=(\sqrt{3}/2)\ a^2$ Lipid tail distances in l_o and l_d domains and lipid tail areas are listed in Table 1. Distances and areas in the lo domains are smaller, as lipid tails in their all-trans configuration are straighter and pack tighter than l_d tails, dominated by gauche defects.

[0250] Membrane peptides are often organized in bundles, whose structure is dominated by α-helical coiled-coils [26, 59-62]. Coiled coils consist of α-helices wound together to form a ropelike structure stabilized by hydrophobic interactions, found in about 10% of the proteins in the human genome [63]. The main feature of this motif is a ~10.8 Å (q||~0.58 $Å^{-1}$) equatorial reflection corresponding to the spacing between adjacent coiled-coils [64-66]. The volume fractions of the peptide, the l_o and l_d lipid domains were determined from the integrated peak intensities of the lipid and peptide signals in FIGS. **5** *d*) to 30:45:25 (l_o lipids:coiled peptides).

[0251] While RBC membranes were reported to consist of ~52% proteins and ~40% lipids [4], the values above indicate a higher fraction of lipids (and cholesterol). The technique is not sensitive to monomeric short peptides, but to the packing of peptide helices, only. These helical regions are likely part of larger trans-membrane proteins. The molecular structure of the RBC membranes is pictured in FIG. **8** *a*).

[0252] In early X-ray diffraction studies of human erythrocytes membranes [67, 68] ghosts were prepared using the Dodge protocol and pellets of the final preparation were imaged. Diffraction patterns with lamellar periodicities between ~55 and ~70 Å were observed and assigned to hemoglobin free membranes, in agreement with our findings. Large amounts of hemoglobin were reported to result in much larger lamellar periodicities of ~110 Å [67]. The electron density in FIG. **5** *a*) agrees qualitatively well with the early electron density in [68], which was assigned to intact, hemoglobin-free erythrocyte membranes.

Membrane Orientation

[0253] The orientation of the RBC membranes in the stack was determined from the 2-dimensional data in FIG. **5** *b*) by radial integration using Hermans orientation function, as described in the Materials and Methods Section. The intensity of the first reflectivity peak as function of the meridional angle (I) is plotted in FIG. **6** *c*). The degree of orientation was determined to be 90.9% (±0.26%). While values of ~97% are reported for synthetic supported membranes [69], the value for the RBC membrane is to the best of our knowledge the highest ever reported for a biological membrane. This high degree of orientation of the RBC membrane on silicon chips is required for a detailed structural characterization of the membranes, in particular to differentiate in-plane and out-of-plane structure.

Determination of Domain Size

[0254] The in-plane diffraction signals in FIG. **5** *d*) are significantly broader than typical Bragg peaks in crystalline materials, indicating that the corresponding phases are small. The domain sizes can be estimated from the peak widths of the corresponding correlation peaks using Scherrer's equation (as detailed in the Materials and Methods Section). Values for the domain size, are listed in Table 1. From these results, RBC membranes consist of small, nanometer sized domains of l_o and l_d lipids and coiled-coil α-helical peptides

The Effect of Aspirin on RBC Membrane Structure

[0255] There is growing evidence for an influence of various pharmaceuticals on lipid membrane organization and stability [70]. In particular, non-steroidal anti-inflammatory drugs (NSAID's) have been shown to disturb bilayer structures in native and model membranes [71, 72]. Aspirin is the most common NSAID and is known to interact with membranes [51, 71]. Aspirin strongly perturbs model membrane structure in a concentration dependent manner and influences human erythrocyte shape [73] and decreases the hydrophobic surface barrier in mucosal membranes, leading to a diffusion of acid and gastrointestinal injury [74] and impacts on protein sorting [75]. Aspirin was previously reported to partition into lipid bilayers and position itself in the lipid head group region [24, 51, 76]. Recently, an interaction between aspirin and cholesterol was reported, as aspirin was observed to reduce the volume of cholesterol plaques in model membranes at elevated cholesterol concentrations of ~40 mol % [76]. Aspirin also inhibits the formation of cholesterol rafts in fluid lipid membranes at physiological cholesterol concentrations [24, 76].

[0256] In this section it is disclosed that: Aspirin partitions in RBC membranes, preferably in l_o lipid domains, and is located in the membrane head group region. Aspirin also reduces membrane thickness and increases lipid tail distances, indicative of a fluidification of the RBC membranes.

[0257] The out-of-plane scattering for RBC membranes containing 1 mM, 1.5 mM, 2 mM, 2.5 mM and 3 mM ASA is shown in FIG. **7** *a*). The curve containing 2.5 mM ASA and the corresponding fit is shown in part b). Data is well fit by 3 series of Bragg peaks, corresponding to l_o, l_d and peptide domains, in agreement with pure RBC membranes.

[0258] Electron density profiles of the l_o lipid domain for RBC membranes and RBC membranes+1 mM aspirin are shown in FIG. **7** *c*). Upon the addition of aspirin, the electron density increases at z~22.8 Å. Under the assumption that a small amount of aspirin does not disturb the bilayer structure significantly, the two densities can be subtracted, and the extra intensity assigned to aspirin molecules. The experiments thus locate aspirin inside the head group region of the RBC membranes, in agreement with results in model phospholipid bilayers [24, 51, 76]. There is only a small effect of aspirin on the electron density of the l_d domains, as shown in FIG. **7** *e*), indicating that aspirin preferably interacts with l_o regions.

[0259] The lamellar spacing, d_z and head group to head group spacing, d_{HH}, of the l_o and l_d lipid domains as function of ASA content are depicted in FIG. **7** *d*). While lamellar spacing and membrane thickness for the l_d lipid domains are not affected by the presence of ASA, the two spacings significantly decrease with increasing aspirin concentrations for the l_o lipid domains. They decrease until lamellar spacing and membrane thickness for l_o and l_d domains coincide at an ASA concentration of 2.5 mM. At this ASA concentration, the overall lamellar spacing of the RBC membranes is reduced to 53.4 Å, the overall membrane thickness to 41.8 Å.

[0260] While the lipid spacing in the ld domain is unchanged by the presence of aspirin, the q||-value of the lo signal slightly shifts to smaller q||-values, indicative of an increase in the distance between lipids from a_{lo}=4.69 Å to a_{lo}=4.85 ÅA, and an increase in tail area from 19.04 $Å^2$ to 20.37 $Å^2$. Lipid domain sizes are approximately independent of aspirin concentration, however, a slight increase in peptide domain size was observed with increasing ASA content. A cartoon of the structure of RBC membranes in the presence of ASA is shown in FIG. **8** *b*).

Conclusions

[0261] Presented here is the preparation of human red blood cell membranes on a chip, i.e., highly aligned multilamellar stacks of RBC membranes applied on silicon wafers. These solid supported RBC membranes are ideally suited for analysis using biophysical techniques and development of sensors for blood tests. Based on the protocol for the preparation of red blood cell ghosts, small uni-lamellar RBC vesicles were produced, which are applied onto functionalized silicon chips and annealed into multi-lamellar, planar membranes. Morphology and molecular structure of the RBC membranes were analyzed by optical microscopy, fluorescent microscopy, UV-vis spectroscopy and X-ray diffraction. These RBC's on a chip present a platform to test the interaction of bacteria and drugs with RBC membranes and determine their molecular mode-of-action in the future.

[0262] The X-ray diffraction measurements present direct experimental evidence that RBC membranes consist of nanometer sized l_o and ld lipid domains, and α-helical coiled-coil peptide domains. The composition of RBC's was determined to be 30:45:25 (l_o:ld :coiled peptides).

[0263] RBC membranes that contain up to 3 mM of ASA were prepared. Presented here is experimental evidence that aspirin partitions in RBC membranes and preferably locates in the head groups region of the l_o lipid domains. ASA led to an increase of the lipid-lipid distance and a decrease of the membranes thickness, indicative of a fluidification of the RBC membranes.

Example 2. Hemolysis Assay Based on a Human Red Blood Cell Membrane (HBLOC) Sensor

[0264] Inventors have developed a method which isolates human red blood cells on a silicon chip for use as a safe and quantitative test for hemolytic bacteria. To develop our human blood cells on a chip, a sample of human blood is exposed to a hypotonic solution which causes the RBC's to burst and empty their contents. A series of sonication and washing steps are then applied to isolate only the RBC membrane, and to remove all hemoglobin and other contaminants. The result is a solution of empty membrane sacks known as RBC "ghosts". This solution is then applied to sensors and allowed to slowly dry, leaving behind stacked sheets of RBC membrane. The sensors use nanostructured gold electrodes, functionalized for the application of the RBC membranes and maximizing the surface area for increased sensitivity of the tests. The coated electrodes are then used as part of a 3-electrode electrochemical cell, where any damage to the cell membrane allows a redox-indicator in solution to access the electrode surface. Under cyclic voltammetry or chronoamperometry measurements the reduction/oxidation of the indicator molecule gives rise to a current that is proportional to the amount of membrane damage.

[0265] Nanostructured gold electrodes have been fabricated and the RBC membranes successfully applied to the sensors (FIG. **9**). Membrane damage was quantitatively measured using ferricyanide as the redox indicator and cyclic voltammetry. To mimic hemolytic activity by bacteria attacking RBC membranes, the membranes were disrupted using a surfactant (sodium dodecyl sulfate, SDS). The voltammograms and bar graph show increases in the reduction and oxidation peak currents as a result of membrane damage and higher electroactive surface available (FIG. **10**).

Example 3. RBC Ghost and Biosensor Preparation Protocol

[0266] Additional experiments were performed with respect to investigating the preparation of RBC ghosts from blood samples and the application of the RBC ghost preparations onto a substrate (silicon wafers) and to form multi-lamellar RBC membrane stacks.

[0267] The following protocol was observed to produce desirable preparations of RBC ghosts for annealing to form multi-lamellar RBC membrane stacks:

[0268] 1. Take blood from volunteer.

[0269] 2. Prepare Buffer:

[0270] a. PBS Buffer: 2 Tablets of PBS in 400 ml Ultra Pure Water

[0271] b. Diluted PBS Buffer: 16 ml of PBS Buffer filled to 500 ml; Adjust the pH to 8 using KOH.

[0272] 3. Wash Blood: Centrifuge Blood at maximum settings for 10 minutes and remove the supernatant (Plasma). Fill the Tube with PBS buffer to ensure a total volume of ~10 ml. Repeat this washing step twice.

[0273] 4. Prepare 24 Eppendorf tubes in an ice bucket.

[0274] 5. Remove the supernatant from the Blood tube after the last Washing step.

[0275] 6. Mix 50 μl of the RBC fraction with 1 ml of diluted PBS buffer in each of the 24 Eppendorf tubes.

[0276] 7. Vortex the tubes.

[0277] 8. Let the tubes sit for 30 minutes.

[0278] 9. Centrifuge the tubes at maximal settings (~20 000×g) for 30 minutes.

[0279] 10. Remove the supernatant. And refill the tubes with 1 ml diluted buffer solution.

[0280] 11. Vortex the tubes.

[0281] 12. Centrifuge the tubes at maximal settings (~20 000×g) for 15 minutes.

[0282] 13. Repeat steps 10 to 12 until the solution is clear.

[0283] 14. The Ghosts may be stored in the Fridge.

[0284] 15. Centrifuge all Eppendorf s at maximal settings (~20 000×g) for 15 minutes.

[0285] 16. Remove the supernatant and combine all Pellets in one Eppendorf. It might be convenient to first combine 2×12 tubes and then combine these pellets.

[0286] 17. Centrifuge the sample at maximal settings (·20 000×g) for 15 minutes.

[0287] 18. Remove or add diluted PBS buffer to ensure a total volume of 0.5 ml. This will result in an RBC membrane concentration of ~14 mg/ml.

[0288] 19. Sonicate the sample: Place the sample in an ice bucket and insert the sonication tip. Set the instrument to 5 second pulses and 50 second breaks at 20% Intensity for 20 minutes. The sample should look milky first but clear up during sonication.

[0289] 20. Centrifuge the sample at maximal settings (~20 000×g) for 20 minutes.

[0290] The following protocol was observed to produce desirable substrates for promoting the formation of multi-lamellar RBC membrane stacks:

[0291] 1. Silicon wafers placed in a Glass dish.

[0292] 2. Fill in 5 ml Hydrogen Peroxide and 15 ml Sulfuric Acid (98%) ("Piranha Solution"). This step ensures the wafer surface is hydrophilic.

[0293] 3. Let the wafers sit for min 20 Minutes.

[0294] 4. The beaker does not need to be heated (room temperature works).

[0295] The following protocol was used for contacting the preparation of RBC ghosts with the prepared silicon substrate:

[0296] 1. Heat the 3d orbital shaker and the metal plate to 37 degrees.

[0297] 2. Set the Shaker speed to 7 and the tilt to 8.

[0298] 3. Take the wafer out of the Piranha solution and rinse it ONLY with Water (no Methanol).

[0299] 4. Dry the wafer with nitrogen gas.

[0300] 5. Place the metal plate on the 3D orbital shaker.

[0301] 6. Place the wafer on the metal plate.

[0302] 7. Slowly apply 100 μl of the Ghost solution onto the wafer.

[0303] 8. Place a plastic lid on top of the wafer and tilt the lid with a Qtip.

[0304] 9. Wait until the wafers look well dried.

[0305] The following protocol was then used to incubate the RBC ghosts on the substrate to promote the formation of multi-lamellar RBC membrane stacks:

[0306] 1. Place the wafers in a glass beaker with a saturated Potassium Sulfate solution.

[0307] 2. Seal the beaker with a lid and parafilm.

[0308] 3. Place the beaker in the incubator at 37 degrees Celsius.

[0309] 4. Let the wafers sit for 3 days.

[0310] FIG. **11** shows images of a biosensor and multi-lamellar RBC membrane stack prepared according to the

protocol of the present example. FIG. **12**(*a*) shows a 2D x-ray image of a biosensor comprising a prepared according to the protocol of the present example. FIG. **12**(*b*) shows the reflectivity Bragg peaks. The narrow peaks go up to an order of 5 which indicates a very well ordered and uniform membrane film.

Example 4: Hybrid Erythrocyte Membranes

[0311] Materials and Methods

[0312] Preparation of Erythrocyte Liposomes

[0313] The detailed protocol is described elsewhere [80]. Briefly: Heparinized blood samples were collected. The blood was washed twice, and the RBCs were isolated by successive centrifugation and replacement of the supernatant with phosphate buffered saline (PBS). The cells were exposed to osmotic stress by mixing hematocrit with lysis buffer (3% PBS, pH 8) at a concentration of 5 vol %. The lysis buffer was pre-chilled to ~4° C. and the reaction tubes were immediately stored on ice to prevent a fast re-closing of the ruptured cells. Hemoglobin and other cellular components were removed through multiple washing steps as described in [80]. The protocol results in a white pellet containing closed empty erythrocyte liposomes.

[0314] The resulting solution was tip sonicated 20 times for 5 s and 55 s breaks each at a power of 100 W. The reaction tube was placed on ice during sonication to prevent the sample from overheating. Afterwards, the tube was centrifuged for 15 min at 20,000×g. The supernatant consisted of a solution of small, nanometer-sized liposomes and is hereafter referred to as the Erythrocyte Liposome Solution. The protocol results in a membrane concentration of ~14 mg/mL [80].

[0315] Preparation of hybrid membrane

[0316] Individual stock solutions of synthetic lipids were prepared by dissolving 1-palmitoyl-2-oleoyl-sn-glycero-3-phospho-L-serine (POPS) or 1-palmitoyl-2-oleoyl-glycero-3-phosphocholine (POPC) in chloroform and 2,2,2-Trifluoroethanol (TFE) (1:1). To produce a hybrid RBC membrane, the lipids were added to a separate glass vial to achieve an overall mass fraction of 10 mass % of POPS (FIGS. **14**-**15**), 10 mass % of POPC (FIG. **16**-**17**), or 50 mass % of POPC (FIG. **18**). The chloroform was removed by light nitrogen flow in the glass vial for ~20 min before resuspending the synthetic lipids in the Erythrocyte Liposome Solution. The mixture was then vortexed and incubated for 30 min to ensure that all of the synthetic lipids had been removed from the bottom surface of the glass vial. The hybrid membrane mixture was then sonicated at 20% intensity with 5 s pulses and 55 s breaks for 20min in an ice bucket. The sample was dried completely using a Vacufuge and incubated at 37° C. for 1 h at 97% relative humidity (RH). This step allows the lipids to anneal and form a homogeneous membrane as previously shown [81]. Following incubation, dilute PBS was added to achieve an overall molar concentration of ~1 mg/ml. This will be referred to as the hybrid membrane solution.

[0317] Electrochemical Impedance Spectroscopy (EIS)

[0318] The setup (FIGS. **13**A-**13**B) consists of a screen-printed electrochemical sensor (BVT TECHNOLOGIES, BVT-AC1) with a silver reference electrode and gold counter- and working electrodes (1 mm diameter) which is mounted in a custom made flow cell. Prior to every experiment, sensors were first immersed in a methanol bath and sonicated for 20 min to remove any organic residues. The sensor was then plasma cleaned immanently before mounting to the flow chamber. EIS spectra were measured using a PalmSens4 potentionstat (PalmSense BV, TheNetherlands). The AC voltage was set to 10 mV (0 V DC offset) and the sensor's impedance was measured for frequencies between 1 mHz and 1 MHz subdivided into 30 logarithmically distributed data points. The liquid flow through the chamber is controlled with a computer-controlled syringe pump. Both the potentiostat as well as the syringe pump were controlled through MATLAB™.

[0319] The Randles circuit (see FIGS. **13**A-**13**B for parameter definition) was found to model signals from a membrane coated and non-coated sensor. However, the interpretation of the double layer term varies for both systems. In the absence of any coating, the double layer impedance originates from the formation of the Gouy-Chapman-layer at the surface of the sensor [82]. In contrast, when coated with a membrane, the double layer term corresponds to the membrane's electrical properties and the Gouy-Chapman-layer can be neglected as it has been suggested previously [83].

[0320] (i) Hybrid RBC membrane with 10 mass % POPS

[0321] A sequence of two buffers was successively pumped into the chamber: (1) Buffer A: Potassium hexacyanoferrate(III) ($K_3[Fe(CN)_6]$) at a concentration of 5 mM. (2) Buffer B: Vesicles formed from the hybrid membrane solution in 5 mM Potassium hexacyanoferrate(III) ($K_3[Fe(CN)_6]$). Buffer A is pumped into the chamber. Ten EIS spectra are recorded in time intervals of ~1 min (left most section in the resulting graphs). Afterwards, Buffer B is pumped into the chamber. EIS spectra are monitored for 90 min in time intervals of ~1 min (right most section in the resulting graphs). The buffer B inside the chamber is exchanged after every 5 measurements.

[0322] (ii) Hybrid RBC membrane with 10 mass % of POPC

[0323] A sequence of two buffers was successively pumped into the chamber: (1) Buffer A: Potassium hexacyanoferrate(III) ($K_3[Fe(CN)_6]$) at a concentration of 5 mM. (2)

[0324] Buffer B: Vesicles formed from the hybrid membrane solution in 5 mM Potassium hexacyanoferrate(III) ($K_3[Fe(CN)_6]$). Buffer A is pumped into the chamber. Ten EIS spectra are recorded in time intervals of ~1 min (left most section in the resulting graphs). Afterwards, Buffer B is pumped into the chamber. EIS spectra are monitored for 90 min in time intervals of ~1 min (right most section in the resulting graphs). The buffer B inside the chamber is exchanged after every 5 measurements.

[0325] (iii) Hybrid RBC membrane with 50 mass % of POPC

[0326] A sequence of three buffers was successively pumped into the chamber: (1) Buffer A: Potassium hexacyanoferrate(III) (K_3 $[Fe(CN)_6]$) at a concentration of 5 mM. (2) Buffer B: Vesicles formed from the hybrid membrane solution in 5 mM Potassium hexacyanoferrate(III) ($K_3[Fe(CN)_6]$). (3) Buffer C: A sample buffer consisting of 25 μg/mL PmB in 5 mM Potassium hexacyanoferrate(III) (K_3 $[Fe(CN)_6]$). In a first step, the flow chamber is flushed with Buffer A. Ten EIS spectra are recorded in time intervals of ~1 min (left most section in the resulting graphs). Afterwards, Buffer B is pumped into the chamber. EIS spectra are monitored for 90 min in time intervals of ~1 min (middle section in the resulting graphs).

[0327] The buffer B inside the chamber is exchanged after every 5 measurements. Finally, Buffer C is pumped into the chamber. EIS spectra are recorded immediately after every movement of the syringe pump (right most section in the resulting graphs).

[0328] Results

[0329] In this assay, a gold sensor mounted in a flow cell was coated with a hybrid erythrocyte membrane. The dielectric properties of the membrane layer were modeled by a series of resistors, a Warburg element and a constant phase element, sketched in FIG. **13**B.

[0330] First, the sensor's dielectric properties were measured 10 times. Only small variations in the fitted parameters are observable indicating a system in equilibrium. Subsequently the hybrid solution was run through the flow cell and a membrane formed on the sensor. Membranes were deposited as the passivating layer on the working Au electrode surface. The redox-active molecule ferricyanide was used as a reporter and added to the buffer used during the impedance experiments. When the membrane was intact, no current from the reduction or oxidation of the reporter was observed, as the lipid membrane prevented the transfer of electrons at the electrode surface. This is indicated by an increased resistance R_0 and increase in the Warburg coefficient as well as decrease in the constant phase element coefficient CPF_0_0 as visible in FIGS. **14**C-**14**E, FIGS. **15**C-**15**E, FIGS. **16**C-**16**E, FIGS. **17**C-**17**E. The later parameter may be understood as a quantification of the membrane's capacitance.

[0331] This experiment clearly demonstrates the formation of insulating membrane layers on the surface of electrode. Importantly, this layer formation occurred in an aqueous environment and did not require drying the electrode.

[0332] Coating a sensor with a hybrid membrane is technically challenging to ensure the structural integrity and functionality of the membranes on the one hand, and to obtain a uniform coating without holes and a constant thickness on the other hand. A particular challenge is the stability of the membrane layer on the sensor's surface in aqueous solutions. Just immersing the sensor in a membrane solution did not result in a defect-free membrane coating. Therefore, the inventors have developed a protocol, where the membrane layer is formed successively, by successively pumping small amounts of membrane solution into the chamber, letting membranes attach to the sensor, and annealing the partial coating before the next injection. The resistance R_0 during the coating process of the graphs (FIGS. **14**A-**18**A) shows a sharp increase followed by slight decrease in each step. The periodicity to this zig-zag pattern corresponds to 5 coating steps and measurements, and correlates with the introduction of fresh Buffer B into the chamber. There is an increase after introducing Buffer B, followed by a slight decrease of the resistance R_0. These two behaviors can be understood by an initial attachment of the membrane to the sensor surface followed by a removal of unstable or incomplete bilayers. The fact that one can identify a further increase in the resistance R_0 whenever fresh membrane buffer was added proves that a single immersion of the sensor with buffer results in insufficient coating. It is thus required to introduce the buffer in multiple steps to archive a both stable and defect free coating. This successive coating protocol aids in providing for complete coverage of the sensor and the formation of a sufficiently thick membrane layer.

[0333] The functionality of the hybrid membrane on the sensor was tested by exposing the hybrid membrane sensor to polymyxin B. This antibiotic acts on bacterial membranes and leads to membrane damage, eventually killing the cell. Eukaryotic membranes on the other hand, are not sensitive to PmB below the toxicity limit. The sample containing 50 mass % POPC was additionally treated with polymyxin B (PmB). This membrane active antibiotics is well known to damage the membrane of gram-negative bacteria. This interaction is highly controlled by cholesterol as well as the presence of anionic lipid molecules. When the membrane is damaged, the aqueous buffer (and therefore the reporter) can access the surface of the electrode, inducing a current across the membrane. The membrane resistance was measured by Electrochemical Impedance Spectroscopy (EIS).

[0334] R_0 initially increased when lipid solution was run through the flow cell and a membrane formed on the sensor following the above protocol. The solution was then switched and buffer containing polymyxin B at a concentration of 25 μg/mL was pumped through the cell. As shown in FIG. **18**A, the resistance R_0 dropped down as the result of break through and pore formation in the membranes. At the same time, the Warburg element recovered to the state of a blank sensor and the constant phase element coefficient was further reduced. This assay and data prove the structural integrity and functionality of the hybrid membranes when applied on the sensor surface.

Example 5: Synthetic *E. coli* Membranes

[0335] Methods and Materials

[0336] Synthetic Small Unilamellar Vesicles

[0337] 1-palmitoyl-2-oleoyl-sn-glycero-3-phosphoethanolamine (POPE), 1-palmitoyl-2-oleoyl-sn-glycero-3-phospho-(1'-rac-glycerol) (POPG) and Cardiolipin (CL) was purchased from Avanti Polar Lipids. All lipids were dissolved in chloroform and mixed in POPE:POPG:CL mass ratio of 67:23.2:9.8 (FIGS. **19**-**22**), 78:21:0 (FIGS. **23**-**26**), 90:0:10 (FIG. **27**-**28**), or 0:80:20 (FIG. **29**). The chloroform was removed by light nitrogen flow in the glass vial for ~20 min before resuspending the sample in 5 mM $K_3[Fe(CN)_6]$ buffer. The volume was adjusted to achieve a concentration of 0.5 mg/ml. This mixture mimics the lipid composition in a E-Coli membrane.

[0338] Electrochemical Impedance Spectroscopy (EIS)

[0339] The setup (FIGS. **13**A-**13**B) consists of a screen printed electrochemical sensor (BVT TECHNOLOGIES, BVT-AC1) with a silver reference electrode and gold counter- and working electrodes (1 mm diameter) which is mounted in a custom made flow cell. Prior every experiment, sensors were first immersed in a methanol bath and sonicated for 20 min to remove any organic residues. The sensor was then plasma cleaned immanently before mounting to the flow chamber. EIS spectra were measured using a PalmSens4 potentionstat (PalmSense BV, TheNetherlands). The AC voltage was set to 10 mV (0 V DC offset) and the sensor's impedance was measured for frequencies between 1 mHz and 1 MHz subdivided into 30 logarithmically distributed data points. The liquid flow through the chamber is controlled with a computer-controlled syringe pump. Both, the potentiostat as well as the syringe pump were controlled through MATLAB.

[0340] The Randles circuit (see FIGS. **13**A-**13**B for parameter definition) was found to model signals from a membrane coated and non-coated sensor. However, the interpretation of the double layer term varies for both systems. In the absence of any coating, the double layer impedance originates from the formation of the Gouy-Chapman-layer at the surface of the sensor [82]. In contrast, when coated with a membrane, the double layer term corresponds the membrane's electrical properties and the Gouy-Chapman-layer can be neglected as it has been suggested previously [83].

[0341] A sequence of three buffers was successively pumped into the chamber: (1) Buffer A: Potassium hexacyanoferrate(III) (K_3 [$Fe(CN)_6$]) at a concentration of 5 mM. (2) Buffer B: Vesicles formed from the synthetic lipids in 5 mM Potassium hexacyanoferrate(III) ($K_3[Fe(CN)_6]$). (3) Buffer C: A sample buffer consisting of 25 μg/mL PmB in 5 mM Potassium hexacyanoferrate(III) ($K_3[Fe(CN)_6]$). In a first step, the flow chamber is flushed with Buffer A. Ten EIS spectra are recorded in time intervals of ~1 min (left most section in the resulting graphs). Afterwards, Buffer B is pumped into the chamber. EIS spectra are monitored for 90 min in time intervals of ~1 min (middle section in the resulting graphs). The buffer B inside the chamber is exchanged after every 5 measurements.

[0342] Finally, Buffer C is pumped into the chamber. EIS spectra are recorded immediately after every movement of the syringe pump (see the right most section in the resulting graphs).

[0343] All experiments were performed at least in duplicates.

[0344] Results

[0345] In this assay, a gold sensor mounted in a flow cell was coated with an *E. coli* mimic membrane. The dielectric properties of the membrane layer were modeled by a series of resistors, a Warburg element and a constant phase element, sketched in FIG. **13**B.

[0346] First, the sensor's dielectric properties were measured 10 times. Only small variations in the fitted parameters were observable indicating a system in equilibrium. Subsequently the *E. coli*-mimic solution was run through the flow cell and a membrane formed on the sensor. Membranes were deposited as the passivating layer on the working Au electrode surface. The redox-active molecule ferricyanide was used as a reporter and added to the buffer used during the impedance experiments. When the membrane was intact, no current from the reduction or oxidation of the reporter was observed, as the lipid membrane prevented the transfer of electrons at the electrode surface. This is indicated by an increased resistance R_0 and increase in the Warburg coefficient as well as decrease in the constant phase element coefficient CPF_0_0 as visible in FIGS. **19**-**29** (C,D,E). The later parameter may be understood as a quantification of the membrane's capacitance.

[0347] This experiment clearly demonstrates the formation of insulating membrane layers on the surface of electrode. Importantly, this layer formation occurred in an aqueous environment and does not require drying the electrode.

[0348] The samples were then treated with polymyxin B (PmB). This membrane active antibiotics is well known to damage the lipid bilayer of gram-negative bacteria. This interaction is highly controlled by cholesterol as well as the presence of anionic lipid molecules. When the membrane is damaged, the aqueous buffer (and therefore the reporter) can access the surface of the electrode. The membrane resistance was measured by Electrochemical Impedance Spectroscopy (EIS).

[0349] The response after the introduction of PmB varied significantly between sensors with different lipid compositions. Phosphatidylglycerol (PG) was identified as critical component. As shown in FIGS. **19**-**27** A and FIG. **29**A, the resistance R_0 first increased. This indicates an accumulation of PmB on the membrane surface. Once a critical concentration was achieved, R_0 dropped as the result of break through and pore formation in the membranes. At the same time, the Warburg element recovered to the state of a blank sensor and the constant phase element coefficient was further reduced.

[0350] This is very different in the absence of PG lipids (FIGS. **27**A and **28**A). Here, the resistance R_0 increased after the introduction of PmB. This indicates a formation of a PmB layer on the membrane's surface without damaging the bilayer. This experiment demonstrates the sensor's ability to reliably detect and quantify antibiotic activity.

Example 6: *E. coli* membranes

[0351] Methods and Materials

[0352] *E-Coli*-based Small Unilamellar Vesicles

[0353] *E. coli* Extract polar lipid extract in Chloroform was purchased from Avanti Polar Lipids (Product number 100600). The original sample was aliquoted for individual measurement runs. The chloroform was removed by light nitrogen flow in the glass vial for ~20 min before resuspending the sample in 5 mM $K_3[Fe(CN)_6$ buffer. The volume was adjusted to achieve a concentration of 0.5 mg/ml.

[0354] Electrochemical Impedance Spectroscopy (EIS)

[0355] The setup (FIGS. **13**A-**13**B) consists of a screen printed electrochemical sensor (BVT TECHNOLOGIES, BVT-AC1) with a silver reference electrode and gold counter- and working electrodes (1 mm diameter) which is mounted in a custom made flow cell. Prior every experiment, sensors were first immersed in a methanol bath and sonicated for 20 min to remove any organic residues. The sensor was then plasma cleaned immanently before mounting to the flow chamber. EIS spectra were measured using a PalmSens4 potentionstat (PalmSense BV, TheNetherlands). The AC voltage was set to 10 mV (0 V DC offset) and the sensor's impedance was measured for frequencies between 1 mHz and 1 MHz subdivided into 30 logarithmically distributed data points. The liquid flow through the chamber is controlled with a computer-controlled syringe pump. Both, the potentiostat as well as the syringe pump were controlled through MATLAB.

[0356] The Randles circuit (see FIGS. **13**A-**13**B for parameter definition) was found to model signals from a membrane coated and non-coated sensor. However, the interpretation of the double layer term varies for both systems. In the absence of any coating, the double layer impedance originates from the formation of the Gouy-Chapman-layer at the surface of the sensor [82]. In contrast, when coated with a membrane, the double layer term corresponds the membrane's electrical properties and the Gouy-Chapman-layer can be neglected as it has been suggested previously [83].

[0357] A sequence of three buffers was successively pumped into the chamber: (1) Buffer A: Potassium hexacyanoferrate(III) ($K_3[Fe(CN)_6]$) at a concentration of 5 mM.

(2) Buffer B: Vesicles formed from the E. coli membrane analog in 5 mM Potassium hexacyanoferrate(III) ($K_3[Fe(CN)_6]$). (3) Buffer C: A sample buffer consisting of 25 μg/mL PmB in 5 mM Potassium hexacyanoferrate(III) ($K_3[Fe(CN)_6]$). In a first step, the flow chamber is flushed with Buffer A. Ten EIS spectra are recorded in time intervals of ~1 min (left most section in the resulting graphs). Afterwards, Buffer B is pumped into the chamber. EIS spectra are monitored for 90 min in time intervals of ~1 min (middle section in the resulting graphs). The buffer B inside the chamber is exchanged after every 5 measurements. Finally, Buffer C is pumped into the chamber. EIS spectra are recorded immediately after every movement of the syringe pump (see the right most section in the resulting graphs).

[0358] Results

[0359] In this assay, a gold sensor mounted in a flow cell was coated with an *E. coli* membrane. The dielectric properties of the membrane were modeled by a series of resistors, a Warburg element and a constant phase element, sketched in FIG. **13**B.

[0360] First, the sensor's dielectric properties were measured 10 times. Only small variations in the fitted parameters were observable indicating a system in equilibrium. Subsequently the *E. coli* membrane solution was run through the flow cell and a membrane formed on the sensor. Membranes were deposited as the passivating layer on the working Au electrode surface. The redox-active molecule ferricyanide was used as a reporter and added to the buffer used during the impedance experiments. When the membrane was intact, no current from the reduction or oxidation of the reporter was observed, as the lipid membrane prevented the transfer of electrons at the electrode surface. This is indicated by an increased resistance R_0 and increase in the Warburg coefficient as well as decrease in the constant phase element coefficient CPF_0_0 as visible in FIGS. **30**C-**30**E and FIGS. **31**C-**31**E. The later parameter may be understood as a quantification of the membrane's capacitance.

[0361] This experiment clearly demonstrates the formation of insulating membrane layers on the surface of electrode. Importantly, this layer formation occurred in an aqueous environment and did not require drying the electrode.

[0362] The samples were then treated with polymyxin B (PmB). This membrane active antibiotics is well known to damage the lipid bilayer of gram-negative bacteria. This interaction is highly controlled by cholesterol as well as the presence of anionic lipid molecules. When the membrane is damaged, the aqueous buffer (and therefore the reporter) can access the surface of the electrode. The membrane resistance was measured by Electrochemical Impedance Spectroscopy (EIS).

[0363] As shown in FIGS. **30**A and **31**A, the resistance R_0 first increased. This indicates an accumulation of PmB on the membrane surface. Once a critical concentration was achieved, R_0 dropped as the result of break through and pore formation in the membranes. At the same time, the Warburg element recovered to the state of a blank sensor and the constant phase element coefficient was further reduced.

[0364] This experiment demonstrates the sensor's ability to reliably detect and quantify antibiotic activity.

Example 7: Renal Membrane Analogues

[0365] Lipid compositions were based on the composition of detergent-susceptible (cholesterol-depleted) renal membranes by Marqueź et al. [84]. 1,2-Dimyristoyl-sn-glycero phosphocholine (DMPC), -phospho-L-serine (DMPS), and -phosphoethanolamine (DMPE) (Avanti Polar Lipids) (2:1:1 mass %), cholesterol (Caledon), and polymyxin B (Sigma-Aldrich) were mixed at desired molecular ratios and dissolved in a mixture of chloroform (Caledon)/2,2,2- trifluoroethanol (TFE) (Sigma-Aldrich). 3 mass % cholesterol was added to the lipid mix, resulting in a 2:1:1:0.2 ratio for DMPC/DMPS/DMPE/Chol.

[0366] Electrochemical Impedance Spectroscopy (EIS)

[0367] The setup (FIGS. **13**A-**13**B) consists of a screen-printed electrochemical sensor (BVT TECHNOLOGIES, BVT-AC1) with a silver reference electrode and gold counter- and working electrodes (1 mm diameter) which are mounted in a custom-made flow cell. Prior to every experiment, sensors were first immersed in a methanol bath and sonicated for 20 min to remove any organic residues. The sensor was then plasma-cleaned before mounting to the flow chamber. EIS spectra were measured using a PalmSens4 potentiostat (PalmSense BV, The Netherlands). The ac voltage was set to 10 mV (0 V DC offset), and the sensor's impedance was measured for frequencies between 1 mHz and 1 MHz subdivided into 30 logarithmically distributed data points. The liquid flow through the chamber was controlled using a computer-controlled syringe pump. Both the potentiostat as well as the syringe pump were controlled through MATLAB.

[0368] The real and imaginary parts of the recorded sensor impedance were fitted simultaneously to the Randles circuit (FIGS. **13**A-**13**B) using the impedance.py Python library (version 1.4.1). The buffer is represented by a single resistor Rs_{ol} in series with a double-layer impedance which consists of a parallel circuit of the double-layer capacitance Cm and double-layer resistance. The double-layer capacitance was modeled by a constant-phase element; the double-layer resistance is a series of a resistor R_m with a Warburg element W_m.

[0369] The Randles circuit was found to model signals from a membrane-coated and noncoated sensor; however, we note that the interpretation of the double-layer term varies for both systems. In the absence of any coating, the double-layer impedance originates from the formation of the Gouy-Chapman layer at the surface of the sensor. [82] In contrast, when coated with a membrane, the double-layer term corresponds to the membrane's electrical properties and the Gouy-Chapman layer can be neglected as it has been suggested previously. [83]

[0370] A sequence of three buffers was successively pumped into the chamber: (1) buffer A: potassium hexacyanoferrate(III) ($K_3[Fe(CN)_6]$) at a concentration of 5 mM. (2) Buffer B: vesicles formed from the cholesterol-depleted renal membrane analogue in 5 mM potassium hexacyanoferrate(III) ($K_3[Fe(CN)_6]$). (3) Buffer C: A sample buffer consisting of either 25 μg/mL PmB, 25 μg/mL of PmB in the erythro-PmBs, or 4.5 mg/mL of erythrocyte liposomes in 5 mM potassium hexacyanoferrate(III) ($K_3[Fe(CN)_6]$). In the first step, the flow chamber is flushed with Buffer A. Ten EIS spectra are recorded in time intervals of ≈1 min. Afterward, Buffer B is pumped into the chamber. EIS spectra are monitored for 90 min in time intervals of min. Finally, Buffer C is pumped into the chamber. The buffer B inside the chamber is exchanged after every 5 measurements. EIS spectra are recorded immediately after every movement of the syringe pump.

[0371] Results

[0372] Nephrotoxicity was tested in vitro in renal membrane analogues. In this assay, a gold sensor mounted in a flow cell is first coated with renal membrane analogues and then treated with the agent. Detergent-susceptible(cholesterol-depleted) renal membranes were deposited on the sensors where membrane composition was taken from Marquei et al. [84]. The dielectric properties of the membrane layer were modeled by a series of resistors, a Warburg element and a constant phase element, sketched in FIGS. **13**A-**13**B.

[0373] Membranes were deposited as a passivating layer on the working Au electrode surface. The redox-active molecule ferricyanide was used as a reporter and added to the buffer used during the impedance experiments. When the membrane is intact, no current from the reduction or oxidation of the reporter is observed as the lipid membrane prevents the transfer of electrons at the electrode surface. When the membrane is damaged, the aqueous buffer (and therefore the reporter) can access the surface of the electrode. The membrane resistance was measured by electrochemical impedance spectroscopy (EIS). PmB, erythrocyte liposomes (the empty delivery system), and erythro-PmBs (antibody-conjugated erythrocyte liposomes with polymyxin B) were then run through the flow cell, and membrane resistance (Rm) was recorded as a function of time.

[0374] Rm initially increased when lipid solution was run through the flow cell and a membrane formed on the sensor. Susceptible renal membrane analogues containing 3 mass % cholesterol was used as they are most sensitive to PmB damage.[85] The solution is then switched, and a buffe containing polymyxin B at a concentration of 25 μg/mL is pumped through the cell. As shown in FIG. **33**, the resistance continues to increase, indicating that PmB attaches to the surface of the membranes. Once a critical PmB concentration is achieved, the Rm drops down as a result of break through and pore formation in the membranes.

[0375] When using erythrocyte liposomes (FIG. **22**), Rm increases after membrane formation indicative of liposome attachment to the renal membrane analogue. Resistance stays high, indicating that the membrane stays intact. When treating the sensor with erythro-PmBs, resistance continuously increases after membrane formation with no sign of leakage and membrane damage. Hence, while free PmB showed clear nephrotoxicity and damage to renal membrane analogues, the erythrocyte liposomes and the erythro-PmBs did not result in damage in the susceptible (cholesterol-depleted) renal membranes.

[0376] While the present application has been described with reference to examples, it is to be understood that the scope of the claims should not be limited by the embodiments set forth in the examples, but should be given the broadest interpretation consistent with the description as a whole.

[0377] All publications, patents and patent applications are herein incorporated by reference in their entirety to the same extent as if each individual publication, patent or patent application was specifically and individually indicated to be incorporated by reference in its entirety. Where a term in the present application is found to be defined differently in a document incorporated herein by reference, the definition provided herein is to serve as the definition for the term.

REFERENCES

[0378] [1] James T Dodge, Carolyn Mitchell, and Donald J Hanahan, "The preparation and chemical characteristics of hemoglobin-free ghosts of human erythrocytes," Archives of biochemistry and biophysics 100, 119-130 (1963).

[0379] [2] G Schwoch and H Passow, "Preparation and properties of human erythrocyte ghosts," Molecular and cellular biochemistry 2, 197-218 (1973).

[0380] [3] Lars Kaestner, "Red blood cell ghosts and intact red blood cells as complementary models in photodynamic cell research," Bioelectrochemistry 62, 123-126 (2004).

[0381] [4] Theodore L Steck, "The organization of proteins in the human red blood cell membrane a review," The Journal of cell biology 62, 1-19 (1974).

[0382] [5] A. J Verkleij, R. F. A Zwaal, B Roelofsen, P Comfurius, D Kastelijn, and L. L. M van Deenen, "The asymmetric distribution of phospholipids in the human red cell membrane. a combined study using phospholipases and freeze-etch electron microscopy," Biochimica et Biophysica Acta (BBA)—Biomembranes 323, 178-193 (1973).

[0383] [6] Narla Mohandas and Patrick G Gallagher, "Red cell membrane: past, present, and future," Blood 112, 3939-3948 (2008).

[0384] [7] T. H. Watts, A. A. Brian, J. W. Kappler, P. Marrack, and H. M. McConnell, "Antigen presentation by supported planar membranes containing affinity-purified I-Ad ," Proc. Natl. Acad. Sci. U.S.A. 81, 7564-7568 (1984).

[0385] [8] G. Pabst, N. Kučerka, M.-P. Nieh, M. C. Rheinstädter, and J. Katsaras, "Applications of neutron and x-ray scattering to the study of biologically relevant model membranes," Chemistry and Physics of Lipids 163, 460-479 (2010).

[0386] [9] Ilya Reviakine and Alain Brisson, "Formation of supported phospholipid bilayers from unilamellar vesicles investigated by atomic force microscopy," Langmuir 16, 1806-1815 (2000).

[0387] [10] John F. Nagle and Stephanie Tristram-Nagle, "Structure of lipid bilayers," Biochim. Biophys. Acta 1469, 159-195 (2000).

[0388] [11] S. H. Chen, C. Y. Liao, H. W. Huang, T. M. Weiss, M. C. Bellisent-Funel, and F. Sette, "Collective dynamics in fully hydrated phospholipid bilayers studied by inelastic x-ray scattering," Phys. Rev. Lett. 86, 740-743 (2001).

[0389] [12] M. C. Rheinstädter, C. Ollinger, G. Fragneto, F. Demmel, and T. Salditt, "Collective dynamics of lipid membranes studied by inelastic neutron scattering," Phys. Rev. Lett. 93, 108107 (2004).

[0390] [13] M. Tanaka and E. Sackmann, "Polymer-supported membranes as models of the cell surface," Nature 437, 656-663 (2005).

[0391] [14] Daillant, E Bellet-Amalric, A Braslau, T Charitat, G Fragneto, F Graner, S Mora, F Rieutord, and B Stidder, "Structure and fluctuations of a single floating lipid bilayer," Proceedings of the National Academy of Sciences of the United States of America 102, 11639-11644 (2005).

[0392] [15] Maikel C. Rheinstädter, Wolfgang Häussler, and Tim Salditt, "Dispersion relation of lipid membrane shape fluctuations by neutron spin-echo spectrometry," Phys. Rev. Lett. 97, 048103 (2006).

[0393] [16] Xinjian Zhou, Jose M Moran-Mirabal, Harold G Craighead, and Paul L McEuen, "Supported lipid bilayer/carbon nanotube hybrids," Nature nanotechnology 2, 185-190 (2007).

[0394] [17] Norbert Kučerka, Mu-Ping Nieh, and John Katsaras, "Fluid phase lipid areas and bilayer thicknesses of commonly used phosphatidylcholines as a function of temperature," Biochimica et Biophysica Acta (BBA)—Biomembranes 1808, 2761 — 2771 (2011).

[0395] [18] Maikel C Rheinstädter, "Lipid membrane dynamics," in Dynamics of Soft Matter: Neutron Applications, edited by Sow- Hsin Chen Victoria Garcia Sakai, Christiane Alba-Simionesco (Springer Science & Business Media, 2011) p. 263.

[0396] [19] Bradley Moores, Elizabeth Drolle, Simon J Attwood, Janet Simons, and Zoya Leonenko, "Effect of surfaces on amyloid fibril formation," PLoS One 6, e25954 (2011).

[0397] [20] Maikel Rheinstädter, Laura Toppozini, and Hannah Dies, "The interaction of bio-molecules with lipid membranes studied by x-ray diffraction," Zeitschrift fur Physikalische Chemie 228, 1105-1120 (2014).

[0398] [21] Maikel C Rheinstädter, "Basic aspects and applications of lipids and protein dynamics," in Liposomes, Lipid Bilayers and Model Membranes: from Basic Research to Application, edited by Mu-Ping Nieh Norbert Kučerka, Georg Pabst and John Katsaras (CRC Press, 2014)

[0399] [22] Drew Marquardt, Richard J Alsop, Maikel C Rheinstädter, and Thad A Harroun, "Neutron scattering at the intersection of heart health science and biophysics," Journal of Cardiovascular Development and Disease 2, 125-140 (2015).

[0400] [23] Kelly Cathcart, Amit Patel, Hannah Dies, Maikel C Rheinstädter, and Cecile Fradin, "Effect of cholesterol on the structure of a five-component mitochondria-like phospholipid membrane," Membranes 5, 664-684 (2015).

[0401] [24] Richard J Alsop, Laura Toppozini, Drew Marquardt, Norbert Kučerka, Thad A Harroun, and Maikel C Rheinstädter, "Aspirin inhibits formation of cholesterol rafts in fluid lipid membranes," Biochimica et Biophysica Acta (BBA)-Biomembranes 1848, 805— 812 (2015).

[0402] [25] Richard J Alsop, Clare L Armstrong, Amna Maqbool, Laura Toppozini, Hannah Dies, and Maikel C Rheinstädter, "Cholesterol expels ibuprofen from the hydrophobic membrane core and stabilizes lamellar phases in lipid membranes containing ibuprofen," Soft matter 11, 4756-4767 (2015).

[0403] [26] Jennifer Tang, Richard J Alsop, Matilda Backholm, Hannah Dies, An-Chang Shi, and Maikel C Rheinstädter, "Amyloid-f3 25-35 peptides aggregate into cross-f3 sheets in unsaturated anionic lipid membranes at high peptide concentrations," Soft matter 12, 3165-3176 (2016).

[0404] [27] Richard J Alsop, Adree Khondker, Jochen S Hub, and Maikel C Rheinstädter, "The lipid bilayer provides a site for cortisone crystallization at high cortisone concentrations," Scientific reports 6, 1-10 (2016).

[0405] [28] J Yang, L K Tamm, T W Tillack, and Z Shao, "New approach for atomic force microscopy of membrane proteins. the imaging of cholera toxin," Journal of molecular biology 229, 286-90 (1993).

[0406] [29] S A Jewell, R W Titball, J Huyet, C E Naylor, A K Basak, P Gologan, C P Winlove, and P G Petrov, "*Clostridium perfringens* α-toxin interaction with red cells and model membranes," Soft matter 11, 7748-61 (2015).

[0407] [30] K. Simons and E. Ikonen, "Functional rafts in cell membranes," Nature 387, 569572 (1997).

[0408] [31] Ka Simons and Mathias J. Gerl, "Revitalizing membrane rafts: new tools and insights," Nat Rev Mol Cell Biol 11, 688-699 (2010).

[0409] [32] Clare L. Armstrong, Drew Marquardt, Hannah Dies, Norbert Kučerka, Zahra Yamani, Thad A. Harroun, John Katsaras, An-Chang Shi, and Maikel C. Rheinstädter, "The observation of highly ordered domains in membranes with cholesterol," PLOS ONE 8, e66162 (2013).

[0410] [33] Sebastian Meinhardt, Richard L. C. Vink, and Friederike Schmid, "Monolayer curvature stabilizes nanoscale raft domains in mixed lipid bilayers," Proc. Natl. Acad. Sci. U.S.A. 110, 4476-4481 (2013).

[0411] [34] Maikel C. Rheinstädter and Ole G. Mouritsen, "Small-scale structures in fluid cholesterol-lipid bilayers," Curr. Opin. Colloid Interface Sci. 18, 440-447 (2013).

[0412] [35] Laura Toppozini, Sebastian Meinhardt, Clare L Armstrong, Zahra Yamani, Norbert Kučerka, Friederike Schmid, and Maikel C Rheinstädter, "Structure of cholesterol in lipid rafts," Physical review letters 113, 228101 (2014).

[0413] [36] Maikel C. Rheinstädter Richard J. Alsop, "Lipid rafts in binary lipid/cholesterol bilayers," in Membrane organization and lipid rafts in the cell and artificial membranes, Cell Biology Research Progress, edited by Angel Catala (Nova, 2016) pp. 17— 42.

[0414] [37] Gerald J Roth, Nancy Stanford, and Philip W Maj eros, "Acetylation of prostaglandin synthase by aspirin," Proc. Natl. Acad. Sci. U.S.A. 72, 3073-3076 (1975).

[0415] [38] Carlo Patrono, Luis A Garc´ia Rodriguez, Raffaele Landolfi, and Colin Baigent, "Low-dose aspirin for the prevention of atherothrombosis," N. Engl. J. Med. 353, 2373-2383 (2005).

[0416] [39] Valerie B ODonnell, Robert C Murphy, and Steve P Watson, "Platelet lipidomics modern day perspective on lipid discovery and characterization in platelets," Circulation research 114, 1185-1203 (2014).

[0417] [40] Sanford J Shattil and Richard A Cooper, "Membrane microviscosity and human platelet function," Biochemistry (Mosc.) 15, 4832-4837 (1976).

[0418] [41] Pannuru Padmavathi, Vaddi Damodara Reddy, Paramahamsa Maturu, and Nallanchakravarthula Varadacharyulu, "Smoking-induced alterations in platelet membrane fluidity and Na+/K+-ATPase activity in chronic cigarette smokers," J Atheroscler Thromb 17, 619-627 (2010).

[0419] [42] Karine Gousset, Willem F Wolkers, Nelly M Tsvetkova, Ann E Oliver, Cara L Field, Naomi J Walker, John H Crowe, and Fern Tablin, "Evidence for a physiological role for membrane rafts in human platelets," J. Cell. Physiol. 190, 117-128 (2002).

[0420] [43] E Beutler, C West, and K G Blume, "The removal of leukocytes and platelets from whole blood," J Lab Clin Med 88, 328-333 (1976).

[0421] [44] Giampaolo Minetti, Stephane Egée, Daniel Mörsdorf, Patrick Steffen, Asya Makhro, Cesare Achilli, Annarita Ciana, Jue Wang, Guillaume Bouyer, Ingolf Bernhardt, Christian Wagner, Serge Thomas, Anna Bogdanova, and Lars Kaestner, "Red cell investigations: Art and artefacts," Blood Reviews 27, 91101 (2013).

[0422] [45] W. B. Grazer, "The red cell membrane and its cytoskeleton," Biochemical Journal 198, 1-8 (1981).

[0423] [46] D. Tortorella and E. London, "Method for efficient pelleting of small unilamellar model membrane vesicles," Analytical Biochemistry 217, 176 — 180 (1994).

[0424] [47] R. Richter, A. Mukhopadhyay, and A. Brisson, "Pathways of lipid vesicle deposition on solid surfaces: A combined QCM-D and AFM study," Biophys. J. 85, 3035-3047 (2003).

[0425] [48] Clare L. Armstrong, Martin D. Kaye, Michaela Zamponi, Eugene Mamontov, Madhusudan Tyagi, Timothy Jenkins, and Maikel C. Rheinstädter, "Diffusion in single solid supported lipid bilayers studied by quasi-elastic neutron scattering," Soft Matter 6, 5864-5867 (2010).

[0426] [49] M. Lucio, C. Nunes, D. Gaspar, K. Golebska, M. Wisniewski, J. L. F. C. Lima, G. Brezesinski, and S. Reis, "Effect of anti-inflammatory drugs in phosphatidylcholine membranes: A fluorescence and calorimetric study," Chemical Physics Letters 471, 300-309 (2009).

[0427] [50] Stephanie Tristram-Nagle, Yufeng Liu, Justin Legleiter, and John F. Nagle, "Structure of gel phase dmpc determined by x-ray diffraction," Biophysical Journal 83, 3324-3335 (2002).

[0428] [51] Matthew A. Barrett, Songbo Zheng, Golnaz Roshankar, Richard J. Alsop, Randy K. R. Belanger, Chris Huynh, Norbert Kučerka, and Maikel C. Rheinstädter, "Interaction of aspirin (acetylsalicylic acid) with lipid membranes," PLoS ONE 7, e34357 (2012).

[0429] [52] Norbert Kučerka, Yufeng Liu, Nanjun Chu, Horia I. Petrache, Stephanie Tristram-Nagle, and John F. Nagle, "Structure of fully hydrated fluid phase DMPC and DLPC lipid bilayers using x-ray scattering from oriented multilamellar arrays and from unilamellar vesicles," Biophys. J. 88, 2626-2637 (2005).

[0430] [53] H. Dies, L. Toppozini, and M. C. Rheinstädter, "The interaction between amyloid-β peptides and anionic lipid membranes containing cholesterol and melatonin," PLOS ONE , 1-17 (2014).

[0431] [54] M. C. Rheinstädter, C. Ollinger, G. Fragneto, F. Demmel, and T. Salditt, "Collective dynamics of lipid membranes studied by inelastic neutron scattering," Phys. Rev. Lett. 93, 108107 (2004).

[0432] [55] R. Welti, D. A. Rintoul, F. Goodsaid-Zalduondo, S. Felder, and D. F. Silbert, "Gel-phase phospholipid in the plasma membrane of sterol-depleted mouse lm cells," The Journal of Biological Chemistry 256, 7528-7535 (1981).

[0433] [56] Danny Poinapen, Laura Toppozini, Hannah Dies, Daniel C W Brown, and Maikel C Rheinstädter, "Static magnetic fields enhance lipid order in native plant plasma membrane," Soft Matter 9, 6804-6813 (2013).

[0434] [57] J. Katsaras, V. A. Raghunathan, E. J. Dufourc, and J. Dufourcq, "Evidence for a two-dimensional molecular lattice in subgel phase DPPC bilayers," Biochemistry 34, 4684-4688 (1995).

[0435] [58] T. T. Mills, J. Huang, G. W. Feigenson, and J. F. Nagle, "Effects of cholesterol and unsaturated dopc lipid on chain packing of saturated gel-phase DPPC bilayers," Gen. Physiol. Biophys. 28, 126-139 (2009).

[0436] [59] Nicole Pinto, Fei-Chi Yang, Atsuko Negishi, Maikel C. Rheinstädter, Todd E. Gillis, and Douglas S. Fudge, "Self-assembly enhances the strength of fibers made from vimentin intermediate filament proteins," Biomacromolecules 15, 574-581 (2014).

[0437] [60] Fei-Chi Yang, Robert D. Peters, Hannah Dies, and Maikel C. Rheinstädter, "Hierarchical, self-similar structure in native squid pen," Soft Matter 10, 5541— 5549 (2014).

[0438] [61] Fei-Chi Yang, Yuchen Zhang, and Maikel C Rheinstädter, "The structure of people's hair," PeerJ 2, e619 (2014).

[0439] [62] Yuchen Zhang, Richard J Alsop, Asfia Soomro, Fei-Chi Yang, and Maikel C Rheinstädter, "Effect of shampoo, conditioner and permanent waving on the molecular structure of human hair," PeerJ 3, e1296 (2015).

[0440] [63] Sébastien Neukirch, Alain Goriely, and Andrew C Hausrath, "Chirality of coiled coils: elasticity matters," Physical review letters 100, 038105 (2008).

[0441] [64] FHC Crick, "Is α-keratin a coiled coil?" Nature 170, 882 — 883 (1952).

[0442] [65] C Cohen and DA Parry, "α-helical coiled coils: more facts and better predictions," Science 263, 488-489 (1994).

[0443] [66] Andrei N Lupas and Markus Gruber, "The structure of α-helical coiled coils," Advances in protein chemistry 70, 37-38 (2005).

[0444] [67] S Knutton, J B Finean, R Coleman, and A R Limbrick, "Low-angle x-ray diffraction and electron-microscope studies of isolated erythrocyte membranes," Journal of cell science 7, 357-371 (1970).

[0445] [68] James B Stamatoff, Samuel Krimm, and Nancy Reid Harvie, "X-ray diffraction studies of human erythrocyte membrane structure," Proceedings of the National Academy of Sciences 72, 531-534 (1975).

[0446] [69] Richard J Alsop, Rafaela Schober, and Maikel Christian Rheinstädter, "Swelling of phospholipid membranes by divalent metal ions depends on the location of the ions in the bilayers," Soft Matter (2016).

[0447] [70] M Lucio, J L F C Lima, and S Reis, "Drug-membrane interactions: significance for medicinal chemistry," Current medicinal chemistry 17, 1795-1809 (2010).

[0448] [71] Lenard M Lichtenberger, Yong Zhou, Vasanthi Jayaraman, Janice R Doyen, Roger G O'Neil, Elizabeth J Dial, David E Volk, David G Gorenstein, Mohan Babu Boggara, and Ramanan Krishnamoorti, "Insight into nsaid-induced membrane alterations, pathogenesis and therapeutics: characterization of interaction of nsaids with phosphatidylcholine," BBA-MOL CELL BIOL L 1821, 994-1002 (2012).

[0449] [72] Catarina Pereira-Leite, Claudia Nunes, and Salette Reis, "Interaction of nonsteroidal anti-inflammatory drugs with mem-branes: In vitro assessment and relevance for their biological actions," Progress in lipid research 52, 571-584 (2013).

[0450] [73] Mario Suwalsky, Jessica Belmar, Fernando Villena, Maria José Gallardo, Malgorzata Jemiola-Rzeminska, and Kazimierz Strzalka, "Acetylsalicylic acid (aspirin) and salicylic acid interaction with the human erythrocyte membrane bilayer induce in vitro changes in the morphology of erythrocytes," Archives of biochemistry and biophysics 539, 9-19 (2013).

[0451] [74] Lenard M Lichtenberger, Yong Zhou, Elizabeth J Dial, and Robert M Raphael, "Nsaid injury to the gastrointestinal tract: evidence that nsaids interact with phospholipids to weaken the hydrophobic surface barrier and induce the formation of unstable pores in membranes," J. Pharm. Pharmacol. 58, 1421-1428 (2006).

[0452] [75] Yong Zhou, Kwang-Jin Cho, Sarah J Plowman, and John F Hancock, "Nonsteroidal anti-inflammatory drugs alter the spatiotemporal organization of ras proteins on the plasma membrane," Journal of Biological Chemistry 287, 16586-16595 (2012).

[0453] [76] Richard J Alsop, Matthew A Barrett, Songbo Zheng, Hannah Dies, and Maikel C Rheinstädter, "Acetylsalicylic acid (asa) increases the solubility of cholesterol when incorporated in lipid membranes," Soft matter 10, 4275-4286 (2014).

[0454] [77] Photoelectric Spectrometry Group and Institut für Spektrochemie und Angewandte Spektroskopie, UV Atlas of Organic Compounds: UV Atlas Organischer Verbindungen , UV Atlas of Organic Compounds: UV Atlas Organischer Verbindungen No. Bd. 2 (Plenum Press, 1966).

[0455] [78] J. F. Nagle and M. C. Wiener, "Relations for lipid bilayers," Biophys. J. 55, 309-313 (1989).

[0456] [79] P. Scherrer, "Bestimmung der Größe und der inneren Struktur von Kollidteilchen mittels R¨ontgenstrahlen," Göttinger Nachrichten Math. Phys. 2, 98-100 (1918).

[0457] [80] Himbert, Sebastian, Richard J. Alsop, Markus Rose, Laura Hertz, Alexander Dhaliwal, Jose M. Moran-Mirabal, Chris P. Verschoor et al. "The molecular structure of human red blood cell membranes from highly oriented, solid supported multi-lamellar membranes." Scientific reports 7, no. 1 (2017): 1-14.

[0458] [81] Himbert, Sebastian, Matthew J. Blacker, Alexander Kihm, Quinn Pauli, Adree Khondker, Kevin Yang, Sheilan Sinjari et al. "Hybrid erythrocyte liposomes: Functionalized red blood cell membranes for molecule encapsulation." Advanced Biosystems 4, no. 3 (2020): 1900185.

[0459] [82] Oldham, Keith B. "A Gouy—Chapman—Stern model of the double layer at a (metal)/(ionic liquid) interface." Journal of Electroanalytical Chemistry 613, no. 2 (2008): 131-138.

[0460] [83] Steinem, Claudia, Andreas Janshoff, Wolf-Peter Ulrich, Manfred Sieber, and Hans-Joachim Galla. "Impedance analysis of supported lipid bilayer membranes: a scrutiny of different preparation techniques." Biochimica et Biophysica Acta (BBA)-Biomembranes 1279, no. 2 (1996): 169-180.

[0461] [84] Márquez M G, Favale N O, Nieto F L, Pescio L G, Sterin-Speziale N. Changes in membrane lipid composition cause alterations in epithelial cell—cell adhesion structures in renal papillary collecting duct cells. Biochimica et Biophysica Acta (BBA)-Biomembranes. 2012 Mar. 1;1818(3):491-501.

[0462] [85] Khondker A, Alsop R J, Dhaliwal A, Saem S, Moran-Mirabal J M, Rheinstädter M C. Membrane cholesterol reduces polymyxin B nephrotoxicity in renal membrane analogs. Biophysical Journal. 2017 Nov. 7;113(9): 2016-28.

1. A biosensor comprising:

a solid substrate having a lipid bilayer compatible surface; and

a multi-lamellar lipid membrane structure localized on the lipid bilayer compatible surface, the multi-lamellar lipid membrane structure being prepared from red blood cells or red blood cell ghosts and comprising one or more synthetic lipids.

2. The biosensor of claim **1**, wherein the one or more synthetic lipids are selected from the group consisting of 1,2-dimyristoyl-sn-glycero-3-phosphocholine (DMPC), 1-palmitoyl-2-oleoyl-glycero-3-phosphocholine (POPC), 1-palmitoyl-2-oleoyl-sn-glycero-3-phospho-L-serine (POPS), 1,2-dimyristoyl-sn-glycero-3-phospho-L-serine (DMPS), and 1-palmitoyl-2-oleoyl-sn-glycero-3-phospho-(1'-rac-glycerol) (POPG).

3. The biosensor of claim **1**, wherein the one or more synthetic lipids comprises a phospholipid, wherein the phospholipid is 18:1, 18:0, 14:0, or 16:0.

4. The biosensor of claim **1**, wherein the one or more synthetic lipids comprises a phosphatidylcholine (PC) and/or a phosphatidylethanolamine (PE).

5. The biosensor of claim **4**, wherein the PC is selected from the group consisting of 1,2-dimyristoyl-sn-glycero-3-phosphocholine (DMPC) and 1-palmitoyl-2-oleoyl-glycero-3-phosphocholine (POPC).

6. The biosensor of claim **4**, wherein the concentration of the PC and/or the PE in the multi-lamellar lipid membrane structure is between about 10 mass % to about 90 mass %, between about 20 mass % to about 80 mass %, between about 30 mass % to about 70 mass %, or between about 40 mass % to about 60 mass %, or between about 45 mass % to about 55 mass %.

7. The biosensor of claim **6**, wherein the concentration of the PC and/or the PE in the multi-lamellar lipid membrane structure is about 10 mass %, about 20 mass %, about 50 mass %, about 80 mass % or about 90 mass %.

8. The biosensor of claim **1**, wherein the one or more synthetic lipids comprises a phosphatidylglycerol (PG) and/or a phosphatidylserine (PS).

9. The biosensor of claim **8**, wherein the PS is selected from the group consisting of 1-palmitoyl-2-oleoyl-sn-glycero-3-phospho-L-serine (POPS) and 1,2-dimyristoyl-sn-glycero phospho-L-serine (DMPS).

10. The biosensor of claim **8**, wherein the PG comprises 1-palmitoyl-2-oleoyl-sn-glycero-3-phospho-(1'-rac-glycerol) (POPG).

11. The biosensor of claim **8**, wherein the concentration of the PG and/or the PS in the multi-lamellar lipid membrane structure is between about 10 mass % to about 50 mass %, between about 20 mass % to about 40 mass %, or between about 25 mass % to about 35 mass %.

12. The biosensor of claim **11**, wherein the concentration of the PG and/or the PS in the multi-lamellar lipid membrane structure is about 10 mass %, about 20 mass %, or about 50 mass %.

13. The biosensor of claim **1**, wherein the multi-lamellar lipid membrane structure further comprises one or more lipids conjugated with polyethylene glycol (PEGylated lipids).

14. The biosensor of claim **13**, wherein the PEG is PEG 350, PEG550, PEG 750, PEG1000, PEG2000, PEG3000, or PEG5000.

15. The biosensor of claim **13**, wherein the one or more PEGylated lipids comprises PEGylated phosphatidylethanolamine (PE).

16. The biosensor of 13, wherein the one or more PEGylated lipids comprises a functionalized PEGylated lipid, the functionalized PEGylated lipid comprises a functionalized group selected from the group consisting of maleimide, biotin and amine.

17. The biosensor of claim **15**, wherein the PEGylated PE is 18:1, 18:0, 14:0, or 16:0.

18. The biosensor of claim **13**, wherein the one or more PEGylated lipids comprises PEGylated cholesterol.

19. The biosensor of claim **13**, wherein the polyethylene glycol is methoxy polyethylene glycol.

20. The biosensor of claim **13**, wherein the concentration of the one or more synthetic lipids is up to about 10 mass %

and the concentration of the PEGylated lipids in the multi-lamellar lipid membrane structure is up to about 10 mass %.

21. A biosensor comprising:

a solid substrate having a lipid bilayer compatible surface; and

a multi-lamellar lipid membrane structure localized on the lipid bilayer compatible surface, the multi-lamellar lipid membrane structure comprises two or more synthetic lipids comprising a phosphatidylethanolamine (PE), a phosphatidylglycerol (PG), a phosphatidylcholine (PC), a phosphatidylserine (PS), a cholesterol, and/or a cardiolipin (CL).

22. The biosensor of claim **21**, wherein the PE comprises 1-palmitoyl-2-oleoyl-sn-glycero-3-phosphoethanolamine (POPE) and/or 1,2-dimyristoyl-sn-glycero-3-phosphoethanolamine (DMPE).

23. The biosensor of claim **21**, wherein the PG comprises 1-palmitoyl-2-oleoyl-sn-glycero-3-phospho-(1'-rac-glycerol) (POPG) and/or1,2-dimyristoyl-sn-glycero-3--phospho-(1'-rac-glycerol) (DMPG).

24. The biosensor of claim **21**, wherein the PC comprises 1,2-dimyristoyl-sn-glycero-3-phosphocholine (DMPC).

25. The biosensor of claim **21**, wherein the PS comprises 1,2-dimyristoyl-sn-glycero-3-phospho-L-serine (DMPS).

26. The biosensor of claim **21**, wherein the two or more synthetic lipids are PE, PG and CL, wherein the concentration of the PE in the multi-lamellar lipid membrane structure is between about 67 mass % to about 71 mass %, the concentration of the PG is in the multi-lamellar lipid membrane structure is between about 23 mass % to about 27 mass %, and the concentration of the CL in the multi-lamellar lipid membrane structure is between about 3 mass % to about 10 mass %.

27. The biosensor of claim **21**, wherein the two or more synthetic lipids are PE and CL, wherein the concentration of the PE in the multi-lamellar lipid membrane structure is about 90 mass % and the concentration of the CL in the multi-lamellar lipid membrane structure is about 10 mass %.

28. The biosensor of claim **21**, wherein the two or more synthetic lipids are PE and PG, wherein the concentration of the PE in the multi-lamellar lipid membrane structure is about 78 mass % and the concentration of the PG in the multi-lamellar lipid membrane structure is about 22 mass %.

29. The biosensor of claim **21**, wherein the two or more synthetic lipids are PG and CL, wherein the concentration of the PG in the multi-lamellar lipid membrane structure is about 80 mass % and the concentration of the CL in the multi-lamellar lipid membrane structure is about 20 mass %.

30. The biosensor of claim **21**, wherein the two or more synthetic lipids are PC, PS, PE and cholesterol.

31. The biosensor of claim **30**, wherein the PC is 1,2-dimyristoyl-sn-glycero-3-phosphocholine (DMPC), the PS is 1,2-dimyristoyl-sn-glycero-3-phospho-L-serine (DMPS), and the PE is 1,2-dimyristoyl-sn-glycero-3-phosphoethanolamine (DMPE).

32. The biosensor of claim **30**, wherein the mass ratio of PC:PS:PE:cholesterol is 2:1:1:0.2 or 2:1:1:0.

33. A method of detecting membrane disruption activity in a sample, the method comprising:

(a) contacting the sample with the biosensor of claim **1**; and

(b) detecting a change in the multi-lamellar lipid membrane structure in response to the sample.

34. The method of claim **33**, wherein the biosensor comprises at least one electrode and detecting the change in the multi-lamellar lipid membrane structure comprises voltammetry, cyclic voltammetry, chronoamperometry, differential multi pulse voltammetry, double potential pulse techniques or additive differential pulse voltammetry.

35. A method of making the biosensor of claim **1**, the method comprising:

(a) preparing an aqueous solution of hybrid membranes comprising membranes prepared from red blood cells or red blood cell ghosts and the one or more synthetic lipids; and

(b) generating the multi-lamellar lipid membrane structure localized on the lipid bilayer compatible surface by successively providing the aqueous solution of hybrid membranes on the lipid bilayer compatible surface.

36. The method of claim **35**, wherein the aqueous solution of hybrid membranes is successively provided on the lipid bilayer compatible surface from 2 to 8 times, preferably 5 times.

37. The method of claim **35**, wherein after each providing of the aqueous solution of hybrid membranes to the lipid bilayer compatible surface, the method further comprises allowing the hybrid membranes to attach to the biosensor, and performing annealing to improve stability and reduce defects in the multi-lamellar lipid membrane structure.

* * * * *